REPORT 549—Part I

AGARD

ADVISORY GROUP FOR AEROSPACE RESEARCH & DEVELOPMENT

64 RUE DE VARENNE PARIS 7E FRANCE

Considerations in the determination of stability and control derivatives and dynamic characteristics from flight data

by Chester H. Wolowicz

★

1966

NORTH ATLANTIC TREATY ORGANIZATION

AGARD REPORT 549 - PART I

NORTH ATLANTIC TREATY ORGANIZATION

ADVISORY GROUP FOR AEROSPACE RESEARCH AND DEVELOPMENT

(ORGANISATION DU TRAITE DE L'ATLANTIQUE NORD)

CONSIDERATIONS IN THE DETERMINATION OF STABILITY AND CONTROL DERIVATIVES AND DYNAMIC CHARACTERISTICS FROM FLIGHT DATA

by

Chester H. Wolowicz

NASA Flight Research Center
Edwards Air Force Base, California, USA

This Report was prepared at the request of the Flight Mechanics Panel of AGARD

CONTENTS

LIST OF TABLES

LIST OF FIGURES

NOTATION

The body system of axes, radian measure, and foot-pound-second units are used throughout the paper unless specifically stated or indicated otherwise. Basic sign conventions are shown in Figure 1. In Section 1, in which a number of axis systems are considered, the subscripts are used to denote quantities referred to the various systems except for the quantities referred to the body system of axes. The subscripts for these quantities are omitted for convenience except to identify coordinates, x_b, y_b, and z_b.

a_s	perpendicular distance from spring to knife edge (Fig. 13), ft
a, A	polynomial coefficients (Section 3)
A_i	cross-sectional area of air-intake duct of jet engine at entrance, ft^2
A_j	cross-sectional area of jet-exhaust duct of jet engine at exit, ft^2
a_x, a_t, a_n	longitudinal, lateral, and normal accelerations of the aircraft at the center of gravity relative to the body system of axes; positive forward, to the right, and up, respectively, g units
$a_{x_i}, a_{t_i}, a_{n_i}$	recorded values of a_x, a_t, and a_n, respectively; corrected for phase lag and misalinement but not for location relative to the center of gravity, g units
b	wing span, ft
b, B	polynomial coefficients (Section 3)
$\bar{c}$	mean aerodynamic chord, ft
c, C	polynomial coefficients (Section 3)
C	spring couple (Section 4), ft lb
C_c	coefficient of axial force along the body x-axis; positive to the rear, $-X/\bar{q}S$
$\bar{C}_{c_u}$	phugoid damping coefficient, $V\frac{\partial C_c}{\partial u} + \frac{2C_c}{\cos\alpha\cos\beta}$
$(\bar{C}_{c_u})_p$	contribution of power to phugoid damping coefficient, $-\left(V\frac{\partial C_T}{\partial u} + \frac{2C_T}{\cos\alpha\cos\beta}\right)$

C_{c_α} = $\frac{\partial C_c}{\partial \alpha}$

$C_{c_{\dot{\alpha}}}$ = $\frac{\partial C_c}{\partial \frac{\dot{\alpha}\bar{c}}{2V}}$

C_{c_q} = $\frac{\partial C_c}{\partial \frac{q\bar{c}}{2V}}$

$C_{c_{\delta_e}}$ = $\frac{\partial C_c}{\partial \delta_e}$

C_D drag coefficient; coefficient of axial force along the stability x-axis, positive to the rear, $-X_s/\bar{q}S$

C_L lift coefficient; coefficient of lift force along the stability z-axis, positive up, $-Z_s/\bar{q}S$

C_{L_t} = $\frac{W}{\bar{q}S}$

C_{L_α} lift-curve slope, $\partial C_L/\partial\alpha$

$C_{L_{\dot{\alpha}}}$ = $\frac{\partial C_L}{\partial \frac{\dot{\alpha}\bar{c}}{2V}}$

C_{L_q} = $\frac{\partial C_L}{\partial \frac{q\bar{c}}{2V}}$

$C_{L_{\delta_e}}$ = $\frac{\partial C_L}{\partial \delta_e}$

$C_l, (C_l)_s, (C_l)_w, (C_l)_o$ coefficient of rolling-moment about the body, stability, wind, and principal x-axis, respectively, (rolling moment)/$\bar{q}$Sb

C_{l_p} damping-in-roll derivative, $\frac{\partial C_l}{\partial \frac{pb}{2V}}$

C_{l_r} = $\frac{\partial C_l}{\partial \frac{rb}{2V}}$

C_{l_β} effective dihedral derivative, $\frac{\partial C_l}{\partial \beta}$

$C_{l_{\dot{\beta}}} = \frac{\partial C_l}{\partial \frac{\dot{\beta} b}{2V}}$

$C_{l_{\delta_a}} \quad \frac{\partial C_l}{\partial \delta_a}$

$C_{l_{\delta_r}} = \frac{\partial C_l}{\partial \delta_r}$

$C_m, (C_m)_s, (C_m)_w, (C_m)_0$ = pitching-moment coefficient about the body, stability, wind, and principal y-axis, respectively, (pitching moment)/$\bar{q}S\bar{c}$

C_{m_0} pitching-moment coefficient abcut the aerodynamic center

$(C_m)_p$ contribution of power to pitching-moment coefficient

C_{m_α} longitudinal-stability derivative, $\frac{\partial C_m}{\partial \alpha}$

$(C_{m_\alpha})_p$ contribution of power to longitudinal stability (Equations (35) and (44))

$C_{m_{\dot{\alpha}}} = \frac{\partial C_m}{\partial \frac{\dot{\alpha}\bar{c}}{2V}}$

$C_{m_q} = \frac{\partial C_m}{\partial \frac{q\bar{c}}{2V}}$

$\bar{C}_{m_u} = V \frac{\partial C_m}{\partial u} + \frac{2C_m}{\cos\alpha \cos\beta}$

$(C_{m_u})_p$ refer to Equations (47), (48), and (49)

$C_{m_{\delta_e}} = \frac{\partial C_m}{\partial \delta_e}$

C_N normal-force coefficient, coefficient of force parallel to body z-axis; positive up, $-Z/\bar{q}S$

$(C_N)_p$ contribution of power to normal-force coefficient

C_{N_α} = $\frac{\partial C_N}{\partial \alpha}$

$(C_{N_\alpha})_p$ variation of contribution of $(C_N)_p$ with angle of attack

$(C_{N_\alpha})_{h.t.}$ variation of normal-force coefficient of horizontal tail with local angle of attack at the tail; coefficient based on horizontal-tail area and local dynamic pressure,

$$\frac{\partial \left(\frac{-Z_{h.t.}}{\bar{q}_{h.t.} S_{h.t.}} \right)}{\partial \alpha_{h.t.}}$$

$(C_{N_\alpha})_{v.t.}$ variation of coefficient of force normal to vertical tail with vertical angle of attack of vertical tail; coefficient based on vertical-tail area and local dynamic pressure,

$$\frac{\partial \left(\frac{Y_{v.t.}}{\bar{q}_{v.t.} S_{v.t.}} \right)}{\partial \alpha_{v.t.}}$$

$C_{N_{\dot{\alpha}}}$ = $\frac{\partial C_N}{\partial \frac{\dot{\alpha}\bar{c}}{2V}}$

C_{N_q} = $\frac{\partial C_N}{\partial \frac{q\bar{c}}{2V}}$

$\bar{C}_{N_u}$ longitudinal phugoid static-stability derivative, $V \frac{\partial C_N}{\partial u} + \frac{2C_N}{\cos \alpha \cos \beta}$

$C_{N_{\delta_e}}$ = $\frac{\partial C_N}{\partial \delta_e}$

$C_n, (C_n)_s, (C_n)_w, (C_n)_0$ yawing-moment coefficient about body, stability, wind, and principal z-axis, respectively, (yawing moment)/$\bar{q}$Sb

C_{n_β} static directional-stability derivative, $\frac{\partial C_n}{\partial \beta}$

$C_{n_{\dot{\beta}}}$ = $\frac{\partial C_n}{\partial \frac{\dot{\beta}b}{2V}}$

C_{n_r} = $\frac{\partial C_n}{\partial \frac{rb}{2V}}$

C_{n_p} = $\dfrac{\partial C_n}{\partial \dfrac{pb}{2V}}$

$C_{n_{\delta_r}}$ = $\dfrac{\partial C_n}{\partial \delta_r}$

$C_{n_{\delta_a}}$ = $\dfrac{\partial C_n}{\partial \delta_a}$

C_T thrust coefficient, (thrust)/$\bar{q}S$

C_{T_u} = $\dfrac{\partial C_T}{\partial u}$

$(C_x)_w$ coefficient of axial force along the wind x-axis, $\dfrac{X_w}{\bar{q}S}$

$C_y, (C_y)_s, (C_y)_w, (C_y)_0$ side-force coefficient parallel to body, stability, wind, and principal y-axis, respectively, $C_y = (C_y)_s$, (Side force)/$\bar{q}S$

C_{y_β} = $\dfrac{\partial C_y}{\partial \beta}$

$(C_{y_\beta})_p$ contribution of power to C_{y_β}

$C_{y_{\dot\beta}}$ = $\dfrac{\partial C_y}{\partial \dfrac{\dot\beta b}{2V}}$

C_{y_r} = $\dfrac{\partial C_y}{\partial \dfrac{rb}{2V}}$

C_{y_p} = $\dfrac{\partial C_y}{\partial \dfrac{rb}{2V}}$

$(C_z)_w$ coefficient of force along the wind z-axis, $\dfrac{Z_w}{\bar{q}S}$

d, D polynomial coefficients (Section 3)

e = 2.178

e, E polynomial coefficients (Section 3)

g		acceleration of gravity, ft/sec^2
g_1	$= \frac{g}{V} \sin \theta, \frac{1}{sec}$	
g_2	$= \frac{g}{V} \cos \theta \sin \phi, \frac{1}{sec}$	
h		altitude, ft
$\bar{H}$		angular-momentum vector of a rotating mass, $I_{rm}\Omega$, lb ft sec
H_x, H_y, H_z		angular momentum of $\bar{H}$ about x , y , z body axes, respectively, lb ft sec
I_{rm}		moment of inertia of rotating mass of engine about its rotating axis, slug ft^2
I_x, I_y, I_z		moments of inertia of aircraft about x , y , z body axes, respectively, slug ft^2
$I_{x_0}, I_{y_0}, I_{z_0}$		moments of inertia of aircraft about x , y , z principal axes, respectively, slug ft^2
$I_{x_s}, I_{y_s}, I_{z_s}$		moments of inertia of aircraft about x , y , z stability axes, respectively, slug ft^2
$I_{x_r}, I_{y_r}, I_{z_r}$		moments of inertia of aircraft about x , y , z reference axes, respectively, slug ft^2
I_{x_c}		moment of inertia of cradle supporting aircraft (Section 4), slug ft^2
I'_x	$= \frac{I_{xz}}{I_x}$	
I'_z	$= \frac{I_{xz}}{I_z}$	
I_{xz}		product of inertia of aircraft referred to body x- and z-axes, slug ft^2
k		stability-augmentation-system gain, sec
K_s		linear spring constant, lb/ft
K		correlation constant (Section 5)
K_t		torsional spring constant, $2K_s a_s^2$, ft lb/rad

l		distance as defined locally at time of discussion, ft
L, M, N		rolling, pitching, and yawing moments about body x , y , z axes, respectively, ft lb
L_i, M_i, N_i		inertial rolling, pitching, and yawing moments about the respective body axes, ft lb
L_{rm}, M_{rm}, N_{rm}		rolling, pitching, and yawing moments due to gyroscopic action of rotating mass of engine, ft lb
$(L)_s, (M)_s, (N)_s$		rolling, pitching, and yawing moments about the stability x , y , z axes, ft lb
$\bar{L}$		rolling acceleration about body x-axis, (rolling moment)/I_x , $1/sec^2$
L_p	$= \frac{\partial L}{\partial p} = C_{l_p} \frac{\bar{q}Sb^2}{2V}$	, ft lb sec
$\bar{L}_p$	$= C_{l_p} \frac{\bar{q}Sb^2}{2VI_x}$	, $\frac{1}{sec}$
$\bar{L}'_p$	$= \frac{\bar{L}_p + \frac{I_{xz}}{I_x} N_p}{1 - \frac{I_{xz}^2}{I_x I_z}}$	, $\frac{1}{sec}$
L_r	$= \frac{\partial L}{\partial r} = C_{l_r} \frac{\bar{q}Sb^2}{2V}$	, ft lb sec
$\bar{L}_r$	$= C_{l_r} \frac{\bar{q}Sb^2}{2VI_x}$	, $\frac{1}{sec}$
$\bar{L}'_r$	$= \frac{\bar{L}_r + \frac{I_{xz}}{I_x} \bar{N}_r}{1 - \frac{I_{xz}^2}{I_x I_z}}$	, $\frac{1}{sec}$
L_β	$= \frac{\partial L}{\partial \beta} = C_{l_\beta} \bar{q}Sb$	, ft lb
$\bar{L}_\beta$	$= C_{l_\beta} \frac{\bar{q}Sb}{I_x}$	, $\frac{1}{sec^2}$
L_{δ_a}	$= \frac{\partial L}{\partial \delta_a} = C_{l_{\delta_a}} \bar{q}Sb$	, ft lb

$\bar{L}_{\delta_a}$ = $C_{l_{\delta_a}} \frac{\bar{q}Sb}{I_x}$, $\frac{1}{sec^2}$

L_{δ_r} = $C_{l_{\delta_r}} \bar{q}Sb$, ft lb

$\bar{L}_{\delta_r}$ = $C_{l_{\delta_r}} \frac{\bar{q}Sb}{I_x}$, $\frac{1}{sec^2}$

m mass of airplane, W/g , slugs

m_a mass rate of air intake of jet engine, slugs/sec

m_i mass rate of jet exhaust, slugs/sec

M Mach number

M_i indicated Mach number

$\bar{M}$ pitching acceleration about body y-axis, (pitching moment)/I_y , $1/sec^2$

M_q = $\frac{\partial M}{\partial q} = C_{m_q} \frac{\bar{q}S\bar{c}^2}{2V}$, ft lb sec

$\bar{M}_q$ = $C_{m_q} \frac{\bar{q}S\bar{c}^2}{2VI_y}$, $\frac{1}{sec}$

M_u = $\frac{\partial M}{\partial u} = \bar{C}_{m_u} \frac{\bar{q}S\bar{c}}{V}$, lb sec

$\bar{M}_u$ = $\bar{C}_{m_u} \frac{\bar{q}S\bar{c}}{I_y}$, $\frac{1}{sec^2}$

M_α = $\frac{\partial M}{\partial \alpha} = C_{m_\alpha} \bar{q}S\bar{c}$, ft lb

$\bar{M}_\alpha$ = $C_{m_\alpha} \frac{\bar{q}S\bar{c}}{I_y}$, $\frac{1}{sec^2}$

$M_{\dot{\alpha}}$ = $\frac{\partial M}{\partial \dot{\alpha}} = C_{m_{\dot{\alpha}}} \frac{\bar{q}S\bar{c}^2}{2V}$, ft lb sec

$\bar{M}_{\dot{\alpha}}$ = $C_{m_{\dot{\alpha}}} \frac{\bar{q}S\bar{c}^2}{2VI_y}$, $\frac{1}{sec}$

M_{δ_e} = $\frac{\partial M}{\partial \delta_e} = C_{m_{\delta_e}} \bar{q}S\bar{c}$, ft lb

$\bar{M}_{\delta_e}$ = $C_{m_{\delta_e}} \frac{\bar{q}S\bar{c}}{I_y}$, $\frac{1}{sec^2}$

$\bar{N}$ yawing acceleration about body z-axis, (yawing moment)/I_z , $1/sec^2$

N_p = $\frac{\partial N}{\partial p} = C_{n_p} \frac{\bar{q}Sb^2}{2V}$, ft lb sec

$\bar{N}_p$ = $C_{n_p} \frac{\bar{q}Sb^2}{2VI_z}$, $\frac{1}{sec}$

$\bar{N}'_p$ = $\frac{\bar{N}_p + \frac{I_{xz}}{I_z} \bar{L}_p}{1 - \frac{I_{xz}^2}{I_x I_z}}$, $\frac{1}{sec}$

N_r = $\frac{\partial N}{\partial r} = C_{n_r} \frac{\bar{q}Sb^2}{2V}$, ft lb sec

$\bar{N}_r$ = $C_{n_r} \frac{\bar{q}Sb^2}{2VI_z}$, $\frac{1}{sec}$

$\bar{N}'_r$ = $\frac{\bar{N}_r + \frac{I_{xz}}{I_z} \bar{L}_r}{1 - \frac{I_{xz}^2}{I_x I_z}}$, $\frac{1}{sec}$

N_β = $\frac{\partial N}{\partial \beta} = C_{n_\beta} \bar{q}Sb$, ft lb

$\bar{N}_\beta$ = $C_{n_\beta} \frac{\bar{q}Sb}{I_z}$, $\frac{1}{sec^2}$

N_{δ_r} = $\frac{\partial N}{\partial \delta_r} = C_{n_{\delta_r}} \bar{q}Sb$, ft lb

$\bar{N}_{\delta_r}$ = $C_{n_{\delta_r}} \frac{\bar{q}Sb}{I_z}$, $\frac{1}{sec^2}$

N_{δ_a} = $\frac{\partial N}{\partial \delta_a} = C_{n_{\delta_a}} \bar{q}Sb$, ft lb

$\bar{N}_{\delta_a}$ = $C_{n_{\delta_a}} \frac{\bar{q}Sb}{I_z}$, $\frac{1}{sec^2}$

p, q, r	rolling, pitching, and yawing velocities, respectively, about body axes, rad/sec
p_0, q_0, r_0	rolling, pitching, and yawing velocities, respectively, about principal axes, rad/sec
p_s, q_s, r_s	rolling, pitching, and yawing velocities, respectively, about stability axes, rad/sec
$\dot{p}, \dot{q}, \dot{r}$	rolling, pitching, and yawing angular accelerations, respectively, about body axes, rad/sec^2
$\dot{p}_0, \dot{q}_0, \dot{r}_0$	rolling, pitching, and yawing accelerations, respectively, about principal axes, rad/sec^2
$\bar{p}$	static pressure, lb/ft^2
$\bar{p}_i$	indicated static pressure, uncorrected recorded pressure, lb/ft^2
$\bar{p}_i, \bar{p}_j$	static pressures acting across inlet of air intake and exhaust, respectively, of jet engine, lb/ft^2
$\bar{p}_T$	stagnation pressure, $\bar{q}_c + \bar{p}$, lb/ft^2
P	period of short-period oscillation, sec
$\bar{q}$	dynamic pressure, $\frac{1}{2}\zeta V^2$, lb/ft^2
$\bar{q}_c$	impact pressure; dynamic pressure of compressible flow (Equations (98) and (99)), lb/ft^2
$\bar{q}_{c_i}$	indicated impact pressure, lb/ft^2
$\bar{q}_{h.t.}, \bar{q}_{v.t.}$	dynamic pressures at the horizontal and vertical tail, respectively, lb/ft^2
R	instantaneous radius of turn (Fig. 27), ft
R	reaction force (Section 4), lb
s	Laplacian operator, $\sigma + i\omega$, $\frac{1}{\text{sec}}$
s_{in}	instrument sensitivity
S	wing area, ft^2
$S_{h.t.}, S_{v.t.}$	horizontal- and vertical-tail areas, respectively, ft^2
t	time, sec

T	thrust due to power, lb
$T_{1/2}$	time required for absolute value of transient short-period oscillation to damp to one-half amplitude, sec
$\frac{1}{T_R}, \frac{1}{T_S}$	roll-subsidence and spiral-divergence roots, respectively, of the lateral-directional characteristic equation, $\frac{1}{sec}$
T_R, T_S	roll-subsidence and spiral-divergence time constants, sec
T_θ	pitch-attitude time constant in numerator of $\frac{q(s)}{\delta_e(s)}$ transfer function, sec
u, v, w	linear velocities relative to body x , y , z axes, respectively, ft/sec
$\dot{u}, \dot{v}, \dot{w}$	linear accelerations relative to body x , y , z axes, respectively, ft/sec^2
$\hat{\Delta u}$	$= \frac{\Delta u}{V}$
$\hat{\Delta \dot{u}}$	$= \frac{\Delta \dot{u}}{V}$
V	airspeed, ft/sec
V_i	velocity of intake air at air intake of jet engine ft/sec
V_j	velocity of jet exhaust, ft/sec
W	weight of aircraft, lb
W_c	weight of cradle (Section 4), lb
x, y, z	distances from the center of gravity along body x , y , z axes, respectively, ft
X, Y, Z	forces along the body x , y , z axes, respectively; positive forward, to the right, and down, respectively, lb
X_g, Y_g, Z_g	components of gravitational force acting along the body x , y , z axes, respectively
X_u	$= \frac{\partial X}{\partial u} = -\bar{C}_{c_u} \frac{\bar{q}S}{V}$, lb sec/ft

$\bar{X}_u = - \bar{C}_{c_u} \frac{\bar{q}S}{mV}$, $\frac{1}{sec}$

$X_\alpha = \frac{\partial X}{\partial \alpha} = - C_{c_\alpha} \bar{q}S$, lb

$\bar{X}_\alpha = - C_{c_\alpha} \frac{\bar{q}S}{mV}$, $\frac{1}{sec}$

$X_\delta = \frac{\partial X}{\partial \delta} = - C_{c_\delta} \bar{q}S$, lb

$\bar{X}_\delta = - C_{c_\delta} \frac{\bar{q}S}{mV}$, $\frac{1}{sec}$

$Y_{v.t.} = - (C_{N_\alpha})_{v.t.} \bar{q}_{v.t.} S_{v.t.}$, lb

$Y_\beta = \frac{\partial Y}{\partial \beta} = C_{y_\beta} \bar{q}S$, lb

$\bar{Y}_\beta = C_{y_\beta} \frac{\bar{q}S}{mV}$, $\frac{1}{sec}$

$(Y)_p$ lateral force in plane of propeller disk due to propeller, lb

$Y_\delta = \frac{\partial Y}{\partial \delta} = C_{y_\delta} \bar{q}S$, lb

$\bar{Y}_\delta = C_{y_\delta} \frac{\bar{q}S}{mV}$, $\frac{1}{sec}$

$Z_u = \frac{\partial Z}{\partial u} = - \bar{C}_{N_u} \frac{\bar{q}S}{V}$, lb sec/ft

$\bar{Z}_u = - \bar{C}_{N_u} \frac{\bar{q}S}{mV}$, $\frac{1}{sec}$

$Z_q = \frac{\partial Z}{\partial q} = - C_{N_q} \frac{\bar{q}S\bar{c}}{2V}$, lb sec

$\bar{Z}_q = - C_{N_q} \frac{\bar{q}S\bar{c}}{2mV^2}$

$Z_\alpha = \frac{\partial Z}{\partial \alpha} = - C_{N_\alpha} \bar{q}S$, lb

$\bar{Z}_{\alpha}$ = $- C_{N\alpha} \frac{\bar{q}S}{mV}$, $\frac{1}{sec}$

$Z_{\dot{\alpha}}$ = $\frac{\partial Z}{\partial \dot{\alpha}} = - C_{N\dot{\alpha}} \frac{\bar{q}S\bar{c}}{2V}$, lb sec

$\bar{Z}_{\dot{\alpha}}$ = $- C_{N\dot{\alpha}} \frac{\bar{q}S\bar{c}}{2mV^2}$

$(Z)_p$ contribution of propulsion system to Z force, lb

$Z_{h.t.}$ = $- (C_{N\alpha})_{h.t.} \bar{q}_{h.t.} S_{h.t.}$, lb

α angle of attack of aircraft

$\Delta\alpha_c$ change in α due to influence of flight-path curvature

α_0 angle of attack of aircraft for zero Z force

$(\alpha)_p$ angle of attack of thrust line relative to airstream velocity at propeller or air intake of jet engine; thrust line considered parallel to x axis

α_p maximum positive or negative angle of attack obtained in a roll maneuver (Fig. 66)

β sideslip angle

$\dot{\beta}$ rate of change of β with time, rad/sec

γ flight-path angle relative to horizontal

γ adiabatic constant

δ_a aileron deflection; positive when left aileron is deflected down

$\delta_{a\beta}$ = $\frac{d\delta_a}{d\beta}$

δ_e elevator deflection; positive when trailing edge is deflected down

δ_r rudder deflection; positive when trailing edge is deflected to the left

$\delta_{r\beta}$ = $\frac{d\delta_r}{d\beta}$

δ_{sp}	angle included between reference x-axis and plane of spring couple (Fig. 15)
Δ	increment
ϵ	angle between body x-axis and principal x-axis; positive when reference is above principal axis at the nose
ϵ_p	upwash angle at the propeller due to such factors as fuselage and wing
ζ	short-period ratio of actual damping to critical damping
ζ_{ph}	phugoid ratio of actual to critical damping
ζ_{in}	instrument damping ratio
η	angle of inclination of principal x-axis relative to stability x-axis; positive when principal x-axis is above stability x-axis at the nose
θ_{rm}	pitch attitude of angular-velocity vector, Ω, of rotating mass of engine relative to body x-axis
μ_b	relative aircraft density, $\frac{m}{\rho S b}$
c	relative aircraft density, $\frac{m}{\rho S \bar{c}}$
μ_0	absolute viscosity, lb sec/in^{-2}
ρ	mass density of air, slugs/ft^3
σ	real part of Laplacian operator, $s = \sigma + iw$
τ	time parameter, $\frac{m}{\rho V S}$, sec
τ'	time constant for simplified stability augmentation system, sec
ψ, θ, ϕ	yaw, pitch, and roll, Euler orientation angles, respectively. (In general aircraft motions, they are normally the orientation angles of the aircraft body axis system to a spatial (earth) reference system. In instrument alinement, they refer to the misalinement of the instrument reference axis system to the aircraft body axis system.)

$\dot{\psi}, \dot{\theta}, \dot{\phi}$	rate of rotation of the Euler orientation angles, rad/sec
$\Delta\psi', \Delta\theta', \Delta\phi'$	yaw, pitch, and roll Euler orientation angles of aircraft body axis system during small perturbations relative to body axis system preceding the perturbations regardless of aircraft attitude preceding perturbations (Fig.4(b)), $\Delta\psi' \simeq \int \Delta r dt$, $\Delta\theta' \simeq \int \Delta q dt$, $\Delta\phi' \simeq \int \Delta p dt$
Φ_d	damping angle
Φ_{ij}	phase angle of vector quantity i relative a vector quantity j
ω_n, ω_{n_d}	undamped and damped natural frequencies, respectively, of the aircraft in short-period modes of oscillation, rad/sec
$\omega_{n_{ph}}, \omega_{n_{d_{ph}}}$	undamped and damped natural frequencies, respectively, of the aircraft in phugoid modes of oscillation, rad/sec
$\omega_{n_{in}}$	undamped natural frequency of instrument, rad/sec
Ω	angular rate of rotation of rotating mass of engine, rad/sec
$\lvert j \rvert$	absolute magnitude of a vector quantity j ; always positive
$[L]$	transformation matrix
$[L]^{-1}$	inverse transformation matrix
$[L]_s, [L]_b$	transform matrices to transform vector quantities from reference axis system to aircraft stability and body axis systems, respectively
$[\alpha]_s$	transformation matrix representing transformation from body to stability axis system
$(\ )_b, (\ )_s, (\ )_w, (\ )_0$	relative to body, stability, wind, and principal axes systems, respectively
$(\ )_p$	contribution due to power

CONSIDERATIONS IN THE DETERMINATION OF STABILITY AND CONTROL DERIVATIVES AND DYNAMIC CHARACTERISTICS FROM FLIGHT DATA

Chester H. Wolowicz

1. INTRODUCTION

The determination of stability and control characteristics from flight data in the form of derivatives and other behavior parameters has become an important part of flight testing. As new concepts in airplanes are developed or the airplane flies in new Mach and altitude regimes, there is the need to verify theory and wind-tunnel data and the various influences on stability characteristics, to provide information not obtained in wind-tunnel studies, and to uncover the sources of discrepancies between prediction and actual flight behavior. Where wind-tunnel data are unavailable or where safety of flight into untested regions is of concern, flight-determined derivatives have been extrapolated to predict airplane behavior prior to flight into these regions.

Because of the exploratory nature of many of the investigations, the practical aspects of determining derivatives and other behavior parameters, such as oscillatory characteristics, from flight data are very important. Experience has shown that a maximum appreciation and understanding of the practical aspects is attained when background knowledge includes an understanding of axis systems, transformations, the equations of motions and the limitations of the equations, techniques used to determine the mass characteristics of the airplane, the installation and behavior of flight test instrumentation, flight test techniques, and the theory and limitations of techniques used to determine the stability and control characteristics from flight data.

Although some of the factors mentioned above, such as axis systems and transformations as well as aspects of the equations of motion, may be found in textbooks, the treatment is generally not oriented toward flight testing. Some of the techniques used in determining stability and control characteristics may be found in technical reports; however, limitations of the techniques occasionally may not be shown. This paper attempts to bring all the factors together to provide a ready reference of pertinent information. It is, in fact, a greatly expanded version of AGARD Report 224*.

It is the purpose of this paper to discuss the various factors that influence the determination of stability and control derivatives and other behavior characteristics from flight data. Included are illustrations of the application of flight derivatives to verification of predictions and to determination of aeroelastic effects, stability criteria, and flight guidance. This paper is intended not only for the practical engineer who is working with flight data but also for the scientist who is attempting to develop new, sophisticated analytical techniques.

---

* *Stability-Derivative Determination From Flight Data* by Chester H. Wolowicz and Euclid C. Holleman, October 1958.

Acknowledgement of investigators whose work has directly contributed to the present paper is made in each section. It is recognized that many noteworthy works of other investigators are not referenced.

2. AXIS SYSTEMS AND COORDINATE TRANSFORMATIONS

2.1 Axis Systems

In the study of the dynamics of the airplane, as many as six orthogonal axis systems may be used simultaneously. An understanding of these systems or reference frames and their relation to the aircraft and its motions at various flight conditions is essential to the proper analysis of flight data. Although a comprehensive treatment of axis systems may be found in Reference 1, a brief treatment of the axis systems is presented in this section.

2.1.1 Body Systems

The body axis system (x_b, y_b, z_b) is body-fixed with its origin at the center of gravity of the airplane. The x_b axis is always parallel to the fuselage reference line and when the center of gravity is in the plane of symmetry, as it normally is, both the x_b and z_b axes are in the airplane's plane of symmetry, as shown in Figure 1. The y_b axis is normal to the plane of symmetry; thus, the body system of axes is angularly invariant with respect to the aircraft structure.

Because of its angular invariance with respect to the aircraft, the body axis system is an excellent frame of reference for mounting flight test instruments. The orientation of the flight test instruments and their consequent output relative to the body axes – especially the linear accelerometer and angular rate and acceleration sensors – make it convenient to determine, from flight data, stability and control parameters with respect to this reference frame. Aside from convenience, this reference frame is the logical frame about which to orient rates, accelerations, and the stability and control parameters in the study of handling-quality criteria, inasmuch as the orientation of the pilot is invariant relative to this frame.

2.1.2 Stability System

The stability axis system (x_s, y_s, z_s) is a special case of the body axis system. Like the body system, the x_s and z_s axes are in the plane of symmetry when the center of gravity is in this plane, and parallel to the plane of symmetry when the center of gravity is not in the plane. Unlike the body system, however, the x_s and z_s axes are angularly variant relative to the fuselage reference line. The z_s axis is perpendicular to the resultant velocity vector and the x_s axis is parallel to the component of the resultant velocity vector projected onto the plane of symmetry, as shown in Figure 1.

The important parametric relationship between the body and stability axes systems is the angle of attack, α, which is the angle between the x_s and x_b axes (Fig. 1).

The stability axis system is commonly used in theoretical subsonic aerodynamics and subsonic wind-tunnel force and moment investigations. It is also employed, on occasion, in place of body axes in flight test investigations of longitudinal stability and control characteristics.

2.1.3 Principal System

The principal axis system (x_0, y_0, z_0) defines the natural axes of rotation of the aircraft. They are the axes which result in maximum and minimum moments of inertia. The orientation of this axis system in the aircraft is a function of the mass distribution of the aircraft and will remain fixed as long as the mass and mass distribution remain fixed. When the lateral distribution of mass is symmetrical relative to the plane of symmetry, which is generally the case, the y_0 axis will coincide with the y_b axis, and the x_0 and z_0 axes will lie in the plane of symmetry, as shown in Figure 1.

The inclination of the x_0 axis (Fig.1) to the x axis of the reference axis system (generally body axes in flight test investigations) has a direct bearing on the inertial moments experienced about the reference axes as reflected in the product of inertia term I_{xz} in the equations of motion and, hence, on the lateral stability of the airplane.

When the principal axes are used as reference axes, as they occasionally are in theoretical and simulator investigations, they are used to simplify the equations of motion by the elimination of the I_{xz} term.

2.1.4 Wind System

The wind axis system is related to the resultant velocity vector and the plane of symmetry of the airplane. As shown in Figure 1, the x_w axis is parallel to the resultant velocity vector and lies in the transverse plane of the stability axes ($x_s y_s$ plane). Consequently, the z_w axis is coincident with the z_s axis. The x_w and y_w axes coincide with their respective counterparts x_s and y_s when the aircraft has zero sideslip.

The important parameters associated with the wind system are the sideslip angle, β, and the angle of climb, γ. By basic definition the angle of sideslip, β, is the angle between the x_w axis and the plane of symmetry and thus lies in the transverse stability axes plane, as shown in Figure 1. It should be noted that not all β-sensors necessarily measure this β; this will be discussed in Section 5 on "Instrumentation". The angle of climb always lies in the vertical plane and is the angle included between the x_w axis and the horizontal plane.

2.1.5 Spatial Reference System

The preceding axis systems are tied in with the plane of symmetry of the airplane with their origins at the center of gravity; as shown in Figure 1. To complete the systems of axes used, at least one inertial, space-fixed, axis system is required. In dealing with general motions of aircraft, this spatial system is generally earth-referenced to describe the motion of the airplane with respect to time for short time intervals. Such a situation is indicated in Figure 2, which shows the relationships of the various axis systems previously described and the relationship of the body axis system with respect to the spatial reference (x_r, y_r, z_r). Shown in the figure are flight path γ, angle of sideslip β, angle of attack α, as well as the Euler orientation angles, ψ, θ, and ϕ of the airplane's body axes relative to the spatial axis system. This is shown in a much simpler format in Figure 3. The sequence of rotations of the Euler angles is important. Generally, the sequence of rotation is

ψ , θ , and ϕ ; this means that the airplane is initially yawed, then pitched, and finally rolled.

It should be noted that $\gamma = \theta - \alpha$ only when the aircraft is unbanked ($\phi = 0$).

2.1.6 Perturbation Reference Frames

In using perturbation theory in stability analysis, Euler angle perturbations may be considered to be superimposed on the unperturbed angles, as shown in Figure 4(a), with the result that the perturbed angles are $\psi + \Delta\psi$, $\theta + \Delta\theta$, and $\phi + \Delta\phi$, or they may be based on a secondary spatial reference frame which is the unperturbed airplane axis system (x_{b_0}, y_{b_0}, z_{b_0}). In Figure 4(b) the unperturbed body axes constitute the secondary spatial reference frame and are oriented to the basic spatial reference frame through the angles ψ , θ , and ϕ . However, the perturbed planes are oriented to the secondary spatial reference plane by $\Delta\psi'$, $\Delta\theta'$, and $\Delta\phi'$, which generally are not the same as $\Delta\psi$, $\Delta\theta$, and $\Delta\phi$.

2.2 Coordinate Transformations

Coordinate transformations are used so frequently in dynamic studies of aircraft that some consideration should be given to this subject. Literature on transformations is extensive and ranges from the classical mathematical treatments (Reference 2, for example) to engineering applications (References 3 and 4, for example). At this time, the most pertinent transformations are considered to serve as guidelines for other transformations that may be desired.

2.2.1 Transformation from Earth Reference Axes to Airplane Axes

Consider X_r , Y_r , and Z_r as generalized vector quantities acting along the coordinates x_r , y_r , z_r , respectively. The transformed vector quantities X , Y , Z acting along x_b , y_b , and z_b axes, respectively, are obtained by performing three successive rotations, ψ , θ , and ϕ , to define the airplane's orientation with respect to the reference axes x_r , y_r , and z_r through a transformation matrix $[L]$ as follows

$$\begin{bmatrix} X \\ Y \\ Z \end{bmatrix} = [L] \begin{bmatrix} X_r \\ Y_r \\ Z_r \end{bmatrix} = [\phi]\ [\theta]\ [\psi] \begin{bmatrix} X_r \\ Y_r \\ Z_r \end{bmatrix} \tag{1a}$$

$$= \begin{bmatrix} 1 & 0 & 0 \\ 0 & \cos\phi & \sin\phi \\ 0 & -\sin\phi & \cos\phi \end{bmatrix} \begin{bmatrix} \cos\theta & 0 & -\sin\theta \\ 0 & 1 & 0 \\ \sin\theta & 0 & \cos\theta \end{bmatrix} \begin{bmatrix} \cos\psi & \sin\psi & 0 \\ -\sin\psi & \cos\psi & 0 \\ 0 & 0 & 1 \end{bmatrix} \begin{bmatrix} X_r \\ Y_r \\ Z_r \end{bmatrix} \tag{1b}$$

$$= \begin{bmatrix} \cos\theta\cos\psi & \cos\theta\sin\psi & -\sin\theta \\ \sin\phi\sin\theta\cos\psi - \sin\psi\cos\phi & \sin\psi\sin\theta\sin\phi + \cos\psi\cos\phi & \sin\phi\cos\theta \\ \cos\psi\cos\phi\sin\theta + \sin\psi\sin\phi & \sin\psi\cos\phi\sin\theta - \cos\psi\sin\phi & \cos\phi\cos\theta \end{bmatrix} \begin{bmatrix} X_r \\ Y_r \\ Z_r \end{bmatrix} \tag{1c}$$

2.2.2 *Transformation from Airplane Axes to Earth Axes*

Since projection from airplane axes to earth axes is an inverse process of the preceding transformation, premultiplication of Equation (1a) by the inverse transformation matrix $[L]^{-1}$ results in

$$\begin{bmatrix} X_r \\ Y_r \\ Z_r \end{bmatrix} = [L]^{-1} \begin{bmatrix} X \\ Y \\ Z \end{bmatrix} . \tag{2a}$$

However, since the orthogonal projections on the airplane axes are being transformed to orthogonal projections on the earth axes, the inverse of the transformation matrix $[L]$ in Equation (1c) is the same as its transpose; thus

$$\begin{bmatrix} X_r \\ Y_r \\ Z_r \end{bmatrix} = \begin{bmatrix} \cos\theta\cos\psi & \sin\phi\sin\theta\cos\psi - \sin\psi\cos\phi & \cos\psi\cos\phi\sin\theta + \sin\psi\sin\phi \\ \cos\theta\sin\psi & \sin\psi\sin\theta\sin\phi + \cos\psi\cos\phi & \sin\psi\cos\phi\sin\theta - \cos\psi\sin\phi \\ -\sin\theta & \sin\phi\cos\theta & \cos\phi\cos\theta \end{bmatrix} \begin{bmatrix} X \\ Y \\ Z \end{bmatrix} . \tag{2b}$$

2.2.3 *Relationship Between Airplane Rates* p , q , *and* r *and Euler Rates* $\dot{\psi}$, $\dot{\theta}$, *and* $\dot{\phi}$

It should be recognized from Figure 5 that, although the airplane rate-vector quantities, p , q , and r are orthogonal, the Euler rate-vector quantities are not. Thus, to obtain the relationships of p , q , and r as functions of $\dot{\psi}$, $\dot{\theta}$, and $\dot{\phi}$, it is necessary to transform $\dot{\psi}$, $\dot{\theta}$, and $\dot{\phi}$ to components along x_r , y_r , and z_r axes and then apply Equation (1c). The first transformation is accomplished rapidly by applying Equation (2b) and considering each Euler quantity as a special case of transformation of a body axis quantity. To wit: in Equation (2b) both ϕ and θ are considered zero for $\dot{\psi}$ and $\dot{\theta}$, and ϕ is considered zero for ϕ . Hence, the resulting transformation to the reference axes will be

$$\begin{bmatrix} X_r \\ Y_r \\ Z_r \end{bmatrix} = \begin{bmatrix} \cos\theta\cos\psi & -\sin\psi & 0 \\ \cos\theta\sin\psi & \cos\psi & 0 \\ -\sin\theta & 0 & 1 \end{bmatrix} \begin{bmatrix} \dot{\phi} \\ \dot{\theta} \\ \dot{\psi} \end{bmatrix} . \tag{3a}$$

Substituting Equation (3a) into Equation (1c) results in the following:

$$\begin{bmatrix} X \\ Y \\ Z \end{bmatrix} = \begin{bmatrix} p \\ q \\ r \end{bmatrix} = \begin{bmatrix} 1 & 0 & -\sin\theta \\ 0 & \cos\phi & \sin\phi\cos\theta \\ 0 & -\sin\phi & \cos\theta\cos\phi \end{bmatrix} \begin{bmatrix} \dot{\phi} \\ \dot{\theta} \\ \dot{\psi} \end{bmatrix} . \tag{3b}$$

To obtain the inverse of Equation (3b), it is necessary to solve for the inverse of the transformation matrix since $\dot{\phi}$, $\dot{\theta}$, and $\dot{\psi}$ are not orthogonal and hence do not

permit the use of the transpose for the inverse. This is accomplished by solving for the inverse matrix $[L]^{-1}$ in the relationship

$$[L]\ [L]^{-1} = \begin{bmatrix} 1 & 0 & 0 \\ 0 & 1 & 0 \\ 0 & 0 & 1 \end{bmatrix} . \tag{4}$$

After solving for $[L]^{-1}$, the inverse of Equation (3b) is determined to be

$$\begin{bmatrix} \dot{\phi} \\ \dot{\theta} \\ \dot{\psi} \end{bmatrix} = \begin{bmatrix} 1 & \sin\phi\tan\theta & \cos\phi\tan\theta \\ 0 & \cos\phi & -\sin\phi \\ 0 & \sin\phi\sec\theta & \cos\phi\sec\theta \end{bmatrix} \begin{bmatrix} p \\ q \\ r \end{bmatrix} . \tag{5}$$

2.2.4 *Transformation of Euler Angles from the Body to the Stability Axis System*

If two different rotation series give the same starting and ending orientation, the matrices representing the rotation series are equal, element for element, in the two transformation matrices. Thus, the Euler angles, ψ_s, θ_s, and ϕ_s, of the stability axes can be derived from the Euler angles, ψ_b, θ_b, and ϕ_b, of the body axes by the following transformation matrix relationship

$$[L]_s = [\alpha]_s [L]_b \tag{6}$$

where $[L]_s$ is the transformation matrix of Equation (1c) using stability axis orientation angles ψ_s, θ_s, and ϕ_s in place of ψ, θ, and ϕ, and $[L]_b$ is the same transformation matrix using body axis orientation angles ψ_b, θ_b, and ϕ_b in place of ψ, θ, and ϕ, if the same successive rotation series is employed. The transformation $[\alpha]_s$ is the matrix representing the transformation from the body to the stability axis system, or

$$[\alpha]_s = \begin{bmatrix} \cos\alpha & 0 & \sin\alpha \\ 0 & 1 & 0 \\ -\sin\alpha & 0 & \cos\alpha \end{bmatrix} . \tag{7}$$

Upon performing the matrix multiplication shown by Equation (6), and checking corresponding elements in the equated results to obtain the most feasible elements for the desired result, the following relationships are arrived at

$$\left.\begin{aligned} \sin\theta_s &= \cos\alpha\sin\theta_b - \sin\alpha\cos\theta_b\cos\phi_b \\ \sin\phi_s &= \frac{\sin\phi_b\cos\theta_b}{\cos\theta_s} \\ \sin\psi_s &= \frac{\cos\alpha\cos\theta_b\sin\psi_b + \sin\alpha\,(\sin\psi_b\cos\phi_b\sin\theta_b - \cos\psi_b\sin\phi_b)}{\cos\theta_s} . \end{aligned}\right\} \tag{8}$$

2.2.5 *Transformation of Aerodynamic Coefficients to Various Axis Systems*

The following transformations are accomplished readily by employing Equation (2b) and replacing ψ, θ, and ϕ in the equation by $-\beta$, α, and 0, respectively. Thus, to transform from body to stability axes, set $\beta = 0$, thereby obtaining

$$\left.\begin{aligned} C_D &= C_c \cos\alpha + C_N \sin\alpha \\ (C_y)_s &= C_y \\ C_L &= -C_c \sin\alpha + C_N \cos\alpha \\ (C_l)_s &= C_l \cos\alpha + C_n \sin\alpha \\ (C_m)_s &= C_m \\ (C_n)_s &= -C_l \sin\alpha + C_n \cos\alpha \ . \end{aligned}\right\} \tag{9}$$

Similarly, to transform from body to wind axes

$$\left.\begin{aligned} (C_x)_w &= -C_c \cos\alpha\cos\beta + C_y \sin\beta - C_N \sin\alpha\cos\beta \\ (C_y)_w &= C_c \cos\alpha\sin\beta + C_y \cos\beta + C_N \sin\alpha\sin\beta \\ (C_z)_w &= -C_L = C_c \sin\alpha - C_N \cos\alpha \\ (C_l)_w &= C_l \cos\alpha\cos\beta + C_m \sin\beta + C_n \sin\alpha\cos\beta \\ (C_m)_w &= C_m \cos\beta - C_l \cos\alpha\sin\beta - C_n \sin\alpha\sin\beta \\ (C_n)_w &= C_n \cos\alpha - C_l \sin\alpha \ . \end{aligned}\right\} \tag{10}$$

Also, for stability to wind axes, set $\alpha = 0$, obtaining

$$\left.\begin{aligned} (C_x)_w &= -C_D \cos\beta + (C_y)_s \sin\beta \\ (C_y)_w &= C_D \sin\beta + (C_y)_s \cos\beta \\ (C_z)_w &= -C_L \\ (C_l)_w &= (C_l)_s \cos\beta + (C_m)_s \sin\beta \\ (C_m)_w &= (C_m)_s \cos\beta - (C_l)_s \sin\beta \\ (C_n)_w &= (C_n)_s \ . \end{aligned}\right\} \tag{11}$$

To transform from wind to stability or body axes, or stability to body axes, use is made of Equation (1c).

2.2.6 *Transformation of Derivatives*

The transformation of derivatives from one axis system to another goes beyond pure kinematic transformations. Longitudinal derivatives are relatively simple in their transformations; lateral-directional derivatives are more complex in transformations. The several examples will illustrate the procedure to obtain derivative transformation. Influence of factors such as power is not considered at this time.

Transformation of longitudinal derivatives is accomplished by direct differentiation of the coefficient equations. This is possible because α and q are not modified by the axis system used. For example, to obtain the derivative of C_L with respect to α in a transformation from body to stability axes, differentiate the equation for C_L in Equation (9) obtaining, on a per radian basis,

$$C_{L_\alpha} = -C_{c_\alpha} \sin\alpha + C_{N_\alpha} \cos\alpha - C_D \ . \tag{12}$$

The transformation of the lateral-directional derivatives is more complicated, inasmuch as the angular rate variables r and p are affected by the transformation. At this time, sideslip angle, β, is not considered to be affected by the transformations because of its definition; however, the type of β-sensor used in flight tests - whether it be a vane, floating cone, or ball nose - does have a bearing on the interpretation of the β readout and the meaning of the derivatives with respect to the sensed β. This is discussed in Section 5.

Consider the transformation of lateral-directional derivatives from the stability to the body axis system. Transformation of the yawing and rolling moment equations is accomplished by

$$\left.\begin{aligned} N &= (N)_s \cos\alpha + (L)_s \sin\alpha \\ L &= (L)_s \cos\alpha - (N)_s \sin\alpha \ , \end{aligned}\right\} \tag{13}$$

where L and N represent rolling and yawing moments, respectively.

However,

$$\left.\begin{aligned} (N)_s &= \left[(C_{n_\beta})_s\beta + (C_{n_r})_s \frac{r_s b}{2V} + (C_{n_{\dot\beta}})_s \frac{\dot\beta b}{2V} + (C_{n_p})_s \frac{p_s b}{2V} + (C_{n_\delta})_s\delta\right] \bar{g}Sb \\ (L)_s &= \left[(C_{l_\beta})_s\beta + (C_{l_r})_s \frac{r_s b}{2V} + (C_{n_{\dot\beta}})_s \frac{\dot\beta b}{2V} + (C_{l_p})_s \frac{p_s b}{2V} + (C_{l_\delta})_s\delta\right] \bar{g}Sb \ . \end{aligned}\right\} \tag{14}$$

It will be necessary to express Δr_s and Δp_s in Equation (14) as functions of Δr and Δp using the transform

$$\left.\begin{aligned} r_s &= r\cos\alpha - p\sin\alpha \\ p_s &= p\cos\alpha + r\sin\alpha \ . \end{aligned}\right\} \tag{15}$$

Upon substituting Equation (15) into (14) and Equation (14) into (13), and regrouping terms,

$$\frac{N}{\bar{g}Sb} = \left[(C_{n_\beta})_s \cos\alpha + (C_{l_\beta})_s \sin\alpha\right]\beta + \left[(C_{n_r})_s \cos^2\alpha + (C_{l_p})_s \sin^2\alpha + (C_{n_p} + C_{l_r})_s \sin\alpha\cos\alpha\right]\frac{rb}{2V} + \left[(C_{n_{\dot\beta}})_s \cos\alpha + (C_{l_{\dot\beta}})_s \sin\alpha\right]\frac{\dot\beta b}{2V} + \left[(C_{n_p})_s \cos^2\alpha - (C_{l_r})_s \sin^2\alpha - (C_{n_r} - C_{l_p})_s \sin\alpha\cos\alpha\right]\frac{pb}{2V} + \left[(C_{n_\delta})_s \cos\alpha + (C_{l_\delta})_s \sin\alpha\right]\delta \qquad (16a)$$

and

$$\frac{L}{\bar{g}Sb} = \left[(C_{l_\beta})_s \cos\alpha - (C_{n_\beta})_s \sin\alpha\right]\beta + \left[(C_{l_p})_s \cos^2\alpha + (C_{n_r})_s \sin^2\alpha - (C_{n_p} + C_{l_r})_s \sin\alpha\cos\alpha\right]\frac{pb}{2V} + \left[(C_{l_{\dot\beta}})_s \cos\alpha - (C_{n_{\dot\beta}})_s \sin\alpha\right]\frac{\dot\beta b}{2V} + \left[(C_{l_r})_s \cos^2\alpha - (C_{n_p})_s \sin^2\alpha - (C_{n_r} - C_{l_p})_s \sin\alpha\cos\alpha\right]\frac{rb}{2V} + \left[(C_{l_\delta})_s \cos\alpha - (C_{n_\delta})_s \sin\alpha\right]\delta \; . \qquad (16b)$$

Summaries of transformations of aerodynamic derivatives from stability to body axis system, and vice versa, are given in Tables I and II.

2.2.7 *Transformation of Moments of Inertia from One Axis System to Another*

Although this topic is covered in applied mechanics literature, an illustrative example is given as a refresher. Also included are tables of transformations for ready reference.

To obtain I_{x_s} in terms of body axes quantities, use is made of the fundamental relation

$$I_{x_s} = \int (y_s^2 + z_s^2)\, dm \; . \qquad (17)$$

Substituting the following transform into Equation (17),

$$\begin{aligned} x_s &= x\,\mathrm{ccs}\,\alpha + z\sin\alpha \\ z_s &= z\cos\alpha - x\sin\alpha \end{aligned} \tag{18}$$

and expanding,

$$\begin{aligned} I_{x_s} &= \left[\int (y_b^2 + z_b^2)\ dm\right]\cos^2\alpha + \left[\int (y_b^2 + x_b^2)\ dm\right]\sin^2\alpha - 2\left[\int x_b z_b dm\right]\sin\alpha\cos\alpha \\ &= I_x\cos^2\alpha + I_z\sin^2\alpha - 2I_{xz}\sin\alpha\cos\alpha \\ &= \tfrac{1}{2}(I_z + I_x) - \tfrac{1}{2}(I_z - I_x)\cos\alpha - I_{xz}\sin 2\alpha\ . \end{aligned}$$

3. EQUATIONS OF MOTION

The equations of motion of an airplane as found in texts on aircraft dynamics (such as Reference 5) and as normally presented in the technical literature, although prosaic in appearance, do contain complexities in the significance of the individual terms. The following discussion is intended to acquaint the reader with the scope of the complexities which may be encountered and which should be recognized and managed in dealing with the equations of motion. An understanding of this matter is important in applying the equations to derivative determination from flight data.

3.1 Inertial Quantities

In all considerations of the inertial portions of the equations of motion, the axis system used has a direct bearing on the expressions for inertial forces; the degree of asymmetry of the mass distribution of the aircraft and the magnitude and violence of the aircraft motions affect the format of the expressions for inertial moments. It is assumed, for the purposes of this paper, that the aircraft behaves as a rigid body. Where aeroelasticity is a factor, it is assumed that proper precautions will have been taken to provide assurance that the rigid-body concept will provide a good degree of approximation.

Inertial quantities arise from the inherent action of the aircraft whose various components act as a rigid-body assembly and from the rotating masses attached to the aircraft.

3.1.1 Inherent Aircraft General Inertial Force Expressions

Inasmuch as our interest lies in the analysis of flight test data oriented to the body axis system, the inertial force expressions applicable to this axis system and for all attitudes of flight are

$$X_i = m(\dot{u} + qw - rv) \tag{19a}$$

$$Y_i = m(\dot{v} + ru - pw) \tag{19b}$$

$$Z_i = m(\dot{w} - qu + pv)\ . \tag{19c}$$

If the stability axis system were employed as the reference instead of the body axis system, $qw = pw = \dot{w} = 0$, inasmuch as there is no linear velocity component along the z-stability axis.

3.1.2 *General Inertial-Moment Expressions*

For the general case where the principal axes are asymmetric to the various planes of the reference axes, the inertial-moment expressions are

$$L_i = I_x\dot{p} + I_{xy}(rp - \dot{q}) - I_{xz}(\dot{r} + pq) + I_{yz}(r^2 - q^2) + (I_z - I_y)qr \qquad (20a)$$

$$M_i = I_y\dot{q} + I_{yz}(rq - \dot{r}) - I_{xy}(\dot{r} + qr) + I_{xz}(p^2 - r^2) + (I_x - I_z)rp \qquad (20b)$$

$$N_i = I_z\dot{r} + I_{xz}(qr - \dot{p}) - I_{yz}(\dot{q} + rp) + I_{xy}(q^2 - p^2) + (I_y - I_x)pq \; . \qquad (20c)$$

Fortunately, situations involving general asymmetry of the aircraft are rare. Normally, the vehicle will have a mass distribution symmetrical relative to the xz-body plane of symmetry, with the result that the principal y-axis coincides with the y-body axis. Under such circumstances, $I_{xy} = I_{yz} = 0$ and the general inertial-moment expressions reduce to the following normally employed form:

$$L_i = I_x\dot{p} - I_{xz}(\dot{r} + pq) + (I_z - I_y)qr \qquad (21a)$$

$$M_i = I_y\dot{q} + I_{xz}(p^2 - r^2) + (I_x - I_z)rp \qquad (21b)$$

$$N_i = I_z\dot{r} - I_{xz}(\dot{p} - qr) + (I_y - I_x)\,pq \; . \qquad (21c)$$

The inertial expressions in Equations (21a, b, c) are nonlinear and thus not suitable for use in the derivation of closed-form stability equations. However, they are required in analog or digital computer study of the motion of the aircraft in general or violent maneuvers and in the analog matching of flight data from such maneuver in attempts to determine the effective values of the stability and control derivatives for the maneuver.

In violent maneuvers, the terms involving pq and rp are particularly important. These terms, as well as qr, are gyroscopic terms. Modern high-performance aircraft tend to have low values of I_x compared to I_y and I_z, with the result that gyroscopic action represented by $(I_x - I_z)rp$ and $(I_y - I_x)pq$, in particular, has been responsible for the uncontrollable, catastrophic roll-coupling behavior of at least one jet aircraft after a deliberate high roll rate input.

When the motions of the aircraft are small or gradual, the inertial-moment expressions may be simplified to

$$L_i = I_x\dot{p} - I_{xz}\dot{r} \qquad (22a)$$

$$M_i = I_y\dot{q} \qquad (22b)$$

$$N_i = I_z\dot{r} - I_{xz}\dot{p} \; . \qquad (22c)$$

3.1.3 Small-Perturbation Inertial Expressions

The classical approach to the study of aircraft dynamic stability and control involves the use of small disturbances (perturbations). Restricting the motions to small deviations from steady-state conditions allows the elimination of non-linear terms from the inertial expressions. Such motions are useful in defining the stability, control, and handling qualities of the aircraft, and the pilot effort or autopilot characteristics required to control the motion. It has been found that the use of small-perturbation theory gives good results and permits the development of analytical expressions.

To arrive at the small-perturbation inertial expressions, replace the individual acceleration and velocity terms in Equations (19a, b, c) and (22a, b, c) by accelerations and velocities made up of disturbances superimposed on equilibrium conditions so that $\dot{u}$, etc., is replaced by $\dot{u} + \Delta\dot{u}$, etc., respectively; expand the product terms; neglect the second-order quantities ($\Delta r \Delta u$, for example); and subtract the initial conditions from the final resulting conditions. The resulting small-perturbation inertial expressions are

$$\Delta X_i = m[\Delta\dot{u} + w\Delta q + q\Delta w - r\Delta v - v\Delta r] \tag{23a}$$

$$\Delta Y_i = m[\Delta\dot{v} + u\Delta r + r\Delta u - w\Delta p - p\Delta w] \tag{23b}$$

$$\Delta Z_i = m[\Delta\dot{w} - u\Delta q - q\Delta u + p\Delta v + v\Delta p] \tag{23c}$$

and

$$\Delta L_i = I_x\Delta\dot{p} - I_{xz}\Delta\dot{r} \tag{24a}$$

$$\Delta M_i = I_y\Delta\dot{q} \tag{24b}$$

$$\Delta N_i = I_z\Delta\dot{r} - I_{xz}\Delta\dot{p} \quad . \tag{24c}$$

Equations (23a, b, c) show that lateral-directional-mode perturbations Δv, Δr, and Δp appear in the longitudinal-mode equations ΔX_i and ΔZ_i, and that the longitudinal-mode perturbations Δu and Δw appear in the lateral-directional-mode equation ΔZ_i. This coupling of the two modes can normally be minimized to permit practical use of the uncoupled practical approximation of Equations (23a, b, c) shown in Equations (25a, b, c). This minimization is achieved in flight test maneuvers such as elevator pulses for perturbation of the longitudinal mode and rudder or aileron pulses for perturbation of the lateral-directional mode initiated during steady wings-level or steady turn flight.

$$\Delta X_i = m[\Delta\dot{u} + w\Delta q] \tag{25a}$$

$$\Delta Y_i = m[\Delta\dot{v} + u\Delta r - w\Delta p] \tag{25b}$$

$$\Delta Z_i = m[\Delta\dot{w} - u\Delta q - q\Delta u] \quad . \tag{25c}$$

3.2 Gyroscopic Couples of Rotating Masses

Spinning masses mounted on the aircraft – such as propellers and rotating elements of engines – possess angular momentum relative to the reference (body) axes and produce gyroscopic couples on the aircraft which could be significant, as was the case on the X-5 airplane[6]. Normally, the gyroscopic couples are negligible; however, the advent of vertical-rising aircraft with tilting engines and the increase in size of propulsion units on high-performance aircraft make it inadvisable to arbitrarily ignore this coupling.

For a rotating mass having a rotating axis in or parallel to the xz-plane of symmetry but at an angle θ_{rm} to the x-body axis (Fig.6), it can be shown from the moment of momentum relation, $\bar{\Omega} \times \bar{H}$ and $H = I_{rm}\Omega$, that the gyroscopic couple about each of the body axes is

$$L_{rm} = qH_z - rH_y = -I_{rm}\Omega q \sin\theta_{rm} \tag{26a}$$

$$M_{rm} = rH_x - pH_z = I_{rm}\Omega(r\cos\theta_{rm} + p\sin\theta_{rm}) \tag{26b}$$

$$N_{rm} = pH_y - qH_x = -I_{rm}\Omega q\cos\theta_{rm} \ . \tag{26c}$$

These rotating mass contributions are added to the inertial moments expressed by Equations (20a, b, c), (21a, b, c), and (22a, b, c).

For small perturbations of the aircraft, the perturbations of the gyroscopic couples resulting from the rotating mass are expressed by

$$\Delta L_{rm} = -I_{rm}\Omega\Delta q\sin\theta_{rm} \tag{27a}$$

$$\Delta M_{rm} = I_{rm}\Omega(\Delta r\cos\theta_{rm} + \Delta p\sin\theta_{rm}) \tag{27b}$$

$$\Delta N_{rm} = -I_{rm}\Omega\Delta q\cos\theta_{rm} \ . \tag{27c}$$

These perturbations are added to Equations (24a, b, c) when significant, in which case, Equations (24a, b, c) will become inter-dependent because of the coupling of the longitudinal-mode and lateral-directional-mode moment equations. It should be noted that, if θ_{rm} were variable, the above relations in Equations (27a, b, c) would have required further expansion and introduced an additional degree of freedom in the form of $\Delta\theta_{rm}$.

3.3 Gravitational Force

The gravity force will not contribute to the moment equations as long as the origin of the axis system is at the centre of gravity.

3.3.1 Components of Gravity Force

With the gravity force W acting along the z_r axis, the expressions for the components of gravity force acting along the body axes are readily deduced from Figure 4(a) to be

$$X_g = -W \sin\theta \tag{28a}$$

$$Y_g = W \cos\theta \sin\phi \tag{28b}$$

$$Z_g = W \cos\theta \cos\phi \ . \tag{28c}$$

These components are subtracted from the inertial-force equations (19a, b, c).

3.3.2 Small Perturbations

Small perturbations of the components of the gravity force may be based on Euler angle perturbations superimposed on the unperturbed angles using the same basic reference frame, or on Euler angle perturbations relative to a secondary spatial reference frame made up of the unperturbed aircraft axis system as discussed in Section 2.1.6. and as shown in Figure 4(b). In this second approach, unperturbed body axes are used as the secondary spatial reference when interest is primarily in perturbations of body-oriented flight test data.

Using the first approach, replace θ and ϕ in Equations (28a, b, c) by $\theta + \Delta\theta$ and $\phi + \Delta\phi$, respectively; expand the resulting trigonometric functions, consider $\cos\Delta\_ \simeq 1$, $\sin\Delta\_ \simeq \Delta\_$, and $\Delta\_\Delta\_ \simeq 0$; and subtract the initial conditions from the result. The resulting small-perturbation expressions are

$$\Delta X_g = -W\Delta\theta \cos\theta \tag{29a}$$

$$\Delta Y_g = W(\Delta\theta \cos\theta \cos\phi - \Delta\theta \sin\theta \sin\phi) \tag{29b}$$

$$\Delta Z_g = -W(\Delta\phi \cos\theta \sin\phi + \Delta\theta \sin\theta \cos\phi) \ . \tag{29c}$$

In the second approach, using the unperturbed body axes as the reference and $\Delta\psi'$, $\Delta\theta'$, and $\Delta\phi'$ (Fig.4(b)) as the Euler angles of the perturbations, the perturbations of the components of gravity are obtained by using Equations (1c) and (28a, b, c). In Equation (1c) the generalized quantities X_r, Y_r, and Z_r are replaced by the expressions for X_g, Y_g, and Z_g, respectively, as given in Equations (28a, b, c); and the Euler angles ψ, θ, and ϕ are replaced by $\Delta\psi'$, $\Delta\theta'$, and $\Delta\phi'$, respectively. The generalized quantities X_b, Y_b, and Z_b in Equation (1c) are now equal to $(X_g + \Delta X_g)$, $(Y_g + \Delta Y_g)$, and $(Z_g + \Delta Z_g)$, respectively. By subtracting the initial conditions (Equations (28a, b, c)) from the resulting perturbed equation after considering $\cos\Delta\_ \simeq 1$, $\sin\Delta\_ \simeq \Delta\_$, and $\Delta\_\Delta\_ \simeq 0$, the perturbation expressions for this second approach will have the following form:

$$\Delta X_g = W(\cos\theta \sin\phi \, \Delta\psi' - \cos\theta \cos\phi \, \Delta\theta') \tag{30a}$$

$$\Delta Y_g = W(\sin\Delta\psi' + \cos\theta \cos\phi \, \Delta\phi') \tag{30b}$$

$$\Delta Z_g = -W(\sin\theta \, \Delta\theta' + \cos\theta \sin\phi \, \Delta\phi') \ . \tag{30c}$$

The advantage in using Equations (30a, b, c) instead of Equations (29a, b, c) is that, for small perturbations during highly banked as well as wings-level flight,

$$\Delta\psi' \simeq \int \Delta r \, dt \tag{31a}$$

$$\Delta\theta' \simeq \int \Delta q \, dt \tag{31b}$$

$$\Delta\phi \simeq \int \Delta p \, dt \, . \tag{31c}$$

To apply such simple integrations to $\Delta\psi$, $\Delta\theta$, and $\Delta\phi$ in Equations (29a, b, c) requires that ϕ and θ be small.

Both Equations (29a, b, c) and (30a, b, c) show coupling of the longitudinal and lateral modes. In both sets of equations, the longitudinal modes (ΔX_g and ΔZ_g) are uncoupled from the lateral-mode perturbations by performing a longitudinal pulse when initial conditions are steady-state. In performing a lateral-directional pulse from steady-state conditions, the lateral-mode expression (30b) is inherently uncoupled from longitudinal perturbations, whereas expression (29b) shows interaction of the longitudinal perturbation $\Delta\theta$ which is excited by the lateral-directional pulse.

When banked and climbing flight are being considered, it may be surmised from the preceding that Equations (30a, b, c) are more amenable than Equations (29a, b, c) to theoretical stability analysis and for analysis of flight data when longitudinal or lateral pulses are applied from initial steady-state conditions.

3.4 Aerodynamic Derivatives

In stability and control investigations based on flight data, the previously discussed inertial, gyroscopic, and gravitational quantities are normally equated to aerodynamic parameters only. This is done primarily to facilitate the analysis of flight data. However, in doing this, the parameters are no longer pure aerodynamic parameters, inasmuch as they will have been modified by influences arising from power and aeroelasticity as well as possible other sources. Generally, these influences can be accounted for and the pure aerodynamic parameter arrived at.

Inasmuch as the equations are set up under the principle of super-position of influences, situations may be encountered in which the accuracy of the results obtained from the equations will deteriorate. This is of particular concern where very rapid control inputs are encountered. Also, inasmuch as the aerodynamic parameters are in the form of derivatives, care must be exercised not to exceed the validity of the derivative.

Finally, there are some limitations in combining several of the derivatives, $C_{n_r} - C_{n_{\dot\beta}}$, for example.

Consideration is given at this time to the above-mentioned factors which have significance in the utilization of aerodynamic derivatives in the equations of motion and in the determination of the derivatives from flight data. For convenience, the conventional derivatives are tabulated overleaf.

Longitudinal Derivatives

$$\bar{C}_{N_u} = V\frac{\partial C_N}{\partial u} + \frac{2C_N}{\cos\alpha\cos\beta} \qquad C_{N_\alpha} = \frac{\partial C_N}{\partial \alpha} \qquad C_{N_{\dot\alpha}} = \frac{\partial C_N}{\partial\left(\frac{\dot\alpha\bar{c}}{2V}\right)} \qquad C_{N_q} = \frac{\partial C_N}{\partial\left(\frac{q\bar{c}}{2V}\right)} \qquad C_{N_\delta} = \frac{\partial C_N}{\partial\delta}$$

$$\bar{C}_{c_u} = V\frac{\partial C_c}{\partial u} + \frac{2C_c}{\cos\alpha\cos\beta} \qquad C_{c_\alpha} = \frac{\partial C_c}{\partial \alpha} \qquad C_{c_{\dot\alpha}} = \frac{\partial C_c}{\partial\left(\frac{\dot\alpha\bar{c}}{2V}\right)} \qquad C_{c_q} = \frac{\partial C_c}{\partial\left(\frac{q\bar{c}}{2V}\right)} \qquad C_{c_\delta} = \frac{\partial C_c}{\partial\delta}$$

$$\bar{C}_{m_u} = V\frac{\partial C_m}{\partial u} + \frac{2C_m}{\cos\alpha\cos\beta} \qquad C_{m_\alpha} = \frac{\partial C_m}{\partial \alpha} \qquad C_{m_{\dot\alpha}} = \frac{\partial C_m}{\partial\left(\frac{\dot\alpha\bar{c}}{2V}\right)} \qquad C_{m_q} = \frac{\partial C_m}{\partial\left(\frac{q\bar{c}}{2V}\right)} \qquad C_{m_\delta} = \frac{\partial C_m}{\partial\delta}$$

Lateral-Directional Derivatives

$$C_{y_\beta} = \frac{\partial C_y}{\partial\beta} \qquad C_{y_{\dot\beta}} = \frac{\partial C_y}{\partial\left(\frac{\dot\beta b}{2V}\right)} \qquad C_{y_r} = \frac{\partial C_y}{\partial\left(\frac{rb}{2V}\right)} \qquad C_{y_p} = \frac{\partial C_y}{\partial\left(\frac{pb}{2V}\right)} \qquad C_{y_\delta} = \frac{\partial C_y}{\partial\delta}$$

$$C_{l_\beta} = \frac{\partial C_l}{\partial\beta} \qquad C_{l_{\dot\beta}} = \frac{\partial C_l}{\partial\left(\frac{\dot\beta b}{2V}\right)} \qquad C_{l_r} = \frac{\partial C_l}{\partial\left(\frac{rb}{2V}\right)} \qquad C_{l_p} = \frac{\partial C_l}{\partial\left(\frac{pb}{2V}\right)} \qquad C_{l_\delta} = \frac{\partial C_l}{\partial\delta}$$

$$C_{n_\beta} = \frac{\partial C_n}{\partial\beta} \qquad C_{n_{\dot\beta}} = \frac{\partial C_n}{\partial\left(\frac{\dot\beta b}{2V}\right)} \qquad C_{n_r} = \frac{\partial C_n}{\partial\left(\frac{rb}{2V}\right)} \qquad C_{n_p} = \frac{\partial C_n}{\partial\left(\frac{pb}{2V}\right)} \qquad C_{n_\delta} = \frac{\partial C_n}{\partial\delta}$$

3.4.1 Significance of the Derivatives

The aerodynamic derivative provides the slope of the curve of the aerodynamic force or moment coefficient, as the case may be, with respect to an independent variable - other independent variables being considered constant - at a particular value of the variable. In analog simulation studies, nonlinear curves are reduced to straight-line segments, each segment being valid only for an incremental range of the independent variable.

In the inverse problem of obtaining derivatives from flight data, the derivative is valid only for the incremental range of disturbance of the independent variable, at the steady-state condition, used in determining the derivative. An example involving a nonlinear variation of C_n with β is shown in Figure 7. In this example, the origin, 0, represents steady state and $(\Delta\beta)_1$ and $(\Delta\beta)_2$ represent two disturbance ranges of the variable. It will be noticed that the derivative obtained may differ appreciably in magnitude because of the nonlinearity of the curve in the disturbance ranges $(\Delta\beta)_1$ and $(\Delta\beta)_2$.

3.4.2 *Unsteady Flow Effects*

In dealing with the derivative concept in accounting for the influence of independent variables on an aerodynamic force or moment coefficient, for example

$$\Delta C_n = C_{n_\beta}\Delta\beta + C_{n_r}\frac{\Delta r b}{2V} + C_{n_{\dot\beta}}\frac{\Delta\dot\beta b}{2V} + C_{n_p}\frac{\Delta p b}{2V} + C_{n_{\delta_r}}\Delta\delta_r ,$$

it is assumed that each derivative contributes to the total as though it acted alone and that the aerodynamic force and moment coefficients are functions of the instantaneous values of the disturbance displacements and velocities, control angles, and their derivatives. Further, the derivatives are based on the variation of the coefficients under near-steady-state conditions of the variable. Although the derivative concept of treating aerodynamic force and moment perturbations has generally worked well, the application to situations of rapidly changing independent variables (unsteady flow conditions), as in the case of a very rapid control displacement or a sharp-edged gust, does not necessarily give correct answers. This is due to apparent mass effects of the air, whose inertia will not produce instantaneous changes in circulation and consequently causes aerodynamic lag. This is illustrated in Figure 8, which shows the variation of C_N as a function of nondimensional time, $\bar{c}/2V$, as a result of a step gust. The derivative concept would show a constant slope curve, whereas the actual variation of $C_N(t)$ would show a lag at the initial instance of the step gust input.

When an aircraft is oscillating sinusoidally, the lift will follow the sinusoidal variation in angle of attack but will be of smaller magnitude and there will be a phase difference between the lift and angle of attack. This unsteady flow effect is a function of reduced oscillating frequency, $\omega\bar{c}/2V$, as well as Mach number. Although the magnitude of C_{N_α} is not normally affected appreciably for normal airplane oscillating frequency conditions, the phase lag may bring about a large change in $C_{N_{\dot\alpha}}$. This may be of considerable importance in pitch damping of tailless aircraft (Ref.7).

In general, all the aerodynamic derivatives behave in a similar manner. Thus, it is seen that attempts to use the derivative concept in analog simulators involving very rapid changes of the independent variables can lead to errors; conversely, determination of derivatives from flight data requires awareness of the maneuvering or unsteady flow factors mentioned which can influence the magnitude of the derivative.

3.4.3 *Derivatives with Respect to* u

Aerodynamic derivatives with respect to u are of concern when phugoid modes are being investigated. Because this mode is often overlooked, these derivatives are generally unfamiliar. Thus, some consideration is given to them at this time for future reference as needed. Consider $-Z = C_N\bar{q}S$. Differentiation with respect to u shows

$$\left.\begin{aligned} -\frac{\partial Z}{\partial u} &= \frac{\partial C_N}{\partial u}\bar{q}S + C_N\rho VS\frac{\partial V}{\partial u} \\ &= \left(V\frac{\partial C_N}{\partial u} + \frac{2C_N}{\cos\alpha\cos\beta}\right)\frac{1}{V}\bar{q}S , \end{aligned}\right\} \qquad (32)$$

where $\partial V/\partial u = 1/(\cos\alpha\cos\beta)$ from $u = V\cos\beta\cos\alpha$. The ΔZ due to change in u is now expressed as

$$-Z_u = \bar{C}_{N_u}\frac{\bar{q}S}{V}. \tag{33}$$

Since

$$\left(V\frac{\partial C_N}{\partial u} + \frac{2C_N}{\cos\alpha\cos\beta}\right)$$

is more than simply the variation of the normal coefficient with respect to velocity, u, it can fittingly be called the effective aerodynamic derivative of C_N with respect to u, or $\bar{C}_{N_u}$. Similarly, the effective aerodynamic derivatives of C_m and C_c with respect to u are

$$\left(V\frac{\partial C_m}{\partial u} + \frac{2C_m}{\cos\alpha\cos\beta}\right) \quad \text{and} \quad \left(V\frac{\partial C_c}{\partial u} + \frac{2C_c}{\cos\alpha\cos\beta}\right),$$

or $\bar{C}_{m_u}$ and $\bar{C}_{c_u}$, respectively.

3.4.4 Derivatives with Respect to q and $\dot{\alpha}$, and r and $\dot{\beta}$

It is customary in reporting flight-determined derivatives, wherein transient oscillations are used in the analysis, to pair the derivatives varying with respect to q and $\dot{\alpha}$ and those varying with respect to r and $\dot{\beta}$. For example

$$\left.\begin{aligned} C_{m_q}\frac{\Delta q\bar{c}}{2V} + C_{m_{\dot{\alpha}}}\frac{\Delta\dot{\alpha}\bar{c}}{2V} &\simeq (C_{m_q} + C_{m_{\dot{\alpha}}})\frac{\Delta q\bar{c}}{2V} \\ \text{and} \\ C_{n_r}\frac{\Delta rb}{2V} + C_{n_{\dot{\beta}}}\frac{\Delta\dot{\beta}b}{2V} &\simeq (C_{n_r} - C_{n_{\dot{\beta}}})\frac{\Delta rb}{2V}. \end{aligned}\right\} \tag{34}$$

Inasmuch as the phenomenon involving $\dot{\alpha}$ is different from that involving q, and the phenomenon involving r is different from that of $\dot{\beta}$, the pairing is valid only when small-perturbation transient oscillations of a maneuver are involved and satisfy the linearized equations of motion. In addition, although the pairing works well for the longitudinal equations whether or not stability or body axes are employed, the validity of the paring for the lateral-directional equations is dependent on the use of the stability system of axes; if body axes are used, the pairing of r and $\dot{\beta}$ derivatives is permissible at low angles of attack.

In performing a small-perturbation longitudinal transient oscillation, the center of gravity of the aircraft tends to move along the flight path as though it were not disturbed; consequently, the amplitude ratio $|\Delta q|/|\Delta\dot{\alpha}|$ is similar to 1.0 and the vector quantities Δq and $\Delta\dot{\alpha}$ are approximately in phase. Thus Δq can be substituted for $\Delta\dot{\alpha}$. In the case of a lateral-directional (Dutch roll) transient oscillation relative to the stability axis system, the aircraft, in tending to

maintain its center of gravity along the flight path as though it were not disturbed, will experience $\Delta r \simeq -\Delta\dot{\beta}$, inasmuch as r and $\dot{\beta}$ are now referred to the same axis system. Thus, the amplitude ratio $|\Delta r|/|\Delta\dot{\beta}|$ is similar to 1.0, but the phase relation is approximately 180°; consequently, the sign of the $\Delta\dot{\beta}$ derivative is changed to minus in pairing r and $\dot{\beta}$ derivatives. In dealing with the body axis system, $|\Delta r|/|\Delta\dot{\beta}|$ and $\Phi_{r\dot{\beta}}$ can differ appreciably from 1.0 and 180°, respectively, at high angles of attack.

It is reiterated that pairing the derivatives is valid only for the special conditions mentioned. On the other hand, it has not been possible to solve for the $\dot{\alpha}$ derivatives independent of the q derivatives, and $\dot{\beta}$ derivatives independent of r derivatives, from flight data with any degree of consistency and confidence.

3.4.5 Power Effects

The propulsive system may have a significant influence on the stability as well as the trim of the airplane. Its force and moment contributions to the equations of motion may be presented as derivatives in the equations. If the power contributions are not accounted for by their own derivatives, they will be reflected in the magnitudes of the aerodynamic stability and control derivatives which will then become, in essence, effective derivatives. A comprehensive treatment of power effects is complex and beyond the scope of this paper. Only major effects are considered, to show how propulsion system derivatives contribute to the effective values of the aerodynamic derivatives.

It is essential at this time to emphasize an important point regarding consideration of the effect of power on stability. True inherent stability of the aircraft with power on can only be evaluated by keeping the settings of the engine and propeller controls fixed during the maneuver. Any maneuver that entails alteration of the propulsion system controls during the maneuver will not provide a true index of the stability from an analysis of the time history of the maneuver.

Influence of propellers: Influences of propellers consist of direct propeller effects and also indirect effects due to the propeller slipstream on the wing-fuselage and the tail surfaces.

Direct propeller effects: Direct propeller effects, as shown in Figure 8, consist of a direct thrust T acting along the thrust axis, and a transverse forve $(Y)_p$, as well as a normal force $(-Z)_p$, perpendicular to the thrust axis in the plane of the propeller disk. The thrust T is a primary function of α and V. Quantitative determination of the normal and transverse forces $(-Z)_p$ and $(Y)_p$ may be accomplished by solving for $(C_{N_\alpha})_p$ and $(C_{y_\beta})_p$, as discussed in References 8 and 9. Actually, the derivatives are of more concern for the purposes of this paper than the actual magnitudes of the forces.

The contributions of the direct propeller effect (Fig.9) on longitudinal and lateral stability are reflected in

$$(C_{m_\alpha})_p = C_{T_\alpha}\frac{Z_p}{\bar{c}} + (C_{N_\alpha})_p\frac{x_p}{\bar{c}} \qquad (35)$$

and

$$(C_{n_\beta})_p = -(C_{y_\beta})_p\frac{x_p}{\bar{c}} . \qquad (36)$$

It is opportune to note the influences of the direct propeller effects on C_{L_α} when performing a transformation from the body to the stability axis system. The net effective C_L and C_D of the aircraft, in the absence of angular rates and for fixed controls, can be expressed as

$$\begin{bmatrix} C_L \\ C_D \end{bmatrix} = \overbrace{\begin{bmatrix} \cos\alpha & -\sin\alpha \\ \sin\alpha & \cos\alpha \end{bmatrix}}^{\text{Aero}} \overbrace{\begin{bmatrix} \sin\alpha_p & \cos\alpha_p \\ -\cos\alpha_p & \sin\alpha_p \end{bmatrix}}^{\text{Power}} \begin{bmatrix} C_N \\ C_c \\ C_T \\ (C_n)_p \end{bmatrix} , \tag{37}$$

where the direct thrust is assumed to be vectored parallel to the body x-axis and $\alpha_p = \alpha + \epsilon_p$. Differentiating Equation (37) with respect to α for C_{L_α}

$$C_{L_\alpha} = (C_{N_\alpha}\cos\alpha - C_{c_\alpha}\sin\alpha) - C_D + C_{T_\alpha}\sin\alpha_p + (C_{N_\alpha})_p\cos\alpha \quad , \tag{38}$$

where C_D is the effective value as shown in Equation (37).

Study of Equation (38) shows that power increases the effective C_{L_α} of the aircraft. On low-performance aircraft, the power effect is generally negligible.

Propeller slipstream: The propeller slipstream influences the distribution of the aerodynamic forces on the aircraft structure as a result of (i) the increase in local velocity over the structure due to and in the propeller slipstream, and (ii) upwash and downwash effects of the rotating slipstream of the propeller. The slipstream can be stabilizing or destabilizing, depending upon the direction of rotation of the propeller and the position of the tail relative to the rotating slipstream. Analytical techniques to quantitatively account for the propeller slipstream effects on the stability of the aircraft have not been satisfactory. Generally, powered models are used to provide engineering data on new designs.

Influence of jet engines: The jet engine has the counterpart of the effects that were shown for the propeller. It provides a direct thrust, shows normal and transverse force effects at the entrance of the intake duct, and – depending on geometry – is capable of influencing the equilibrium and stability of the aircraft by inflow of air into the jet exhaust. Unlike the propeller, the influence of the jet engine on the tail surfaces, and hence the stability of the airplane, is amenable to analytical techniques to quantitatively account for these effects.

The thrust produced on the aircraft equipped with a jet engine is equal, as shown in Figure 10, to the vectorial change in momentum of the air and fuel passing through the engine plus the resultant of the pressure forces acting across the inlet and outlet areas. Where the intake and exhaust are in line with the thrust axis and the x-body axis

$$\begin{aligned} T &= C_r\bar{q}S \\ &= m_j V_j - m_\alpha V\cos\alpha_p + (\bar{p}_i A_i - \bar{p}_j A_j) \quad . \end{aligned} \tag{39}$$

A change in direction of the momentum vectors at intake or exhaust relative to the x-body axis brings into being forces normal to the body x-axis. Where the jet exhaust is parallel to the x-body axis, the component of the normal force in the xz-plane of symmetry is expressed by

$$\left.\begin{aligned}(-Z)_p &= (C_N)_p\,\bar{q}S \\ &= m_\alpha V \sin\alpha_p \\ &= \left(\frac{m_\alpha V \sin\alpha_p}{\bar{q}S}\right)\bar{q}S\ .\end{aligned}\right\} \tag{40}$$

Similarly, a normal force in the transverse plane is in evidence during a sideslip, or

$$\left.\begin{aligned}(Y)_p &= (C_y)_p\,\bar{q}S \\ &= -m_\alpha V \sin\beta \\ &= \left(-\frac{m_\alpha V \sin\beta}{\bar{q}S}\right)\bar{q}S\ .\end{aligned}\right\} \tag{41}$$

A jet-induced inflow toward the jet axis at the tail may affect the stability of the aircraft if design precautions have not been taken. As a result of the jet exhaust spreading out behind the engine, a turbulent mixing of the air outside of the jet stream with the jet exhaust takes place along the boundary of the jet stream (see Figure 11). The drawing in of the air from outside the stream is jet-induced inflow. A horizontal tail located in this jet-induced inflow field will be subjected to jet-induced downwash angles. Thus, the angle of attack of the tail would be modified and pitching moments would be created that would affect the stability as well as the equilibrium of the aircraft.

The quantitative effects of the jet-induced downwash at the tail can be calculated by using the theory developed by Ribner[10]. This theory allows for curvature of the jet due to angle of attack of the aircraft. It is also applicable to determination of jet-induced sidewash of the vertical-tail surfaces at asymmetric power conditions or during sideslip.

In the absence of suitable design precautions, such as boattailing of the exhaust to shield the tail surfaces from the inflow effect, the change in pitching and yawing moments resulting from the jet-induced downwash $(\Delta\alpha_{h.t.})_p$ and sidewash $(\Delta\alpha_{v.t.})_p$, respectively, can be expressed by

$$(\Delta M_{h.t.})_p = (C_{N\alpha})_{h.t.}(\Delta\alpha_{h.t.})_p\bar{q}_t S_t x_{h.t.} \tag{42}$$

$$(\Delta N_{v.t.})_p = -(C_{N\alpha})_{v.t.}(\Delta\alpha_{v.t.})_p\bar{q}_t S_t x_{v.t.} \tag{43}$$

where $x_{h.t.}$ and $x_{v.t.}$ are negative values with tails aft of the center of gravity.

The variations of forces and moments due to the jet engine are primarily functions of α, β, and V, assuming that control settings are constant. From the preceding it may be readily deduced that

$$\Sigma(C_{N_\alpha})_p = \frac{m_a V \cos\alpha_p}{\bar{q}S}\frac{\partial\alpha_p}{\partial\alpha} + (C_{N_\alpha})_{h.t.}\frac{\bar{q}_t S_{h.t.}}{\bar{q}S}\frac{\partial(\alpha_{h.t.})_p}{\partial\alpha} \tag{44a}$$

$$\Sigma(C_{m_\alpha})_p = C_r\frac{z_p}{\bar{c}} + \frac{m_a V\cos\alpha_p}{\bar{q}S}\frac{x_p}{\bar{c}}\frac{\partial\alpha_p}{\partial\alpha} + (C_{N_\alpha})_{h.t.}\frac{\bar{q}_t S_{h.t.}x_{h.t.}}{\bar{q}S\bar{c}}\frac{\partial(\alpha_{h.t.})_p}{\partial\alpha} \tag{44b}$$

$$\Sigma(C_{y_\beta})_p = -\frac{m_a V\cos\beta}{\bar{q}S} - (C_{N_\alpha})_{v.t.}\frac{\bar{q}_t S_{v.t.}}{\bar{q}Sb}\frac{\partial(\alpha_{v.t.})_p}{\partial\alpha} \tag{45a}$$

$$\Sigma(C_{n_\beta})_p = -\frac{m_a V\cos\beta}{\bar{q}S}\frac{x_p}{b} - (C_{N_\alpha})_{v.t.}\frac{\bar{q}_t S_{v.t.}x_{v.t.}}{\bar{q}Sb}\frac{\partial(\alpha_{v.t.})_p}{\partial\alpha} \tag{45b}$$

where x_p is positive when the air intake is forward of the center of gravity and $x_{v.t.}$ is negative with vertical tail aft of the center of gravity, and

$$(\bar{C}_{c_u})_p = -\left(V\frac{\partial C_T}{\partial u} + \frac{2C_T}{\cos\alpha\cos\beta}\right)_p \tag{46}$$

$$(\bar{C}_{m_u})_p = \left(V\frac{\partial C_m}{\partial u} + \frac{2C_m}{\cos\alpha\cos\beta}\right)_p \tag{47}$$

where

$$(C_m)_p = C_T\frac{z_p}{\bar{c}} + \frac{m_a V\sin\alpha_p}{\bar{q}S}\frac{x_p}{\bar{c}} + (C_{N_\alpha})_{v.t.}(\Delta\alpha_{v.t.})_p\frac{\bar{q}_t S_{h.t.}x_{h.t.}}{\bar{q}S\bar{c}} \tag{48}$$

and

$$\left(\frac{\partial C_m}{\partial u}\right)_p \simeq \frac{\partial C_T}{\partial u}\frac{z_p}{\bar{c}} + \frac{m_a\sin\alpha_p}{\bar{q}S}\frac{x_p}{\bar{c}} \quad . \tag{49}$$

3.4.6 Aeroelastic Effects

The preceding discussions assumed that the aircraft was rigid. This assumption was permissible in the past; however, modern aircraft flying at high speed under dynamic-pressure conditions are subject to degrees of flexibility of component parts which cannot, at times, be ignored and which affect the stability of the aircraft[11-16]. The contribution of aeroelastic deformation to derivatives is dependent primarily on aircraft geometry and dynamic pressure as well as structural rigidity and Mach number. Aeroelastic phenomena may be considered in two separate parts: static and dynamic aeroelastic effects.

When aerodynamic loading takes place at a sufficiently slow rate in comparison to the natural frequency of vibration of the pertinent part of the structure to permit the assumption of static deformation of the structure, the influence of aeroelasticity can be accounted for by modifying the derivatives. Illustrations of steady-state distortions which have been serious in the past are aileron reversal and wing divergence. Today, such factors as thinner wings and more flexible fuselages have magnified the effects of structural flexibility on stability and control of aircraft.

If the aerodynamic loading frequency were to approach the structural frequency of the pertinent component, the structural deformation would produce perturbations in the aerodynamic forces and moments which have to be accounted for by the introduction of additional appropriate derivatives in the equations of motion and the introduction of additional equations, which would be elasticity equations.

3.4.7 Other Effects

The preceding discussion has included major factors which influence analysis and account for discrepancies between wind-tunnel and flight data; however, it does not account for all factors. Other factors could include jet pluming, flow separations associated with movements of shock waves, and fuel sloshing. Since one never knows what phenomena will occur, it is imperative to have an open mind in trying to account for discrepancies in comparisons of data.

3.5 Summary of the Equations of Motion

The various dynamic relations which have been discussed are pertinent to an understanding of the equations of motion and the conditioning of data to the equations. The influence of power and structural flexibility on the various aerodynamic parameters (coefficient and stability derivatives) was stressed, and it was pointed out that the net result of these influences, or modifiers, was the emergence of an effective aerodynamic parameter.

It is easily recognized that the introduction into the equations of motion of each individual modifier to the aerodynamic parameters would result in a cumbersome set of equations. It is more practical to let the normally accepted stability symbol (C_{n_β}, for example) represent the effective value than to list all modifiers. In so doing, one should be aware of the various sources which contribute to the magnitude of the effective parameter in order to properly account for these contributions during an analog investigation, or other study, in which wind-tunnel and calculated data are used. On the other hand, in the inverse problem of determining coefficients and derivatives from flight data, a discrepancy in trends as well as magnitude between wind-tunnel and flight data will suggest possible influences from sources not accounted for by tunnel data.

3.5.1 General Equations

The following assumptions are made with regard to the equations of motion summarized in Table IV:

(i) The airplane behaves as a rigid body in that the moments of inertia, inclination of principal axes, etc., are not affected significantly.

(ii) The airplane is symmetrical about the xz-plane with regard to geometry and mass distribution.

(iii) The axes of rotating elements on the aircraft are fixed in a direction relative to the body reference axes.

(iv) The earth is flat. Aircraft speeds are assumed to be insufficient to include earth curvature in the equations.

(v) The forcing frequency of a disturbance is sufficiently far removed from the natural frequency of the pertinent part of the structural components to permit the disturbance to be considered as a static load and the effect of deformation to be accounted for by modification of the aerodynamic parameters.

(vi) Each aerodynamic parameter is an effective parameter, in that it includes all sources contributing to its net value.

Although listed in Table IV for completeness, experience has shown C_{y_p}, C_{y_r}, $C_{y_{\dot{\beta}}}$ and C_{c_q} and $C_{c_{\dot{\alpha}}}$ to be normally negligible.

3.5.2 *Small-Perturbation Equations*

The general equations of motion in Table IV are suitable for analog and digital programing which involves large disturbances and nonlinear terms, they are not suitable for analytical purposes. For such purposes, it is necessary to linearize the equations at least to an engineering degree of accuracy. This is accomplished by restricting their applications to small perturbations, as has been discussed previously. In addition, the perturbations are referred to a secondary spatial reference frame, discussed in Section 2.1.6, which is the unperturbed airplane axis system shown in Figure 4(b). Using the secondary reference system for small perturbations permits the use of Equations (31a, b, c), which simplifies analysis and extends the validity of the linearized perturbation equations to maneuvers involving high pitch attitude and large bank angles.

The uncoupled, linearized perturbation equations are shown in Table V in a format which generally constitutes the basis for application to derivative determination. The assumptions listed for the general equations of motion are also valid for the equations in this table. In addition, it is assumed that the maneuvers are such as to minimize the errors in the g terms arising from the approximation of the gravity terms shown in Equations (40a, b, c). Also, it is assumed that the gyroscopic couples of rotating elements are not significant, which may not always be the case. The equations are complete within the limits of the assumptions, and analysis would reveal all modes of longitudinal and lateral motions.

Omission of the longitudinal force equation and the $\hat{\Delta u}$ terms in the longitudinal equations (50a, b, c) would remove the phugoid mode from the analysis of the longitudinal motions, leaving only the short-period mode. This short-period format of the longitudinal equations is the one usually employed. Although the small-perturbation equations shown in Table V are frequently used in the format shown to develop relations for derivative determination, it is also desirable to list the equations in an operational format as Laplacian transforms with Laplace operator s.

Using Laplace transforms enables the dynamic properties of the airplane to be defined by a series of transfer functions relating the various responsive motions of the airplane to disturbing inputs. The transfer functions are extensively used in stability and control, handling qualities, and automatic flight control investigations to assess the effects of configuration changes, the effects of particular stability derivatives, and the effects of changes in automatic control systems. They are also helpful in obtaining stability derivatives from flight data.

With zero initial conditions and inputs due only to control deflections, the Laplace transforms of the small-perturbation equations of motion take on the operational forms shown in Table VI as Equations (62a, b, c) and (63a, b, c). The notations $\bar{X}_u$, $\bar{M}_\alpha$, etc., shown in the equations, are a convenient means of listing the parameters.

3.6 Determination of the Roots of the Determinant of the Lateral-Directional Small-Perturbation Equations

The following discussion regarding the determination of the roots of the determinant of the lateral-directional small-perturbation equations is based on Reference 17. Although the main points are brought out at this time, recourse should be made to the reference for more detailed considerations.

3.6.1 The Determinant

Using the Laplace transform format of the lateral-directional equations (Equations (63a, b, c) in Table VI), the determinant of these equations may be expressed in either of two formats, as follows:

(i) When expressed as

$$As^4 + Bs^3 + Cs^2 + Ds + E = 0 , \tag{65}$$

then

$$\left.\begin{aligned}
A &= I'_X I'_Z - 1 \\
B &= (\bar{L}_p + I'_X \bar{N}_p) + (\bar{N}_r + I'_Z \bar{L}_r) - (I - I'_X I'_Z)\bar{Y}_\beta \\
C &= (\bar{N}_p \bar{L}_r - \bar{N}_r \bar{L}_p) - (\bar{L}_p + I'_X \bar{N}_p)\bar{Y}_\beta - (\bar{N}_r + \bar{I}'_Z \bar{L}_r)\bar{Y}_\beta - \\
&\qquad - [(1 - I'_X \sin\alpha)\bar{N}_\beta - (\sin\alpha - I'_Z)\bar{L}_\beta] \\
D &= (\bar{N}_\beta \bar{L}_p - \bar{N}_p \bar{L}_\beta) + (\bar{N}_r \bar{L}_{\mu} - \bar{N}_p \bar{L}_{\cdot})\bar{Y}_\beta + g_1(\bar{N}_\beta + I'_Z \bar{L}_\beta) - \\
&\qquad - g_2(\bar{L}_{\mu} + I'_X \bar{N}_\beta) + (\bar{N}_\beta \bar{L}_r - \bar{N}_r \bar{L}_\beta)\sin\alpha \\
E &= g_1(\bar{L}_\beta \bar{N}_p - \bar{L}_p N_\beta) - g_2(\bar{N}_\beta \bar{L}_r - \bar{N}_r \bar{L}_\beta) \quad .
\end{aligned}\right\} \tag{66}$$

(ii) When expressed as

$$s^4 + bs^3 + cs^2 + ds + e = 0 , \tag{67}$$

then

$$\left.\begin{aligned} b &= -\bar{L}'_p - \bar{N}'_r - \bar{Y}_\beta \\ c &= -(\bar{N}'_p\bar{L}'_r - \bar{N}'_r\bar{L}'_p) + \bar{L}'_p\bar{Y}_\beta + \bar{N}'_r\bar{Y}_\beta + \bar{N}'_\beta - \bar{L}'_\beta \sin\alpha \\ d &= -(\bar{N}'_\beta\bar{L}'_p - \bar{N}'_p\bar{L}'_\beta) - (\bar{N}'_r\bar{L}'_p - \bar{N}'_p\bar{L}'_r)\bar{Y}_\beta - g_1\bar{N}'_\beta + \\ &\qquad g_2\bar{L}'_\beta - (\bar{N}'_\beta\bar{L}'_r - \bar{N}'_r\bar{L}'_\beta)\sin\alpha \\ e &= -g_1(\bar{L}'_\beta\bar{N}'_p - \bar{L}'_p\bar{N}'_\beta) + g_2(\bar{N}'_\beta\bar{L}'_r - \bar{N}'_r\bar{L}'_\beta) , \end{aligned}\right\} \tag{68}$$

where the primed values are equal to

$$\bar{N}'_i = \frac{\bar{N}_i + I'_z\bar{L}_i}{1 - I'_xI'_z} \quad \text{and} \quad \bar{L}'_i = \frac{\bar{L}_i + I'_x\bar{N}_i}{1 - I'_xI'_z} . \tag{69}$$

The determination of the roots of the determinant is dependent upon the modes of motion of the aircraft. The modes may be:

(a) Lateral phugoid (coupling of spiral and roll modes) and Dutch roll.

(b) Spiral divergence, roll subsidence, and oscillatory (Dutch roll).

3.6.2 Determination of the Roots when Lateral Phugoid and Dutch Roll Modes Exist

The determinant (Eqn.(67)) can be approximated by the following biquadratic

$$\left[s^2 + \left(b - \frac{d}{c}\right)s + \left(c - \frac{e}{c} - \frac{bd}{c}\right)\right]\left[s^2 + \frac{d}{c}s + \frac{e}{c}\right] = 0 , \tag{70}$$

in which the first and second quadratics represent the Dutch roll and lateral phugoid modes, respectively.

Two sets of conditions must be satisfied if Equation (70) is to be applicable[17]:

(a) The approximate nature of Equation (70) requires that $e/c^2 \ll 1$ and $bd/c^2 \ll 1$ to assure validity of the equation.

(b) It is necessary that $d^2 - 4ed < 1$ in order that the lateral phugoid exist.

Reference 17 points out, on the basis of limited experience, that, for values of e/c^2 of approximately 0.05 or less, bd/c^2 can be as large as 0.25 and $d^2/4ec$ as low as 0.005 without compromising the engineering accuracy of Equation (70). Thus, the

equation applies if

$$\frac{e}{c^2} \ll 1 , \qquad \frac{bd}{c^2} < 0.25 , \qquad 0.005 < \frac{d^2}{4ec} < 1 . \tag{71}$$

The second quadratic in Equation (70) expresses the lateral phugoid very simply; thus,

from $$s^2 + \frac{d}{c} s + \frac{e}{c}$$

and $$\left.\begin{aligned} \omega_{n_{ph}} &\simeq \frac{e}{c} \\ 2\zeta_{ph}\omega_{n_{ph}} &\simeq \frac{d}{c} . \end{aligned}\right\} \tag{72}$$

The first quadratic in Equation (70) is unwieldy. It is simpler to determine the characteristics of the Dutch roll mode by the following factored form of determinant

$$(s^2 + 2\zeta\omega_n s + \omega_n^2)(s^2 + 2\zeta_{ph}\omega_{n_{ph}} s + \omega_{n_{ph}}^2) = 0 . \tag{73}$$

Expansion of this determinant and comparison with Equation (67) shows that

$$\left.\begin{aligned} b &= 2\zeta\omega_n + 2\zeta_{ph}\omega_{n_{ph}} \\ c &= \omega_n^2 + \omega_{n_{ph}}^2 + (2\zeta\omega_n)(2\zeta_{ph}\omega_{n_{ph}}) \\ d &= (2\zeta_{ph}\omega_{n_{ph}})\omega_n^2 + (2\zeta\omega_n)\omega_{n_{ph}}^2 \\ e &= \omega_{n_{ph}}^2\omega_n^2 , \end{aligned}\right\} \tag{74}$$

Since $\omega_{n_{ph}}^2$ and $(2\zeta_{ph}\omega_{n_{ph}})$ are obtained from Equation (72), ω_n^2 and $(2\zeta\omega_n)$ can now be determined from Equations (74) or

$$\left.\begin{aligned} 2\zeta\omega_n &= b - 2\zeta_{ph}\omega_{n_{ph}} \\ \omega_n^2 &= c - \omega_{n_{ph}} - (2\zeta\omega_n)(2\zeta_{ph}\omega_{n_{ph}}) . \end{aligned}\right\} \tag{75}$$

3.6.3 Determination of the Roots when Spiral Divergence, Roll Subsidence, and Dutch Roll Modes Exist

When the spiral divergence, roll subsidence, and Dutch roll modes constitute the lateral-directional characteristics of the airplane, which is normally the case, the determinant as represented by Equation (67) may be factored in the following terms characterizing these modes:

$$\left(s + \frac{1}{T_S}\right)\left(s + \frac{1}{T_R}\right)\left(s^2 + 2\zeta\omega_n^2 + \omega_n^2\right) = 0 . \tag{76}$$

The coefficients b , c , d and e (Equation (68)) in terms of the factors of Equation (76) are

$$\left.\begin{aligned} b &= 2\zeta\omega_n + \frac{1}{T_R} + \frac{1}{T_S} \\ c &= \omega_n^2 + 2\zeta\omega_n \left(\frac{1}{T_R} + \frac{1}{T_S}\right) + \frac{1}{T_R T_S} \\ d &= \omega_n^2 \left(\frac{1}{T_R} + \frac{1}{T_S}\right) + 2\zeta\omega_n \frac{1}{T_R T_S} \\ e &= \omega_n^2 \frac{1}{T_R T_S} \ . \end{aligned}\right\} \tag{77}$$

When the spiral-mode root, $1/T_S$, is much less than the roll subsidence root, $1/T_R$, as it usually is, the coefficients b , c , d , and e may be approximated to a good degree of accuracy by

$$\left.\begin{aligned} b &\simeq 2\zeta\omega_n + \frac{1}{T_R} \\ c &\simeq \omega_n^2 + 2\zeta\omega_n \frac{1}{T_R} \\ d &\simeq \omega_n^2 \frac{1}{T_R} \ . \end{aligned}\right\} \tag{78}$$

Eliminating $1/T_R$ in Equation (78)

$$\left.\begin{aligned} c &\simeq (2\zeta\omega_n) \frac{d}{\omega_n^2} + \omega_n^2 \\ d &\simeq (2\zeta\omega_n) + \frac{d}{\omega_n^2} \ . \end{aligned}\right\} \tag{79}$$

Eliminating $2\zeta\omega_n$ in Equations (79) provides an accurate solution of ω_n^2 within the limitation that

$$\frac{1}{T_S} \ll \frac{1}{T_R}$$

or

$$(\omega_n^2)^3 - c(\omega_n^2)^2 + bd(\omega_n^2) - d^2 = 0 \ . \tag{80}$$

Eliminating ω_n^2 in Equations (79) to solve for $2\zeta\omega_n^2$ within the limitation that $1/T_S << 1/T_R$ results in

$$(2\zeta\omega_n)^3 - 2b(2\zeta\omega_n)^2 + (c + b^2)(2\zeta\omega_n) + (d - cb) = 0 . \tag{81}$$

The roll-subsidence root, $1/T_R$, may now be obtained from coefficient b or d in Equation (78) or

$$\left.\begin{aligned} \frac{1}{T_R} &= \frac{d}{\omega_n^2} \\ \frac{1}{T_R} &= b - 2\zeta\omega_n \end{aligned}\right\} \tag{82}$$

The spiral-divergence root, $1/T_S$, may now be approximated from any one of the coefficient expressions in Equations (77), such as

$$\frac{1}{T_S} \simeq \frac{e}{\omega_n^2(1/T_R)} . \tag{83}$$

4. MASS CHARACTERISTICS

The airplane mass characteristics – weight, location of the center of gravity, moments of inertia, and inclination of principal axis – significantly affect airplane motions. Errors in the knowledge of these quantities are reflected directly in the flight-determined derivatives and may govern the validity of the derivatives in comparisons with wind-tunnel data. Although possible inaccuracies in the knowledge of the inertia characteristics must be given serious consideration in comparisons of flight-determined derivatives with wind-tunnel data, these derivatives have been used effectively in flight-guidance simulator studies.

The weight and horizontal location of the center of gravity are always determined experimentally. Inasmuch as the vertical location of the center of gravity, moments of inertia, and location of the principal axis are difficult to determine experimentally, manufacturer's estimates are usually relied upon. These estimates are considered to be of sufficient accuracy for most work involving flight tests. If more precise data are required, they should be determined by using experimental techniques.

It would be highly desirable to determine all of the mass characteristics experimentally. This is not always feasible because of the lack of proper facilities. Large, flexible aircraft, such as the Boeing B-52, offer practical problems, in that experimentally determined rolling moments of inertia with wings drooped would not be representative of flight conditions. The following discussion of the experimental determination of mass characteristics of aircraft is intended to serve as a guideline in setting up suitable facilities for use with most categories of aircraft.

4.1 Weight and Center-of-Gravity Location

The weight and longitudinal position of the center of gravity relative to the horizontal reference line of the airplane for the empty and gross weight conditions can be obtained easily by leveling the airplane on suitable scales or electronic weighing cells. With weighing cells, two of the cells (R_1 and R_2) are usually located at the wing jackpoints and the third cell (R_3) is located at some convenient distance, l, forward or aft of the wing jackpoints. The horizontal position of the center of gravity relative to the jackpoints is then determined from

$$\Delta l = \frac{R_3 l}{\Sigma R} . \tag{84}$$

For aircraft operating on conventional fuels, the variation of the center of gravity with fuel consumption can usually be defined adequately by weighing the airplane at several fuel levels, providing there is a predetermined sequence or mode of operation in obtaining the fuel from the various fuel cells. When the aircraft is equipped with fuel cells from which the fuel can be drawn selectively, the center of gravity position becomes a function of the sequence in drawing off the fuel from the various cells as well as the weight of the fuel. In some instances, it has been found necessary to account for fuel-tank shape and airplane attitude. Where hazardous fuels are used, the center of gravity is determined experimentally for the no-fuel condition only; the effect of fuel on the center of gravity position is calculated. The horizontal location of the center of gravity is experimentally obtained at least to within 0.01 mean aerodynamic chord, which is considered adequate for derivative determination.

During flight tests, the center of gravity is obtained by observing the total amount of fuel consumed and subtracting it from the takeoff weight. Reference to a chart showing the variation of weight with center of gravity provides the desired answer.

An accurate knowledge of the vertical location of the center of gravity is pertinent to the experimental derivative studies, insofar as experimental determination of moments of inertia and comparison with wind-tunnel data are concerned. The vertical center of gravity can be obtained by static or oscillatory techniques. For the static test techniques, the airplane is placed in various pitch or roll attitudes. For the roll approach (Fig. 12), the airplane is mounted in a horizontal, wings-level attitude on knife edges alined with respect to each other in the plane of symmetry of the aircraft. By rolling the airplane to various attitude angles and measuring the reaction R_1, moment arm y_1, and the roll angle ϕ, using a clinometer, the vertical position of the center of gravity is obtained from the equation

$$z_\alpha = \frac{R_1 Y_1 - W Z_c \sin\phi}{W \sin\phi} . \tag{85}$$

For rigid aircraft of the order of 15,000 lb, and under carefully controlled conditions, the vertical position is considered to be determinable to within 1 inch.

To determine the vertical position of the center of gravity from free-oscillation tests, any one of several techniques may be used. The simplest technique consists of changing the equivalent torsional spring constant for pitching or rolling moment of inertia tests. For rolling-oscillation tests with the setup shown in Figure 13 and

with small damping effects – a necessary condition for successful tests – the equations of motion for the two spring conditions are

$$(I_x + I_{x_c} + mz^2 + m_c z_c^2)\ddot{\phi}_1 + (K_{t_1} - Wz - W_c z_c)\phi_1 = 0 \qquad (86a)$$

$$(I_x + I_{x_c} + mz^2 + m_c z_c)\ddot{\phi}_2 + (K_{t_2} - Wx - W_c z_c)\phi_2 = 0 \; . \qquad (86b)$$

Considering $\phi_1 = A \cos \omega_1 t$ and $\phi_2 = B \cos \omega_2 t$, it is found upon solving Equations (86a, b) for z, the vertical distance from the knife edge to the center of gravity, that

$$z = \frac{K_{t_2} - K_{t_1}(p_1/p_2)^2}{W[1 - (p_1/p_2)^2]} - \frac{W_c z_c}{W} \; . \qquad (87)$$

The equivalent torsional spring constant, K_t, may be changed from K_{t_1} to K_{t_2} by changing the linear springs or the distance a which is perpendicular to the spring (see Figure 13). The change in linear springs is probably the more desirable approach.

Inasmuch as the rolling-oscillation test setup discussed constitutes an inverted pendulum, it is imperative that the equivalent torsional spring constant, K_t, be greater than $Wz + W_c z_c$ for stability of setup. Also, the accuracy of the results depends upon avoiding secondary spring actions of tiebacks and structural flexibility, which could inadvertently result in a lower effective spring constant than expected because of an equivalent series action of the secondary unwanted spring action with the intended spring.

4.2 Moments of Inertia

The moments of inertia of an airplane are usually calculated during the design phase and are based on estimated weights and centroid locations for various parts of the aircraft. These calculated moments of inertia are considered to be adequate for most analyses when the results are to be used in simulator studies. However, should experimental determination of the inertia be required, methods are available (see References 18 to 21). The methods are generally restricted to rigid aircraft and to aircraft whose weight, as well as the safety precautions of the experiment, will permit pivoting the aircraft on knife edges and suspending it from overhead cables.

Schematic representation of typical methods for determining the rolling and pitching moments of inertia are illustrated in Figures 13 and 14, respectively. Equation (86) is applicable to the determination of rolling moments of inertia in accord with Figure 13, with consideration given to the proper interpretation of the lengths z and z_c to the mountings shown. In Figure 14, cradle weight is zero. The yawing moment of inertia may be safely determined from a cable-suspension method used to determine the inclination of the principal axis (Figures 15 and 16), which is discussed subsequently.

Unless precautions are taken in every detail of an experimental setup, difficulties may be encountered because of flexibility of experimental components, which will alter the effective spring constant, K_t, or modify the free-oscillation pivotal point relative to the center of gravity of the aircraft. In one instance of determining the pitching moment of inertia when the aircraft was supported at the wing jackpoints and

oscillated with the spring at the nose, the wing section which had been considered rigid was observed to flex as the aircraft oscillated. This flexing caused the axis of rotation to shift forward and downward from the line through the jackpoints.

A common fault is the use of flexible cables as tiebacks for the springs and connection from the spring to the aircraft. Under no condition should flexible connections be used, inasmuch as they constitute springs in series with the actual intended springs employed; thus, the system from tieback to aircraft represents a much softer spring than intended. It should also be noted that, on some aircraft, attaching the spring to the aft portion of the fuselage would be an error, since the aft portion of the fuselage would constitute a relatively flexible structure and alter the effective spring constant.

Serious errors can also result when knowledge of the center-of-gravity location is inaccurate and when the line of action of the spring from the attach point to the aircraft is not perpendicular to the plane formed by the axis of rotation and the point of spring attachment on the aircraft (Fig. 13).

Generally, the inertia characteristics are determined for no-fuel conditions because fuel sloshing tends to bring in a beat action in the oscillatory motions. When determination is attempted with fuel onboard, the difference in oscillatory modes between the sloshing fuel and the aircraft should be as large as is practical, with due regard to safety of the setup, to minimize the beat action and permit determination of the natural frequency of oscillation of the aircraft.

Measuring the inertias of very large aircraft is difficult and is compounded with flexible aircraft. Such measurements are not in the realm of the methods discussed. A unique facility designed to enhance the feasibility for determining the moments of inertia of large aircraft about all three axes is located at the US Air Force Flight Test Center, Edwards, California, USA. Its capabilities cover a weight range from 30,000 to 300,000 lb and moments of inertia from 250,000 to 10×10^6 slug ft^2. The facility enables the determination of aircraft moments of inertia from measurements of changes in pendulum characteristics resulting from the addition of an aircraft to a freely oscillating platform. The basic elements of the facility consist of the platform, a control console for activating various systems which ready the platform for oscillation, and an instrumentation console for regulating the amplitude and measuring the period of the oscillations. The platform is an integral cruciform structure 110 ft long and 80 ft wide, with its loading surface flush with the surrounding floor space. The apparatus employs special hydrostatic bearings (identical to those used in the 200 in. Palomar telescope) to support the platform, which is lockable in two axes with oscillation about the axis of interest.

To contend with the problem of aircraft flexibility, stiffening jacks are used to support the aircraft structure. As a result of the stiffening operation, flexibility effects are considered to be less than 4% in roll and 2% in pitch.

The experimental error in the methods discussed is of the order of ±5% or less.

4.3 Inclination of Principal Axis

The inclination of the principal axis of the airplane is one of the more difficult quantities to determine experimentally. An error of $1/4^\circ$ in the value of the inclination of the principal axis can significantly affect some of the derivatives. The method of Reference 22 is considered accurate to $1/6^\circ$.

This method consists of finding the direction of the restoring-moment vector which produces no rolling moment relative to the body x-axis during the yawing oscillations of the airplane as a spring mass system while suspended by means of a cable attached to a hoisting sling. Figure 15 shows schematically, and Figure 16 shows photographically, a general arrangement of the setup. The airplane is suspended at a horizontal pitch attitude, and yaw restraint is provided by two sets of springs whose lines of action lie in a common plane. The springs should provide a pure couple action. The restoring-moment vector acts normal to the plane of the springs. The springs may be attached to short, rigid mounting brackets located below the wings equidistant from the plane of symmetry or to brackets mounted below the fuselage ahead of and behind the center of gravity. In this respect, the wing mounting arrangement is most convenient and less time-consuming. It is essential that the springs provide a pure couple action.

As the airplane oscillates in yaw with various inclinations of the plane of the spring couple (angle δ_{sp} in Figure 15), some coupling is present between yaw N and roll L, which results in a certain amount of rolling oscillation. This is shown in the following equations where the subscript r denotes the reference attitude of the airplane:

$$I_{x_r}\dot{p}_r - I_{x_r z_r}\dot{r}_r = L \tag{88}$$

$$I_{z_r}\dot{r}_r - I_{x_r z_r}\dot{p}_r = N . \tag{89}$$

At some one value of δ_{sp}, however, the rolling motion accompanying the yawing motion is zero ($|p|/|r| = 0$). In this situation the preceding equations reduce to

$$\begin{aligned} - I_{x_r z_r}\dot{r}_r &= L \\ I_{z_r}\dot{r}_r &= N . \end{aligned} \tag{90}$$

However, as shown in Figure 15,

$$\tan \delta_{sp} = \frac{-L}{N} . \tag{91}$$

Hence

$$\tan \delta_{sp} = \frac{I_{x_r z_r}}{I_{z_r}} . \tag{92}$$

Inasmuch as the inclination of the principal axis is given by the wellknown expression

$$\tan 2\epsilon = \frac{2I_{x_r z_r}}{I_{z_r} - I_{x_r}} , \tag{93}$$

substitution of Equation (92) for I_{xz_r} in Equation (93) gives

$$\tan 2\epsilon = \frac{2I_{z_r} \tan \delta_{sp}}{I_{z_r} - I_{x_r}} . \tag{94}$$

The value of I_{z_r} is determined as a byproduct of the test by using

$$I_{z_r} \simeq \frac{C \cos \delta_{sp}}{\omega^2} . \tag{95}$$

However, I_{x_r} must be determined from other tests.

Figure 17 shows a typical experimental plot of the variation of $|p|/|r|$ with δ_{sp} for determining the value of δ_{sp} at which $|p|/|r|$ is zero. In obtaining the tests points shown in the figure, the flight test roll- and yaw-rate gyros mounted in the airplane were used to obtain oscillograph records for determining $|p|/|r|$ from the transient oscillations.

The measured values of moments of inertia relative to the reference axes and the determined inclination of the principal axes may be used to determine the principal moments of inertias, I_{x_0} and I_{z_0}, by using the following equations

$$I_{x_0} = I_{x_r} - I_{x_r z_r} \tan \epsilon \tag{96}$$

$$I_{z_0} = I_{z_r} + I_{x_r z_r} \tan \epsilon . \tag{97}$$

Although no mention was made of the effects of air mass on the experimental values of moments of inertia, the effects should be considered and corrections applied if necessary. Reference 23 provides formulas to correct for air-mass effects.

Formulas for transferring moments of inertia from one set of axes to another were presented in Section 3.1.

5. INSTRUMENTATION

Basic to an analysis of flight data is the instrumentation. Considerable instrumentation research has been in progress and many flight test instruments have been developed to improve the linearity of response, resolution, dynamic response characteristics, readability, ruggedness, and reliability of calibrations over varying operating conditions and extended periods of time. In addition, the application of the instruments requires knowledge of mounting accuracy, sources of error in the flight records, and methods of correcting the errors. Inadequate appreciation of the instrument characteristics, mounting accuracy, and possible influence of sources of error serves as a detriment to the successful application of new techniques of analysis as well as a detriment to the analysis by approximate methods.

In the following discussion, sufficient guidelines are presented to show the care required in the selection, installation, and calibration of instruments to minimize errors in the analysis of flight data. Individual instruments may differ from one organization to another and the degree of sophistication in instruments and recorders will vary with the individual investigation; however, the principals of operation of the sensors are generally the same.

5.1 Mach Number, Altitude, and Dynamic Pressure

Accurate determination of Mach number is of fundamental importance in flight testing high-speed aircraft. The principal methods, discussed in detail in References 24 and 25, are based upon the following relationship for subsonic conditions ($M < 1.0$)

$$\frac{\bar{q}_c}{\bar{p}} = \left[\left(1 - \frac{\gamma - 1}{2} M^2\right)^{\gamma/(\gamma-1)} - 1\right] = (1 + 0.2M)^{7/2} - 1 . \qquad (98)$$

For supersonic conditions ($M > 1.0$), the equation is modified to include the loss in total pressure behind the shock wave

$$\frac{\bar{q}_c}{\bar{p}} = \frac{\gamma + 1}{2} M^2 \left(\frac{\frac{\gamma + 1}{2} M^2}{\frac{2\gamma}{\gamma + 1} M^2 - \frac{\gamma - 1}{\gamma + 1}}\right)^{1/(\gamma-1)} - 1 = 1.2M^2 \left(\frac{5.76M^2}{5.6M^2 - 0.8}\right)^{5/2} - 1 . \qquad (99)$$

The impact pressure $\bar{q}_c$ and the static pressure p are measured by using a pitot-static head and pressure recorders. The maximum Mach number as well as dynamic pressure which can be determined by using pitot-static heads is of the order of 3.5. Higher speeds are primarily dependent upon inertial platforms and radar. Dynamic pressures at Mach numbers is the approximate range of 2.5 to 8.0 can be determined through the use of a spherical flow-direction sensor and a total- (stagnation) pressure technique.

5.1.1 Pitot-Static Head ($M < 3.5$)

Much research has been done on various types and configurations of total-pressure heads to reduce angularity effects[26, 27]. The type shown in Figure 18 is used widely. This head has an external cylindrical shape, a cylindrical chamber, and a 10^o slant profile. It is insensitive (zero error) to angle-of-attack from -5^o to 20^o and up to 10^o of sideslip. The error is less than 1% in the angle-of-attack range from -10^o to 25^o and $\pm 10^o$ sideslip.

The arrangement of the static-pressure orifices on the head has been found to be pertinent in increasing the range of insensitivity of the orifices to flow angularities. The arrangement used has been determined from tests of orifice configurations[28, 29]. The two identical sets or arrangements shown in Figure 18 are each circumferential, with four orifices on the top, six on the bottom, and one on the bottom centerline behind the others. The two sets of static-pressure orifices are used to provide for separate pressure systems. One set of static orifices is used for the pilot's instruments, the other set for flight test recording instruments to minimize the time lag of response that would be encountered with a common system. The arrangement of the orifices in each set provides an increased range of insensitivity to angle-of-attack; however, it is not as insensitive to sideslip. Large static-pressure errors are encountered at sideslip angles greater than 3^o. Since constant sideslip angles are seldom encountered, the static-pressure data can be readily faired.

Installation of the pitot-static head: Installation of the pitot-static head requires consideration of the complicated flow field of the airplane, which is a function of the airplane configuration as well as Mach number and attitude. Errors in pitot-static-head readings resulting from this flow field are referred to as position errors. The static-pressure orifices are particularly affected by position errors at subsonic speeds; thus, precautions are taken to mount the pitot-static head as far ahead of the airplane as is practical.

Of the various types of installations of the pitot-static head – such as nose boom, wing boom, and fuselage – the nose-boom installation is the most suitable for minimizing position errors. In this installation, shown in Figure 19, the head is mounted on a boom extending as far ahead of the nose of the airplane as is practical. As reported in Reference 29, the amount of error in Mach number due to position error in the static-pressure measurements can be related to certain physical measurements on the airplane. This is shown in Figures 20 and 21, which are reproduced from Reference 30. In Figure 20, the error in Mach number due to static-pressure error is plotted as a ratio of boom length to the maximum effective fuselage diameter for subsonic, transonic, and supersonic speeds. In Figure 21, the variation in Mach number error with Mach number is plotted for two airplanes having boom-length-to-fuselage-diameter ratios of 0.60 and 0.95. Above a Mach number of 1.05, the position error drops to zero. The Mach number at which the position error drops to zero is dependent upon the nose-boom geometry and is the Mach number at which the shock wave ahead of the airplane crosses over the static-pressure orifices.

Wing-boom installations of the pitot-static head are subject to several disadvantages, including possible susceptibility to the shock wave caused by the wing as well as the shock wave caused by the fuselage. This complicates the calibration and makes it more difficult for the pilot to fly at the desired Mach number in the regions where the shock waves are in the vicinity of the orifices. Wing booms are usually more sensitive to sideslip and subject to more lag in response because of the longer tubing required.

Fuselage installations of the head are subject to position errors, which are difficult to estimate.

Calibration: Calibration of the pitot-static head, fortunately, involves only the determination of the position error for the static pressure – the total pressure is not affected by position error. Various methods that have been used include the pacer method, the fly-by (tower-pass) method, and modifications of the basic radar-phototheodolite method[24]. The pacer method requires the use of a pacer airplane with a calibrated system and special flights for calibration purposes. The fly-by method requires 1g flight at extremely low altitudes past an instrumented course. This latter method not only requires special flights, but is hazardous and limited to Mach numbers of about 0.8.

The radar-phototheodolite method has the advantage of providing calibration data during routine research flights. The method makes use of a radiosonde unit to measure static-pressure and temperature variations of the atmosphere with altitude. It also requires ground equipment consisting of a radar unit, a phototheodolite, a chronograph, and three cameras. One of the cameras photographs the radar scope and gives the slant range; the target camera gives the correction to the elevation scales; and the third camera gives the elevation scale. The airplane itself is equipped with a radar beacon

to assist in tracking. The three cameras and the airplane's internal records are synchronized by means of the chronograph. The radar-phototheodolite unit determines the range and elevation angle of the airplane from which the true geometric altitude of the airplane is determined (within ±100 ft) as a function of time.

A cross plot of the radar-phototheodolite data (airplane altitude vs. time) with the radiosonde results (free-stream static pressure vs. altitude) provides a plot of true free-stream static pressure as a function of time. Since the time base of the airplane's indicated static-pressure records is synchronized with the radar-phototheodolite, a comparison of the airplane's indicated static-pressure records with the cross plot provides the position error, $\Delta\bar{p}$, of the static head. The corrected static pressure may now be obtained from the relation $\bar{p} = \bar{p}_i + \Delta\bar{p}$. The true impact pressure is now determined from $\bar{q}_c = \bar{p}_T - \bar{p} = \bar{q}_{ci} - \Delta\bar{p}$.

True Mach number: True Mach number is determined from tables of $\bar{q}_c/\bar{p}$ as functions of Mach number based on Equations (98) and (99). The indicated Mach number, M_i , as determined from $\bar{p}_i$, $\bar{q}_{ci}$, and the tables, is plotted against the corrected Mach number, M , to provide a calibration curve, such as shown in Figure 22, for the pitot-static-head installation on the airplane. Generally, calibration data points for four or five flights are used before the calibration curve is finalized. The scatter, ΔM , in calibration points is usually within ±0.01 at subsonic and supersonic speeds and within ±0.02 at transonic speeds.

Pressure altitude: Altitude is generally expressed in terms of "pressure altitude", which is the altitude in the standard atmosphere tables corresponding to the corrected static pressure. The corrections for a given pitot-static pressure system are obtained in the form $\bar{p}_i/\bar{p}$ vs. M . The curve for this relationship is derived from the Mach number calibration of the system and the position error for the static pressure determined as a ratio of the true static pressure by the following equations from Reference 25:

When $M < 1.0$,

$$\frac{\Delta\bar{p}}{\bar{p}} = \frac{-1.4M^2}{1 + 0.2M^2}\left(\frac{\Delta M}{M}\right) . \tag{100}$$

When $M > 1.0$,

$$\frac{\Delta\bar{p}}{\bar{p}} = \left(\frac{4.0}{5.6M^2 - 0.8} - 2\right)\left(\frac{\Delta M}{M}\right) . \tag{101}$$

In routine tests, the pressure ratio $\bar{p}_i/\bar{p}$ is divided by $\bar{p}_i$ to obtain $\bar{p}$, which is used to determine the pressure altitude.

Dynamic pressure: The dynamic pressure, $\bar{q}$, is determined from the simple relation

$$\bar{q} = 0.7\bar{p}M^2 . \tag{102}$$

5.1.2 *Use of Spherical Flow-Direction Sensor to Obtain Dynamic Pressure*

In the absence of true Mach number, such as when flight is beyond the practical limit of the pitot-static tube ($M \simeq 3.5$), a technique has been evolved to obtain the dynamic pressure, in the higher supersonic and hypersonic regions, directly from the total-pressure port of a spherical flow-direction sensor[31]. The flow-direction sensor, described in more detail in Section 5.3, is a movable sphere mounted at the nose of the airplane to form a "ball nose". The total-pressure port vectors into the resultant velocity at the sensor.

Inasmuch as $\bar{q} = 0.7\,\bar{p}M^2$ and, from the Rayleigh pitot formula,

$$\frac{\bar{p}}{\bar{p}_r} = f(M) ,$$

where

$$f(M) = \left[\frac{2}{(\gamma + 1)M^2}\right]^{\gamma/(\gamma+1)} \left[\frac{2\gamma M^2 - (\gamma - 1)}{\gamma + 1}\right]^{1/(\gamma+1)} , \qquad (103)$$

the dynamic pressure can be expressed as

$$\bar{q} = 0.7\bar{p}[f(M)]\bar{p}_T \qquad (104)$$

or

$$\frac{\bar{q}}{\bar{p}_T} = F(M) . \qquad (105)$$

A plot of $\bar{q}/p_T$ versus M (Fig. 23(a)) shows that this ratio varies only about 5% in the Mach range above 2.5. As a result of this small variation in $\bar{q}/p_T$ at the higher Mach numbers, it was suggested that an "indicated" dynamic pressure, $\bar{q}_i$, could be expressed as

$$\bar{q}_i = K\bar{p}_T . \qquad (106)$$

Figure 23(b) shows the ratio of indicated to true dynamic pressure, $\bar{q}_i/\bar{q}$, for two values of K. Using $K = 0.526$, $\bar{q}$ is 5% high at $M = 2.1$ and 2.5% low at $M = 7$.

5.1.3 *Pressure-Recording Instruments*

Selection of the pressure-recording instruments and their ranges for a given installation depends on the altitude and Mach number range over which a specified attainable Mach number accuracy is desired. When tests are to be conducted at one altitude, it is no problem to select a pressure-recording instrument to provide the requisite accuracy. For tests conducted over a large range of altitudes, the requisite accuracy may be attained by using a combination of limited-range instruments. Considerations of the pressure time lag require that the instrument volume remain as small as possible, thus necessitating an evaluation of instrument accuracy with consideration for the errors caused by the added time lag of multiple-instrument installation.

The lag in response at the recorder servo or pilot display, as the case may be, can be calculated from the following formula (from Reference 32), which takes into account the sense line, instrument volume, and pressure

$$\lambda = \frac{128\mu_0 l(V_0 l)}{\pi \bar{p} D^4} , \qquad (107)$$

where

λ = lag in response, sec

μ_0 = viscosity of the fluid, lb sec/in^{-2}

l = length of sense line, in

Vol = instrument volume, in^{-3}

$\bar{p}$ = mean pressure in sense line, lb/in^2

D = diameter of sense line, in .

Several ranges of instruments are available for both the static-pressure and total-pressure recorders. For the static-pressure recorders, the lower-range instruments require temperature calibration. Hysteresis and friction errors, and temperature errors, should be within ±1/2% of range or better.

5.2 Control Position Transmitters

Control position transmitters, commonly referred to as CPT units, sense the control-surface deflections and must be accurate and sensitive enough to measure small deflections. Transmitters of the sliding contactor type change the ratio of resistance in two arms of a Wheatstone bridge circuit. Any variation in the resistance of the arms unbalances the circuit and causes current to flow to the recording galvanometer (see Figure 24).

In a properly installed system, the phase lag between the transmitter and the recorder should be negligible. The errors due to hysteresis, zero shift, temperature, accelerations, or vibrations should also be negligible.

The transmitters are firmly mounted at the control surfaces to eliminate the effect of control-system deformations. The spanwise location of the transmitter gives an approximate spanwise surface deflection.

Zero checks are made before and after each flight to detect any zero shift in the galvanometer recording system.

5.3 Angle-of-Attack and Sideslip

5.3.1 Vane-Type Flow-Direction Sensors

Of the various types of flow-direction devices for sensing angle of attack and sideslip up to a Mach number of approximately 3.0, good accuracy and reliability is

obtained with a counterbalanced, freely turning vane mounted on a nose boom, which also serves as a mount for the pitot-static head (Fig. 19). Each vane is directly connected to a synchro transmitter within the boom, which is electrically connected to a synchro receiver mounted in a recorder located within the airplane. It should be noted that, although the α-vane measures the aerodynamic α, the β-vane measures a β referenced to the body axis system of the airplane.

Inherent accuracy: Hysteresis in the system is practically nil. Friction introduces an error of less than $\pm 0.1^{\circ}$. In an optical recorder system, the unbalance of a balanced optical recorder element may cause a trace deflection equivalent to 0.05° per g of acceleration. Temperature has no direct effect on sensitivity. Natural frequency and damping of the system should be of the order to 10 c/s and 0.65, respectively, to provide flat response to within $\pm 1\%$ for sinusoidal inputs up to 6 c/s.

Mounting: The angle-of-attack and angle-of-sideslip vanes are mounted on a nose boom extending forward as far as possible to minimize the effects of upwash and shock wave. In this respect, vanes are mounted 1½ maximum fuselage diameters ahead of the airplane when feasible. Figure 25, reproduced from Reference 30, shows the theoretical effects of upwash from the nose boom and fuselage at low speeds. Wing upwash was not considered.

The boom and its mount should be sufficiently stiff to minimize deflections due to inertia and air loads. Particular care must be taken to aline the longitudinal axis of the boom with the longitudinal body axis of the airplane and the vane struts to the boom so that the angle-of-attack and angle-of-sideslip vane struts are parallel to the body y and z axes, respectively. The rear vane is for sideslip and projects vertically downward. The recorder is mounted in any convenient location.

Field checks: The final calibration of a transmitter-recorder combination is made in place on the airplane with the aid of a calibration fixture that provides an accurate alinement of the vane with the boom and the zero of the calibration quadrant. Calibrations should be made in increments of about 2° to detect nonlinearities. Calibration should be performed both before and after flight.

The vanes should be given periodic checks for alinement with their pivotal shafts and for friction. An extension of the chordline of the vane should be within 0.005 in. of alinement with the center of the shaft.

Correction of recorded data: The angle-of-attack and angle-of-sideslip vanes measure local flow direction. The effects of boom bending due to inertia and air loads, flow components resulting from angular velocities, flight-path curvature, and upwash due to the boom, fuselage, and wings introduce errors in the measured flow angles with respect to the true airplane angle-of-attack or sideslip. In addition, phase lag and dynamic amplification of the sensing-recording system introduce additional errors in the recording of the vane indications. The magnitude of each effect must be investigated and corrections made to the recorded data wherever pertinent to the analysis for determination of derivatives.

Bending of the boom results in errors in vane indications, inasmuch as the vane is referenced to the axis of the boom. As pointed out in Reference 30, deflections due to aerodynamic loading have been negligible; however, where very long booms are used or extremely long, flexible fuselages are being dealt with, bending corrections may be

determined from calculated aerodynamic loading[31]. Boom-bending error resulting from inertia loads is accounted for through static deflection calibration of the boom.

Upwash error resulting from the boom, fuselage, and wing is generally considered negligible and within the accuracy of the methods of analysis employed. This may not necessarily be true. In a boom-vane installation on a large bomber where the vane was one fuselage diameter ahead of the nose, the upwash error in angle-of-attack at subsonic speeds was of the order of 4%. On other large aircraft having fuselages of larger cross section, the influence was much larger. Upwash error due to the boom itself may be measured by wind-tunnel calibration of the system[28, 34]. The effect of upwash at subsonic speeds at the vane due to the fuselage can be calculated by the method of Reference 35. The effect of upwash at subsonic speeds due to the wing can be calculated by the equations in Reference 36 for unswept wings and the methods of Reference 37 for swept wings. At supersonic speeds, the wing and fuselage do not contribute any upwash effects to the vane.

The angle-of-attack sensor is also subject to pitch-rate effects of flight-path curvature. Corrections for flight-path curvature (Fig. 26) may be significant at subsonic speeds; whereas, pitch-rate corrections may be significant from the subsonic through the low supersonic speed range. Corrections for flight-path curvature affect magnitude primarily; whereas, corrections for pitch rate affect phase angle primarily. This is illustrated in Figure 27, which shows the graphical time-vector determination of the absolute amplitude of the corrected angle of attack as a ratio of the indicated amplitude for an aircraft performing small-perturbation, free-oscillation maneuvers at a Mach number of 0.8 at 40,000 ft. The presentation considers only corrections for flight-path curvature and pitch-rate affects and is based on the equation

$$\alpha \simeq \alpha_i + \frac{x_v g}{V^2}\left(a_n - \cos\theta\cos\phi\right) + \frac{x_v}{V} q \ . \qquad (108)$$

The solution shows the influence of the flight-path curvature to be of the order of 3%.

Flight-path curvature in yaw has a negligible effect on the sideslip vane. Correction for yaw-rate and roll-rate effects should be considered. The approximate expression for correcting the indicated sideslip for angular-rate effects is

$$\beta \simeq \beta_i - \frac{x_v}{V} r + \frac{z_v}{V} p \ . \qquad (109)$$

5.3.2 *Spherical Hypersonic Flow-Direction Sensor*

The spherical flow-direction sensor shown in Figure 28 was designed to replace the α and β vane-type sensors at the higher supersonic Mach numbers and dynamic pressure where the combined temperature and aerodynamic loads exceed the limitations of the vane-type sensor[38]. The spherical sensor is a null-seeking, hydraulically operated, electronically controlled servo-mechanism. It has pressure measurements as its sole sensing inputs. It operates on the principle that when two static ports are located on the great circle of a sphere, a null reading will result when the bisector of the included angle of the two static ports is parallel to the fluid stream immediately in front of the sensor. The rotation of the bisecting line relative to a reference gives the inclination of the fluid stream relative to the reference.

When the spherical sensor is in the zero position (axis alined with the airplane), the α-ports are 42° above and below the reference line in the vertical plane of symmetry of the aircraft and the β-ports are 42° on either side of the reference line in the transverse plane.

The sphere constitutes the outer gimbal of a two-gimbal pivot system in which the outer gimbal is pivoted to the inner gimbal whose pivotal axis is fixed and is normal to the plane of symmetry of the airplane. As the sensing sphere seeks null readings in each of its two sets of static-pressure ports, the gimbals rotate about their respective axes. The inner gimbal, rotating about its fixed axis, which is normal to the plane of symmetry, sweeps an angle α in the plane of symmetry. The outer gimbal, whose pivotal axis is mounted on the inner gimbal and remains in the plane of symmetry at all times, sweeps an angle β in a plane which is perpendicular to the plane of symmetry; this plane is the transverse plane of the stability axis system of the aircraft. The α and β angles picked off by synchros are the aerodynamic α and β angles of the airplane.

The inherent accuracy of the spherical sensor is of the order of $\pm 0.5^{\circ}$ or better for dynamic pressures in excess of 20 lb/ft^2. At high angles of attack in excess of approximately 26° at low dynamic pressures of about 40 lb/ft^2 and less, the α indications are subject to large errors, possibly due to flow interference of the lip on the collar of the housing.

5.4 Angular Velocities and Accelerations

The angular velocity and angular acceleration relative to any one axis can be sensed by individual sensors or sensed and recorded in a convenient packaged unit. Figures 39(a) and 39(b) show the details of the angular-velocity aspect of a NACA designed, packaged unit which includes the recorder. The angular acceleration sensing and recording involves a relatively small extension of this unit. The operation of the unit depends upon the precessional force of a restrained gyro motor when the unit is subjected to an angular rate about an axis which is perpendicular to both the axis of rotation of the gyro motor and the axis of rotation of the gimbal rings. The gyroscopic element is the rotor of a synchronous motor. The sensitive element is restrained by a precision helical spring. The moving system is damped by rotating an aluminium disk in the field of a strong permanent magnet. The angular-velocity measurement is made by optically recording on the film the angular displacement of the gimbal. Sensitivity of the angular-velocity recorder can be adjusted by rotating the actuator arm along the mirror staff tail.

Angular acceleration is obtained by differentiating the gimbal motion. The differentiation is accomplished by mounting a coil in a magnetic field and driving it from the damping shaft so that it rotates with speed proportional to the angular velocity of the gimbal. The output voltage, which is proportional to the angular acceleration, is recorded on the film by a self-contained reflecting galvanometer.

5.4.1 Inherent Accuracy

In well-designed angular-velocity systems, the reading accuracy is of the order of 0.5% of full scale or better; the errors due to friction and hysteresis are less than 1% of full scale, and the change in sensitivity from large changes in temperature should

be as small as possible. Errors due to linear accelerations of 5g should be less than 1%. The sensor should provide flat response characteristics within ±1% for all anticipated impressed frequencies. The phase lag (time lag) is a function of damping ratio and undamped natural frequency of the sensor.

Recorded angular accelerations are subject to the errors found in the angular-velocity record. In the NACA acceleration-velocity packaged unit, additional errors are introduced by the acceleration recording galvanometer; inasmuch as the angular-acceleration pickup is a differentiation device, the response and phase lag of the accelerometer and velocity portions of the unit are similar.

5.4.2 *Mounting and Corrections*

It is important that the instrument mounting be rigid. Although small-amplitude, high-frequency vibrations may not be apparent on the velocity trace, the vibrations can introduce considerable noise in the acceleration trace.

Angular-velocity gyros are subject to coupling errors caused by an interference (airplane) angular velocity about the spin axis of the gyro rotor. Care should be exercised in orienting the instrument during mounting so as to subject its spin axis to the minimum interference angular velocity. A mathematical study of the coupling error is presented in Reference 39. The interference angular velocity (also known as the q rate) affects the sensitivity of the instrument, the undamped natural frequency, and the damping ratio. The extent of the errors is a function of the gimbal tilt, which, itself, is a function of the gyro sensitivity in spring-restrained instruments and the magnitude of the interference angular velocity. This is illustrated in Figure 40 for an angular-velocity unit having a static sensitivity of 0.256 radian per radian per second. A decrease in sensitivity would reduce the coupling error; however, a decrease is not always desirable. To minimize the coupling error for any one instrument, the axes should be oriented as follows:

Desired Velocity	*Input Axis*	*Spin Axis*	*Output Axis*
Roll rate, p	x	z	y
Pitch rate, q	y	z	x
Yaw rate, r	z	y	x

Alinement of the sensing-recording units should be within ±0.2° of correct orientation with relation to the body axes. Undetected misalinement has been known to result in erroneous values of highly pertinent derivatives, which resulted in misleading results in analog-simulated rolling characteristics. In any correction for misalinement, it is pertinent that the recorded values be corrected for phase lag of the instrument prior to insertion in the correction equations. Simultaneously, the response of the instrument should be checked, if there is any appreciable deviation from the damping ratio of 0.65, to ascertain the percentage error in magnitude of the indicated quantity due to the dynamics of the instrument. Misalinements in the mounting of the unit may be accounted for by using the equations shown in Figure 31.

5.5 Linear Accelerations

In general, flight testing is done with the beam-type linear accelerometers which are available as single-component or three-component units. Drag determination is frequently made with single-component units[30]. The beam-motion restraining force is generally supplied by a pair of opposed helical springs. The sensitivity and undamped natural frequency are dependent upon the springs used.

5.5.1 Inherent Accuracy

In properly designed beam-type linear accelerometers, sensitivity and zero changes from random causes are less than 0.5% of full scale. The sensor should have a damping ratio of 0.65 and a sufficiently high undamped natural frequency to provide flat response characteristics within ±1% for impressed frequencies up to 60% of the undamped natural frequency of the sensor. Each linear accelerometer is affected by an interacting acceleration acting along the beam. The effect is generally small but should not be arbitrarily ignored.

5.5.2 Mounting and Corrections

The instrument should be mounted as close to the center of gravity of the airplane as possible. It should be rigidly fastened on a rigid mounting attached to the primary structure of the airplane to avoid or at least minimize extraneous vibratory accelerations. It should be alined to within ±0.2° of correct orientation with relation to all three reference axes. When the instrument is not mounted at the center of gravity of the airplane, corrections of the indicated readings to the center of gravity must be made by using the expressions shown in Figure 32. The equations for normal acceleration, a_n, and transverse acceleration, a_t, can be linearized and corrections thus simplified by mounting the accelerometers in the plane of symmetry along the x-axis.

5.6 Phase Lag and Response

Since several individually recorded quantities are utilized in the determination of various derivatives, it is important that the phase-lag (time-lag) characteristics of each recording instrument be taken into consideration. For systems where all the quantities can be recorded on electrical galvanometers, it is generally possible to equalize the individual phase lags by proper choice of the frequency response of the recording system. Where this is not possible, as in the use of certain of the self-recording NASA instruments, phase-lag corrections must be considered and applied to bring all pertinent quantities into correct time relationship.

Phase-lag corrections must be applied before making any corrections for misalinement. Corrections for misalinement must be made before correcting the vane and linear-accelerometer records to the center of gravity of the airplane.

Because of the nature of the control inputs, phase-lag corrections can be applied simply by shifting the data time scale[40], as in the determination of control derivatives, or by correcting phase-angle relationships, as in the time-vector method of analysis. This is accomplished by determining the undamped natural frequency of the airplane from free-oscillation maneuvers and Figure 33. Amplitude corrections are not required, since the instruments have flat response characteristics.

When the instruments are not sufficiently damped to provide flat response characteristics, corrections to the magnitudes of the recorded quantities may be determined from Figure 34.

5.7 Ranges and Sensitivity

Instruments used for studies of general handling qualities have relatively low sensitivities in order to accommodate the normal flight range and are used for approximate evaluation of derivatives in conjunction with these studies. For accurate evaluation of the derivatives, using small disturbance maneuvers, sensitive gyros and accelerometers are installed to supplement or replace those used for the handling-qualities studies. The ranges and sensitivities of the instruments are usually selected after studying flight test records of small-perturbation maneuvers performed over a Mach number range during pilot familiarization flights when the airplane is equipped with general-purpose flight test instruments. The increase in sensitivity of any one instrument must be accomplished with discretion, inasmuch as an optimum sensitivity is attained beyond which any increase may result simply in a false sense of accuracy.

Table VII shows the characteristics of instruments which are desirable for derivative investigations for one high-performance airplane when the pulsed free-oscillation maneuver is employed. The listed instrument natural frequencies are more than adequate to maintain flat response characteristics during forced portions of the maneuver up to the anticipated maximum frequencies for all recorded quantities.

5.8 Pulse Code Modulation (PCM) Data-Acquisition Systems

In the preceding considerations of instrumentation, emphasis was placed on factors that affect the accuracy of individual sensors. Self-contained sensor-recorded units are compact, reliable, and accurate. The use of sensors wired to remote recorders can introduce degradation in the accuracy of the overall sensor-recorder system; however, such systems are used to keep the instrumentation volume to a minimum where space is a prime factor and a large number of parameters are involved. As the number of sensed and recorded parameters increases, the time lag in the recovery of the data for the user increases. In flight test investigations where the bulk of the instrumentation is a serious problem or where the number of parameters recorded may constitute a serious time lag in the recovery of the data for the user, a sophisticated data-acquisition system is available to alleviate these problems. This system, originated to fulfill the needs of the space industry, in which transducers of superior quality are used, is capable of handling the data to reasonable accuracy (0.2% to 1%). The system, referred to as the PCM system, converts the analog signal from the sensor to digital format and records the digitized data on tape on a time-sharing basis.

Figure 35(a) shows a schematic drawing of an airborne PCM system. The analog signals from the sensors go to a PCM encoder to convert the signal to an identification coded, digitized format. The coded, digitized signals are then recorded in parallel on an onboard tape recorder on a time-sharing basis. To recover the data, the taped signals are processed through a PCM decommutation, which identifies (unscrambles) the individual sensor signals, to a format computer to provide real-time data outputs in the form of strip charts or oscillograph readouts for an immediate look at the data. The real-time data are also transmitted to a general-purpose computer which tabulates, plots, or performs complex manipulation of the data in engineering units.

Where weight is a serious factor, Figure 35(b) shows a schematic drawing of the PCM system using telemetry. The main differences between the telemetered and airborne PCM systems involves the transmission of the coded, digitized signals in series to the decommutator (instead of parallel to the recorder), which provides time synchronization of the signals before the signals are taped. In processing the data, the format computer properly identifies the individual data channels for real-time data output.

As stated earlier, the PCM system is a sophisticated operation. One installation at the NASA Flight Research Center, Edwards, California, is designed to handle 15,400 data samples per second from 77 to a maximum of 800 data sources.

6. FLIGHT TEST TECHNIQUES

Determination of the flight test techniques to be used in obtaining stability and control derivatives from flight data is governed by a number of factors, including the methods of analysis to be employed. Successful mathematical methods of analysis have been limited to the linearized form of the equations of motion and thus restrict the maneuvers to small perturbations. Inasmuch as stability derivatives are functions of angle of attack and Mach number and, to some extent, aeroelasticity of the airframe, the controlled variables are Mach number, load factor, and pressure altitude. For safety of flight, the investigation of the stability and control characteristics is usually initiated with a gradual buildup of maneuvers at high altitude where the natural frequency and damping of the airplane are lower than at low altitudes and thus permit better control. It is desirable, when feasible, to have the maneuvers performed with the airplane weight within such limits over the derivative-determination phase of the flight test program that the effects of changes in center-of-gravity position and moments of inertia will be negligible.

The important factors to be considered in flight testing for stability and control derivatives are discussed in the following sections.

6.1 Mach Number and Altitude

Flight test maneuvers are generally performed at 1g initial conditions at constant Mach number and altitude. Normally, some variations in these quantities are accepted if the resultant change in dynamic pressure is not more than 5% over that portion of the maneuver encompassed in the analysis. In regions where large Mach number effects exist (Fig.36), tests should be conducted at close Mach number intervals with more rigid requirements at constant Mach number and altitude. Failure to trim the aircraft to the desired Mach number and to maintain that Mach number during the maneuver in regions of rapidly varying characteristics may produce a scatter of data and an erroneous analysis.

The very nature of flight testing requires, for expediency, plotting the results of analysis as a function of Mach number, with each curve representing a constant-altitude condition. Figure 37, taken from Reference 41, shows the influence of altitude on flight test data on one supersonic aircraft.

6.2 Angle of Attack and Load Factor

The variation in airplane characteristics with angle of attack is determined by performing maneuvers at different altitudes with 1g trim conditions prevailing prior to the perturbation, or at constant altitude with the maneuver performed during a stabilized constant-g pushover or turn. It should be noted that it is difficult to obtain good maneuvers during stabilized turns; exceptional piloting skill is required. Figures 37 and 38 show the influence of load factor on stability characteristics. In instances where the aeroelasticity of the structure is nil (dynamic pressure effects are nil), a combination of the two techniques will result in the determination of the variation of the derivatives over an extended range of angle of attack. Should aeroelasticity of the structure be a factor to contend with, the results from the two techniques will differ for the same angle of attack, Mach number, and center of gravity.

6.3 Aeroelasticity

Aeroelastic deformation of the structure assumes increasing significance as the aircraft increases in size and slenderness and operates at increasing dynamic pressures. Supersonic transport designs are flexible in order to keep the structural weight down, the payload high, and the range capability a maximum. To apply theoretical flexibility corrections to rigid wind-tunnel data for comparisons with flight data provides an intuitive basis in ascertaining flexibility effects. When such comparisons are employed and a definite disagreement is evident in the comparison in regard to level and trends of the stability and control parameters as a function of Mach number, it may become difficult to locate the source of the discrepancy – wind-tunnel data or predicted flexibility corrections. Thus, a more positive approach is required to assess flexibility effects.

The stability and control derivatives should be essentially invariant for a rigid airplane as long as Mach number, angle-of-attack, and the center of gravity are constant (assuming Reynolds number effects to be a minor factor). Thus, any direct approach to investigating flexibility effects based on flight data should show the variation of the stability parameters – obtained at the same Mach number, angle-of-attack, and center of gravity – as a function of dynamic pressure. Although Mach number and center-of-gravity control is straightforward, the angle-of-attack is a problem.

The location of the angle-of-attack sensor exposes the sensor to errors resulting from structural deformations, in addition to the other sources discussed in Section 5.3. Hence, it is more judicious to use the life coefficient C_L in lieu of angle-of-attack α. Thus, from a practical point of view, a direct investigation of aeroelastic effects should be based on a comparison of flight data for different dynamic-pressure conditions obtained at the same Mach number, lift coefficient, and center of gravity.

An effective, flexible, and simple flight-planning procedure to determine the flight test conditions as a function of weight and altitude to provide constant M, C_L, and center of gravity can be achieved by using a nomograph such as that in Figure 39. In this nomograph W, M, C_L, and $\bar{q}$ are variables, and center of gravity is constant. The nomograph is based on the following two basic relations for 1g flight:

$$W = C_L \bar{q} S \tag{110}$$

and

$$\bar{q} = 0.7 \bar{p} M^2 . \tag{111}$$

It assumes the weight distribution, which could influence structural deformation, to be essentially constant. Inasmuch as C_L is a constant for any one Mach number condition being investigated, the following expression is readily derived from the above equations and constitutes the basis for the nomograph:

$$\frac{W_2}{W_1} = \frac{\bar{p}_2}{\bar{p}_1} . \qquad (112)$$

The subscripts 1 and 2 denote the initial and compatible second condition. It will be noticed that, for any one initial weight W_1 at altitude h_1 (as typified by pressure $\bar{p}_1$), the vehicle will have to be at a weight W_2 at altitude h_2 to maintain the same C_L at the selected constant Mach number.

To illustrate the use of the nomograph, consider an aircraft to have a weight of 411×10^3 lb at the time a stability maneuver was performed at Mach 2.34 at 55×10^3 ft. These initial conditions, which have been spotted on Figure 39, show the dynamic pressure to be 730 lb/ft^2. If it is desired to perform the next stability maneuver at $\bar{q}_2 = 450$ lb/ft^2, the intersection of $\bar{q}_2$ (450) and the constant Mach line (2.34) determines the new altitude, h_2, to be 65×10^3 ft. The intersection of the constant-altitude line with the constant M, C_L, center-of-gravity line extended from condition 1 determines the weight ($W_2 = 252 \times 10^3$ lb) required to provide the same M and C_L at condition 2 as was present at the time of the stability maneuver at condition 1 (center-of-gravity being constant).

The nomograph is invaluable in systematic flight planning for determination of aeroelastic effects. It permits on-the-spot changes in planned flight conditions. It also accentuates the large changes in weight required to obtain significant changes in dynamic pressure to assure aeroelastic flight data which will be outside the area of experimental error of uncertainty.

6.4 Control Inputs

The method of analysis selected governs the control input. The magnitude and duration of the input influence the magnitude of the perturbation. In the case of an aerodynamic coefficient that is highly nonlinear with respect to an independent variable, different magnitudes of the perturbation may result in different magnitudes of the derivative of the coefficient in analyzing flight data. Thus, in comparing flight results with wind-tunnel data, it is essential that the wind-tunnel value of the derivative be based not only on the same trim condition but also on the same magnitude of perturbation as the flight data.

Where nonlinearity of the coefficients is not a factor and, in lieu of increase of instrument scale factor, larger perturbations of the independent variables are desired to provide more accurate readability of the records, larger control inputs or complex control inputs may be used. Figure 40 shows the increase in amplitudes of recorded quantities resulting from a change in control input.

6.5 Maneuvers

Maneuvers performed for determination of stability and control derivatives from flight data should be compatible with the requirements of the method of analysis to be

employed. Current practical methods of analysis, whether they involve approximate equations solving for individual derivatives or comprehensive techniques solving a number of derivatives, have limitations in their utility; as a result, different types of maneuvers are employed within the range of their individual limitations to obtain the derivatives. As a generality, it might be said that typical handling-quality maneuvers are employed in the determination of derivatives wherein analytical techniques are used. Included are longitudinal elevator-pulse maneuvers, pullups and push-overs, pullups and releases, rudder-pulse and aileron-pulse maneuvers, constant-heading sideslips, recovery from sideslip, and rudder-fixed rolls.

When flight maneuvers applicable to analytical technique for derivative determination are not available or usable, the airplane response to random inputs is analyzed to give limited stability data. This is accomplished effectively with the aid of an analog computer, using a technique involving the matching of analog and flight time histories.

6.5.1 Pulse Maneuvers

The simple pulse maneuver, shown in Figure 41 for a longitudinal perturbation, is the current mainstay for derivative determination. Normally, for this maneuver the airplane is trimmed at the desired angle-of-attack, altitude, and Mach number, and a free oscillation is initiated by an abrupt pulse – an elevator pulse for longitudinal oscillation, a rudder or aileron pulse for lateral-directional oscillations. The resulting free-oscillation of the aircraft is allowed to damp out with the controls held fixed at the initial trim setting. With an irreversible control system, this is easily accomplished by releasing the controls. On tailless aircraft, even small inadvertent control inputs during the free oscillation can significantly affect the damping and, hence, the damping derivatives. Moderate inadvertent control inputs can affect the period of oscillation, as well as the damping, and then influence the static derivative results as well.

Free oscillations are also initiated by release of controls at the end of a sideslip maneuver and at the end of pullup and push-over maneuvers.

In investigating the effects of angle of attack and load factor when utilizing the pulse maneuver in an elevated g turn, the application of the pulse technique is limited by the difficulty of performing a good maneuver. Difficulty has been experienced during the maneuver in holding the proper bank angle to maintain constant load factor and Mach number. With a conventional control system, exceptional piloting skill is required to maintain fixed control during the airplane oscillations at elevated g . The use of the airplane damper as a device for applying a known deflection signal to excite the desired unaugmented oscillations (Fig. 42) offers a means of improving the quality of the data for elevated g conditions as well as 1g conditions.

In well-performed pulse maneuvers and lightly damped oscillations, it is possible to determine a 2-second period to within 0.02 second. Good accuracy in damping can be measured for damping ratios less than 0.2. The accuracy of period and damping measurements becomes rather poor for damping ratios greater than about 0.3.

6.5.2 *Constant-Heading Sideslip Maneuvers*

In the absence of pertinent and applicable pulse-maneuver data or in an effort to complement such data, the constant-heading sideslip maneuver can be used to determine the weathercock and effective dihedral derivatives C_{n_β} and C_{l_β}, provided control-effectiveness derivatives are available from other maneuvers.

Because of frequent loose usage of terminology, the expression "steady sideslip" is used when "constant-heading sideslip" is meant. Actually, a sideslip can be accomplished, as shown in Figure 43, as a wings-level sideslip in which yaw rate and, hence, a changing heading is involved, as a constant-heading sideslip in which a constant linear flight path is maintained ($r = \dot{r} = 0$), or as a combination of these two variations of sideslipping maneuvers. The distinctions in the variation of the sideslip maneuver affect the parameters involved in the analysis of the flight data and the format of the equations employed.

It is difficult to perform the sideslip maneuver as a steadily increasing sideslip at a constant heading without experiencing angular rate and acceleration transients. A more successful approach to the maneuver is to increase the sideslip in increments in order to damp out the angular rates at each increment before proceeding to the next increment. Although this manner of accomplishing the maneuver involves more time, it is justified by the refinement and resulting usable data.

6.5.3 *Pullup and Push-Over Maneuver*

This maneuver, or any one of its variations, is intended primarily for handling-qualities investigations. However, the control-effectiveness parameter, $C_{m_{\delta_e}}$, can be mathematically determined from the initial phases of the maneuver. The maneuver is useful also in determining the other longitudinal derivatives by analog-matching techniques.

6.5.4 *Recovery-From-Sideslip Maneuver*

This maneuver has been valuable for determining lateral-directional derivatives by the analog-matching technique. Good conditioning is achieved by first reducing rudder input to half the value present at the end of a constant-heading sideslip and then releasing it. This maneuver is considered in more detail in Section 7.8.4.

6.5.5 *Elevated-g Turn Maneuver*

The use of this maneuver in derivative determination was discussed in Section 6.5.1.

6.5.6 *Roll Maneuver (Rudder-Fixed)*

This maneuver lends itself to the determination of C_{l_p} and $C_{l_{\delta_a}}$, even though it is primarily a handling-qualities maneuver. In its execution, the roll is initiated by an abrupt aileron step input. The initial phase of the maneuver, up to maximum roll rate, is the useful portion for derivative analysis. The initial phase involves negligible sideslip, an essential factor in its utility for derivative analysis.

6.6 General Comments

The maneuvers discussed constitute those commonly used in mathematical analysis of flight data for derivative determination wherein approximate expressions for determining individual derivatives or a more comprehensive technique, such as the graphical time-vector method, is employed. Many of the approximate expressions and the time-vector method are dependent upon control-fixed free-oscillation data which are not usable when damping is high, thus leaving a vacuum for mathematical analysis of suitable data. Least squaring of the equations of motion has not been too successful, inasmuch as proper conditioning of the motions is difficult to establish and the requisite accuracy of the recorded data appears to be lacking. In the absence of suitable mathematical techniques, recourse is made to analog matching of higher damped oscillations and response to random inputs.

At times, it is desirable to perform maneuvers for power-off as well as power-on conditions to investigate the influence of inflow effects of jet exhausts and possibly other jet-exhaust effects. This may not be operationally feasible for jet engines. Jet-exhaust effects of rocket-engine aircraft have been studied by performing free-oscillation maneuvers just prior to and immediately following power cutoff. Only limited ranges of the records were usable for the power-off oscillations because of the decelerations and changes in altitude.

The analysis of data of a complete flight program for the determination of stability derivatives can be tedious and exacting. The number of computations necessary for an effective analysis of the data makes it apparent that systematic procedures are helpful. Tabulation forms, such as shown in Table VIII, that include many pertinent flight quantities have proved to be helpful.

7. ANALYSIS OF FLIGHT DATA

Of the many methods proposed for determination of stability and control derivatives, only a few are practical for a relatively rapid determination of the derivatives using approximate equations. The limitations of these equations must be known in order to avoid improper applications. Of the more comprehensive techniques of analysis proposed, the graphical time-vector method appears to be the most practical and provides reliable results within the limits of its applications. When analytical techniques are not applicable, analog matching of flight data has proven to be a practical technique for determining derivatives from flight data. In the following sections, the preceding techniques are discussed at some length. Comments on other detailed methods are also included.

Inasmuch as flight-test instruments are referenced to the body-fixed axes, the derivatives are considered with respect to these axes. Conversion of the derivatives from the body to the stability system of axes, if required, is accomplished by the equations listed in Section 2.2.

7.1 Fundamentals of the Time-Vector Approach

Inasmuch as some of the approximate equations are based on time-vector considerations, it is opportune to briefly discuss time-vector properties. Time-vector methods of analysis make use of the time-invariance of the amplitude and phase relations between

the degrees of freedom of an exponentially damped sinusoidal oscillating system (second-order linear system) and the differential and integrals of the degrees of freedom to determine the values of these amplitude and phase relations, or to determine the constants of the system of equations.

Consider the damped, transient, sinusoidal, small-perturbation oscillation of the rolling degree of freedom. This simple system is described by

$$\Delta\dot{p} + 2\zeta\omega_n\Delta p + \omega_n^2\Delta\phi' = 0 \ . \tag{113}$$

The solution to this equation is

$$\Delta\phi' = |\Delta\phi'|e^{-\zeta\omega_n t}\cos\omega_{n_d}t \ , \tag{114}$$

where

$$\omega_{n_d} = \omega_n\sqrt{(1-\zeta^2)} \ . \tag{115}$$

Differentiating with respect to time t ,

$$\left.\begin{aligned}\Delta p &= |\Delta\phi'|\omega_n e^{-\zeta\omega_n t}\left[\zeta\cos(\omega_{n_d}t+\pi) + \sqrt{(1-\zeta^2)}\cos\left(\omega_{n_d}t+\frac{\pi}{2}\right)\right] \\ &= |\Delta\phi'|\omega_n e^{-\zeta\omega_n t}\cos\left(\omega_{n_d}t+\frac{\pi}{2}+\Phi_d\right) \ ,\end{aligned}\right\} \tag{116}$$

where Φ_d is the damping angle

$$\Phi_d = \tan^{-1}\frac{\zeta}{\sqrt{(1-\zeta^2)}} \ . \tag{117}$$

Similarly

$$\Delta\dot{p} = |\Delta\phi'|\omega_n^2 e^{-\zeta\omega_n t}\cos(\omega_{n_d}t+\pi+2\Phi_d) \ . \tag{118}$$

Equations (114), (116), and (118) show that the amplitudes of these equations shrink at the same rate and the phase relationship between the amplitudes is time invariant. The amplitudes of the first and second derivatives of $\Delta\phi'$ are equal to the amplitude of $\Delta\phi'$ multiplied by the undamped natural frequency, ω_n , and by ω_n^2 , respectively. The phase of the derivatives is a function of the damping angle, Φ_d , which is a function of the damping ratio, ζ . As shown in Figure 44, velocity vector $\overrightarrow{\Delta p}$ leads the displacement vector $\overrightarrow{\Delta\phi'}$ by $(90 + \Phi_d)$, and the acceleration vector $\overrightarrow{\Delta\dot{p}}$ leads the displacement vector $(180 + 2\Phi_d)$.

Where more than one degree of freedom is involved in the damped, sinusoidal, transient oscillation system, and the frequency is common to all the freedoms involved, the instantaneous absolute values of the rotating vectors may be considered as ratios (referred to as amplitude ratios) and the phase relations of the ratios established. These ratios of the rotating vectors and their corresponding phase angles are time invariant. As a result, the instantaneous value of any one degree of freedom may be readily determined if the characteristics of any one of the motions are known and

the amplitude ratio and phase angle relative to the characteristic motion are known. For example, if the known characteristic motion is

$$\Delta r = \Delta r\, e^{-\zeta\omega_n t} \cos(\omega_{n_d} t) \tag{119}$$

and, if $|\Delta\beta|/|\Delta r|$, $|\Delta p|/|\Delta r|$, $\Phi_{\beta r}$, and Φ_{pr} are known, then

$$\beta = \left(\frac{|\Delta\beta|}{|\Delta r|}\right) |\Delta r| e^{-\zeta\omega_n t} \cos(\omega_{n_d} t + \Phi_{\beta r}) \tag{120}$$

$$p = \left(\frac{|\Delta p|}{|\Delta r|}\right) |\Delta r| e^{-\zeta\omega_n t} \cos(\omega_{n_d} t + \Phi_{pr}) \ . \tag{121}$$

The time invariance of the amplitude ratios and their phase angles permits the representation of any one of the linearized equations of motion by vectors. For example, by substituting Equations (119), (120), and (121) and the differentials of Equations (119) and (121) into the linearized, small-perturbation, rolling-moment equation, the following format is obtained, using the Δr vector as the reference for the amplitude ratios and phase angles

$$\frac{I_x}{\bar{q}Sb}\frac{|\Delta\dot{p}|}{|\Delta r|}\angle\Phi_{\dot{p}r} - \frac{I_{xz}}{\bar{q}Sb}\frac{|\Delta\dot{r}|}{|\Delta r|}\angle\Phi_{\dot{r}r} - C_{l_p}\frac{|\Delta p|}{|\Delta r|}\frac{b}{2V}\angle\Phi_{pr} - (C_{l_r} - C_{l_{\dot{\beta}}})\frac{|\Delta r|}{|\Delta r|}\frac{b}{2V}\angle\Phi_{rr} = 0 \ , \tag{122}$$

where

$$\frac{|\Delta\dot{p}|}{|\Delta r|} = \omega_n \frac{|\Delta p|}{|\Delta r|} \ , \qquad \frac{|\Delta\dot{r}|}{|\Delta r|} = \omega_n \ , \qquad \frac{|\Delta r|}{|\Delta r|} = 1 \ , \qquad \text{and} \qquad \Phi_{rr} = 0 \ . \tag{123}$$

The vector properties described, plus the requirement that the vector polygon representing any one equation must close, make possible the determination of two unknown derivatives in any one equation. The accuracy with which the unknown derivatives are determined is dependent not only on the accuracy of the amplitude ratios used but also on the accuracy of the phase angle and the sensitivity of the unknown derivative to small errors in the phase angles.

It should be noted that the introduction of cross-coupling terms into the equations of motion would result in nonlinear equations and, hence, time-variant relations of the cross-coupling terms relative to the other terms.

7.2 Basic Flight Data

Application of many of the simpler equations for determining derivatives requires an evaluation of the period and damping; whereas, application of the time-vector method requires, in addition, the determination of amplitude and phase relationships. These quantities are obtained from the free-oscillation portion of the pulse maneuver, as illustrated in Figure 45. The spacing of the peaks of the oscillatory motions determines the damped natural period, and a comparison of these peaks for the different oscillatory quantities determines their phase relationship. Determination of the

phase relationships by an averaging process, typified by the table in Figure 45, has provided more consistent data than obtained by single readings. The first line of the example table lists the time of occurrence of consecutive plus and minus peaks of the roll rate Δp . Similarly, the second line lists the plus and minus peaks of the yaw rate Δr . The third line lists the time difference of the first two lines in each column. Since the yaw rate Δr is the reference in this instance, the signs in the third line indicate that the roll rate Δp lags the yaw rate Δr . The values in the third line are averaged and converted to degrees.

It will be noticed in Figure 45 that a yawing divergence is evident in the yaw-rate record. To isolate the oscillatory motions and determine the time to damp the oscillations, exponential curves are drawn as shown. A semilog plot of the double amplitudes included between the exponential outlines of each motion versus time establishes the time to damp of the oscillations (Fig. 46). A comparison of the plotted double amplitudes of the variables determines the amplitude ratios.

As stated earlier, accuracy of measuring period and damping becomes rather poor for damping ratios greater than about 0.3. Generally, configurations tested at moderate and high altitudes and without damper augmentation have been rather lightly damped so that free-oscillation methods of analysis can be applied with good accuracy.

The damping ratio ζ , damping angle Φ_d , and the undamped natural frequency ω_n , are obtained, for both short-period and phugoid free-oscillations, from the following relations:

$$\zeta = \sin\left[\tan^{-1}\left(\frac{0.693P}{2\pi T_{1/2}}\right)\right] \tag{124}$$

$$\Phi_d = \tan^{-1}\left(\frac{0.693P}{2\pi T_{1/2}}\right) \tag{125}$$

$$\omega_n^2 = \omega_{n_d}^2 + \omega_n^2\zeta^2 = \left(\frac{2\pi}{P}\right)^2 + \left(\frac{0.693}{T_{1/2}}\right)^2 . \tag{126}$$

7.3 Determination of α and β From Free Oscillations in the Absence of or Questionable α and β Data

7.3.1 Longitudinal Free Oscillations

Should the α records be unavailable or questionable in free-oscillation longitudinal data and the pitch-rate records available, $|\Delta\alpha|/|\Delta q|$ and $\Phi_{\alpha q}$ may be obtained by using time-vector techniques. Once these quantities are determined, it is a simple matter to plot α as a function of time or, of more immediate concern, to determine $|\Delta a_n|/|\Delta\alpha|$ for use in determining C_{N_α} .

The complete procedure for determining $|\Delta\alpha|/|\Delta q|$, $\Phi_{\alpha q}$, and $|\Delta a_n|/|\Delta\alpha|$ is shown in Figure 47. The procedure involves the application of the following linearized auxiliary equation to correct the sensed normal acceleration, a_{n_i} , to the center of

gravity of the aircraft, as shown in Figure 47(a),

$$\frac{\Delta a_n}{\Delta q} \angle \Phi_{a_n q} = \frac{|\Delta a_{n_i}|}{|\Delta q|} \angle \Phi_{a_{n_i} q} - \frac{x}{g} \frac{|\Delta \dot{q}|}{|\Delta q|} \angle \Phi_{\dot{q} q} \tag{127}$$

and the vector application of Equation (56b) (Table V) in Figure 47(b) in the format

$$\frac{|\Delta a_n|}{|\Delta q|} \angle \Phi_{a_n q} - \frac{V}{g} \frac{|\Delta q|}{|\Delta q|} \angle \Phi_{q q} + \frac{V}{g} \frac{|\Delta \dot{\alpha}|}{|\Delta q|} \angle \Phi_{\dot{\alpha} q} = 0 \tag{128}$$

to solve for $\Phi_{\alpha q}$ and

$$\frac{|\Delta \alpha|}{|\Delta q|} = \frac{\frac{V}{g} \frac{|\Delta \dot{\alpha}|}{|\Delta q|}}{\omega_n \frac{V}{g}} , \tag{129}$$

which now permits the determination

$$\frac{|\Delta a_n|}{|\Delta \alpha|} = \frac{\frac{|\Delta a_n|}{|\Delta q|}}{\frac{|\Delta \alpha|}{|\Delta q|}} . \tag{130}$$

When the vector quantities Δa_{n_i} and Δa_n are approximately in phase and $\Delta \dot{q}$ is approximately 90^o out of phase with Δa_n, which is usually the case, the vector Equation (127) may be solved by the simple algebraic format

$$\frac{|\Delta a_n|}{|\Delta q|} \simeq \frac{|\Delta a_{n_i}|}{|\Delta q|} + \frac{x}{g} \omega_n . \tag{131}$$

7.3.2 Lateral-Directional Free Oscillations

Should the β records be unavailable or questionable in free-oscillation lateral-directional data, and yaw-rate records available, $|\Delta\beta|/|\Delta r|$ and $\Phi_{\beta r}$ may be obtained by using a vector solution of the following linearized auxiliary equation to correct the transverse accelerometer record to the center of gravity of the aircraft,

$$\frac{|\Delta a_t|}{|\Delta r|} \angle \Phi_{a_t r} = \frac{|\Delta a_{t_i}|}{|\Delta r|} \angle \Phi_{a_{t_i} r} - \frac{x}{g} \frac{|\Delta \dot{r}|}{|\Delta r|} \angle \Phi_{\dot{r} r} + \frac{z}{g} \frac{|\Delta \dot{p}|}{|\Delta r|} \angle \Phi_{\dot{p} r} , \tag{132}$$

and the application of equation (59) in the format

$$-2\tau \frac{|\Delta \dot{\beta}|}{|\Delta r|} \angle \Phi_{\dot{\beta} r} = 2\tau \frac{|\Delta r|}{|\Delta r|} \angle \Phi_{r r} - 2\tau\alpha \frac{|\Delta p|}{|\Delta r|} \angle \Phi_{p r} - C_L \sin\theta \frac{|\Delta \psi'|}{|\Delta r|} \angle \Phi_{\psi' r} -$$

$$- C_L \cos\theta \cos\phi \frac{|\Delta \phi'|}{|\Delta r|} \angle \Phi_{\phi' r} - C_L \frac{|\Delta a_t|}{|\Delta r|} \angle \Phi_{a_t r} , \tag{133}$$

where

$$\frac{|\Delta\dot{r}|}{|\Delta r|} = \omega_n , \qquad \Phi_{rr} = 0 ,$$

and

$$\frac{|\Delta\dot{\beta}|}{|\Delta r|} = \frac{1}{\omega_n}\frac{|\Delta r|}{|\Delta r|} = \frac{1}{\omega_n} , \qquad \Phi_{\dot{\beta}r} = \Phi_{rr} - (90 + \Phi_d) = -(90 + \Phi_d) .$$

Figure 48 shows the application of Equations (132) and (133) to the determination of $|\Delta\beta|/|\Delta r|$, $\Phi_{\beta r}$, and $|\Delta a_t|/|\Delta\beta|$. Upon solving for $|\Delta\beta|/|\Delta r|$ and $\Phi_{\beta r}$ from the graphical solution of Equation (133), it is a simple matter to obtain parameters with β as a base, for example

$$\frac{\Delta p}{\Delta\beta} = \frac{|\Delta p|}{|\Delta r|}\frac{|\Delta r|}{|\Delta\beta|} \qquad \text{and} \qquad \Phi_{p\beta} = \Phi_{pr} - \Phi_{\beta r} .$$

7.4 Equations for Longitudinal Control and Stability Derivatives

The nature of the input and the ensuing free oscillations of the longitudinal-pulse maneuver permit the use of relatively simple methods of analysis in determining longitudinal control and stability derivatives. These methods give results comparable to those from the more complicated methods investigated. Only the simple methods are discussed at this time and only data from these methods are presented. Unless otherwise stated, it is to be assumed that stability augmentation systems are not operational during the maneuver and that the aircraft behaves similarly to a rigid structure, in that its behavior can be represented by the linearized small-perturbation equations.

7.4.1 Control-Effectiveness Derivative, $C_{m_{\delta_e}}$

The control-effectiveness derivatives are determined from the initial portion, approximately 0.2 second, of a rapid pulse maneuver (Fig.49). During this part of the maneuver, the airplane response is almost entirely pitch acceleration, with the result that the pitch control-effectiveness derivative can be determined from

$$C_{m_{\delta_e}} = \frac{I_y}{\bar{q}S\bar{c}}\frac{\Delta\dot{q}}{\Delta\delta_e} . \tag{134}$$

In similar fashion, the change in normal-force coefficient due to elevator deflection can be determined from

$$C_{N_{\delta_e}} = \frac{W}{\bar{q}S}\frac{\Delta a_n}{\Delta\delta_e} . \tag{135}$$

With the preceding restriction in mind, it is desirable, for accuracy, to read the peak control input and acceleration response with a disregard of the phase lag between the two, as shown in Figure 49. It has been found that the time difference in peak values of control input and acceleration response is primarily the result of instrument

phase lag and, to a lesser extent, air-mass inertia effects. Analysis by this method requires instruments with flat response characteristics extending to relatively high frequencies (8 c/s).

Pulses applied at slower rates, and thus extending over a longer time interval, may require inclusion of damping and angle-of-attack terms in the equation, especially α. This may necessitate the inclusion of instrument phase-lag corrections for q and α.

7.4.2 Slope of the Normal-Force-Coefficient Curve

From the short-period free-oscillation data of the airplane with the controls fixed, the variation of the normal-force coefficient with angle of attack may be evaluated from

$$C_{N_\alpha} \simeq \frac{W}{\bar{q}S} \frac{|\Delta a_n|}{|\Delta\alpha|} = C_L \cdot \frac{|\Delta a_n|}{|\Delta\alpha|} . \qquad (136)$$

This expression neglects the pitching-velocity and angle-of-attack-rate terms of the short-period form of the normal-force equation (Equation (58), Table V). These terms have been found to be negligible, as will be noticed in the typical vector diagram (Fig. 50) of the vector form of this equation wherein the pitch rate was used as the base of the amplitude ratios.

In instances where "free-oscillation data" have inadvertent inputs of the elevator and the angle-of-attack data have been ascertained as reliable, C_{N_α} may be determined by selecting those portions of the time history in which the elevator is at its steady-state position and plotting a_n versus α for a number of data points which encompass the range of a_n on the records. The slope of the plotted points is $|\Delta a_n|/|\Delta\alpha|$. This fundamental technique, which involves some labor, may still be the simplest technique where a control-fixed free oscillation is heavily damped and thus precludes the determination of $|\Delta a_n|/|\Delta\alpha|$ by other means.

The derivative C_{N_α} may be converted to the effective lift-curve slope, C_{L_α}, which includes the contribution of power, by using Equation (38). The inclusion or exclusion of the power term depends upon the influence of power. For conventional low-performance aircraft, $\bar{C}_{L_\alpha} \simeq C_{N_\alpha}$ at small angles-of-attack.

7.4.3. The Derivative $(C_{N_q} + C_{N_{\dot\alpha}})$

As explained in Section 3.4, the phenomenon involving $\dot\alpha$ is different from that involving q. The pairing of the derivatives as $(C_{N_q} + C_{N_{\dot\alpha}})$ is valid only for longitudinal small-perturbation, free-oscillation maneuvers. In this maneuver, Δq and $\Delta\dot\alpha$ vectors are approximately in phase and $|\Delta\dot\alpha|/|\Delta q| \simeq 1$, thus permitting the pairing. Determination of the individual derivatives C_{N_q} and $C_{N_{\dot\alpha}}$ has thus far defied solution.

The determination of $(C_{N_q} + C_{N_{\dot\alpha}})$ itself is difficult. It may be readily deduced from the vector diagram (Fig. 50) of the following vector form of the short-period mode of Equation (58),

$$C_L \frac{|\Delta a_n|}{|\Delta q|} \angle\Phi_{a_n q} + C_{N_\alpha} \frac{|\Delta\alpha|}{|\Delta q|} \angle\Phi_{\alpha q} + (C_{N_q} + C_{N_{\dot\alpha}}) \frac{|\Delta q|}{|\Delta q|} \frac{\bar c}{2V} \angle\Phi_{qq} = 0 , \qquad (137)$$

that

$$(C_{N_q} \quad {}_N\dot\alpha) \simeq \frac{\left(C_{N_\alpha} \frac{\Delta\alpha}{\Delta q}\right) \Phi_{a_n q}}{\frac{|\Delta q|}{|\Delta q|} \frac{\bar c}{2V}} \simeq \frac{2V\, C_{N_\alpha}}{\omega_n \bar c} \Phi_{a_n q} . \qquad (138)$$

The individual quantities in Equation (138) show that the degree of success in determining $(C_{N_q} + C_{N_{\dot\alpha}})$ is dependent upon the accuracy with which $\Phi_{a_n\alpha}$ is determined. This phase angle is small, of the order of a few degrees, and, even with the best records and instrumentation, the error in readability of $\Phi_{a_n q}$ from the records could be of the order of the angle itself. Thus, it is very difficult to determine this derivative to a reasonable degree of accuracy.

7.4.4 Pitching-Moment Static Stability and Damping Derivatives, C_{m_α} and $(C_{m_{\dot q}} + C_{m_{\dot\alpha}})$

The equations for the pitching-moment stability derivatives are based on the normal-force equation

$$mu\Delta q - m\Delta\dot w \simeq C_{N_\alpha} \bar q S \Delta\alpha \qquad (139)$$

obtained from the short-period form of Equations (56b) and (58b) and on the short-period form of the pitching-moment equation (Equation (58c))

$$I_y \Delta\dot q = \left(C_{m_\alpha}\Delta\alpha + C_{m_q}\Delta q \frac{\bar c}{2V} + C_{m_{\dot\alpha}}\Delta\dot\alpha \frac{\bar c}{2V}\right) \bar q S \bar c .$$

Differentiating Equation (139) with respect to time and substituting for $\Delta\dot q$ and Δq in Equation (58c) provides the following

$$\Delta\ddot\alpha + \frac{1}{2\tau}\left[C_{N_\alpha} - \frac{m\bar c^2}{2I_y}\left(C_{m_q} + C_{m_{\dot\alpha}}\right)\right]\Delta\dot\alpha - \left[C_{m_\alpha} + \frac{C_{m_q} C_{N_\alpha}}{4\mu_c}\right]\frac{\bar q S \bar c}{I_y}\Delta\alpha = 0 . \qquad (140)$$

Since (140) is a second-order linear differential equation of the form

$$\Delta\ddot\alpha + 2\zeta\omega_n\Delta\dot\alpha + \omega_n^2\Delta\alpha = 0 , \qquad (141)$$

then

$$C_{m_\alpha} = -\frac{I_y}{\bar q S \bar c}\omega_n^2 - \frac{1}{4\mu_c} C_{m_q} C_{N_\alpha} \simeq -\frac{I_y}{\bar q S \bar c}\omega_n^2 \qquad (142)$$

and

$$\left.\begin{aligned}(C_{m_q} + C_{m_{\dot{\alpha}}}) &= \frac{2I_y}{m\bar{c}^2}\left[C_{N_\alpha} - 4\tau\zeta\omega_n\right] \\ &= \frac{2I_y}{m\bar{c}^2}\left[C_{N_\alpha} - 4\tau\left(\frac{0.693}{T_{1/2}}\right)\right] .\end{aligned}\right\} \tag{143}$$

The approximate form of the C_{m_α} equation (Equation (142)), in which the term $C_{m_q}\ (C_{N_\alpha}/4\mu_c)$ is omitted, results in a small error of the order of 3% or less.

Attempts to determine C_{m_q} and $C_{m_{\dot{\alpha}}}$ as individual quantities required a precision of flight data and analysis of these data that is difficult to achieve. The difficulty arises primarily from the acuteness of the phase angle, $\Phi_{\dot{\alpha}q}$, which is generally of the order of a few degrees; an error of 1^o in this phase angle can result in large errors in the solution.

7.4.5 The Phugoid Static Stability and Damping Derivatives C_{c_u} *and* C_{N_u}

Unlike the short-period mode of oscillation in which the velocity is essentially non-variant and the angle of attack is variant, the long-period (phugoid) mode of oscillation involves velocity perturbations and essentially constant angle-of-attack. This implies that any variations in aerodynamic forces during the phugoid are primarily the result of perturbations of the normal and axial forces due to the velocity perturbations, that is to say that $\bar{C}_{c_u}$ and $\bar{C}_{N_u}$ in Equations (58a) and (58b) are the only derivatives of concern.

Upon dividing Equations (56a) and (56b) by V and substituting these equations for Δa_x and Δa_n in Equations (58a) and (58b), respectively, and neglecting second-order effects, the following approximate expressions are obtained for a phugoid initiated from steady-state horizontal flight:

$$\Delta\dot{u} + \bar{C}_{c_u}\frac{\bar{q}S}{mV}\Delta u + \frac{g}{V}\Delta\theta' = 0 \tag{144}$$

and

$$-\bar{C}_{N_u}\frac{\bar{q}S}{mV}\Delta u + \Delta q = 0 . \tag{145}$$

The characteristic equation of the phugoid described by these two equations is a second-order linear differential equation which takes the Laplace form

$$s^2 + \left(\bar{C}_{c_u}\frac{\bar{q}S}{mV}\right)s + \frac{g}{V}\left(\bar{C}_{N_u}\frac{\bar{q}S}{mV}\right) = 0 . \tag{146}$$

It is readily recognized that

$$\bar{C}_{c_u}\frac{\bar{q}S}{mV} = 2\zeta_{ph}\omega_{n_{ph}} \tag{147}$$

and

$$\bar{C}_{N_u} \frac{g\bar{q}S}{mV^2} = \omega_{n_{ph}}^2 \quad . \tag{148}$$

Transposing these two equations results in the following approximate equations for determining $\bar{C}_{N_u}$ and $\bar{C}_{c_u}$ from flight data

$$\bar{C}_{N_u} \simeq \frac{2m\omega_{n_{ph}}}{\rho gS} \tag{149}$$

and

$$\bar{C}_{c_u} \simeq \frac{2mV\zeta_{ph}\omega_{n_{ph}}}{\bar{q}S} = \frac{2m\zeta_{ph}\omega_{n_{ph}}}{\rho VS} \quad . \tag{150}$$

The flight values of ζ_{ph} and $\omega_{n_{ph}}$ are determined from the phugoid oscillations in accordance with Equations (124) and (126).

An interesting byproduct of this brief consideration of the phugoid parameters suggests itself. If C_{N_u} can be considered to be similar to $2C_N$, then Equation (148) takes on the approximate form

$$\omega_{n_{ph}} \simeq \frac{g}{V}\sqrt{\left(\frac{2C_N\bar{q}S}{W}\right)} = \frac{g}{V}\sqrt{2} \quad . \tag{151}$$

Thus, the phugoid frequency, $\omega_{n_{ph}}$, is approximately a function of velocity, V, only.

7.4.6 Corrections for Effects of Stability Augmentation System in Determining Derivatives from Short-Period Oscillations

In performing a pulse maneuver with the stability augmentation system engaged, the ensuing transient short-period oscillation of the aircraft will be characterized by a period of oscillation and a damping ratio which will be different from those obtained with the pitch stability augmentation system off (Fig.51). With the system on, the period will decrease with increasing damping provided by the system; whereas, normally, the period increases with increase in inherent unaugmented damping. This is due to the system gain and the time constant. Thus, the gain and time constant are factors to be considered in equations for determining the stability derivatives, as is brought out in Reference 42. The subsequent discussion is based on this reference.

The following procedure for determining C_{m_α} and $(C_{m_q} + C_{m_{\dot{\alpha}}})$ from flight data which includes stability augmentation effects has been useful but is of limited utility. The principal value of the ensuing discussion is the insight gained into the complications which may be encountered in data which include stability augmentation effects. For rigid-aircraft perturbations about a mean flight path, the Laplace transformed short-period mode two-degree-of-freedom longitudinal equations of motion may be represented in approximate, but practical, form as

$$(s - \bar{M}_q)\Delta q + (-\bar{M}_{\dot{\alpha}}s - \bar{M}_\alpha)\Delta\alpha = \bar{M}_{\delta_e}\Delta\delta_e \tag{152}$$

$$-\Delta q + (s - \bar{Z}_\alpha)\Delta\alpha = \bar{Z}_{\delta_e}\Delta\delta_e \quad . \tag{153}$$

In the absence of pilot input, the transfer function for a damper with a first-order time lag may be represented by

$$\frac{\Delta\delta_e(s)}{\Delta q(s)} = \frac{k}{1 + \tau' s} \simeq k(1 - \tau' s) \ . \tag{154}$$

Substituting Equation (154) into Equations (152) and (153) results in the following determinant

$$\begin{vmatrix} \left[(1 + \bar{M}_{\delta_e} k\tau')s + (-\bar{M}_q - \bar{M}_{\delta_e} k)\right] & (-\bar{M}_{\dot{\alpha}} s - \bar{M}_\alpha) \\ \left[(\bar{Z}_{\delta_e} k\tau')s + (-1 - \bar{Z}_{\delta_e} k)\right] & (s - \bar{Z}_\alpha) \end{vmatrix} = 0 \ , \tag{155}$$

whose characteristic equation is

$$\begin{aligned} &(1 + M_{\delta_e} k\tau' + M_{\dot{\alpha}} Z_{\delta_e} k\tau')s^2 + \\ &\quad + \left[-\bar{Z}_\alpha - \bar{M}_q - \bar{M}_{\dot{\alpha}} - \bar{M}_{\delta_e} k - \bar{Z}_\alpha \bar{M}_{\delta_e} k\tau' - (\bar{M}_{\dot{\alpha}} - \bar{M}_\alpha)\bar{Z}_{\delta_e} k\right] s + \\ &\quad + (-\bar{M}_\alpha + \bar{Z}_\alpha \bar{M}_q + \bar{Z}_\alpha \bar{M}_{\delta_e} k - \bar{M}_\alpha \bar{Z}_{\delta_e} k) = 0 \ . \end{aligned} \tag{156}$$

Considering only those terms in Equation (156) which thus far have been shown to be significant, the short-period longitudinal frequency and damping of the aircraft with a first-order time-lag pitch damper are

$$(\omega_n')^2 \simeq \frac{-\bar{M}_\alpha}{1 + \bar{M}_{\delta_e} k\tau'} \tag{157}$$

$$2\zeta'\omega_n' \simeq \frac{-(\bar{Z}_\alpha + \bar{M}_q + \bar{M}_{\dot{\alpha}} + \bar{M}_{\delta_e} k)}{1 + \bar{M}_{\delta_e} k\tau'} \ . \tag{158}$$

Solving these equations for C_{m_α} and $(C_{m_q} + C_{m_{\dot{\alpha}}})$,

$$C_{m_\alpha} \simeq \left(\frac{I_y}{\bar{q}S\bar{c}} + C_{m_{\delta_e}} k\tau'\right)(\omega_n')^2 \tag{159}$$

$$(C_{m_q} + C_{m_{\dot{\alpha}}}) = \frac{2I_y}{m\bar{c}^2}\left[C_{N_\alpha} - 4\tau\left(\frac{0.693}{T'_{1/2}}\right)\left(1 + \bar{M}_q k\tau'\right) - \frac{mV\bar{c}}{I_y} kC_{m_{\delta_e}}\right] \ . \tag{160}$$

From the above, it is seen that C_{m_α} is readily determined for a first-order linear pitch-damper system. The determination of $(C_{m_q} + C_{m_{\dot{\alpha}}})$, on the other hand, may offer a problem, inasmuch as C_{m_q} in M_q is not readily determined by itself.

If the pitch-damper system is not a first-order linear system, which is the case for many systems, analytical solutions for C_{m_α} and $(C_{m_q} + C_{m_{\dot{\alpha}}})$ are impractical. In such instances, analog techniques are applied in attempts to extract these derivatives.

7.4.7 Representative Results

Typical time histories, the flight-determined period and damping ratios, and the flight-determined longitudinal stability derivatives of the D-558-II research airplane have been reproduced in Figures 52, 53, and 54 from Reference 43. Most of the data were obtained from the all-rocket-powered version of the airplane; the remainder of the data is based on the jet- and rocket-powered version.

These data have been used to illustrate representative results because they show the need for a concentration of flight test data in the transonic zone to establish the extent of any abrupt changes of the derivatives and to show the influence of altitude on this particular aircraft. Because the results did not include control effectiveness, Figure 55 shows representative data from Reference 42 for $C_{m_{\delta_e}}$. All data shown were obtained from wings-level pulse maneuvers and are typical of those that can be obtained from good flight techniques – which include control of flight variables, pilot skill, and instrumentation – and careful application of the methods of analysis discussed.

The maximum deviation from the faired value in the stability derivatives shown in Figure 54 is of the order of 5% for C_{N_α}, 10% for C_{m_α}, and 20% for $(C_{m_q} + C_{m_{\dot{\alpha}}})$; deviation of this order of magnitude occur in only a minor portion of the data analyzed. The maximum deviation of $C_{m_{\delta_e}}$ in Figure 55 is difficult to assess because the data shown were obtained over a large range of altitudes and elevation trim settings; however, the maximum deviation from faired values would be of the order of 10%, which would be representative.

7.5 Equations for Lateral-Directional Stability and Control Derivatives

The lateral-directional control and stability derivatives are not as readily and reliably determined by the use of approximate equations as are the longitudinal derivatives, because of the more complex behavior of the airplane and the larger number of derivatives involved. In the following discussion, unless otherwise stated, it is again assumed that stability augmentation systems are not operational during the maneuver and that the aircraft's perturbed behavior can be represented by the linearized perturbation equations.

7.5.1 Control-Effectiveness Derivatives

The basic procedures for determining lateral and directional control effectiveness are similar to those previously discussed for longitudinal control effectiveness. However, the expressions for lateral-directional control effectiveness are complicated by the need to account for the possible influence of the inclination of the principal axis as well as the aerodynamic terms. Tests with a conventional high-performance airplane utilizing a rapid control pulse or step input showed that the directional control derivative, $C_{n_{\delta_r}}$, could be determined to good accuracy by considering only the inertia term. For example,

$$\left.\begin{aligned} C_{n_{\delta_r}} &= \left[\frac{I_z}{\bar{q}Sb}\Delta\dot{r} - \frac{I_{xz}}{\bar{q}Sb}\Delta\dot{p} - (C_{n_r} - C_{n_{\dot{\beta}}})\frac{b}{2V}\Delta r - C_{n_p}\frac{b}{2V}\Delta p - C_{n_\beta}\Delta\beta\right]\frac{1}{\delta_r} \\ 100 &= \quad 98 \quad - \quad 0 \quad + \quad 2 \quad - \quad 0 \quad - \quad 0 \quad , \end{aligned}\right\} \qquad (161)$$

where the magnitudes of the individual terms are given as percentages of the answer. This simplification in determining $C_{n_{\delta_r}}$ may not be applicable to other aircraft.

For the roll-control derivative, $C_{l_{\delta_a}}$, consideration must be given to the aerodynamic derivative terms. For example, using the same high-performance airplane and a rapid aileron control input,

$$\left.\begin{aligned} C_{l_{\delta_a}} &= \left[\frac{I_x}{\bar{q}Sb}\Delta\dot{p} - \frac{I_{xz}}{\bar{q}Sb}\Delta\dot{r} - C_{l_p}\frac{b}{2V}\Delta p - C_{l_r}\frac{b}{2V}\Delta r - C_{l_\beta}\Delta\beta\right]\frac{1}{\delta_a} \\ 100 &= \quad 73 \quad - \quad 4 \quad + \quad 31 \quad - \quad 0 \quad - \quad 0 \quad . \end{aligned}\right\} \tag{162}$$

The cross-control derivatives, $C_{n_{\delta_a}}$ and $C_{l_{\delta_r}}$, can be evaluated by using Equations (161) and (162), respectively. The cross-control derivatives are usually of smaller magnitude and are therefore more difficult to determine. It appears that all aerodynamic terms may require consideration, as shown in the following example of the analysis for $C_{n_{\delta_a}}$. The flight quantities were obtained from the records as shown in Figure 56. The time difference in the peaks of the control input and the accelerations is due to the phase lag of the instruments. The acceleration and angular-rate records have essentially the correct phase relationship with respect to each other in this instance. The magnitudes of the individual terms as percentages of the answer are

$$\left.\begin{aligned} C_{n_{\delta_a}} &= \left[\frac{I_z}{\bar{q}Sb}\Delta\dot{r} - \frac{I_{xz}}{\bar{q}Sb}\Delta\dot{p} - (C_{n_r} - C_{n_{\dot{\beta}}})\frac{b}{2V}\Delta r - C_{n_p}\frac{b}{2V}\Delta p - C_{n_\beta}\Delta\beta\right]\frac{1}{\delta_a} \\ 100 &= \quad 206 \quad - \quad 141 \quad + \quad 10 \quad + \quad 9 \quad + \quad 16 \quad . \end{aligned}\right\} \tag{163}$$

It will be noticed that the produce-of-inertia term is particularly significant in this example. An error in principal-axis inclination would significantly affect the answer. For instance, in this example an error of $1/4^\circ$ in the inclination of the principal axis (3°) would result in an error of 12% in $C_{n_{\delta_a}}$.

7.5.2 The Side-Force Derivative, C_{y_β}

This derivative, which contributes to the Dutch roll mode of oscillation and is an index of the pilot's ability to sense transverse accelerations, can be determined from the equation

$$C_{y_\beta} \simeq \frac{W}{\bar{q}S}\frac{|\Delta a_t|}{|\Delta\beta|} . \tag{164}$$

The ratio $|\Delta a_t|/|\Delta\beta|$ is obtained from the control-fixed transient oscillations resulting from a pulse maneuver. If the β record is suspect or missing, the ratio may be determined from the a_t and r records as explained in Section 7.3.2 and Figure 48. This indirect technique for obtaining $|\Delta a_t|/|\Delta\beta|$ is analogous to that for obtaining $|\Delta a_n|/|\Delta\alpha|$ and considers C_{y_p}, C_{y_r}, and C_{y_β} as negligible.

7.5.3 The Directional-Stability Derivative, C_{n_β}

The static directional-stability derivative is one of primary importance, and good accuracy is required in its measurement. Although a number of closed-form equations have been used, each possesses limitations which, if not recognized, can lead to erroneous answers. Several of the equations are based on various degrees of degradation of the following expression, the derivation of which was based on the solution of the determinant of the linearized lateral-directional small-perturbation equations (Equations (61a), (61b), and (61c)). The expression includes all but the most negligible quantities.

$$\left(1 - \frac{I_{xz}}{I_x} \sin\alpha\right) C_{n_\beta} = \frac{I_z}{\bar{q}Sb}\left[\omega_n^2 - (2\zeta\omega_n)^2 - 2\zeta\omega_n\left(\frac{\bar{q}S}{mV}\right) C_{y_\beta}\right] - \left[\frac{I_{xz}}{I_z} - \sin\alpha\right]\frac{I_z}{I_x} C_{l_\beta} -$$

$$- \frac{b}{2V}\left\{2\zeta\omega_n\left[\frac{I_z}{I_x}(C_{l_p} - C_{l_\beta}\sin\alpha) + (C_{n_r} - C_{n_{\dot\beta}})\right] + C_{l_p}(C_{n_r} - C_{n_{\dot\beta}})\frac{\bar{q}Sb}{I_x}\frac{b}{2V}\right\} -$$

$$- \frac{b}{2V}\left\{C_{y_\beta}\frac{\bar{q}S}{mV}\left(C_{n_r} + C_{l_p}\frac{I_z}{I_x}\right) - \frac{g\cos\theta}{V} C_{l_\beta} C_{n_r}\frac{\bar{q}Sb}{I_x\omega_n^2}\right\} . \qquad (165)$$

This equation shows that when C_{n_β} is small, that is, of the order of 0.08 per radian (0.0014 per deg) or less, the ordinarily insignificant damping terms become important. In such instances, C_{l_p} is particularly significant.

When C_{n_β} is of an order higher than 0.0014, Equation (165) can be reduced to the following workable equation

$$C_{n_\beta} \simeq \frac{I_z}{\bar{q}Sb}\omega_n^2 + \alpha\frac{I_z}{I_x} C_{l_\beta} - \frac{I_{xz}}{I_x} C_{l_\beta} . \qquad (166)$$

This expression can also be obtained by differentiating an approximate form of Equation (61a) to provide

$$\Delta\ddot\beta = -\Delta\dot r + \alpha\Delta\dot p + \frac{\bar{q}S}{mV} C_{y_\beta}\Delta\dot\beta$$

and also using Equations (61a) and (61c) with the assumption that C_{l_p}, C_{l_r}, $C_{l_{\dot\beta}}$, and C_{n_p} are all equal to zero. Substitutions result in the following linear differential equation,

$$\Delta\ddot\beta - \left[\frac{\bar{q}S}{mV} C_{y_\beta} - \frac{\bar{q}Sb^2}{2VI_z}(C_{n_r} - C_{n_{\dot\beta}})\right]\Delta\beta +$$

$$+ \left[\frac{\bar{q}Sb}{I_z} C_{n_\beta} - \alpha\frac{\bar{q}Sb}{I_x} C_{l_\beta} + \frac{I_{xz}}{I_xI_z} C_{l_\beta}\bar{q}Sb\right]\Delta\beta = 0 , \qquad (167)$$

in which the frequency term is identical to Equation (166).

The fact that C_{n_β} is a function of C_{l_β} in Equation (166) may result in questionable values of C_{n_β} if C_{l_β} is estimated from wind-tunnel data rather than flight data, especially when flexibility effects as well as other phenomena may appreciably alter the wind-tunnel values of C_{l_β} .

An approximation of Equation (166) provides the following simple expression, which is of limited utility:

$$C_{n_\beta} = \frac{I_z}{\bar{q}Sb} \omega_n^2 \quad . \tag{168}$$

The expression has been used successfully on occasions when angle-of-attack and dihedral effects were small. At low indicated airspeeds, where these effects are not small, the discrepancy can be 50% or more.

Values of C_{n_β} have also been obtained from constant-heading sideslip maneuvers using the expression

$$C_{n_\beta} = -(C_{n_{\delta_r}} \delta_{r_\beta} + C_{n_{\delta_a}} \delta_{a_\beta}) \quad . \tag{169}$$

This simple expression is obtained from Equations (61b) and (61c) with the stipulation that angular rates and accelerations are zero during the sideslip maneuver. The successful use of this equation is dependent upon the accurate determination of the apparent stability parameters δ_{r_β} and δ_{a_β} as well as the control-effectiveness derivatives. The results obtained from Equation (169) have shown a relatively poor consistency in the supersonic speed range, primarily because of the difficulty of obtaining sufficient sideslip angle at supersonic conditions to make accurate determination of the apparent stability parameters.

In instances where the influence of I_{xz} and C_{n_p} is negligible, an accurate equation for C_{n_β} , without the necessity of relying on C_{l_β} , has been derived from the yawing-moment equation

$$\frac{I_z}{\bar{q}Sb} \Delta\dot{r} - (C_{n_r} - C_{n_\beta}) \frac{b}{2V} \Delta r - C_{n_\beta} \Delta\beta = 0 \tag{170}$$

and the following expressions for a transient oscillatory sinusoidal motion:

$$\left.\begin{aligned}
\Delta\dot{r} &= \frac{|\Delta\dot{r}|}{|\Delta r|} |\Delta r| e^{-\zeta\omega_n t} \cos(\omega_{n_d} t + \Phi_{\dot{r}r}) = \omega_n |\Delta r| e^{-\zeta\omega_n t} \cos\left(\omega_{n_d} t + \frac{\pi}{2} + \Phi_d\right) \\
\Delta r &= |\Delta r| e^{-\zeta\omega_n t} \cos(\omega_{n_d} t + \Phi_{rr}) = |\Delta r| e^{-\zeta\omega_n t} \cos\omega_{n_d} t \\
\Delta\beta &= \frac{|\Delta\beta|}{|\Delta r|} |\Delta r| e^{-\zeta\omega_n t} \cos(\omega_{n_d} t + \Phi_{\beta r}) \quad .
\end{aligned}\right\} \tag{171}$$

Substituting expressions (171) into Equation (170), expanding by trigonometric identities, and regrouping results in

$$\left[-\frac{I_z}{\bar{q}Sb}\omega_n \cos\Phi_d + C_{n_\beta}\frac{|\Delta\beta|}{|\Delta r|}\sin\Phi_{\beta r}\right]\sin\omega_{n_d}t -$$

$$-\left[\frac{I_z}{\bar{q}Sb}\omega_n \sin\Phi_d + (C_{n_r} - C_{n_{\dot\beta}})\frac{b}{2V} + C_{n_\beta}\frac{|\Delta\beta|}{|\Delta r|}\cos\Phi_{\beta r}\right]\cos\omega_{n_d}t = 0 . \qquad (172)$$

The first bracketed quantity is a summation of components perpendicular to the Δr vector; the second is a summation of components parallel to the Δr vector. Hence

$$-\frac{I_z}{\bar{q}Sb}\omega_n \cos\Phi_d + C_{n_\beta}\frac{|\Delta\beta|}{|\Delta r|}\sin\Phi_{\beta r} = 0 \qquad (173)$$

and

$$\frac{I_z}{\bar{q}Sb}\omega_n \sin\Phi_d + (C_{n_r} - C_{n_{\dot\beta}})\frac{b}{2V} + C_{n_\beta}\frac{|\Delta\beta|}{|\Delta r|}\cos\Phi_{\beta r} = 0 . \qquad (174)$$

Considering only Equation (173) at this time, if the phase angle $\Phi_{\beta r}$ is of the order of 90° and the damping angle is small – which are the conditions normally encountered – then $\sin\Phi_{\beta r}$ and $\cos\Phi_d$ will each be similar to 1 and Equation (173) can be transposed to

$$C_{n_\beta} \simeq \frac{I_z}{\bar{q}Sb}\frac{|\Delta r|}{|\Delta\beta|}\omega_n . \qquad (185)$$

This equation provides accurate values of C_{n_β}, provided it is used within the limitations imposed in its derivation.

Table IX lists the results of the application of Equations (165), (166), and (168) to flight data of the F-104 and YF-102. The values of C_{n_β}, as determined by Equation (165), are used as reference values. For the F-104, Equation (156) shows good correlation with the reference value because of the high value of C_{n_β}, whereas the simple frequency equation (Equation (168)) shows poor agreement. For the YF-102, which has a low value of C_{n_β} for the flight condition shown, Equation (166) shows a significant discrepancy with reference C_{n_β} and points up the influence of the damping terms when C_{n_β} is small. For this same case, it will be observed that the simple frequency equation is unworkable.

A relative comparison of the results obtained for the F-100 airplane using Equations (166), (168), and (169) and the results obtained using the more comprehensive graphical time-vector method (to be discussed later) are shown in Figure 57. Considering the graphical time-vector results as most representative for the airplane, it will be observed that the simple frequency equation (Equation (168)) would show poorest correlation at low subsonic speeds due to angle-of-attack and dihedral effects not accounted for in the equation, whereas Equation (169) shows poorest results in the supersonic region because of the difficulty in obtaining accurate values of δ_{r_β} and δ_{a_β}.

Table X compares the values of C_{n_β} determined from analog matching of oscillatory maneuvers of the X-15 airplane with values of C_{n_β} determined from Equations (166) and (175). The values of I_{xz} and C_{n_p} are essentially equal to zero on this vehicle. The agreement between analog values of C_{n_β} and the equations is good. In Equation (166), the agreement is due to the high value of C_{n_β}. Equation (175) would be the more desirable to use on this airplane because it does not depend on the use of C_{l_β} for a solution.

7.5.4 The Effective Dihedral Derivative, C_{l_β}

Several simple equations for C_{l_β} are available with limitations on their utility, as in the case with most simplified equations.

Values of C_{l_β} can be obtained from the constant-heading sideslip maneuver using the expression

$$C_{l_\beta} = -(C_{l_{\delta_r}}\delta_{r_\beta} + C_{l_{\delta_a}}\delta_{a_\beta}) \quad . \tag{176}$$

The derivation of this expression and circumstances limiting its accuracy are identical to that brought out for its counterpart (Equation (169)).

A comparison of C_{l_β} determined by Equation (176) and the more comprehensive graphical time-vector method is shown in Figure 58 for the F-100 airplane. At low Mach numbers, the results from the sideslip equation (Equation (176)) compare favorably with the time-vector results; at high Mach numbers, a large discrepancy exists between the two methods. Even though C_{l_β} is not one of the derivatives determined most accurately by the time-vector method, the vector method is the most practical analytical means available for evaluating this derivative.

In instances where the influence of I_{xz} is negligible, it is possible to combine Equations (166) and (175) to obtain

$$C_{l_\beta} \simeq \frac{1}{\alpha}\frac{I_x\omega_n^2}{\bar{q}Sb}\left[\frac{|\Delta r|}{|\Delta\beta|}\frac{1}{\omega_n} - 1\right] \quad . \tag{177}$$

The use of this equation is subject to the additional restriction that it should not be used when C_{n_β} is small, as was noted in the discussion of Equation (166). Also, the equation must be used with caution when the angle-of-attack is less than about 3° or 4°. When the angle-of-attack is less, $(|\Delta r|/|\Delta\beta|)(1/\omega_n)$ may approach 1.0 and the error in reading $|\Delta r|/|\Delta\beta|$ from the flight records may result in an error in $(|\Delta r|/|\Delta\beta|)(1/\omega_n)$ that may exceed the net magnitude of the parenthesized quantity. If the β record is the major contributor to inaccuracy in the amplitude ratio, the technique discussed in Section 7.3.2 may be employed to determine the ratio without recourse to the actual β record.

A final precaution regarding the use of Equation (177) is in order. At very low angles-of-attack, the error in the flight-determined values of α can produce large errors in the equation; also, as α approaches zero, the equation approaches an indeterminate form, inasmuch as the bracketed quantity itself approaches zero.

7.5.5 The Damping-in-Roll Derivative, C_{l_p}

Simple expressions for the determination of C_{l_p} are dependent upon a roll maneuver initiated from wings-level flight by a step input of the ailerons. The derivations of the expressions impose the restrictions that yaw due to aileron, $C_{n_{\delta_a}}$, sideslip due to the effective dihedral, C_{l_β}, and product-of-inertia effect are negligible. If these highly restrictive conditions are satisfied, the following relation can be employed

$$C_{l_p} = -C_{l_{\delta_a}} \frac{\Delta\delta_a}{\Delta p_1 \frac{b}{2V}} . \tag{178}$$

In using this equation, $C_{l_{\delta_a}}$ can be determined from the initial part of the control input as discussed in Section 7.5.1 and Δp_1 is determined at some time point, t_1, on the roll-rate time history where $\Delta\dot{p}$ is zero – the region of steady-state roll.

If desired, the separate determination of $C_{l_{\delta_a}}$ can be avoided by solving for

$$\frac{C_{l_{\delta_a}}}{C_{l_p}} = -\frac{\Delta p_1}{\Delta\delta_{a_1}} \frac{b}{2V} \tag{179}$$

and substituting this ratio into the equation

$$C_{l_p} = \frac{I_x}{\bar{q}Sb} \Delta\dot{p}_2 \left[\frac{1}{\Delta p_2 \frac{b}{2V} + \frac{C_{l_{\delta_a}}}{C_{l_p}} \Delta\delta_{a_2}} \right] , \tag{180}$$

resulting in the format

$$C_{l_p} = \frac{2I_x V}{\bar{q}Sb^2} \Delta\dot{p}^2 \left[\frac{1}{\Delta p_2 - \Delta p_1 \frac{\Delta\delta_{a_2}}{\Delta\delta_{a_1}}} \right] . \tag{181}$$

In these last two equations, the subscript 2 indicates that $\Delta\dot{p}$ and Δp were obtained at a time point 2 on the roll-rate time history, preferably at the point of maximum rolling acceleration.

Although the restrictions imposed at the beginning of this section seriously limit the application of these equations, the last equation (Equation (181)) is interesting in that it shows that C_{l_p} can be obtained without requiring the solution of $C_{l_{\delta_a}}$.

7.5.6 The Effective Damping-in-Yaw Derivative, $(C_{n_r} - C_{n_{\dot\beta}})$

It was pointed out in Section 3.4.4 that C_{n_r} and $C_{n_{\dot\beta}}$ may be combined as an equivalent derivative, $(C_{n_r} - C_{n_{\dot\beta}})$, only for oscillatory maneuvers, providing the stability axis system is being considered or that the angle-of-attack is small if the body axis system is used. When the body axis system is employed, this is tantamount to saying that when the amplitude ratio $|\Delta\psi'|/|\Delta\beta| \simeq 1$, at $\alpha < 3^o$ or so, C_{n_r} and $C_{n_{\dot\beta}}$ may be combined as an equivalent derivative for yaw rates.

The combined derivatives are frequently shown in the results of analysis of oscillatory motions relative to body axes, even though this amplitude-ratio condition is exceeded. When this is done, it means that an effective value of C_{n_r} has been obtained which includes the influence of $C_{n_{\dot{\beta}}}$ and the results of the analysis based on the use of the actual $|\Delta\psi'|/|\Delta\beta|$ have produced an answer which is equivalent to the net contribution of Δr and $\Delta\dot{\beta}$ to ΔC_n in terms of Δr .

An approximate equation for $(C_{n_r} - C_{n_{\dot{\beta}}})$ is obtained directly from the damping term of the second-order differential equation (Equation (167)). Inasmuch as

$$2\zeta\omega_n = \frac{\bar{q}S}{mVC_{y_\beta}} - \frac{\bar{q}Sb^2}{2VI_z}(C_{n_r} - C_{n_{\dot{\beta}}}) , \tag{182}$$

a transposition results in

$$(C_{n_r} - C_{n_{\dot{\beta}}}) = -\frac{2I_z}{b^2}\left(\frac{2\zeta\omega_n V}{\bar{q}S} + \frac{C_{y_\beta}}{m}\right) . \tag{183}$$

Considering the assumptions made in deriving Equation (167), from which Equation (183) was obtained, and the stipulations regarding the combining of C_{n_r} and $C_{n_{\dot{\beta}}}$, it may be stated that Equation (183) will provide better accuracy when $|\Delta\psi'|/|\Delta\beta| \simeq 1$ and as $|\Delta p|/|\Delta\beta|$ decreases to satisfy the condition that C_{l_p} and C_{n_p} have a negligible influence on the equation.

An approximate equation for $(C_{n_r} - C_{n_{\dot{\beta}}})$ which has been used successfully in the X-15 airplane flight test program was derived from Equation (174)

$$\frac{I_z}{\bar{q}Sb}\omega_n \sin\Phi_d + (C_{n_r} - C_{n_{\dot{\beta}}})\frac{b}{2V} + C_{n_\beta}\frac{|\Delta\beta|}{|\Delta r|}\cos\Phi_{\beta r} = 0 .$$

This equation is a summation of yawing-moment components parallel to the Δr vector during a free-oscillation maneuver and is subject to the restrictions that I_{xz} and C_{n_p} have a negligible influence on the yawing moment.

Since $\Phi_{\beta r}$ generally varies only a few degrees from 90° for angles-of-attack less than about 15°, and since the damping angle is small, the preceding equation can be reduced and transposed to

$$\left.\begin{aligned}(C_{n_r} - C_{n_{\dot{\beta}}}) &\simeq -\zeta\omega_n \frac{I_z}{\bar{q}Sb\,\frac{b}{2V}} \\ &= -\frac{1.386VI_z}{\bar{q}Sb^2T_{1/2}} .\end{aligned}\right\} \tag{184}$$

Analog records of free-oscillation maneuvers of the X-15 airplane, on which C_{n_p} and I_{xz} are essentially zero, were analyzed for $(C_{n_r} - C_{n_{\dot{\beta}}})$ by using Equations (183) and (184). The results, presented in Table XI, show that the latter equation was better suited for determination of the effective damping-in-yaw derivative, for angles-of-attack up to approximately 12°, than Equation (183) for this vehicle.

7.5.7 Correlation for Effects of Stability Augmentation System in Determining Lateral-Directional Derivatives from Dutch Roll Oscillations

When lateral and directional stability augmentation systems having first-order time lags are operational during a Dutch roll (free-oscillation) maneuver, the effects of the augmentation system on the frequency and damping of the oscillations and on $|\Delta r|/|\Delta\beta|$ may be accounted for in the same manner as was done for the longitudinal mode of oscillation in Section 7.4.6.

7.6 The Graphical Time-Vector Technique

The graphical time-vector method of analysis[44-47], the principles of which were discussed and applied in the initial part of this section, is the most common manual technique used for determining the lateral and directional derivatives. Successful application is dependent upon availability of control-fixed, Dutch roll oscillation data wherein the damping ratio is less than approximately 0.3 to permit definition of the period of oscillations, the log decrement of the damping of oscillations, amplitude ratios, and phase angles.

7.6.1 Advantages

One advantage of the method is that the procedure is manual, and the analyst is afforded a graphical presentation of various factors affecting the solution.

Another advantage is that it is possible to obtain solutions when the β-vane records are available, suspect, or when it is desired to avoid applying corrections to these records. Bypassing the β records was discussed in Section 7.3.2. It was shown that the vector polygon of the transverse-acceleration equation is essential in the solution of the amplitude ratio, $|\Delta\beta|/|\Delta r|$, and the phase angle, Φ_{β_r}. Both of these quantities are used in the vector polygons of the rolling- and yawing-moment equations to determine C_{n_β} and C_{l_β} when the vector is used as the base for the amplitude ratios in the equations, as in Figures 59(a) and 59(b). The phase angle is used in the orientation of the $\Delta\beta$ vector in relation to the Δr vector and provides a more accurate value of Φ_{β_r} than can usually be obtained directly from flight records. The amplitude ratio, $|\Delta\beta|/|\Delta r|$, is used to extract C_{n_β} and C_{l_β} from the determined values of $C_{n_\beta}|\Delta\beta|/|\Delta r|$ and $C_{l_\beta}|\Delta\beta|/|\Delta r|$ in Figures 59(a) and 59(b).

7.6.2 Disadvantages

One disadvantage is that the development of a definite technique is required on the part of the analyst to minimize what would otherwise constitute a rather time-consuming and tedious effort to obtain a consistent and reliable set of results.

Another disadvantage is that only two of the three derivatives in each of the rolling and directional moment equations may be determined by means of the vector diagram, thus necessitating an estimate or a wind-tunnel value of one of the derivatives in each of the equations. Since C_{n_p} and C_{l_r} terms in the vector diagrams (Figures 59(a) and 59(b)) are the smallest vectors, it is customary to estimate these quantities. The errors in the estimated values of C_{n_p} will affect $(C_{n_r} - C_{n_{\dot\beta}})$ primarily; the errors in C_{l_r} will generally affect C_{l_p} primarily, but to a much smaller extent. For low angles-of-attack, $(C_{n_r} - C_{n_{\dot\beta}})$ may be estimated by using Equations (183) or (184) within the limits of their applicability.

7.6.3 Application of the Graphical Time-Vector Technique to the Determination of C_{n_β} , $(C_{n_r} - C_{n_{\dot\beta}})$, C_{l_β} , *and* C_{l_p}

Figures 59(a) and 59(b) show the application of the graphical time-vector technique to the determination of C_{n_β} , $(C_{n_r} - C_{n_{\dot\beta}})$, C_{l_β} , and C_{l_p} . The amplitude ratio, $|\Delta p|/|\Delta r|$, and the phase angle, Φ_{pr} , were determined from a semilog plot such as that in Figure 46. The ratio $|\Delta\beta|/|\Delta r|$ and phase angle $\Phi_{\beta r}$ were obtained from a transverse-acceleration diagram as discussed in Section 7.3.2. The remaining required amplitude ratios and phase angles were determined as follows

$$\left.\begin{aligned} \frac{|\Delta\dot p|}{|\Delta r|} &= \omega_n \frac{|\Delta p|}{|\Delta r|} \; ; \qquad \Phi_{\dot p r} = \Phi_{pr} = (90 + \Phi_d) \\ \frac{|\Delta\dot r|}{|\Delta r|} &= \omega_n \; ; \qquad \Phi_{\dot r r} = 90 + \Phi_d \\ \frac{|\Delta r|}{|\Delta r|} &= 1 \; ; \qquad \Phi_{rr} = 0 \; . \end{aligned}\right\} \tag{185}$$

The derivatives C_{n_p} and C_{l_r} , which have relatively small influences in this instance, were obtained from wind-tunnel data. Assuming there is no question of the accuracy of the data, the tunnel data should be based on oscillatory tests, inasmuch as the flight data are based on an oscillatory maneuver.

With the various known vector quantities properly oriented in the respective diagrams, the diagrams were closed and the unknown vectors determined by drawing the unknown vectors in their proper phase-angle directions, Φ_{pr} and $\Phi_{\beta r}$. The newly determined vectors, such as $-C_{n_\beta}(|\Delta\beta|/|\Delta r|)$ and $(C_{n_r} - C_{n_{\dot\beta}})$ (b/2V) , were then reduced to obtain C_{n_β} , $(C_{n_r} - C_{n_{\dot\beta}})$, C_{l_β} , and C_{l_p} .

Figures 60(a) and 60(b), from Reference 43, show the results of the application of the graphical time-vector technique to the rocket-powered D-558-II research airplane. An interesting aspect of the results is the influence of power on the stability characteristics of this airplane.

At times there may appear to be an incompatibility within wind-tunnel data when the data are compared to flight-determined derivatives. It then becomes imperative to resolve the discrepancy within the tunnel data and between the tunnel data and the flight data. This is illustrated in the following example wherein C_{n_β} was relatively low.

Dynamic model tests of a relatively rigid high-performance aircraft at a set Mach number and $\alpha = 6.6^\circ$ showed that $C_{n_p} = 0.01$ and $(C_{n_r} - C_{n_{\dot\beta}}) = -0.14$. Tunnel data also showed C_{n_β} to be equal to 0.055 on the basis of static tests and equal to 0.0757 on the basis of oscillatory tests. Flight data obtained from time histories of convergent transient oscillations of the quality shown in Figure 45 indicated that, when the wind-tunnel value of $C_{n_p} = 0.01$ was used in the time-vector solution, C_{n_β} was equal to 0.071 and $(C_{n_r} - C_{n_{\dot\beta}})$ was equal to 0.313. It was obvious that $(C_{n_r} - C_{n_{\dot\beta}}) = 0.313$ was not representative of the true characteristics of the aircraft in the Dutch roll mode, since its positive value indicated an oscillatory divergence, whereas flight data showed oscillatory convergence.

A check of the phase angle Φ_{pr} (-104^{o}) by several analysts showed agreement within a few degrees. It was decided that a reasonable spread of uncertainty for the quality of data - corrected for instrument phase lag - would permit Φ_{pr} to be $105^{o} \pm 5^{o}$; at worst, the uncertainty would be $\pm 10^{o}$. Accordingly, solutions for C_{n_β} and $(C_{n_r} - C_{n_{\dot\beta}})$ were obtained by using various values of C_{n_p} and Φ_{pr} (within the spread of uncertainty). The results shown in Figure 61 in the form of a grid plot indicate the sensitivity of the determined values of C_{n_β} and $(C_{n_r} - C_{n_{\dot\beta}})$ to C_{n_p} and Φ_{pr} and the incompatibility of the wind-tunnel data. The tunnel data were incompatible even when allowances were made for unvertainties in inertia characteristics and readability of flight data.

Use was made of approximate Equation (183) with due consideration to the limitations of the equation for higher angle-of-attack conditions to aid in establishing the magnitude of $(C_{n_r} - C_{n_{\dot\beta}})$. For the test condition of an angle-of-attack of 6.6^{o}, the -0.458 value of $(C_{n_r} - C_{n_{\dot\beta}})$ obtained by Equation (183) could be in error to the extent of 100% or so. Hence, it was estimated that the correct value of $(C_{n_r} - C_{n_{\dot\beta}})$ was closer to -0.20 than -0.458. Also, considering that the state of the art in obtaining $(C_{n_r} - C_{n_{\dot\beta}})$ from wind-tunnel tests was more reliable than in obtaining C_{n_p}, the tunnel value (-0.14) of $(C_{n_r} - C_{n_{\dot\beta}})$ was surmised to be representative of the true value of this derivative. Uncertainties in the inertia characteristics required that some deviation be allowed in this value in obtaining $(C_{n_r} - C_{n_{\dot\beta}})$ from flight data. It was, therefore, concluded that the results of the analysis should lie within the shaded area shown in Figure 61. Within this area, the value of C_{n_β} (0.054) compatible with $\Phi_{pr} = -104^{o}$ and $(C_{n_r} - C_{n_{\dot\beta}}) = -0.14$ was considered to be a mean value and was used as an analytical result. The corresponding value of C_{n_p} should have been approximately -0.04.

The best accuracy in determining C_{n_β} and $(C_{n_r} - C_{n_{\dot\beta}})$ is obtained when $|\Delta p|/|\Delta r|$ is small, at which time the influence of C_{n_p} is relatively small. When the roll-to-yaw ratio is large, it may be advantageous to estimate $(C_{n_r} - C_{n_{\dot\beta}})$ and attempt to solve for C_{n_p}. For low angles-of-attack, $(C_{n_r} - C_{n_{\dot\beta}})$ may be estimated by using Equations (183) or (184) within the limitations of their applicability.

The best accuracy in determining C_{l_β} and C_{l_p} is obtained when the roll-to-yaw ratio is large. At this time, the influence of C_{l_r} is relatively small. In either case, the static derivatives, C_{n_β} and C_{l_β}, are determined more accurately than the rotary derivatives, $(C_{n_r} - C_{n_{\dot\beta}})$ and C_{l_p}.

It was previously pointed out that the accuracy of analysis becomes rather poor for damping ratios greater than 0.3. Although a good approximation of the damping ratio for heavily damped aircraft may be obtained by comparing flight records with records of heavily damped motions - the damping ratio of which is known - it becomes difficult to draw accurately the exponential envelopes of the oscillatory motions to obtain reliable values of amplitude ratios.

7.7 Other Analytical Techniques

The preceding discussions regarding determination of derivatives from flight data have shown various limitations. The graphical time-vector technique, although the most successful, is not usable for damping ratios in excess of about 0.3, requires control-fixed transient oscillation data, and requires the assumption of some deriva-

tives, which may, at times, cause difficulties in solutions. To overcome the limitations of the preceding techniques, a number of methods have been proposed for the comprehensive determination of derivatives (References 48-54, for example). Some have been successful in practice; others have not. In most instances, the degree of sophistication involved in the proposals requires automatic data-reduction equipment and the time and effort does not warrant their use when analog equipment is available for application of analog-matching techniques. Several of the methods are considered in the following sections.

7.7.1 Least Squaring of the Equations of Motion

A logical and straightforward method, on the sophisticated side, for determining derivatives from flight data is the application of the least-squaring technique to the linearized equations of motion. Flight quantities at discrete time points are substituted into the equations of motion. Many more data points are selected than the number of unknowns, and a least-squares process is applied to evaluate the unknown derivatives. As logical and simple as the approach may be, it has not been employed too successfully for several reasons, including: difficulty in properly conditioning the maneuver, instrumentation accuracy, phase lags between instruments, insufficient amplification of recorded data to provide precise readability, noise in data readout, and instrument alinement.

One of the more successful attempts to apply this technique was reported in Reference 48. To excite all the lateral-directional modes and give measurable control inputs without exceeding the limits of the linearized equations of motion, the following control input program was used:

> "From trimmed level flight, step the rudder causing the airplane to yaw and then roll due to dihedral effect. When the bank angle reaches approximately 20 degrees, apply a step aileron deflection such that the airplane will roll toward a level flight attitude. In order to obtain a sufficiently long record of the response to aileron, the airplane is allowed to roll to an opposite bank angle of 20 degrees before stopping the recording and initiating recovery".

A typical time history of this maneuver is shown in Figure 62. All instruments had similar response characteristics and high recording sensitivity which was compatible with calibration-sensitivity spread and calibration spread. Alinement of instruments was within $\pm 0.3^{\circ}$. Recorded data were clean. It was found that noise in the readout data significantly affected the results. Twenty discrete time points used for the least-squaring process were considered sufficient.

The results, reproduced in Figures 63(a) and 63(b), show the degree of consistency obtained after the greater-than-usual precautions were taken to provide conditions that would be compatible with the needs of the technique. The requirements for this technique are undoubtedly similar to those necessary to make other promising techniques workable, such as the method of Reference 49. This method is also an equation-of-motion technique utilizing the Fourier transform, a method function to remove dependence on initial and end conditions, and a least-squaring procedure.

7.7.2 Frequency-Response Method

Methods have been proposed (References 50-52 for example) to determine stability and control derivatives by using frequency-response data obtained from flight tests. The method of Reference 52 encompasses the solution of all derivatives through a complex procedure. Other methods, such as that of Reference 51, provide only limited results based on various degrees of approximation.

The method of Reference 52 replaces the time plane with the frequency plane. Amplitude ratios and phase relationships of airplane response to control input from frequency-response analysis of a pulse maneuver[51, 55] provide real and imaginary quantities. The complex quantities at discrete frequencies are substituted into least-squared equations solving for the derivatives desired. The method is simple in theory; however, considerable care, work, and time are involved in the application, and some experience is necessary in the selection of discrete frequencies. These factors minimize interest in further studies of the method, especially where time is of the essence in obtaining a relatively quick look at the flight values. Automatic data-reduction equipment would greatly expedite the frequency-response analysis and would be useful for the other computations required.

7.8 Analog-Matching Techniques

When flight data are of such a nature as to preclude the successful use of the graphical time-vector technique or the approximate equations, and when time and expense will not permit the use of an experimentation with more sophisticated techniques, recourse is usually made to the analog to determine the derivatives that will provide the best match of the analog time history with the flight time history of a maneuver.

The use of the analog should be considered as a last resort, to be used only when other techniques cannot be applied. It is not a "cure-all", for it can produce erroneous answers under certain conditions and still provide a good match with the flight time history of a maneuver.

7.8.1 Conventional and High-Speed Repetitive Operation (REPOP) Analog Matching

The mathematical model of the aircraft for the analog computer is provided by the airplane equations of motion; when attitude records (such as ψ and ϕ) are available and used in the matching process, transformation equations are included to transform aircraft angular rates about the body axes to angular rates about Euler axes.

Generally, the simplest mathematical model compatible with the needs of an investigation is used to reduce the number of analog components required and to expediate solutions. A five-degree-of-freedom mathematical model, involving the general equations of motion, is employed when longitudinal and lateral-directional cross-coupling effects are factors in the responses of the airplane during the maneuver. When such cross-coupling effects are not factors to be contended with, the longitudinal and lateral-directional motions can be treated independently and as two separate analog programs using the linearized equations. Under such circumstances, the longitudinal program is treated as a two-degree-of-freedom case (with velocity a constant) unless phugoid is being considered, which is not often; and the lateral-directional program is treated as a three-degree-of-freedom case. Small-perturbation equations may be used

to advantage in such instances, particularly when datums of angular rates and Euler attitudes may be suspect and angular accelerations have excessive noise or are not available.

Initial estimates of stability and control derivatives to be used in the mathematical model are obtained from available theoretical and/or wind-tunnel values. If possible, flight-determined derivatives obtained through the use of the approximate equations are employed. In the absence of the preceding, the best estimates possible are made. Initial estimates are required to establish reasonable scaling factors for the manually adjusted derivative potentiometers to save operational time.

Inasmuch as errors in initial conditions shift the amplitude or rotate the response time history, provisions are made on the analog to program initial conditions through manually controlled potentiometers.

Flight test inputs in the form of aileron and rudder deflections are reproduced on function generator components of the analog in as faithful a reproduction as possible within the limits of the function generators, which have a finite number of breakpoints. When these inputs are introduced into the mathematical model, the analog computes a response.

In conventional analog-matching, the response is recorded by a strip recorder. The recorded response is then compared with the actual flight time history, which is reproduced on clear plastic to overlay on the analog time history. A mismatch indicates the need to modify the values of the derivatives, possibly change signs of several of them, and possibly modify the initial conditions. These changes are made by using a judicious trial-and-error process until a match is obtained.

The conventional matching technique is laborious because of the need to manually match a strip record with the overlay every time a programed condition is modified in order to study the effect of the modification and assess the next condition to be modified. The conventional technique may require from several days to a week to obtain a match.

High-speed repetitive operation (REPOP) matching differs from the conventional in several basic aspects[56]. The strip recorder is replaced by an oscilloscope and the response to inputs is projected onto the scope, which has an overlay fastened to it. The projected response appears as a stationary time history as a result of an automatic high-speed recycling of the response computation. The maximum recycling speed for fidelity is governed by the time span of the time history to be matched and the frequency-response characteristics of the function generator. Where a cycling rate of 250 cycles per second may provide fidelity for a 3- or 4-second time history, it may cause serious distortions in projections onto the scope if a 10-second time history is projected.

High-speed repetitive operation matching relieves the operator of manual matching of the time history, permits him to make rapid modifications of derivatives and initial conditions, and allows him to observe effectively the influence of a modification on the response. When an optimum match is achieved on the scope, a strip record is made and matched with an overlay to check the fidelity of the scope match and to retain a record of the resulting match. A REPOP match can normally be achieved in 4 to 8 hours.

7.8.2 Advantages of the Analog-Matching Technique

The analog-matching technique for derivative determination, in effect, accomplishes what sophisticated analytical techniques (see the preceding section) have attempted. It enables the determination of derivatives under circumstances where approximate equations and the graphical time-vector technique fail. It does not rely upon definite restrictive maneuvers, although there are some maneuvers that cannot be solved for. Test data showing inadvertent inputs and subsequent disturbances may be used.

7.8.3 Limitations of the Analog-Matching Technique

The success of every technique discussed for determining derivatives was contingent upon the proper conditioning of the maneuvers involved. This is no less true of the analog-matching technique. A Dutch roll maneuver, induced by a control pulse, in which no spiral- or roll-subsidence modes are significantly evident, is generally impossible to match with a unique set of derivatives. It will be found that any number of combinations of derivatives will provide a match. A maneuver involving continuous oscillation of the control surfaces, as would be the case of lateral-directional oscillatory motions with the lateral-directional stability augmentation system on, will also be very difficult to match with a unique set of derivatives.

A properly conditioned lateral-directional maneuver for use on the analog to permit determination of a unique set of derivatives for a match should excite the roll and spiral modes as well as Dutch roll oscillations. The likelihood of obtaining a unique set of derivatives is increased when the maneuver is conditioned to include a rudder disturbance of a step-like nature, a transient oscillation, and an aileron disturbance – not necessarily in this order – as was mentioned in Section 7.7.1 and also illustrated in a recovery-from-sideslip maneuver which is considered in the next section.

Also, as was mentioned in Section 7.6.3, better accuracy will be achieved in the major directional derivatives when the $|\Delta p|/|\Delta r|$ ratio of the dynamic characteristics is low (minimizing influence of C_{n_p}), and in the major lateral derivatives when the $|\Delta p|/|\Delta r|$ ratio is high (minimizing the influence of C_{l_r}). It may be concluded, then, that C_{n_p} and C_{l_r} are normally difficult to determine to any respectable degree of accuracy. The possibility of determining C_{l_r} appears to improve with increasing tendency of the aircraft to roll off during a maneuver.

7.8.4 Application of the Analog-Matching Technique

Figure 64 shows the results of an analog match of a "recovery-from-sideslip" maneuver at a Mach number of 1.84 and an altitude of 49,400 ft. The match is typical for this aircraft, which had negative effective dihedral and adverse aileron yaw for the match shown. Rigid wind-tunnel data corrected for flexibility effects on the actual vehicle predicted practically zero effective dihedral and proverse yaw due to aileron. It was impossible to substantiate the predicted values on the analog, and only one combination of derivatives would provide the match.

The following procedure is typical of that employed in arriving at the analog match of the flight data which did not include rolling and yawing accelerations:

(i) The mathematical model was represented by three lateral-directional small-perturbation equations

$$\Delta\dot{\beta} = \frac{g}{V}\sin(\phi_0 + \Delta\phi) - \Delta r + \alpha_0\Delta p + \frac{\bar{q}S}{mV}(C_{y_\beta}\Delta\beta + C_{y_{\delta_r}}\Delta\delta_r + C_{y_{\delta_a}}\Delta\delta_a) - \frac{g}{V}\sin\phi_0$$

$$\Delta\dot{p} = \frac{I_{xz}}{I_x}\Delta\dot{r} + \frac{\bar{q}Sb}{I_x}\left[C_{l_\beta}\Delta\beta + \frac{b}{2V}(C_{l_p}\Delta p + C_{l_r}\Delta r) + C_{l_{\delta_r}}\Delta\delta_r + C_{l_{\delta_a}}\Delta\delta_a\right]$$

$$\Delta\dot{r} = \frac{I_{xz}}{I_z}\Delta\dot{p} + \frac{\bar{q}Sb}{I_z}\left[C_{n_\beta}\Delta\beta + \frac{b}{2V}(C_{n_r}\Delta r + C_{n_p}\Delta p) + C_{n_{\delta_r}}\Delta\delta_r + C_{n_{\delta_a}}\Delta\delta_a\right] .$$

(ii) In addition, the following transformation was employed to determine the change in Euler roll angle, which attained magnitudes of the order of 20^o on occasions in the maneuvers under consideration

$$\Delta\dot{\phi} = \Delta p - (r_0 + \Delta r)\theta_0\cos(\phi_0 + \Delta\phi) - r_0\theta_0\cos\phi_0$$

(iii) Finally, the outputs of the mathematical model were applied to the following two equations to modify analog values of $\Delta\beta$ and Δa_t to correspond to the indicated values of the flight data:

$$\Delta\beta_i = \Delta\beta + \frac{x_v}{V}\Delta r - \frac{z_v}{V}\Delta p$$

$$\Delta a_{t_i} = -\sin(\phi_0 + \Delta\phi) + \sin\phi_0 + \frac{v}{g}(\Delta\dot{\beta} + \Delta r - \alpha_0\Delta p) -$$

$$- y_{instr}\left(\frac{\cancel{2r\Delta r} \simeq 0 + 2p\Delta p}{g}\right) + x_{instr}\frac{\Delta\dot{r}}{g} - z_{instr}\frac{\Delta\dot{p}}{g} .$$

(iv) Starting with the arbitrarily selected time zero (as in Figure 64) for the time history to be matched:

(a) C_{n_β} was adjusted for approximate frequency match.

(b) The control derivatives were adjusted to provide an initial rough match in the magnitudes of r and ϕ.

(c) Potentiometers for $\dot{r}_0$ and $\dot{\beta}_0$ were adjusted to roughly aline r and β traces of the analog with flight data; similarly, potentiometers for $\dot{\phi}_0$ and $\dot{p}_0$ were adjusted to roughly aline ϕ and p traces. These actions involved the following analog integration

$$\Delta r = \int(\dot{r}_0 + \Delta\dot{r})dt , \qquad \Delta\beta = \int(\dot{\beta}_0 + \Delta\dot{\beta})dt ,$$

$$\Delta p = \int(\dot{p}_0 + \Delta\dot{p})dt , \qquad \Delta\phi = \int(\dot{\phi}_0 + \Delta\dot{\phi})dt .$$

(d) Since adjustment of $\dot{\phi}_0$ and $\dot{p}_0$ modifies alinement of analog and flight traces of r and β, step (c) was reiterated as many times as necessary to obtain a rough alinement of analog and flight traces of r, β, ϕ, and p.

(e) Attention was then focused on the r trace to obtain a more refined match of this trace by more cautiously adjusting C_{n_r}, C_{n_β}, $C_{n_{\delta_a}}$, and $C_{n_{\delta_r}}$. This operation necessitated adjustment of C_{l_β}, $C_{l_{\delta_a}}$, C_{l_p}, and C_{l_r} to keep the p trace in line.

It should be noted that the preceding five steps (iv) (a)-(e), which constitute an initial phase of operation to obtain an approximate match, involve about 1 hour. The explanation of the procedure is, by necessity, brief. It will be readily appreciated that the steps are iterative to keep the frequency of disturbance, the magnitude of disturbances of the various traces, and alinement of analog and flight time histories compatible.

The second phase of the analog-matching process involved the following operations:

(f) With the r trace roughly matched, attention was focused on the ϕ and p traces by manipulating the C_{l_β}, C_{l_p}, and C_{l_r} derivatives and the lateral-control derivatives as necessary. During this operation, fine adjustments were required and made on the r and β traces (as per step (iv) (e)).

(g) With ϕ, p, r, and β traces matched as closely as possible, attention was focused on the a_t trace. This involved C_{y_β}, $C_{y_{\delta_a}}$, and $C_{y_{\delta_r}}$.

The last phase of the analog-matching operation involved making fine adjustments to initial conditions (to compensate for probable errors) and fine adjustments to the derivatives, in essence, performing an iterative procedure of the preceding operations. The second and last phase of the analog-matching process generally involved 3 to 4 hours and, at times, more.

7.8.5 Accuracy of Results in Analog-Matching of Flight Data

As mentioned previously, the accuracy of the results in analog-matching of flight data is largely dependent upon the conditioning of the maneuver. For the longitudinal derivatives, results from a pullup-and-release maneuver of an advanced high-performance aircraft showed the following accuracies based on the amount the derivatives could be changed before a trend toward mismatch became evident:

(1) For a strong maneuver:

C_{N_α}	10%	C_{m_α}	5%
$C_{N_{\delta_e}}$	20% to 30%	$C_{m_{\delta_e}}$	10%
$(C_{N_q} + C_{N_{\dot{\alpha}}})$	200% or more	$(C_{m_q} + C_{m_{\dot{\alpha}}})$	20% to 30%

(2) For a weak maneuver:

C_{N_α}	20%	C_{m_α}	10%
$C_{N_{\delta_e}}$	100%	$C_{m_{\delta_e}}$	20%
$(C_{N_q} + C_{N_{\dot{\alpha}}})$	200% or more	$(C_{m_q} + C_{m_{\dot{\alpha}}})$	40%

The accuracies of the lateral-directional derivatives obtained from analog-matching of well-conditioned, release-from-sideslip maneuvers of the same aircraft are shown in the following tabulation, along with the factors which influence the accuracy:

C_{n_β} – 5%	True for any rudder release involving more than one cycle of oscillation.
C_{l_β} – 5% to 15%	Depended upon oscillatory characteristics of ϕ and magnitude of β, after rudder release.
C_{y_β} – 5% to 20%	Depended on the magnitude of the a_t oscillations and the average slope of β from release to steady value.
C_{n_r} – 5% to 30%	Depended upon the amount of transients the aircraft was allowed to go through before controls were applied again.
C_{n_p} – 5% to 30%	Depended upon the magnitude of the roll rate during oscillation. Higher roll rate showed better accuracy.
C_{l_p} – 5% to 30%	Depended upon the magnitude of the roll rate during oscillation. Higher roll rate showed better accuracy.
C_{l_r} – 5% to 50%	Depended upon magnitude and oscillatory characteristics of rolloff. Larger rolloff showed better accuracy.
$C_{n_{\delta_r}}$ – 5%	True for any rapid rudder input.
$C_{l_{\delta_a}}$ – 5% to 15%	Depended upon the magnitude of the control input.
$C_{n_{\delta_a}}$ – 5% to 30%	
$C_{l_{\delta_r}}$ – 10% to 30%	
$C_{y_{\delta_r}}$ – 5% to 50% or more	
$C_{y_{\delta_a}}$ – 40% to 100% or more	

These results may be considered typical of what may be expected in analog-matching of flight data obtained from properly conditioned maneuvers. The accuracies may well be typical of those that may be expected when comprehensive analytical techniques are used.

8. APPLICATION OF FLIGHT DERIVATIVES

If wind-tunnel data and theory were infallible, it stands to reason that there would be no need for flight determination of derivatives. However, such is not the case. As new concepts in aircraft were developed, either with regard to physical geometry or propulsion systems, and as aircraft fly in new Mach and altitude regimes, there is the need to verify aerodynamic theory and wind-tunnel data and various influences of aeroelastic deformations of prototype structures on stability characteristics; to provide supplementary information not obtained in limited wind-tunnel studies; and to uncover the source of discrepancies between predictions and actual flight behavior. The following discussions provide some insight into several of these areas.

8.1 Verification of Wind-Tunnel Data and Theory

As the Mach capability of the airplane increases, the technology in wind-tunnel testing becomes more critical with regard to model construction, support of the model, and interpretation of the tunnel data. Whereas theory depends upon wind-tunnel data for verification, or to fill in gaps where theory fails, the wind-tunnel may depend upon flight data, as new regimes of flight unfold, to verify testing techniques.

Flight data pointed out the need for a greater concentration of test points in the transonic region to accurately define the stability characteristics in this region (Fig. 54). Flight data showed also that it was not sufficient to use a cold jet stream to simulate the exhaust of rocket engines. Figure 60 shows the effect of the jet exhaust of the D-558-II research airplane on the lateral-directional stability characteristics of the vehicle in the supersonic region. The destabilizing influence of power was the result of a pluming of the hot jet exhaust and consequent formation of a lambda shock wave at the juncture of the vertical tail and the fuselage. During Dutch roll oscillations, the shock wave on the leeward side of the vertical tail moved forward, while on the windward side it remained attached to the jet exit. This phenomenon it not common; it was the result of overexpansion of the jet exhaust and the proximity of the trailing edge of the vertical stabilizer to the jet exhausts.

Another illustration of discrepancy between flight and predicted data involved elevator setting for 1g flight. A comparison of the variation of predicted and flight-determined elevator settings with Mach number showed increasing discrepancy with increasing Mach number for a constant center-of-gravity position. In this instance, involving aeroelastic effects, predictions showed reasonably close correlation of C_{N_α} with flight data; whereas, C_{m_α} and $C_{m_{\delta_e}}$ showed a difference in trend as well as level. Preliminary study of the problem showed a need to consider C_{m_0} as well as C_{m_α} and $C_{m_{\delta_e}}$. Thus, the following pitching-moment equation for trimmed unaccelerated level flight, based on Equation (53b) (Table IV), was used and constituted the major consideration in arriving at the most likely causes for the discrepancy between predicted and flight trim settings of the elevator

$$C_{m_0} + C_{m_\alpha}(\alpha + \alpha_{C_N=0}) + C_{m_{\delta_e}}\delta_e = 0 . \qquad (186)$$

The angle-of-attack $(\alpha + \alpha_{C_N=0})$ was replaced by its equivalent

$$\alpha + \alpha_{C_N=0} = \frac{C_N}{C_{N_\alpha}} \qquad (187)$$

to determine both predicted and flight values of C_{m_0} by the following new format of Equation (186), which is the slope-intercept expression for solving C_{m_0}, or

$$C_{m_0} = \frac{C_{m_\alpha}}{C_{N_\alpha}} C_N - C_{m_{\delta_e}} \delta_e \tag{188}$$

Also, Equation (186) was transposed to solve for

$$\delta_e = -\frac{C_{m_0}}{C_{m_{\delta_e}}} - \frac{C_{m_\alpha}(\alpha + \alpha_{C_N=0})}{C_{m_{\delta_e}}} . \tag{189}$$

A comparison of predicted and flight values of the ratios in Equation (189) showed the values of the ratio $C_{m_\alpha}/C_{m_{\delta_e}}$ to be essentially the same; however, $C_{m_0}/C_{m_{\delta_e}}$ differed in line with the discrepancy in δ_e. Calculation of the static margin using $C_{m_\alpha}/C_{N_\alpha}$, which was employed in determining C_{m_0}, also showed a discrepancy between prediction and flight. In the final analysis, it appeared that the major source of discrepancy between predicted and flight longitudinal trim elevator settings was due primarily to the differences in C_{m_0} and $C_{m_{\delta_e}}$.

An illustration of a discrepancy between wind-tunnel and flight data involving power effects and aeroelasticity is shown in Figure 65. This instance concerned the F-100 airplane (Fig.16), which is considered to be a relatively rigid aircraft and has its air-intake nozzle at the nose. As shown in Figure 65, the variation of the wind-tunnel value of C_{n_β} with Mach number has roughly the same trend as the flight-determined value. However, there is an appreciable difference in level that is well beyond the difference to be expected due to the values of moments of inertias; values are known to within 5% at best. The results of an investigation to trace the sources of the discrepancy showed appreciable moment of momentum effects of air-intake flow and aeroelasticity effects of the vertical tail. When the basic rigid tunnel data were corrected for these two factors, fairly good correlation was achieved with the flight data (Fig.65).

A technique in tracking down inconsistencies in wind-tunnel data involving C_{n_β}, C_{n_p}, and $(C_{n_r} - C_{n_{\dot\beta}})$ was illustrated in Section 7.6.3.

8.2 Effects of Aeroelasticity

The effects of aeroelastic deformation of the structural components on the stability and control characteristics of the aircraft are of prime concern, particularly in large transport designs, as pointed out in Section 6.3. The illustration of aeroelastic effects shown in Figure 65 represents an intuitive approach in accounting for a discrepancy between wind-tunnel and flight data. This approach presumes the basic rigid tunnel data to be correct. It also presumes that aeroelasticity effects are simple enough to permit reasonably reliable calculation of corrections to the data.

As aircraft increases in size and slenderness, and operate at increasing dynamic pressures, aeroelastic deformations of the structure assume increasing significance. The influence of aeroelastic deformations on the stability and control characteristics is difficult to predict on the basis of theory. The deformations of the various components of the structure affect the shock patterns of the airflow which, in turn,

affect the stability and control characteristics in a much more complex manner than the aeroelastic deformation of one or two surfaces on a relatively rigid aircraft. Rigid-model data may be questionable because of the uncertainties in the true rigidity of the model and model supports and interference effects. Thus, a more positive approach is required to assess flexibility effects to verify and improve theory and develop tunnel techniques.

A flight test technique for determining aeroelasticity effects on stability and control characteristics is outlined in Section 6.3. The technique, as presented, is somewhat simplified in that the lifting components of thrust is considered to be negligible. This approximation simplifies flight planning, monitoring, and making on-the-spot changes in flight conditions of W and h for maneuvers at constant M, approximately constant C_L due to aerodynamic lift alone, and constant center-of-gravity. An average of the postflight-determined values of

$$C_L = \frac{W - T \sin \theta}{\bar{q}S} \tag{190}$$

for the test points on the "constant M, C_L, and center-of-gravity line" in Figure 39 - such as points 1 and 2 - will constitute the representative value of C_L for these test points. The maximum deviation from actual C_L is within the experimental error of the investigation. The stability and control derivatives of these points, when plotted against dynamic pressure, define a curve which shows the effect of aeroelasticity on the derivatives. The curve represents only one M, C_L due to aerodynamic lift alone, and center-of-gravity condition.

8.3 Stability Criteria

Considerations of the stability of an airplane include not only its inherent stability, which is its behavior without pilot inputs following an initial disturbance, but also its behavior in response to pilot inputs. In general, the study of the stability of an airplane involves the effect of derivatives on the increase or decrease of the stability. It is an objective study. When the stability of the airplane is considered in the light of the degree of pilot's acceptance of the airplane, and pilot ratings are introduced, the study becomes subjective and is referred to as a handling-qualities study. As may be readily surmised, one study complements the other.

Any extensive discussion of handling qualities, which integrates the pilot as a human servosystem constituting a feedback loop in the control system, is beyond the scope of this paper. It would involve the study of human factors and is affected by the pilot's technical background as well as the depth of piloting background, the types of aircraft flown, orientation and types of displays in the cockpit, and general cockpit environment. The art and science of handling-qualities investigations is covered extensively in the literature (References 57-65, for example).

8.3.1 Longitudinal Short-Period Oscillation, ω_n

The response of the airplane to an elevator input or gust disturbance will normally include a longitudinal short-period oscillation. An oscillatory condition by itself indicates a static oscillatory stability. Positive, neutral, or negative dynamic oscillatory stability is dependent upon the presence of positive, zero, or negative damping characteristics, respectively. A study of the longitudinal characteristics involves both static oscillatory stability and damping.

The undamped natural frequency (static oscillatory stability) is a measure of the longitudinal stiffness of the airplane - analogous to a spring-mass system. This longitudinal stiffness is represented by

$$\left.\begin{aligned} \omega_n^2 &= -(\bar{M}_\alpha + \bar{M}_q \bar{Z}_\alpha) \\ &= -\left(C_{m_\alpha}\bar{q} + C_{m_q} C_{N_\alpha} \frac{\bar{q}}{2\mu_c}\right) \frac{S\bar{c}}{I_y} . \end{aligned}\right\} \tag{191}$$

It will be noted that for any one mass distribution and configuration of the airplane, the longitudinal stiffness is a direct function of $C_{m_\alpha}\bar{q}$ primarily. Thus, the oscillatory frequency of the airplane will decrease with decreasing C_{m_α} and decreasing $\bar{q}$.

It should be noted that when C_{m_α} is zero, a degree of longitudinal stiffness (static oscillatory stability) will be present as evidenced by the $C_{m_q} C_{N_\alpha}$ term in the equation, providing C_{m_q} is negative - a normal situation. The contribution of this term to longitudinal stiffness will increase with increase in C_{N_α} , decrease in mass-density parameter, μ_c , and increase in dynamic pressure, $\bar{q}$.

In maneuvering flight, the pilot feels the effect of longitudinal oscillatory stiffness in the stick force per unit normal acceleration.

8.3.2 Longitudinal Short-Period Damping

The longitudinal short-period damping is expressed either as the actual damping coefficient or as a damping ratio. The damping coefficient (ft lb sec/rad) is dependent upon the aerodynamic derivatives C_{N_α} and $(C_{m_q} + C_{m_{\dot\alpha}})$, as shown in the equation

$$\left.\begin{aligned} 2\zeta\omega_n &= -\left[\bar{Z}_\alpha + (\bar{M}_q + \bar{M}_{\dot\alpha})\right] \\ &= \frac{C_{N_\alpha}\bar{q}S}{mV} - (C_{m_q} + C_{m_{\dot\alpha}}) \frac{\bar{q}S\bar{c}^2}{2VI_y} \\ &= C_{N_\alpha}\rho V \frac{S}{2m} - (C_{m_q} + C_{m_{\dot\alpha}})\, \rho V \frac{S\bar{c}^2}{4I_y} . \end{aligned}\right\} \tag{192}$$

A decrease in C_{N_α} or the negative value of $(C_{m_q} + C_{m_{\dot\alpha}})$ will decrease the damping coefficient, $2\zeta\omega_n$. It will be noticed that the magnitude of the coefficient is also dependent upon the mass density of the air ζ and airspeed V , as well as upon the airplane's mass characteristics and configuration.

The damping ratio ζ as may readily be surmised from the preceding, is obtained from

$$\left.\begin{aligned} \zeta = \frac{2\zeta\omega_n}{2\omega_n} &= -\frac{\bar{Z}_\alpha + (\bar{M}_q + \bar{M}_{\dot\alpha})}{2\sqrt{-\bar{M}_\alpha}} \\ &= \frac{C_{N_\alpha}\sqrt{\rho}\sqrt{\left[\frac{SI_y}{8m^2\bar{c}}\right]} - (C_{m_q} + C_{m_{\dot\alpha}})\sqrt{\rho}\sqrt{\left[\frac{S\bar{c}}{32I_y}\right]}\,\bar{c}}{\sqrt{(-C_{m_\alpha})}} . \end{aligned}\right\} \tag{193}$$

Thus, for any one mass characteristic and configuration of the airplane, the damping ratio ζ is a function of $\sqrt{\rho}$, C_{N_α}, $(C_{m_q} + C_{m_{\dot{\alpha}}})$, and $\sqrt{(-C_{m_\alpha})}$.

8.3.3 Longitudinal Short-Period lead Term, $-\bar{Z}_\alpha$

The parameter $-\bar{Z}_\alpha$, which is a function of C_{N_α}, is a longitudinal short-period lead term which affects the lead of the pitch rate q with respect to the control input δ_e and angle-of-attack as shown by the transfer functions

$$\frac{q(s)}{\delta_e(s)} = \frac{-\bar{M}_{\delta_e}\bar{Z}_\alpha \left(s + \frac{1}{T_\theta}\right)}{s^2 + 2\zeta\omega_n s + \omega_n^2} = \frac{\left(\frac{C_{m_{\delta_e}}\bar{q}S\bar{c}}{I_y}\right)\left(\frac{C_{N_\alpha}\bar{q}S}{mV}\right)\left(s + \frac{1}{T_\theta}\right)}{s^2 + 2\zeta\omega_n s + \omega_n^2} \tag{194a}$$

and

$$\frac{\alpha(s)}{\delta_e(s)} = \frac{\bar{M}_{\delta_e}}{s^2 + 2\zeta\omega_n s + \omega_n^2} . \tag{194b}$$

As shown in Reference 64, the time for peak amplitude of q due to a step input decreases with decreasing $-\bar{Z}_\alpha$. If $-\bar{Z}_\alpha$ becomes sufficiently small in comparison to ω_n, the response to a step input can be disconcerting. It may be characterized in a tracking task by an initial increase in pitch attitude of the airplane followed by dwell, possibly with the airplane aimed at the target; but, then, with no further control input, there will be a subsequent increase in the attitude. This type of behavior may give the pilot the feeling that the airplane is unstable.

A low value of $-\bar{Z}_\alpha$ may cause the pilot to experience a looseness in pitch, pitch-rate overshoot, lack of control precision, and higher control forces. On the other hand, a high value of $-\bar{Z}_\alpha$ may cause a tendency to overcontrol, exceed normal g, and, in general, give the impression that the control is too sensitive.

8.3.4 The Dutch Roll Oscillation, ω_n

The Dutch roll mode of oscillation, represented by the following equation, based on an approximation of the second equation in Equations (78), is a measure of directional stiffness

$$\begin{aligned}\omega_n^2 &= \bar{N}'_\beta - \bar{L}'_\beta \sin\alpha + (\bar{N}'_r + \bar{L}'_p)Y_\beta \\ &\simeq \left(\frac{C_{n_\beta}}{I_z} - \frac{\alpha}{I_x} C_{l_\beta} + \frac{I_{xz}}{I_x I_z} C_{l_\beta}\right) \bar{q}Sb .\end{aligned} \tag{195}$$

Insofar as derivatives are concerned, C_{n_β} and C_{l_β} are normally the only derivatives of any consequence in defining the frequency of this mode of oscillation. Of these two derivatives, C_{n_β} is dominant. It should be noticed that when the static directional stability is zero ($C_{n_\beta} = 0$), there is still some degree of oscillatory stability, providing the effective dihedral is positive ($C_{l_\beta} = -$) and the product of inertia is negative, or vice versa. Some aspects of the controllability of the airplane when C_{n_β} is near zero and slightly negative are reported in Reference 60.

8.3.5 Dutch Roll Damping Coefficient, $2\zeta\omega_n$

The Dutch roll damping coefficient represented by the following equation, based on an approximation of the first equation in Equations (78), gives the measure of the dynamic stability of the Dutch roll mode

$$2\zeta\omega_n = -\bar{N}'_r - \bar{Y}_\beta - \bar{L}'_p$$

$$\simeq -\left[\frac{b^2}{2VI_z}(C_{n_r} - C_{n_{\dot\beta}}) + \frac{C_{y_\beta}}{mV} + \frac{b^2}{2VI_x}C_{l_p}\right]\bar{q}S \quad . \tag{196}$$

This equation shows the interaction of the more dominant derivatives affecting the damping ratio. The equation is more accurate than that shown as Equation (182) in that it includes C_{l_p} .

8.3.6 Dutch roll damping Ratio, ζ

On the basis of Equations (195) and (196), the damping ratio can be approximated to at least the first degree of approximation by

$$\zeta = \frac{-\bar{N}'_r - \bar{Y}_\beta - \bar{L}'_p}{2\sqrt{\bar{N}'_\beta}}$$

$$\simeq \frac{-\left[\frac{b}{2VI_z}(C_{n_r} - C_{n_{\dot\beta}}) + \frac{C_{y_\beta}}{mVb} + \frac{b}{2VI_x}C_{l_p}\right](\bar{q}Sb)^{\frac{1}{2}}}{2\left(\frac{C_{n_\beta}}{I_z} + \frac{I_{xz}}{I_xI_z}C_{l_\beta}\right)^{\frac{1}{2}}} \quad . \tag{197}$$

The Dutch roll damping ratio is strongly affected by $\bar{N}'_r$ and $\bar{N}'_\beta$. An increase in the negative value of $\bar{N}'_r$ not only increases the damping ratio, ζ , but also improves the stability of the spiral mode. Increasing $\bar{N}'_\beta$ not only increases directional stiffness but also the Dutch roll damping ratio, which may be desirable. Decreasing $\bar{N}'_\beta$ increases the bank angle that is induced by a given amount of sideslip in the Dutch roll motion, a characteristic which could be detrimental to maneuvering control of the airplane. In addition, decreasing $\bar{N}'_\beta$ increases the amount of Dutch roll disturbance in the roll mode response to a step aileron input – as reflected in the parameter $(\omega_\phi/\omega_n)^2$ to be discussed – and can disturb and mislead the pilot.

8.3.7 Stability Criteria for Aileron-Only Roll Control, ω_ϕ/ω_n

The roll parameter, ω_ϕ/ω_n , is the roll numerator to Dutch roll frequency ratio of ϕ/δ_e response function. It is represented by

$$\frac{\omega_\phi}{\omega_n} = \left[1 - \frac{\bar{L}'_\beta\bar{N}'_{\delta_a}}{\bar{N}'_\beta\bar{L}'_{\delta_a}}\right]^{\frac{1}{2}}$$

$$= \left[1 - \frac{\left(\frac{C_{n_{\delta_a}}}{C_{l_{\delta_a}}} + \frac{I_{xz}}{I_z}\right)\left(\frac{C_{l_\beta}}{C_{n_\beta}} + \frac{I_{xz}}{I_z}\right)}{1 + \frac{I_{xz}}{I_x}\frac{C_{l_\beta}}{C_{n_\beta}}}\right]^{\frac{1}{2}} \quad . \tag{198}$$

The parameter is a measure of the amount by which the Dutch roll motion is excited when aileron inputs (rudder fixed) are made by the pilot. It is particularly important in the roll tracking task in which the pilot-airplane combination can exhibit considerably different lateral-directional oscillatory tendencies than would be exhibited by the airplane alone. It provides a good index regarding the increase or decrease in stability of the airplane during the aileron-alone roll tracking task.

When $\omega_\phi/\omega_n = 1$, there is no yaw due to aileron inputs and there is little or no Dutch roll motion in response to aileron input. When $\omega_\phi/\omega_n < 1$, the pilot-airplane combination in an aileron-only tracking task will exhibit an effective damping ratio in roll tracking tasks greater than the Dutch roll damping ratio. When $\omega_\phi/\omega_n > 1$, the effective damping ratio will be less than the Dutch roll damping ratio and the roll that results from aileron input is augmented by the roll due to sideslip; this can cause stability problems in the roll tracking task, especially when the Dutch roll damping ratio is small and $|\phi|/|\beta|$ is large.

Equation (198) shows significant interaction of stability, control, and inertia parameters affecting ω_ϕ/ω_n . The interplay of $C_{n_{\delta_a}}$, C_{l_β} , and I_{xz} is important, inasmuch as these parameters may have either plus or minus values. Normally, $C_{n_{\delta_a}}$ and C_{l_β} are the controlling parameters; thus, if the effective dihedral is positive ($C_{l_\beta} < 0$), $C_{n_{\delta_a}}$ will have to be adverse ($C_{n_{\delta_a}} < 0$) to assure $\omega_\phi/\omega_n < 1$ and a stabilizing action during the roll tracking task.

8.3.8 Dutch Roll Stability Criteria, $|\phi|/|\beta|$

The amplitude ratio $|\phi|/|\beta|$ is a characteristic of the Dutch roll oscillations and is thus independent of any excitations of control inputs. Its mathematical relationship to derivatives is given by

$$\frac{|\phi|}{|\beta|} = \frac{\bar{L}'_\beta}{\bar{N}'_\beta}\left[\frac{1 + \dfrac{\bar{N}'_\beta \bar{L}'^2_r}{\bar{L}'^2_\beta}}{1 + \dfrac{\bar{L}'^2_p}{\bar{N}'_\beta}}\right]^{\frac{1}{2}} . \qquad (199)$$

The complex interaction of the derivative parameters makes it difficult to determine pilot sensitivity to $|\phi|/|\beta|$. However, if the airplane has high directional stiffness ($\omega_n > 1$), low $|\phi|/|\beta|$, reasonable $\zeta > 0.1$, and adverse yaw due to aileron, the pilot generally does not bother to coordinate turns by using rudder, inasmuch as the lateral-directional stiffness keeps sideslip small and the low value of $|\phi|/|\beta|$ keeps roll due to sideslip small (Ref.64).

If $|\phi|/|\beta|$ is large (of the order of 4 or more), rudder coordination becomes necessary in maneuvering to keep sideslip small in order to minimize the roll due to sideslip. If the airplane is characterized by favorable yaw due to aileron ($C_{n_{\delta_a}} > 0$) as well as high values of $|\phi|/|\beta|$, the pilot uses a cross-coordination of rudder and aileron controls (right aileron and left rudder) to prevent excessive rolls in maneuvers (Ref.64). It is not difficult to achieve coordination of controls, providing the airplane is not excited by external disturbances. However, because this cross-coordination is unnatural, the pilot is more critical of favorable yaw due to aileron ($C_{n_{\delta_a}} > 0$) than adverse yaw due to aileron ($C_{n_{\delta_a}} < 0$).

8.3.9 Roll-Subsidence Root, $1/T_R$

The roll-subsidence root, $1/T_R$, is influenced most significantly by the parameters shown in the following equation, which is based on the third equation of Equations (78)

$$\left.\begin{aligned} \frac{1}{T_R} &\simeq -\bar{L}'_p + \frac{\bar{L}'_\beta}{\bar{N}'_\beta}\left(\bar{N}'_p - \frac{g}{V}\right) \simeq -\bar{L}'_p \\ &= -C_{l_p}\frac{\bar{q}Sb^2}{2VI_x} . \end{aligned}\right\} \tag{200}$$

As shown, the roll subsidence is dominated by the damping-in-roll derivative, C_{l_p} .

The roll-subsidence root has a direct influence on the steady-state roll rate in response to a specific aileron deflection. When the root is large, the damping in roll is high and the pilot controls the bank angle by commanding and adjusting roll rate. When it is small, the pilot controls bank angle by commanding and adjusting rolling acceleration.

8.3.10 Spiral-Divergence Root, $1/T_S$

The spiral-divergence root, $1/T_S$, is affected primarily by the parameters shown in the following equation, which is based on Equation (83),

$$\frac{1}{T_S} \simeq T_R \frac{g}{V}\frac{(\bar{L}'_\beta\bar{N}'_r - \bar{L}'_r\bar{N}'_\beta)}{\bar{N}'_\beta} . \tag{201}$$

The spiral mode can be convergent, neutrally stable, or divergent. Thus, for the purpose of defining the spiral stability boundary, the equation can be shown as a spiral stability criterion

$$\left.\begin{array}{rll} L_\beta N_r - N_\beta L_r & \left\{\begin{array}{ll} > 0 & \text{spirally convergent} \\ = 0 & \text{neutral spiral stability} \\ < 0 & \text{spirally divergent} . \end{array}\right. \\ \text{or, as an approximation,} & & \\ C_{l_\beta}C_{n_r} - C_{n_\beta}C_{l_r} & & \end{array}\right\} \tag{202}$$

It will be noticed that spiral stability is dependent upon the interaction of four derivatives. Since C_{n_β} is normally positive and C_{n_r} and C_{l_β} are normally negative, it is well to have C_{l_r} negative. Under any circumstance, $C_{l_\beta}C_{n_r}$ should be greater than $C_{n_\beta}C_{l_r}$ for spiral stability.

A divergent spiral mode will result in the airplane performing an increasing nose-down and tightening turn accompanied by an increase in speed and loss in altitude.

8.4 Flight Guidance

Research vehicles that incorporate new concepts of aerodynamic configuration, or research vehicles designed for flight in previously unexplored regions of flight (Mach and altitude), usually have a considerable amount of wind-tunnel investigations performed on models to check their stability and control characteristics. Despite the

comprehensiveness of the tunnel tests, there will be gaps in the data. In addition, there is normally a certain amount of reserve in placing complete confidence in the data. As a result, the flight envelope is built up gradually, using stability and control maneuvers to obtain flight-determined stability and control derivatives to verify wind-tunnel data.

Agreement in the comparisons results in a more rapid buildup of the flight envelope; disagreement involves a slowdown until the flight data can be reduced and cautiously extrapolated. The most representative values of the stability and control characteristics are used in stability criteria and are programed into a flight simulator, in which the pilot simulates the intended mission and emergency conditions to reduce the amount of risk that would otherwise be involved in actual flight. The simulator normally uses the general equations of motion for a mathematical model.

When roll-coupling instability became a physical reality with the loss of several F-100 airplanes, considerable effort was expended at the NASA Flight Research Center in flight and simulator studies of the problem[66, 67]. Because of the complex nature of the motions, guidance of the flight program using analog computations was desirable. In a roll investigation of this type, a small increase in aileron deflection can produce large effects on airplane motions. It has been graphically demonstrated on several occasions that flight guidance based on linear extrapolation of flight data at small aileron deflections can be highly misleading and dangerous Figure 66 shows a representative comparison of the measured excursions in angle of-attack and angle-of-sideslip obtained in 360° rolls with those predicted by using flight-determined derivatives. The good agreement has been demonstrated in most instances in which flight-determined derivatives have formed the basis of calculations. Consequently, the use of such guidance in flight planning has proved invaluable. The use of wind-tunnel and theoretical derivatives in analog studies has not been as successful.

9. CONCLUDING REMARKS

This paper has attempted to bring together the various factors that should be known by the engineer who is concerned with the determination of stability and control characteristics from flight data or the use of these flight-determined characteristics in handling-qualities research.

The discussions have been tempered with practical considerations. The various factors discussed and the observations made are the result of experience in working with flight data, developing techniques, comparing the data with predictions, and investigating the causes of discrepancies,

The theoretical background, approximations, and limitations of the mathematical relations employed have been given careful consideration. The problems encountered with several of the more sophisticated techniques have been presented with the hope that any new comprehensive technique that may be proposed will take into consideration some of the practical problems with instrumentation and development of maneuvers to properly condition the flight data for the technique.

The pulse maneuver, properly executed, has been found to be generally adequate in exciting motions required for stability-derivative analysis as well as for determining the characteristics of the oscillatory modes if adequate instrumentation and alinement are provided.

For longitudinal-derivative analysis, simple equations utilizing period and damping of the oscillatory mode of the airplane were shown to be as satisfactory as more comprehensive methods.

For lateral-directional derivative analysis, the graphical time-vector method was shown to be the most satisfactory manual method of analysis. Simple approximate methods are useful if applied with caution.

Control effectiveness can usually be obtained by relating the peak acceleration to rapid control inputs. Consideration must be given to aerodynamic contributions if reasonable accuracy is to be realized.

The analog-matching technique for determining derivatives from flight data was shown to be a valuable method of analysis for use in the absence of data suitable for analytical techniques. However, the analog-matching technique has limitations in that data must be properly conditioned in order to obtain unique answers. The accuracy of the results obtained from this technique and the effect of the type of maneuver on the accuracy may well provide the clue to what may be expected from sophisticated techniques that may be proposed.

The use of flight data to verify wind-tunnel results and theory was discussed and illustrated. The possible inadequacy of comparisons of flight data with predictions for determining aeroelastic effects was pointed out and a flight-planning technique explained to permit determination of aeroelastic effects from flight data alone.

Present instrumentation and methods of analysis are adequate for extracting derivatives from flight data for use in most flight-guidance simulator studies and detection of characteristics which have not been predicted in the wind-tunnel.

REFERENCES

1. Wright, John — *A Compilation of Aerodynamic Nomenclature and Axes Systems.* US Naval Ordnance Laboratory (White Oak, Silver Springs, Md.), NOLR 1241, August 1962.

2. Frazier, R.A. et al. — *Elementary Matrices.* Cambridge University Press, 1938.

3. Abzug, Malcolm J. — *Kinematics and Dynamics of Fully-Maneuvering Airplanes.* Douglas Aircraft Co., Inc. (El Segundo Plant), Rept. No. ES 16144, June 23, 1952.

4. Thelander, J.A. — *Aircraft Motion Analysis.* Air Force Flight Dynamics Laboratory, Wright-Patterson Air Force Base, Tech. Doc. Rept. 64-70, March 1965.

5. Duncan, W.J. — *The Principles of the Control and Stability of Aircraft.* Cambridge University Press, 1952.

6. Videan, Edward N. — *Flight Measurements of the Dynamic Lateral and Longitudinal Stability of the Bell X-5 Research Airplane at 58.7° Sweepback.* NACA RM H55H10, 1955.

7. Pinsker, W.J.G. — *A Note on the Dynamic Stability of Aircraft at High Subsonic Speeds when Considering Unsteady Flow.* Report Aero 2378, Royal Aircraft Establishment, R & M 2904, British ARC, May 1950.

8. Ribner, H.S. — *Notes on the Propeller and Slip-Stream in Relation to Stability.* NACA Wartime Report L25, 1944.

9. Ribner, Herbert S. — *Formulas for Propellers in Yaw and Charts of the Side-Force Derivative.* NACA Report 819, 1945.

10. Ribner, H.S. — *Field of Flow About a Jet and Effects of Jets on Stability of Jet-Propelled Airplanes.* NACA Wartime Report L213, 1946.

11. Pearce, B.F. et al. — *Analytical Study of Approximate Longitudinal Transfer Functions for a Flexible Airframe.* ASD-TDR-62-279 (Contract No. AF33(616)-7657), Aero. Systems Div., US Air Force Systems Command, June 1962.

12. Pearce, B.F. — *Topics on Flexible Airplane Dynamics.* Part I. *Residual Stiffness Effects in Truncated Modal Analysis.* ASD-TDR-63-334 (Contract No. AF33(657)-8374), Aero. Systems Div., US Air Force Systems Command, July 1963.

13. Frueh, F.J. Zisfein, M.B. — *Numerical Approximation Method for Flexible Flight Vehicle Transfer Function Factors.* ASD-TDR-62-1063 (Contract No. AF33(616)-7906), Aero. Systems Div., US Air Force Systems Command, March 1963.

14. Milne, R.D. — *Dynamics of the Deformable Aeroplane.* R & M 3345, British ARC, September 1964.

15. Huntley, E. — *The Longitudinal Response of a Flexible Slender Aircraft to Random Turbulence.* Report Aero. 2691, Royal Aircraft Establishment, August 1964.

16. Cole, Henry A. Jr. et al. — *Experimental and Predicted Longitudinal and Lateral-Directional Response Characteristics of a Large Flexible 35° Swept-Wing Airplane at an Altitude of 35,000 Feet.* NACA Report 1330, 1957.

17. Ashkenas, Irving L. McRuer, Duane T. — *Approximate Airframe Transfer Functions and Application to Single Sensor Control Systems.* Tech. Report 58-82 (ASTIA No. AD 151925), Wright Air Development Center, US Air Force, June 1958.

18. Turner, Howard L. — *Measurement of the Moments of Inertia of an Airplane by A Simplified Method.* NACA TN 2201, 1950.

19. Notess, Charles B.; Woodward, Claude R. — *An Investigation of the Experimental Determination of Aircraft Inertia Characteristics.* Tech. Rept. 53-207, Wright Air Development Division, US Air Force, July 1953.

20. Woodward, Claude R. — *Handbook of Instructions for Experimentally Determining the Moments of Inertia and Product of Inertia of Aircraft by the Spring Oscillation Method.* Tech. Rept. 55-415 (ASTIA No. AD 97104), Wright Air Development Center, US Air Force, June 1955.

21. Cole, Henry A. Jr.; Bennion, Francis L. — *Measurement of the Longitudinal Moment of Inertia of a Flexible Airplane.* NACA TN 3870, 1951. (Supersedes RM A55J21).

22. Boucher, Robert W. et al. — *A Method for Measuring the Product of Inertia and the Inclination of the Principal Longitudinal Axis of Inertia of an Airplane.* NACA TN 3084, 1954.

23. Malvestuto, Frank S. Jr.; Gale, Lawrence J. — *Formulas for Additional Mass Corrections to the Moments of Inertia of Airplanes.* NACA TN 1187, 1947.

24. Brunn, Cyril D.; Stillwell, Wendell H. — *Mach Number Measurements and Calibration During Flight at High Speeds and at High Altitudes Including Data for the D-558-II Research Airplane.* NACA RM H55J18, 1956.

25. Zalovcik, John A. — *A Radar Method of Calibrating Airspeed Installations on Airplane in Maneuvers at High Altitudes and at Transonic and Supersonic Speeds.* NACA TN 1979, 1949.

26. Gracey, William et al. — *Wind-Tunnel Investigation of a Number of Total Pressure Tubes at High Angles-of-Attack. Subsonic Speeds.* NACA TN 2331, 1951. (Supersedes NACA RM L50G19.)

27. Gracey, William et al. — *Wind-Tunnel Investigation of a Number of Total Pressure Tubes at High Angles-of-Attack. Supersonic Speeds.* NACA TN 2261, 1951.

28. Pearson, Albin O.; Brown, Harold A. — *Calibration of a Combined Pitot-Static Tube and Vane-Type Flow Angularity Indicator at Transonic Speeds and at Large Angles-of-Attack or Yaw.* NACA RM L52F24, 1952.

29. Gracey, William; Scheithauer, Elwood F. — *Flight Investigation at Large Angles-of-Attack of the Static-Pressure Errors of a Service Pitot-Static Tube Having a Modified Orifice Configuration.* NACA TN 3159, 1954.

30. Beeler, De E. et al. — *Flight Techniques for Determining Airplane Drag at High Mach Numbers.* NACA TN 3821, 1956.

31. Fischel, Jack
Webb, Lannie D.
Flight-Informational Sensors, Display, and Space Control of the X-15 Airplane for Atmospheric and Near-Space Flight Missions. NACA TN D-2407, 1964.

32. Wildhack, W.A.
Pressure Drop in Tubing in Aircraft Instrument Installations. NACA TN 593, 1937.

33. Allen, H. Julian
Perkins, Edward W.
A Study of Effects of Viscosity on Flow Over Slender Inclined Bodies of Revolution. NACA Report 1048, 1951. (Supersedes NACA TN 2044.)

34. Sinclair, Archibald R.
Mace, William D.
Wind-Tunnel Calibration of a Combined Pitot-Static Tube and Vane-Type Flow-Angularity Indicator at Mach Numbers of 1.61 and 2.01. NACA TN 3808, 1956.

35. Yaggy, Paul F.
A Method for Predicting the Upwash Angles Induced at the Propeller Plane of a Combination of Bodies with an Unswept Wing. NACA TN 2528, 1951.

36. Glauert, H.
The Elements of Aerofoil and Airscrew Theory. Cambridge University Press, 1947 (Reprinted 1948).

37. Rogallo, Vernon L.
Effects of Wing Sweep on the Upwash at the Propeller Planes of Multiengine Airplanes. NACA TN 2795, 1952.

38. Wolowicz, Chester H.
Gossett, Terrence D.
Operational and Performance Characteristics of the X-15 Spherical, Hypersonic Flow-Direction Sensor. NACA TN D-3070, 1965.

39 Muzzey, C.L.
Kidd, E.A.
Measurement and Interpretation of Flight Test Data for Dynamic Stability and Control. Report No. CAL-60, Cornell Aeronautical Laboratory, April 9, 1954.

40. Seckel, Edward
Systematic Errors. Vol.IV, Part IV A, *AGARD Flight Test Manual*, North Atlantic Treaty Organization, 1963 (rev.).

41. Wolowicz, Chester H.
Time-Vector Determined Lateral-Derivatives of a Swept-Wing Fighter-Type Airplane with Three Different Vertical Tails at Mach Numbers Between 0.70 and 1.48. NACA RM H56C20, 1956.

42. Yancey, Roxanah B.
et al.
Aerodynamic-Derivative Characteristics of the X-15 Research Airplane as Determined from Flight Tests for Mach Numbers from 0.6 to 3.4. NASA TN D-1060, 1962.

43. Wolowicz, Chester H.
Effects of Jet Exhausts on Flight-Determined Longitudinal and Lateral Dynamic Stability Characteristics of the Douglas D-558-II Research Airplane. NASA RM H57G09, 1957.

44. Doetsch, K.H.
The Time Vector Method for Stability Investigations. Report Aero 2495, Royal Aircraft Establishment, August 1953.

45. Breuhaus, Waldemar O. — *Résumé of the Time Vector Method as a Means for Analyzing Aircraft Stability Problems.* Tech. Report 52-299 (Contract No.AF33(038)-20659, RDO No. 461-1-2), Wright Air Development Center, US Air Force, November 1952.

46. Sternfield, L. — *A Vector Method Approach to the Analysis of the Dynamic Lateral Stability of Aircraft.* Journal of the Aeronautical Sciences, Vol. 21, April 1954, pp. 251-256.

47. Wolowicz, Chester H. — *Time-Vector Determined Lateral Derivatives of a Swept-Wing Fighter-Type Airplane with Three Different Vertical Tails at Mach Numbers Between 0.70 and 1.48.* NACA RM H56C20, 1956.

48. Gowin, Norman E. — *Lateral Stability Investigation of an F-100A Airplane.* Tech. Rept. 57-563 (ASTIA No. AD 131052), Wright Air Development Center, US Air Force, November 1957.

49. Shinbrot, Marvin — *On the Analysis of Linear and Nonlinear Dynamical Systems From Transient-Response Data.* NACA TN 3288, 1954.

50. Greenberg, Harry — *A Survey of Methods for Determining Stability Parameters of an Airplane From Dynamic Flight Measurements.* NACA TN 2340, 1951.

51. Triplett, William C. et al. — *The Dynamic-Response Characteristics of a 35° Swept-Wing Airplane as Determined From Flight Measurements.* NACA Report 1250, 1955.

52. Donegan, James J. et al. — *Determination of Lateral-Stability Derivatives and Transfer-Function Coefficients From Frequency-Response Data for Lateral Motions.* NACA Report 1225, 1955. (Supersedes NACA TN 3083.)

53. Klawans, Bernard B. White, Jack A. — *A Method Utilizing Data on the Spiral, Roll-Subsidence, and Dutch Roll Modes for Determining Lateral Stability Derivatives From Flight Measurements.* NACA TN 4066, 1957.

54. Schumacher, Lloyd E. — *A Method for Evaluating Aircraft Stability Parameters From Flight Test Data.* Tech. Rept. 52-71, Wright Air Development Center, US Air Force, June 1952.

55. Eggleston, John M. Mathews, Charles W. — *Application of Several Methods for Determining Transfer Functions and Frequency Response of Aircraft From Flight Data.* NACA Report 1204, 1954.

56. Rampy, John M. Berry, Donald T. — *Determination of Stability Derivatives from Flight Test Data by Means of High Speed Repetitive Operation Analog Matching.* FTC-TDR-64-8, US Air Force Flight Test Center, May 1964.

57. Ashkenas, Irving L.
McRuer, Duane T.
Approximate Airframe Transfer Functions and Applications to Single Sensor Control Systems. Tech. Rept. 58-82 (ASTIA No. AD 151025), Wright Air Development Center, US Air Force, June 1958.

58. Sadoff, Melvin
The Effects of Longitudinal Control-System Dynamics on Pilot Opinion and Response Characteristics as Determined from Flight Tests and from Ground Simulator Studies. NASA MEMO 10-1-58A, 1958.

59. Creer, Brent Y.
et al.
A Pilot Opinion Study of Lateral Control Requirements for Fighter-Type Aircraft. NASA MEMO 1-29-59A, 1959.

60. Taylor, Lawrence W. Jr.
Day, Richard E.
Flight Controllability Limits and Related Human Transfer Functions as Determined from Simulator and Flight Tests. NASA TN D-746, 1961.

61. Ashkenas, Irving L.
McRuer, Duane T.
The Determination of Lateral Handling Quality Requirements from Airframe-Human Pilot System Studies. Tech. Rept. 59-135, Wright Air Development Center, US Air Force, June 1959.

62. Jex, Henry.
Cromwell, Charles H. III
Theoretical and Experimental Investigation of Some New Longitudinal Handling Qualities Parameters. Tech. Rept. ASD-TR-61-26, Wright-Patterson Air Force Base, US Air Force, June 1962.

63. Ashkenas, I.L.
McRuer, D.T.
A Theory of Handling Qualities Derived from Pilot-Vehicle System Considerations. Aerospace Engineering, Vol.21, pp.60,61, 83-102, February 1962.

64. Newell, F.D.
Criteria for Acceptable Representation of Airplane Dynamic Responses in Simulators Used for Pilot Training. Tech. Rept. NAVTRADEVCEN 1146-1, US Naval Training Device Center (Port Washington, NY) October 1962.

65. Durand, T.S.
Jex, H.R.
Handling Qualities in Single-Loop Roll Tracking Tasks: Theory and Simulator Experiments. Tech. Doc. Report ASD-TDR-62-505, Wright-Patterson Air Force Base, US Air Force, November 1962.

66. Weil, Joseph
Day, Richard E.
An Analog Study of the Relative Importance of Various Factors Affecting Roll Coupling. NACA RM H56A06, 1956.

67. Weil, Joseph
Application of Analytical Techniques to Flight Evaluations in Critical Control Areas. AGARD Report 369, 1961.

TABLE I

Transformation of Derivatives from Stability to Body Axis

$C_{N_\alpha} = C_{L_\alpha} \cos\alpha + C_{D_\alpha} \sin\alpha + C_C$	
$C_{C_\alpha} = C_{D_\alpha} \cos\alpha - C_{L_\alpha} \sin\alpha - C_N$	
$C_{m_\alpha} = (C_{m_\alpha})_s$	
$C_{n_\beta} = (C_{n_\beta})_s \cos\alpha + (C_{l_\beta})_s \sin\alpha$	
$C_{n_r} = (C_{n_r})_s \cos^2\alpha + (C_{l_p})_s \sin^2\alpha + (C_{n_p} + C_{l_r})_s \sin\alpha\cos\alpha$	
$C_{n_{\dot\beta}} = (C_{n_{\dot\beta}})_s \cos\alpha + (C_{l_{\dot\beta}})_s \sin\alpha$	
$C_{n_p} = (C_{n_p})_s \cos^2\alpha - (C_{l_r})_s \sin^2\alpha - (C_{n_r} - C_{l_p})_s \sin\alpha\cos\alpha$	
$C_{n_\delta} = (C_{n_\delta})_s \cos\alpha + (C_{l_\delta})_s \sin\alpha$	
$C_{l_\beta} = (C_{l_\beta})_s \cos\alpha - (C_{n_\beta})_s \sin\alpha$	
$C_{l_r} = (C_{l_r})_s \cos^2\alpha - (C_{n_p})_s \sin^2\alpha - (C_{n_r} - C_{l_p})_s \sin\alpha\cos\alpha$	
$C_{l_{\dot\beta}} = (C_{l_{\dot\beta}})_s \cos\alpha - (C_{n_\beta})_s \sin\alpha$	
$C_{l_p} = (C_{l_p})_s \cos^2\alpha + (C_{n_r})_s \sin^2\alpha - (C_{n_p} + C_{l_r})_s \sin\alpha\cos\alpha$	
$C_{l_\delta} = (C_{l_\delta})_s \cos\alpha - (C_{n_\delta})_s \sin\alpha$	

TABLE II

Transformation of Derivatives from Body to Stability Axis

C_{L_α}	$= C_{N_\alpha} \cos\alpha - C_{C_\alpha} \sin\alpha - C_D$
C_{D_α}	$= C_{C_\alpha} \cos\alpha + C_{N_\alpha} \sin\alpha + C_L$
$(C_{m_\alpha})_s$	$= C_{m_\alpha}$
$(C_{n_\beta})_s$	$= C_{n_\beta} \cos\alpha - C_{l_\beta} \sin\alpha$
$(C_{n_r})_s$	$= C_{n_r} \cos^2\alpha + C_{l_p} \sin^2\alpha - (C_{l_r} - C_{n_p}) \sin\alpha\cos\alpha$
$(C_{n_{\dot\beta}})_s$	$= C_{n_{\dot\beta}} \cos\alpha - C_{l_{\dot\beta}} \sin\alpha$
$(C_{n_p})_s$	$= C_{n_p} \cos^2\alpha - C_{l_r} \sin^2\alpha + (C_{n_r} - C_{l_p}) \sin\alpha\cos\alpha$
$(C_{n_\delta})_s$	$= C_{n_\delta} \cos\alpha - C_{l_\delta} \sin\alpha$
$(C_{l_\beta})_s$	$= C_{l_\beta} \cos\alpha + C_{n_\beta} \sin\alpha$
$(C_{l_r})_s$	$= C_{l_r} \cos^2\alpha - C_{n_\beta} \sin^2\alpha + (C_{n_r} - C_{l_p}) \sin\alpha\cos\alpha$
$(C_{l_{\dot\beta}})_s$	$= C_{l_{\dot\beta}} \cos\alpha + C_{n_{\dot\beta}} \sin\alpha$
$(C_{l_p})_s$	$= C_{l_p} \cos^2\alpha + C_{n_r} \sin^2\alpha + (C_{l_r} + C_{n_p}) \sin\alpha\cos\alpha$
$(C_{l_\delta})_s$	$= C_{l_\delta} \cos\alpha + C_{n_\delta} \sin\alpha$

TABLE III

Transformation of Moments of Inertia from One Axis System to Another

Body to Stability

$$I_{x_s} = \tfrac{1}{2}(I_x + I_z) - \tfrac{1}{2}(I_z - I_x)\cos 2\alpha - I_{xz}\sin 2\alpha$$

$$I_{y_s} = I_y$$

$$I_{z_s} = \tfrac{1}{2}(I_x + I_z) + \tfrac{1}{2}(I_z - I_x)\cos 2\alpha + I_{xz}\sin 2\alpha$$

$$I_{x_s z_s} = \tfrac{1}{2}(I_x - I_z)\sin 2\alpha + I_{xz}\cos 2\alpha$$

Stability to Body

$$I_x = \tfrac{1}{2}(I_{x_s} + I_{z_s}) - \tfrac{1}{2}(I_{z_s} - I_{x_s})\cos 2\alpha + I_{x_s z_s}\sin 2\alpha$$

$$I_y = I_{y_s}$$

$$I_z = \tfrac{1}{2}(I_{z_s} + I_{x_s}) + \tfrac{1}{2}(I_{z_s} - I_{x_s})\cos 2\alpha - I_{x_s z_s}\sin 2\alpha$$

$$I_{xz} = I_{x_s z_s}\cos 2\alpha - \tfrac{1}{2}(I_{x_s} - I_{z_s})\sin 2\alpha$$

Principal to Stability

$$I_{x_s} = \tfrac{1}{2}(I_{x_0} + I_{z_0}) - \tfrac{1}{2}(I_{z_0} - I_{x_0})\cos 2\eta$$

$$I_{y_s} = I_{y_0}$$

$$I_{z_s} = \tfrac{1}{2}(I_{x_0} + I_{z_0}) + \tfrac{1}{2}(I_{z_0} - I_{x_0})\cos 2\eta$$

$$I_{x_s z_s} = \tfrac{1}{2}(I_{x_0} - I_{z_0})\sin 2\eta$$

Stability to Principal

$$I_{x_0} = \tfrac{1}{2}(I_{x_s} + I_{z_s}) - \tfrac{1}{2}(I_{z_s} - I_{x_s})\cos 2\eta + I_{x_s z_s}\sin 2\eta$$

$$I_{y_0} = I_{y_s}$$

$$I_{z_0} = \tfrac{1}{2}(I_{x_s} + I_{z_s}) + \tfrac{1}{2}(I_{z_s} - I_{x_s})\cos 2\eta - I_{x_s z_s}\sin 2\eta$$

$$I_{x_0 z_0} = 0 = I_{x_s z_s}\cos 2\eta - \tfrac{1}{2}(I_{x_s} - I_{z_s})\sin 2\eta$$

(Continued)

Principal to Body

$$I_x = \tfrac{1}{2}(I_{x_0} + I_{z_0}) - \tfrac{1}{2}(I_{z_0} - I_{x_0}) \cos 2\epsilon$$

$$I_y = I_{y_0}$$

$$I_z = \tfrac{1}{2}(I_{x_0} + I_{z_0}) + \tfrac{1}{2}(I_{z_0} - I_{x_0}) \cos 2\epsilon$$

$$I_{xz} = -\tfrac{1}{2}(I_{x_0} - I_{z_0}) \sin 2\epsilon$$

Body to Principal

$$I_{x_0} = \tfrac{1}{2}(I_x + I_z) - \tfrac{1}{2}(I_z - I_x) \cos 2\epsilon - I_{xz} \sin 2\epsilon$$

$$I_{y_0} = I_y$$

$$I_{z_0} = \tfrac{1}{2}(I_x + I_z) + \tfrac{1}{2}(I_z - I_x) \cos 2\epsilon + I_{xz} \sin 2\epsilon$$

$$I_{x_0 z_0} = 0 = I_{xz} \cos 2\epsilon + \tfrac{1}{2}(I_x - I_z) \sin 2\epsilon$$

TABLE IV – General Equations of Motion

Velocity Components

$$u = V\cos\beta\cos\alpha \quad (50a) \qquad v = V\sin\beta \quad (50b) \qquad w = V\cos\beta\sin\alpha \quad (50c)$$

Linear Acceleration Equations

$$a_x = (\dot{u} + wq - vr + g\sin\theta)\frac{1}{g} \quad (51a) \qquad a_t = (\dot{v} - wp + ur - g\cos\theta\sin\phi)\frac{1}{g} \quad (51b)$$

$$a_n = -(\dot{w} - uq + vp - g\cos\theta\cos\phi)\frac{1}{g} \quad (51c)$$

Force Equations

$$W_{a_x} = -\left[\bar{C}_{c_u}\frac{\Delta u}{V} + C_{c_\alpha}\alpha + C_{c_q}\frac{q\bar{c}}{2V} + C_{c_{\dot\alpha}}\frac{\dot\alpha\bar{c}}{2V} + \Sigma C_{c_\delta}\delta\right]\bar{q}S \quad (52a) \qquad W_{a_t} = \left[C_{y_\beta}\beta + C_{y_r}\frac{rb}{2V} + C_{y_{\dot\beta}}\frac{\dot\beta b}{2V} + C_{y_p}\frac{pb}{2V} + \Sigma C_{y_\delta}\delta\right]\bar{q}S \quad (52b)$$

$$W_{a_n} = \left[\bar{C}_{N_u}\frac{\Delta u}{V} + C_{N_\alpha}\alpha + C_{N_q}\frac{q\bar{c}}{2V} + C_{N_{\dot\alpha}}\frac{\dot\alpha\bar{c}}{2V} + \Sigma C_{N_\delta}\delta\right]\bar{q}S \quad (52c)$$

Moment Equations

$$I_x\dot{p} + (I_z - I_y)qr - I_{xz}(\dot{r} + pq) - I_{rm}\Omega q\sin\theta_{rm} = \left[C_{l_\beta}\beta + C_{l_p}\frac{pb}{2V} + C_{l_r}\frac{rb}{2V} + C_{l_{\dot\beta}}\frac{\dot\beta b}{2V} + \Sigma C_{l_\delta}\delta\right]\bar{q}Sb \quad (53a)$$

$$I_y\dot{q} - (I_z - I_x)pr - I_{xz}(r^2 - p^2) + I_{rm}\Omega(r\cos\theta_{rm} + p\sin\theta_{rm}) = \left[C_{m_0} + C_{m_u}\frac{\Delta u}{V} + C_{m_\alpha}\alpha + C_{m_q}\frac{q\bar{c}}{2V} + C_{m_{\dot\alpha}}\frac{\dot\alpha\bar{c}}{2V} + \Sigma C_{m_\delta}\delta\right]\bar{q}S\bar{c} \quad (53b)$$

$$I_z\dot{r} + (I_y - I_x)pq - I_{xz}(\dot{p} - rq) - I_{rm}\Omega\cos\theta_{rm} = \left[C_{n_\beta}\beta + C_{n_r}\frac{rb}{2V} + C_{n_{\dot\beta}}\frac{\dot\beta b}{2V} + C_{n_p}\frac{pb}{2V} + \Sigma C_{n_\delta}\delta\right]\bar{q}S\bar{b} \quad (53c)$$

Transformations for Angular Rates

$$p = \dot\phi - \dot\psi\sin\theta \quad (54a) \qquad \dot\theta = q\cos\phi - r\sin\phi \quad (55a)$$

$$q = \dot\theta\cos\phi + \dot\psi\cos\theta\sin\phi \quad (54b) \qquad \dot\phi = p + (q\sin\phi + r\cos\phi)\tan\theta \quad (55b)$$

$$r = \dot\psi\cos\theta\cos\phi - \dot\theta\sin\phi \quad (54c) \qquad \dot\psi = (q\sin\phi + r\cos\phi)\sec\theta \quad (55c)$$

TABLE V

Linearized Small-Perturbation Equations of Motion

Longitudinal Equations

$$\Delta a_x \simeq \left[\Delta\dot{u} + w\Delta q + g\cos\theta\cos\phi\,\Delta\theta'\right]\frac{1}{g} \tag{56a}$$

$$\Delta a_n \simeq -\left[\Delta\dot{w} - u\Delta q - q\Delta u + g\sin\theta\,\Delta\theta'\right]\frac{1}{g} \tag{56b}$$

$$\Delta\theta' \simeq \int\Delta q\,dt \tag{57}$$

$$W\Delta a_x = -\left[\bar{C}_{c_u}\frac{\Delta u}{V} + C_{c_\alpha}\Delta\alpha + \Sigma C_{c_\delta}\Delta\delta\right]\bar{q}S \tag{58a}$$

$$W\Delta a_n = \left[\bar{C}_{N_u}\frac{\Delta u}{V} + C_{N_\alpha}\Delta\alpha + C_{N_q}\frac{\Delta q\bar{c}}{2v} + C_{N_{\dot\alpha}}\frac{\Delta\dot\alpha\bar{c}}{2V} + \Sigma C_{N_\delta}\Delta\delta\right]\bar{q}S \tag{58b}$$

$$I_y\Delta\dot{q} = \left[\bar{C}_{m_u}\frac{\Delta u}{V} + C_{m_\alpha}\Delta\alpha + C_{m_q}\frac{\Delta q\bar{c}}{2v} + C_{m_{\dot\alpha}}\frac{\Delta\dot\alpha\bar{c}}{2V} + \Sigma C_{m_\delta}\Delta\delta\right]\bar{q}S\bar{c} \tag{58c}$$

Lateral-Directional Equations

$$\Delta a_t \simeq \left[\Delta\dot{v} + u\Delta r - w\Delta p - g\left(\sin\theta\,\Delta\psi' + \cos\theta\cos\phi\,\Delta\phi'\right)\right]\frac{1}{g} \tag{59}$$

$$\Delta\psi' \simeq \int\Delta r\,dt \tag{60a}$$

$$\Delta\phi' \simeq \int\Delta p\,dt \tag{60b}$$

$$W\Delta a_t = \left[C_{y_\beta}\Delta\beta + \Sigma C_{y_\delta}\Delta\delta\right]\bar{q}S \tag{61a}$$

$$I_x\Delta\dot{p} - I_{xz}\Delta\dot{r} = \left[C_{l_\beta}\Delta\beta + C_{l_p}\frac{\Delta pb}{2V} + C_{l_r}\frac{\Delta rb}{2V} + C_{l_{\dot\beta}}\frac{\Delta\dot\beta b}{2V} + \Sigma C_{l_\delta}\Delta\delta\right]\bar{q}Sb \tag{61b}$$

$$I_z\Delta\dot{r} - I_{xz}\Delta\dot{p} = \left[C_{n_\beta}\Delta\beta + C_{n_p}\frac{\Delta pb}{2V} + C_{n_r}\frac{\Delta rb}{2V} + C_{n_{\dot\beta}}\frac{\Delta\dot\beta b}{2V} + \Sigma C_{n_\delta}\Delta\delta\right]\bar{q}Sb \tag{61c}$$

TABLE VI

Laplace Transform Format of Small-Perturbation Equations of Motion

Longitudinal

$$\begin{bmatrix} (s - \bar{X}_u) & (s\sin\alpha + g_2) & -\bar{X}_\alpha \\ (q + \bar{Z}_u) & (s\cos\alpha + \bar{Z}_q s - g_1) & -(s - \bar{Z}_{\dot{\alpha}} s - \bar{Z}_\alpha) \\ -\bar{M}_u & s(s - \bar{M}_q) & -(\bar{M}_{\dot{\alpha}} s + \bar{M}_\alpha) \end{bmatrix} \begin{bmatrix} \Delta u \\ \Delta\theta' \\ \Delta\alpha \end{bmatrix} = \Delta\delta \begin{bmatrix} \bar{X}_\delta \\ -\bar{Z}_\delta \\ \bar{M}_\delta \end{bmatrix} \tag{62a}$$

(62b)

(62c)

Lateral-Directional

$$\begin{bmatrix} (s - \bar{Y}_\beta) & (s\cos\alpha - g_1) & -(s\sin\alpha + g_2) \\ -\bar{L}_\beta & -s(I'_x s + \bar{L}_r) & s(s - \bar{L}_p) \\ -\bar{N}_\beta & s(s - \bar{N}_r) & -s(I'_z s - \bar{N}_p) \end{bmatrix} \begin{bmatrix} \Delta\beta \\ \Delta\psi' \\ \Delta\phi' \end{bmatrix} = \Delta\delta \begin{bmatrix} \bar{Y}_\delta \\ \bar{L}_\delta \\ \bar{N}_\delta \end{bmatrix} \tag{63a}$$

(63b)

(63c)

where

$$g_1 = (g/V)\sin\theta \tag{64a}$$

$$g_2 = (g/V)\cos\theta\cos\phi \tag{64b}$$

TABLE VII

Desirable Characteristics of Instruments for Free-Oscillation Maneuver

Function	*Range*	*Sensitivity (per inch deflection)*	*Undamped natural frequency (c/s)*	*Damping ratio*
α , deg	±10	5.0	8 or more	0.65
β , deg	±10	4.0	8 or more	0.65
q , radian/sec	±0.2	0.2	8 or more	0.65
$\dot{q}$, radian/sec^2	±0.5	0.5	8 or more	0.65
r , radian/sec	±0.1	0.1	8 or more	0.65
$\dot{r}$, radian/sec^2	±0.4	0.4	8 or more	0.65
p , radian/sec	±0.2	0.2, rudder pulses	8 or more	0.65
	±0.6	0.6, aileron pulses	8 or more	0.65
$\dot{p}$, radian/sec^2	±0.6	0.6, rudder pulses	8 or more	0.65
	±6.0	6.0, aileron pulses	8 or more	0.65
a_n , g units	±1	1.0	8 or more	0.65
a_t , g units	±0.3	0.3, rudder pulses	8 or more	0.65
	±0.6	0.6, aileron pulses	8 or more	0.65

TABLE VIII

Format used by NASA Flight Research Center to Record Actual Conditions at Time of Maneuver

Trace	Instrument		Scale factors	
	Nat. freq	Damp ratio	Flt's. 20 →	Flt's.
p	6.75	0.65	0.511	
r	6.75	.65	.126	
a_t	19.50	.65	.490	
β	10.50	.65	10.30	

β-vane location

X_v = _____ ; Z_v = _____

Linear accelerometer location

X = _____ ; Y = _____ ; Z = _____

S = _____

1	2	3	4	5	6	7	8	9	10
Comment	Flt.-Run	h_p, ft	M	V, fps	Dynamic pressure, $\bar{q}$	Weight, W, lb	C.G., % MAC	$C_{L_t} = \frac{W}{\bar{q}S}$	Density, ρ, slugs/ft^3
	20-17	40,320	0.745	723	142	23,800	28.7	0.237	.000573

Trace	Instrument		Scale factors	
	Nat. freq	Damp. ratio	Flt's. 10 →	Flt's.
α	10.5	.65	10.6	
a_n	32.0	.65	5.17	
δ_r			13.4	
δ_a			16.7	

Airplane _____

Configuration _____

_____

11	12	13	14	15	16	17	18	19
α, deg / a_n-trim, g units	δ_e-trim, deg	Control input, $\Delta\delta$, deg	Period, P, sec	$T_{1/2}$, sec	$\omega_{n_d} = \frac{2\pi}{P}$	Damping angle $\Phi_d = \tan^{-1}\left(\frac{1103P}{T_{1/2}}\right)$	Damping ratio $\zeta = \sin\Phi_d$	Undamped nat. freq. $\omega_n = \omega_{n_d}/\cos\Phi_d$
6.5 / .93		-7.55	3.66	2.92	1.72	7.56	0.131	1.73

TABLE IX

Airplane	*M*	*Altitude, ft*	α, *deg*	*Reference* C_{n_β} *(Eq. (6-53))*	C_{n_β} *, per radian*	
					Equation (6-54)	*Equation (6-56)*
F-104	0.94	41 000	4.9	0.46	0.46	0.57
YF-102	0.74	40,000	6.6	0.054	0.043	0.106

TABLE X

$\alpha/M/h$	15/0.8/60	3.5/0.8/40	6.6/1.2/60	14/1.6/80	10/2.0/80	5/2.0/80
Analog value of C_{l_β}	-0.084	-0.021	-0.032	-0.074	-0.0164	-0.0034
Analog value of C_{n_β}	0.259	0.641	0.640	0.367	0.445	0.508
Equation (166)	0.266	0.661	0.663	0.360	0.434	0.498
Equation (175)	0.278	0.679	0.674	0.383	0.451	0.504

TABLE XI

$\alpha/M/h$*	15/0.8/60	3.5/1.0/40	18/1.2/80	6.6/1.2/80	14/2.0/80	10/2.0/80	5/2.0/80
Analog value of $(C_{n_r} - C_{n_{\dot\beta}})$	-1.58	-1.734	-1.71	-1.92	-2.09	-2.55	-2.58
Equation (184)	-2.50	-1.43	-2.96	-1.81	-4.77	-2.76	-2.68
Equation (183)	-4.22	-1.647	-4.69	-2.36	-8.46	-4.41	-4.39

* h = altitude/1000

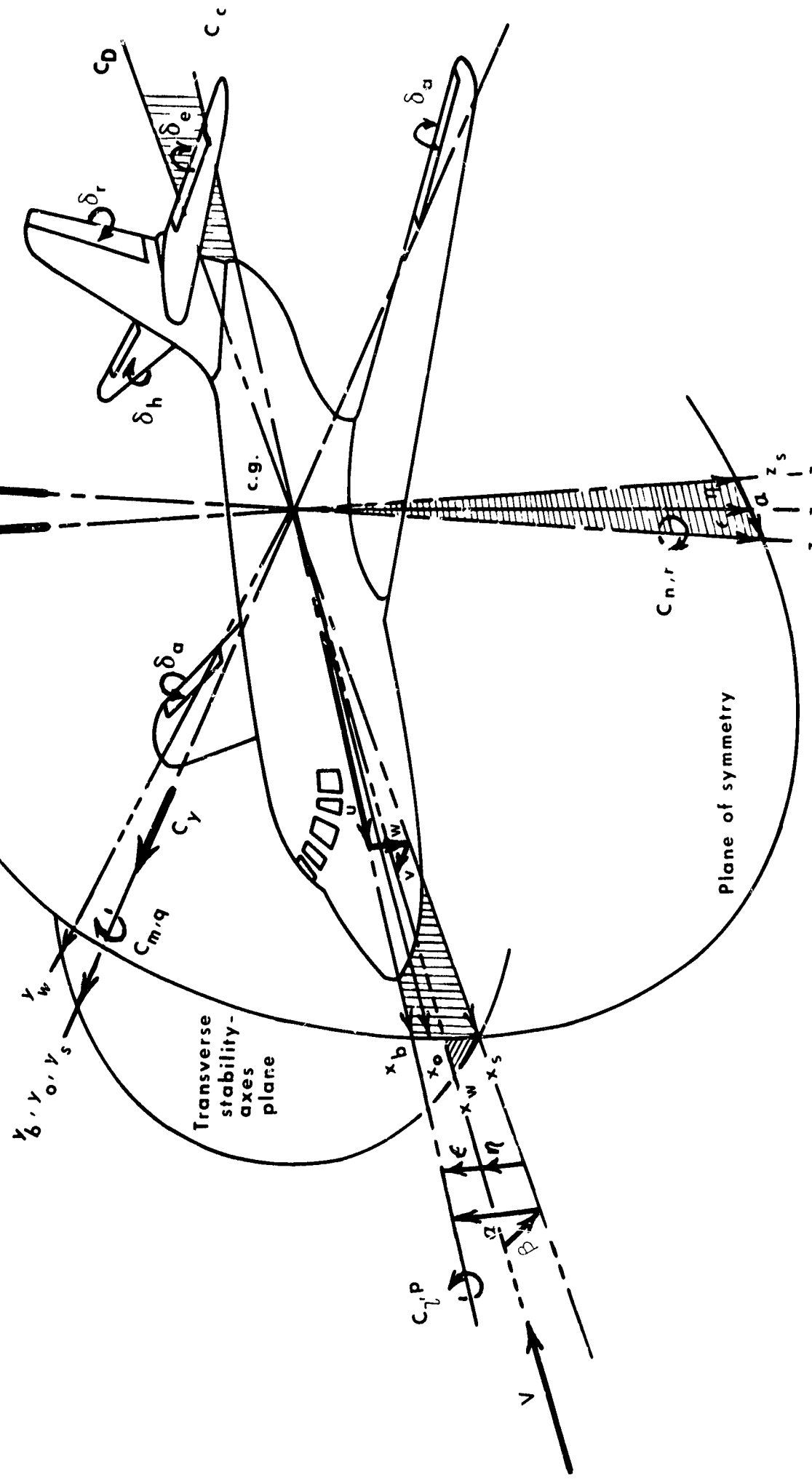

Fig. 1 Definition of body, stability, principal, and wind axis systems, control deflections, and force and moment coefficients

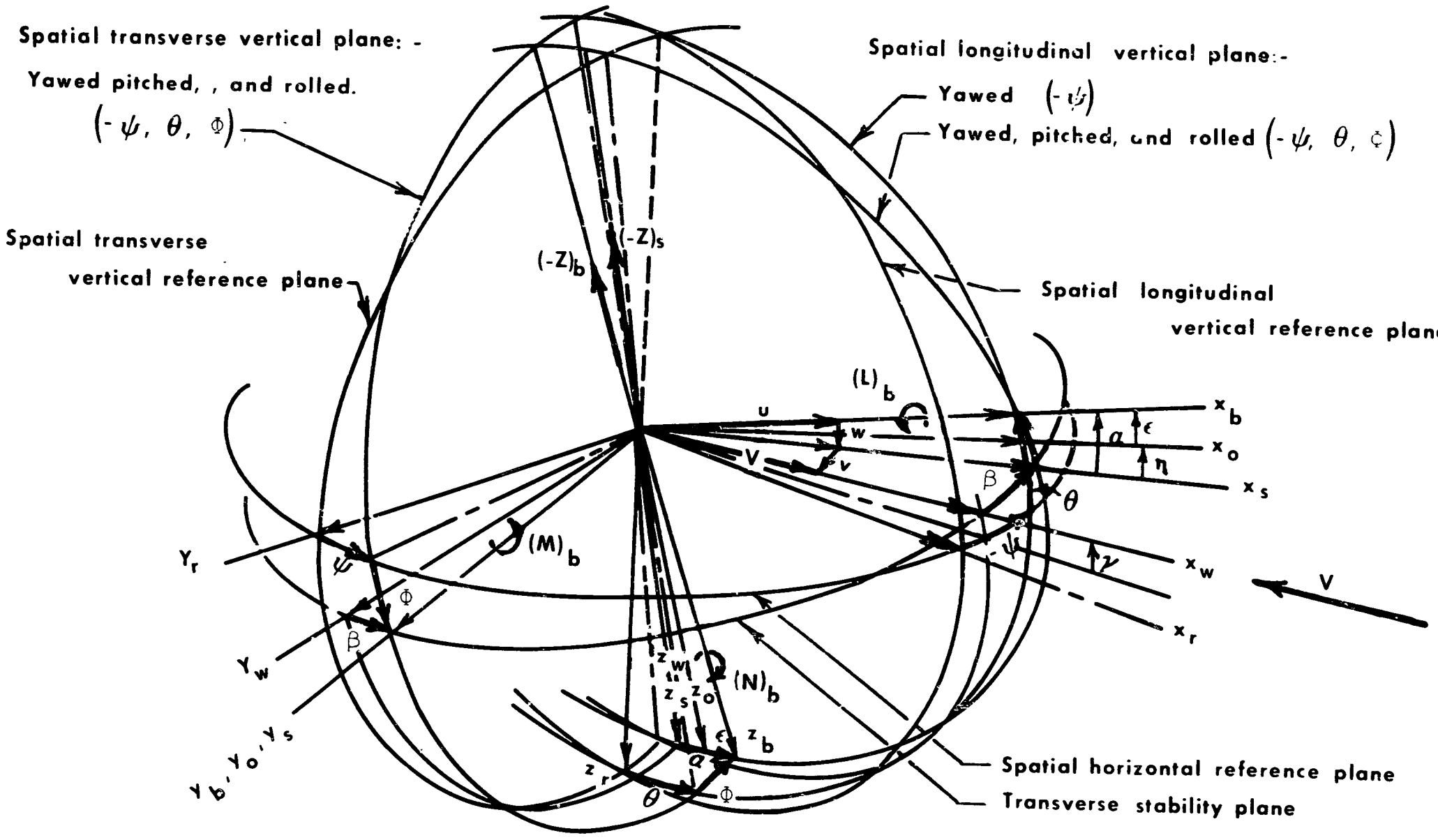

Fig. 2 Relationship of body, stability, principal, wind, and spatial-reference orthogonal axes systems when body x-axis is rotated in sequence through $-\psi$, θ, and ϕ

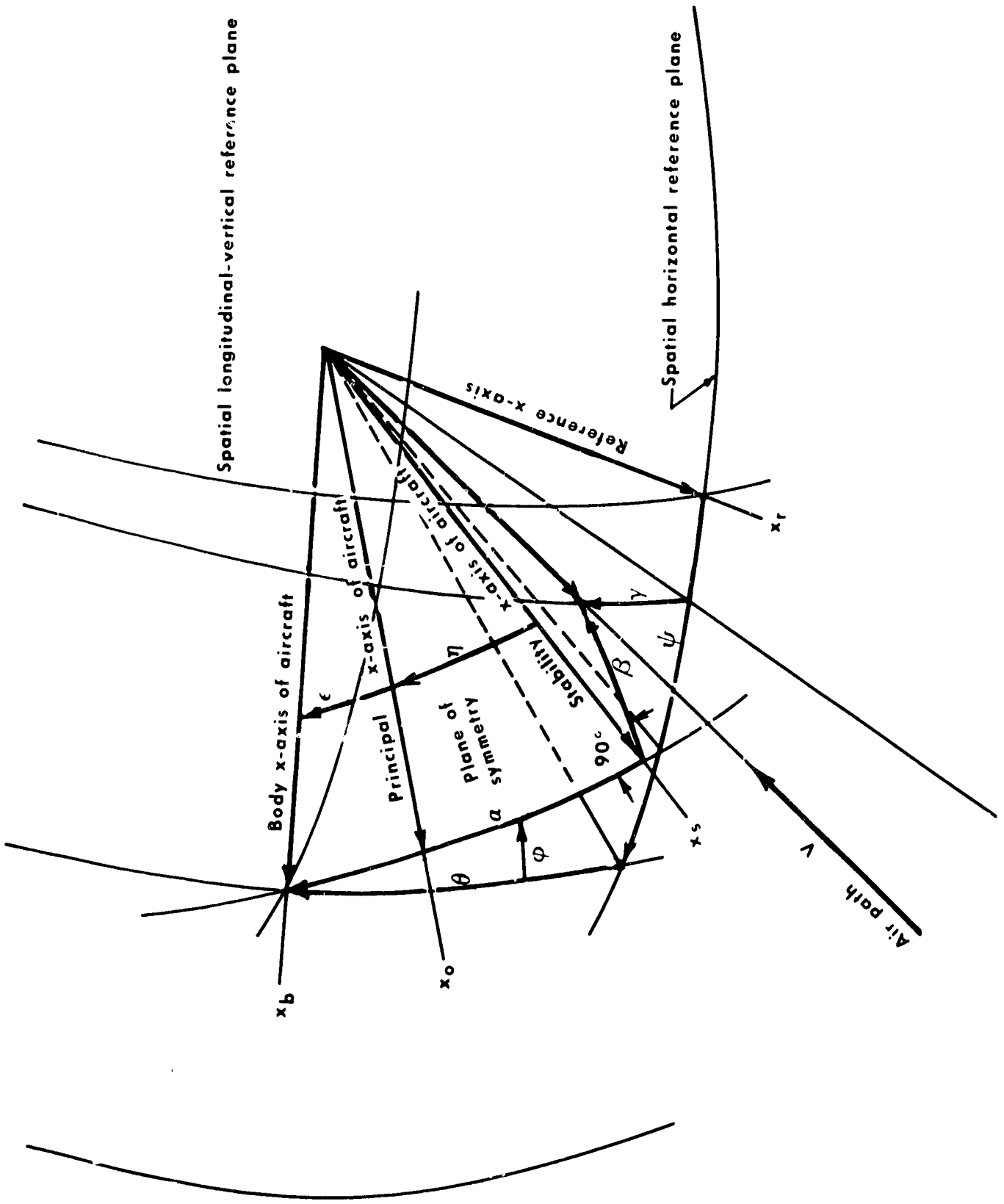

Fig. 3 Relationship of aerodynamic angles α, β, and γ; axes and Euler angles ψ, θ, and ϕ

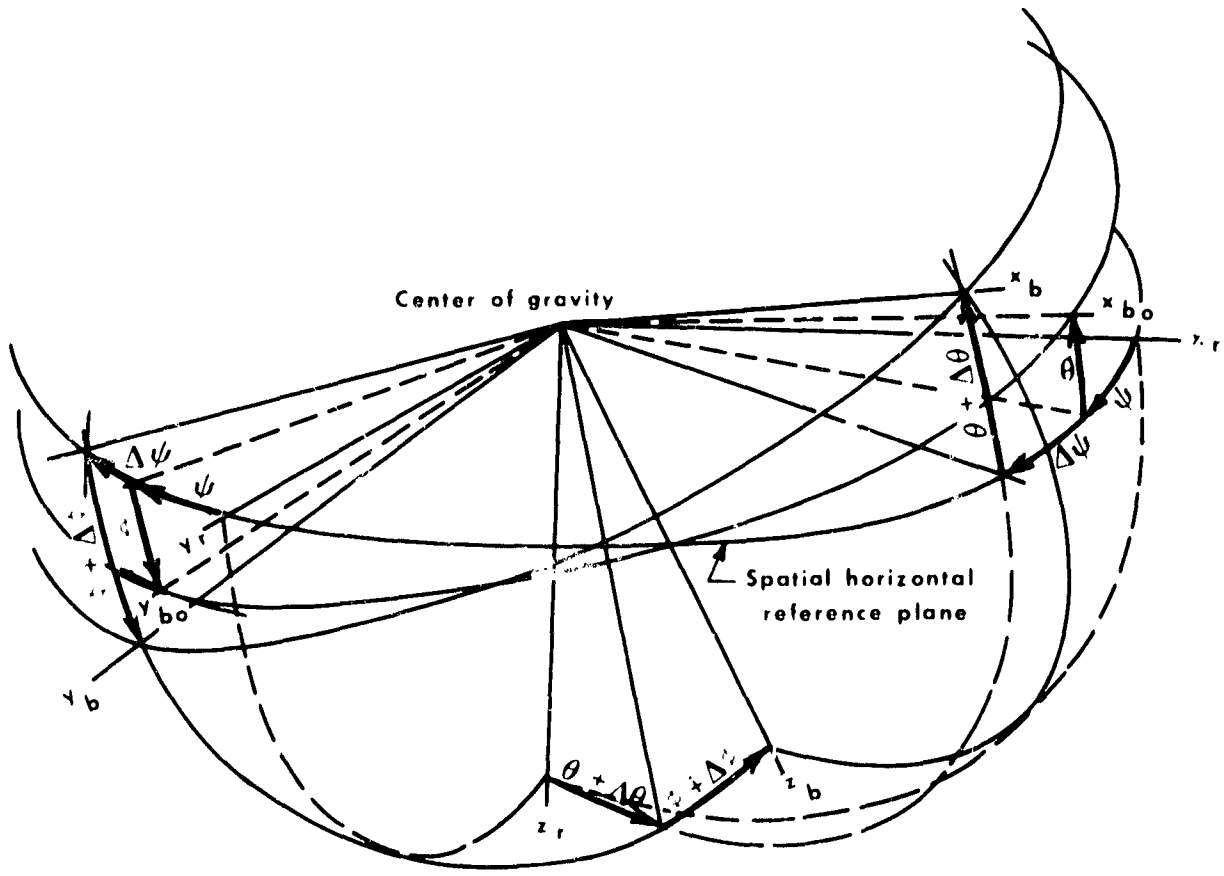

(a) Euler angle perturbation referred to the $x_r y_r z_r$ basic reference frame

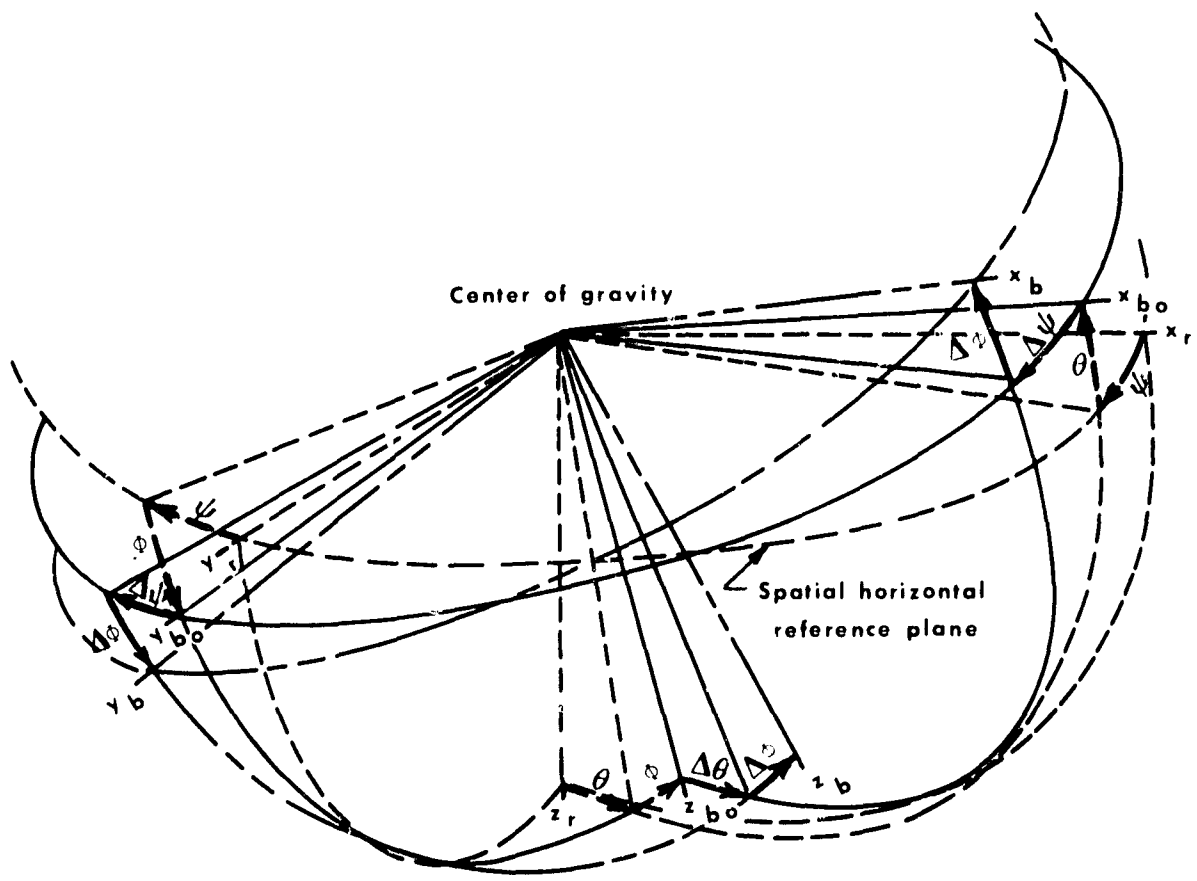

(b) Euler angle perturbation referred to $x_{b_0} y_{b_0} z_{b_0}$ axes serving as a secondary spatial reference

Fig. 4 Several methods of considering Euler angle perturbations

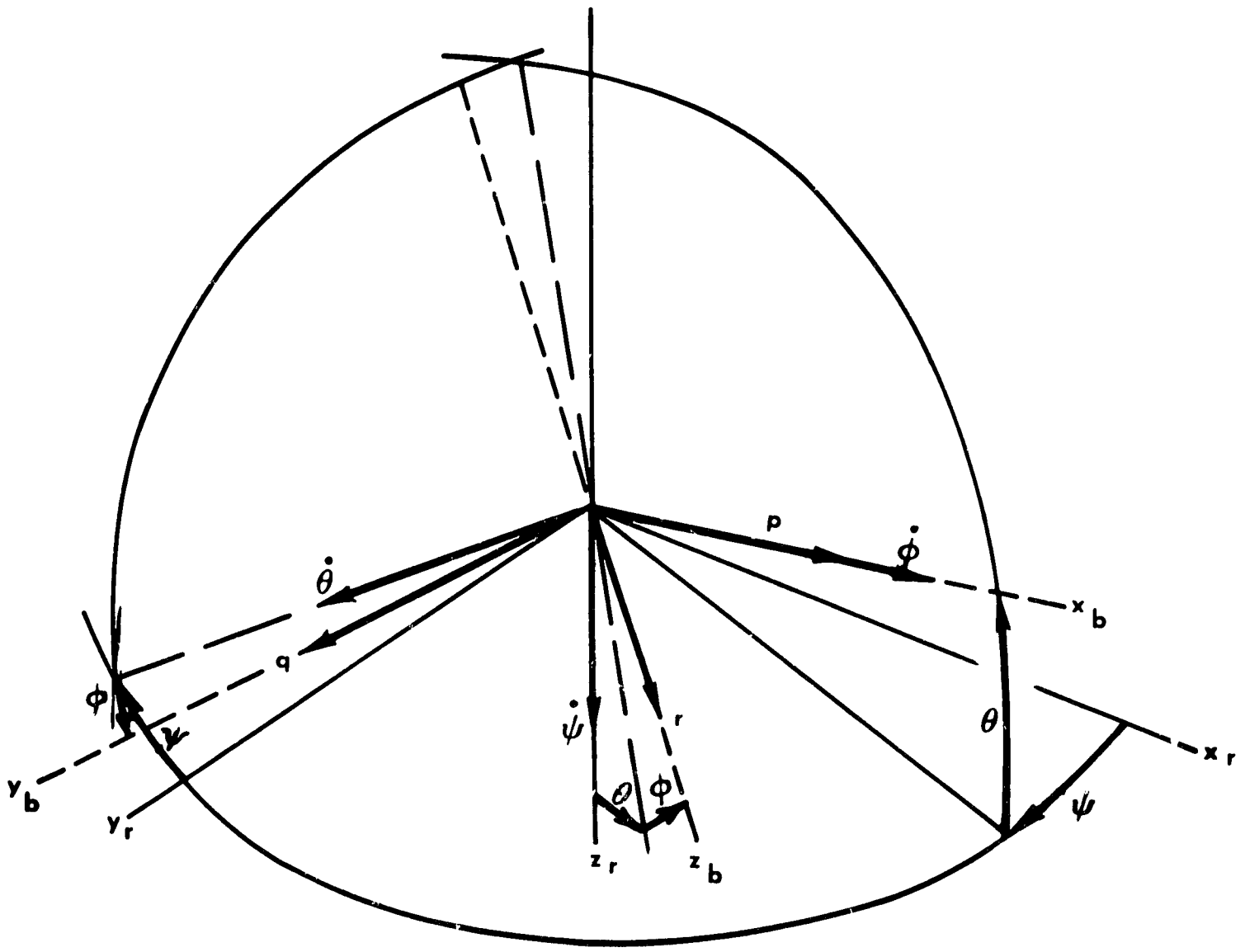

Fig.5 Relation of p , q , and r about body axes and Euler angle rates $\dot{\psi}$, $\dot{\theta}$, and $\dot{\phi}$

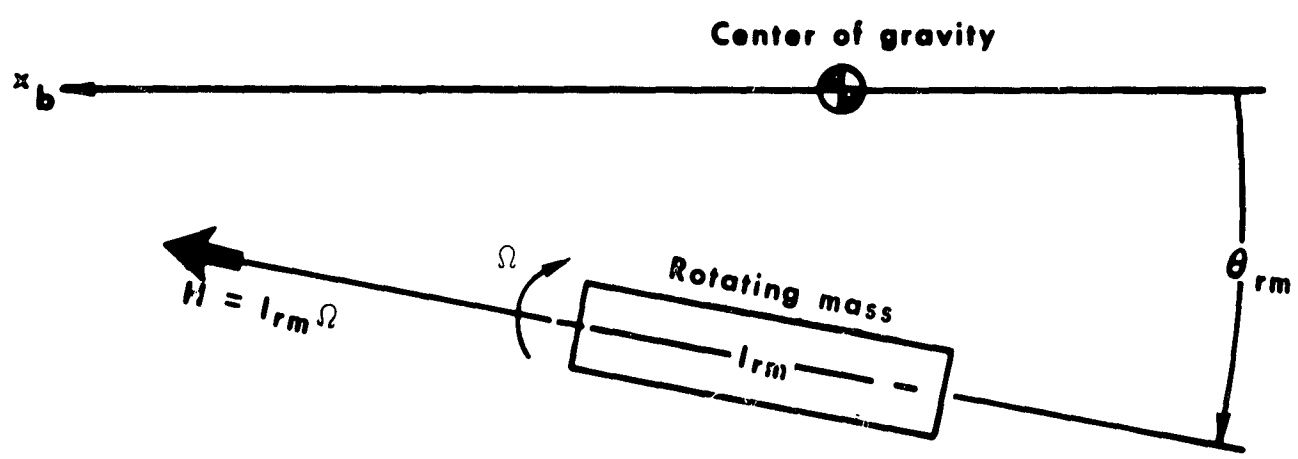

Fig.6 Pertinent relationships of rotating mass for gyroscopic couple consideration. Rotating axis parallel to xz-plane of symmetry

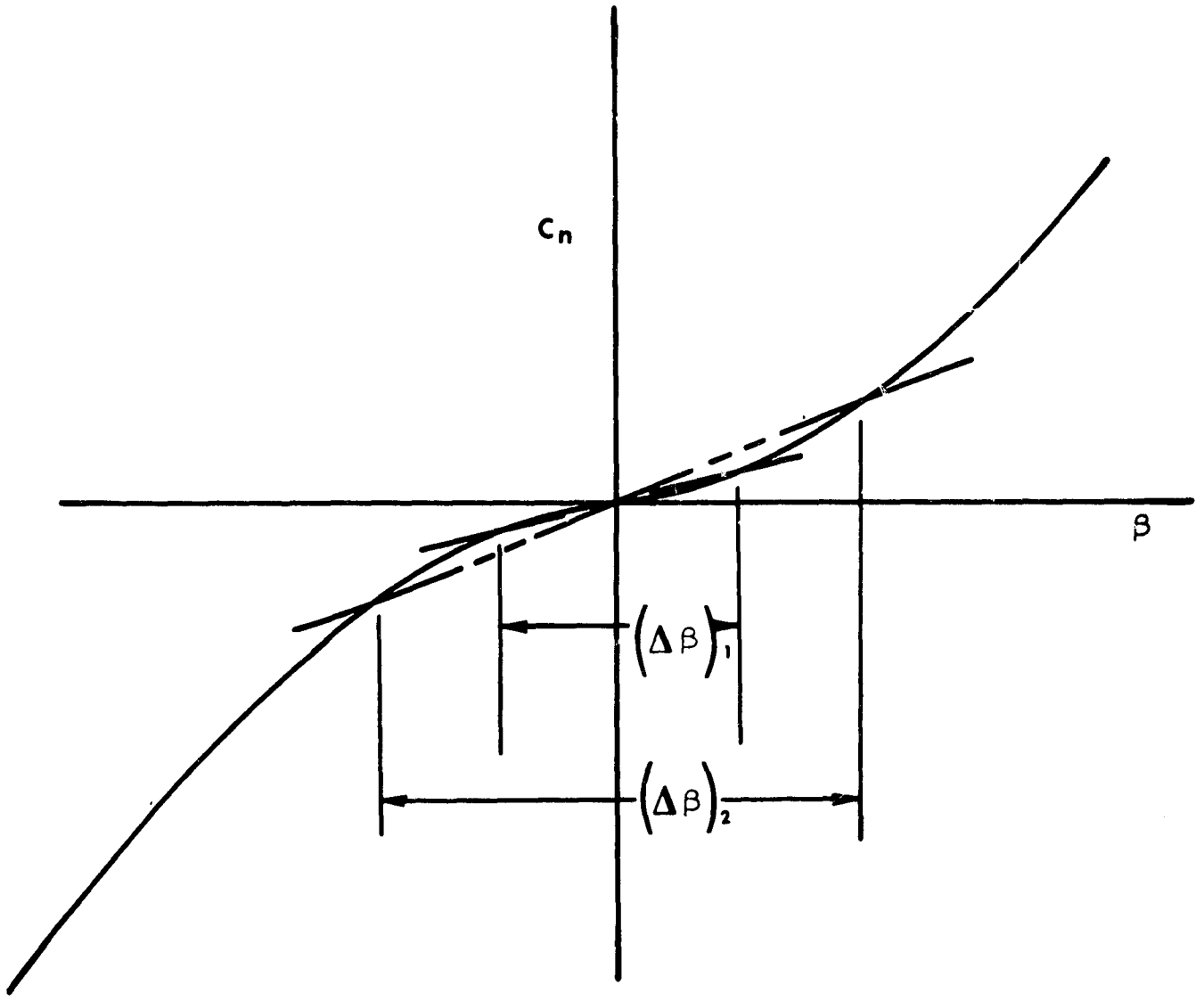

Fig.7 An example of the influence of ranges of disturbances such as $(\Delta\beta)_1$ and $(\Delta\beta)_2$ on the value of a derivative

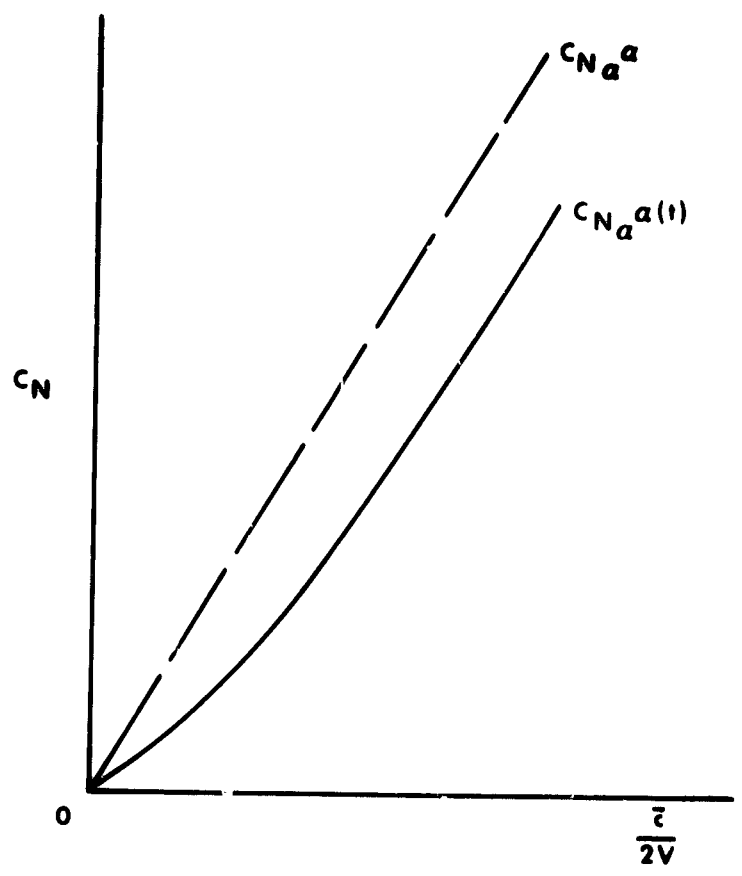

Fig.8 Effect of time lag of modification of vortex flow about lifting surface on the change in C_N following initial instant change in α

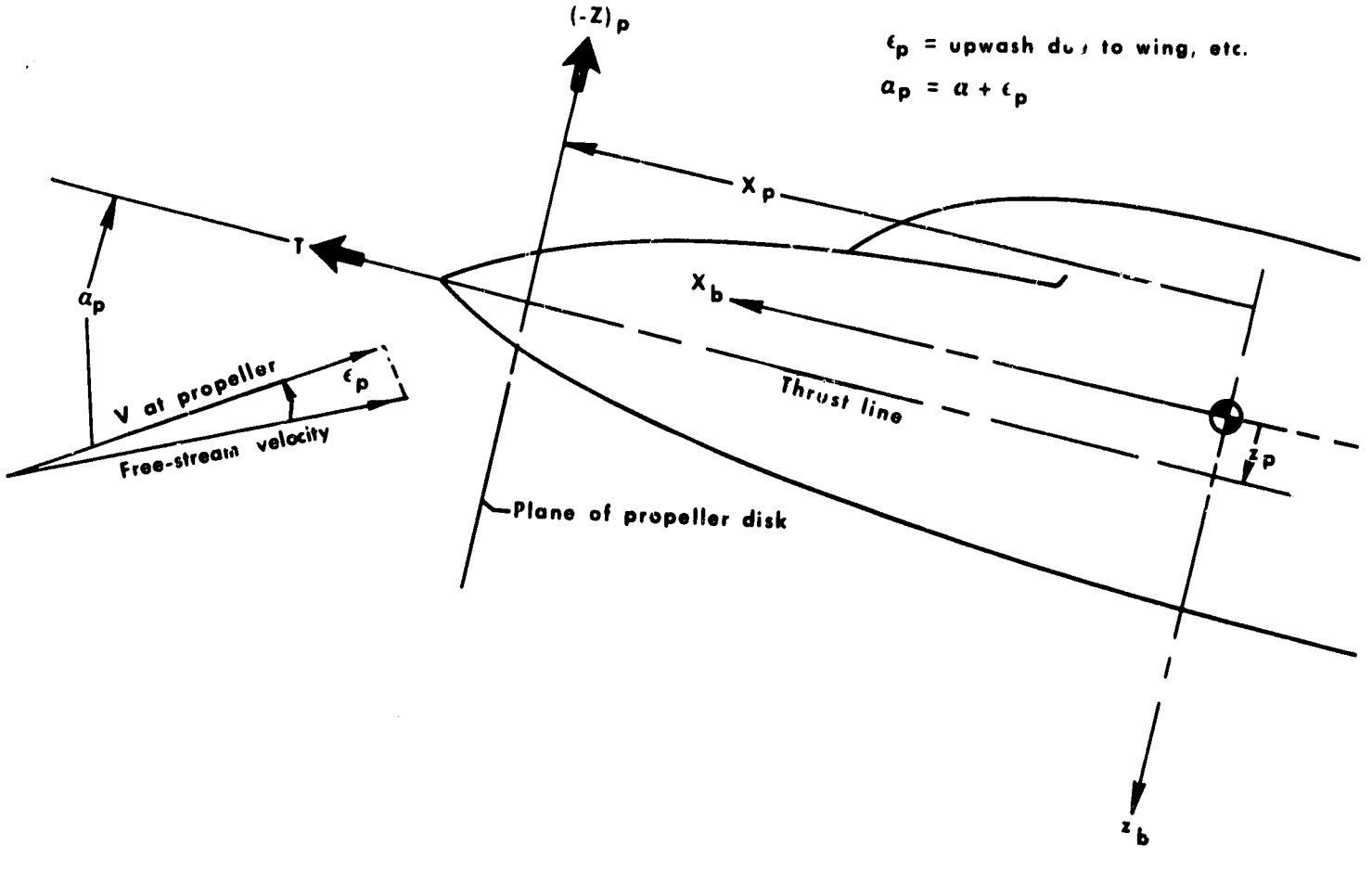

Fig.9 Direct propulsive effects of propeller

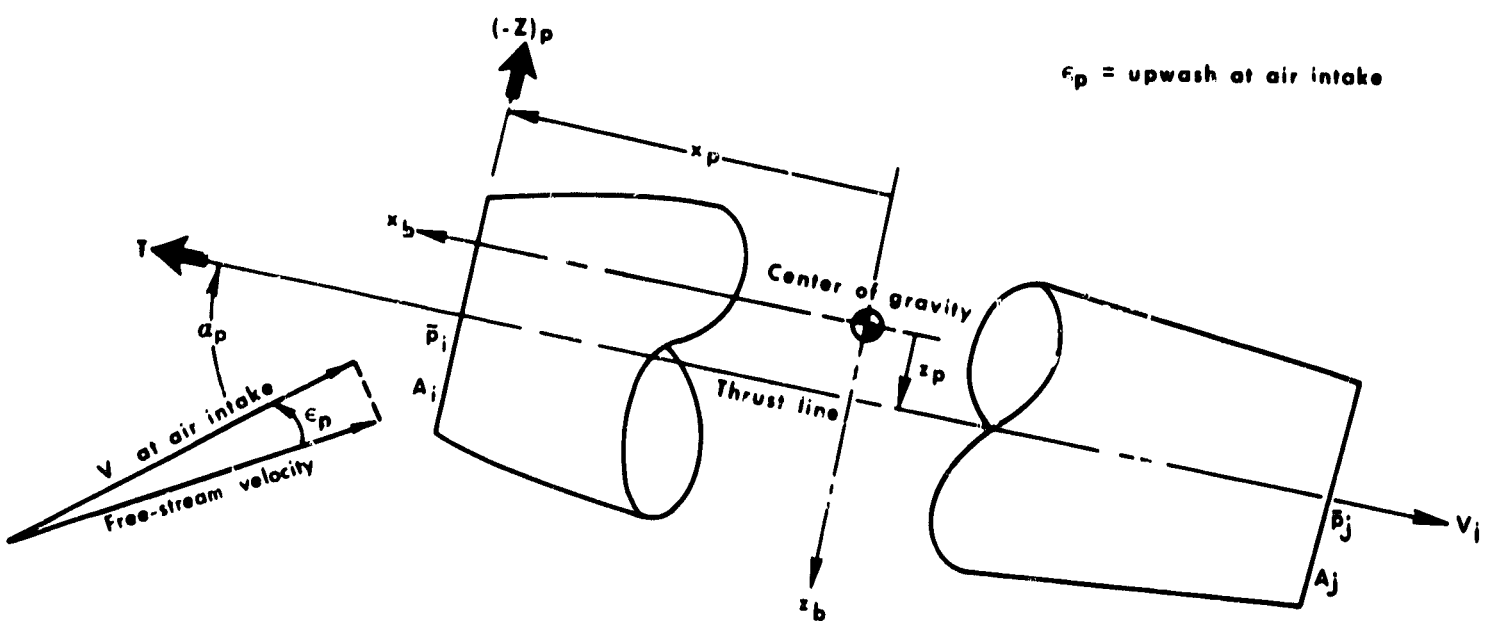

Fig. 10 Direct propulsive effects of jet engine

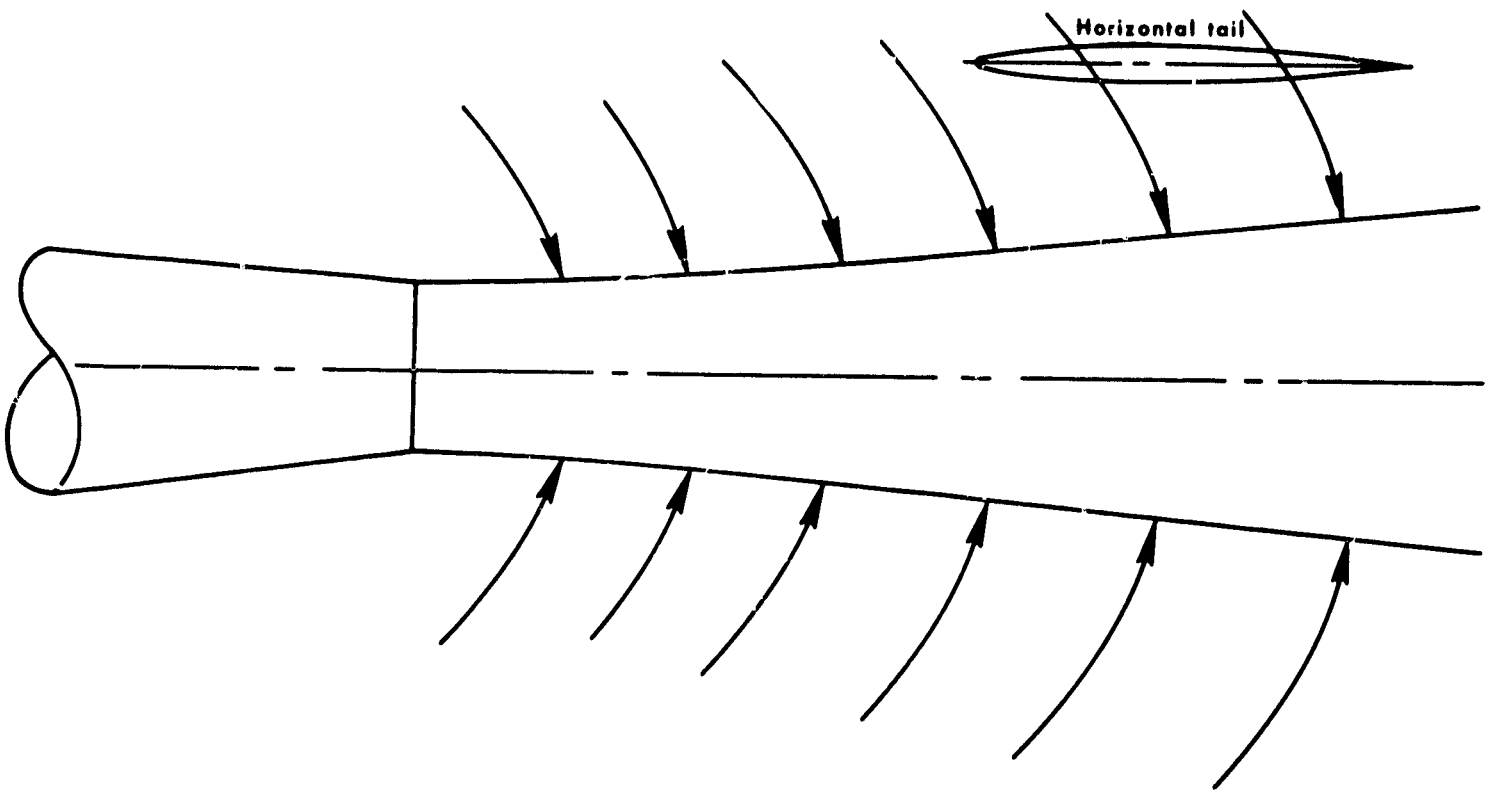

Fig. 11 Jet-exhaust inflow effect on horizontal tail

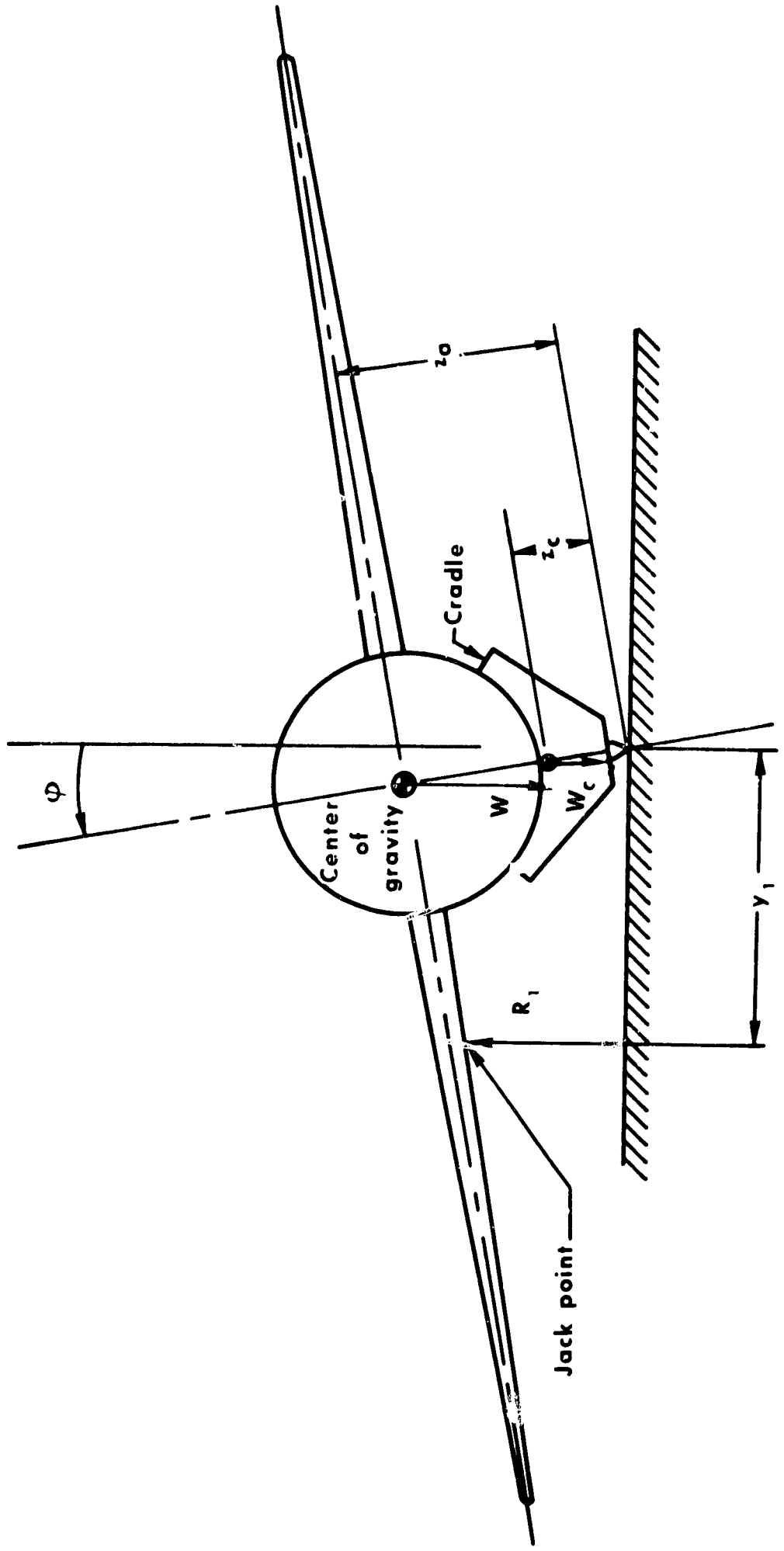

Fig. 12 Determination of vertical position of center-of-gravity by tilting aircraft in roll

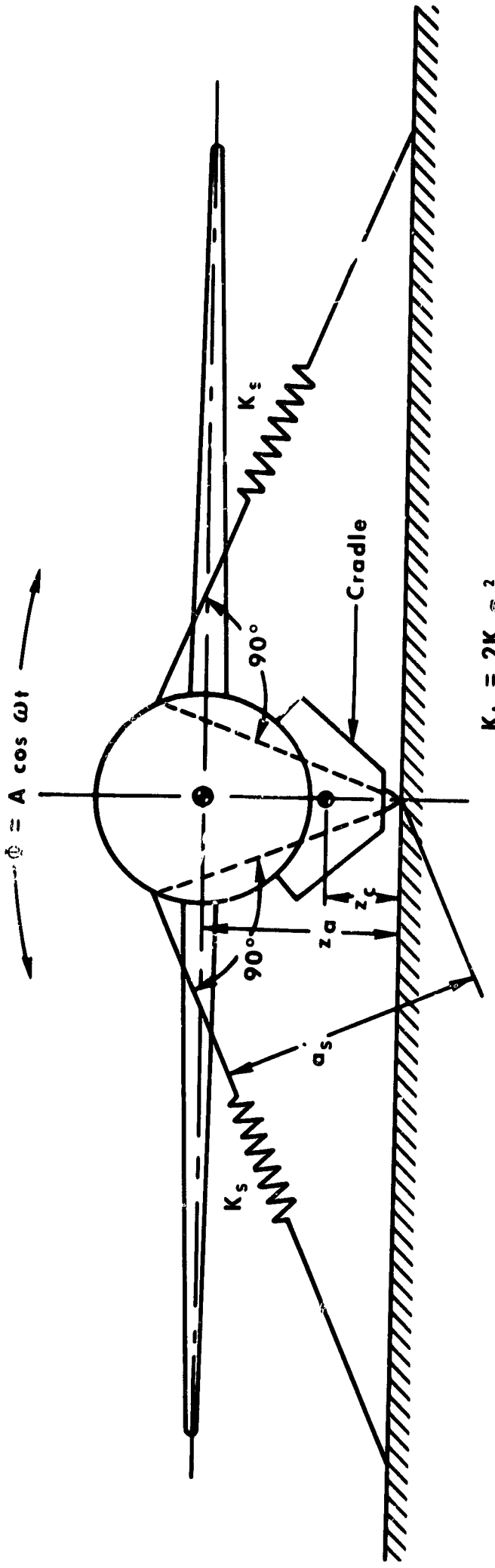

Fig. 13 Determination of vertical center-of-gravity and rolling moments of inertia by rolling oscillations

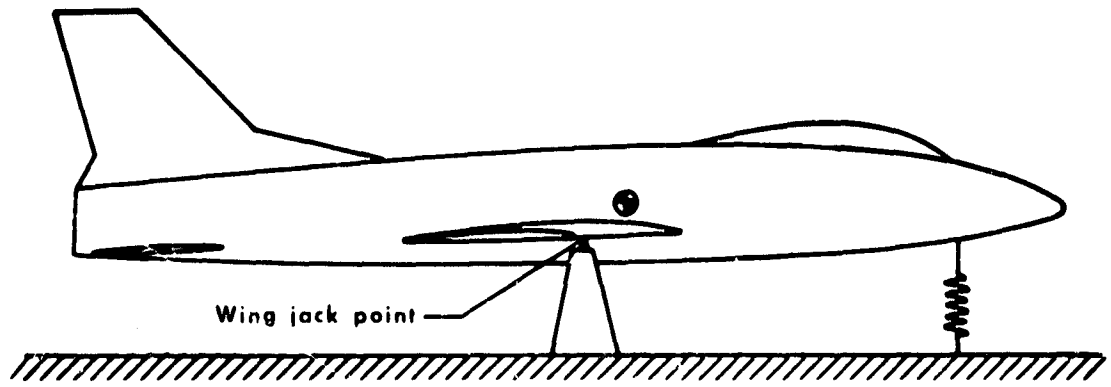

Fig. 14 Determination of pitching moment of inertia

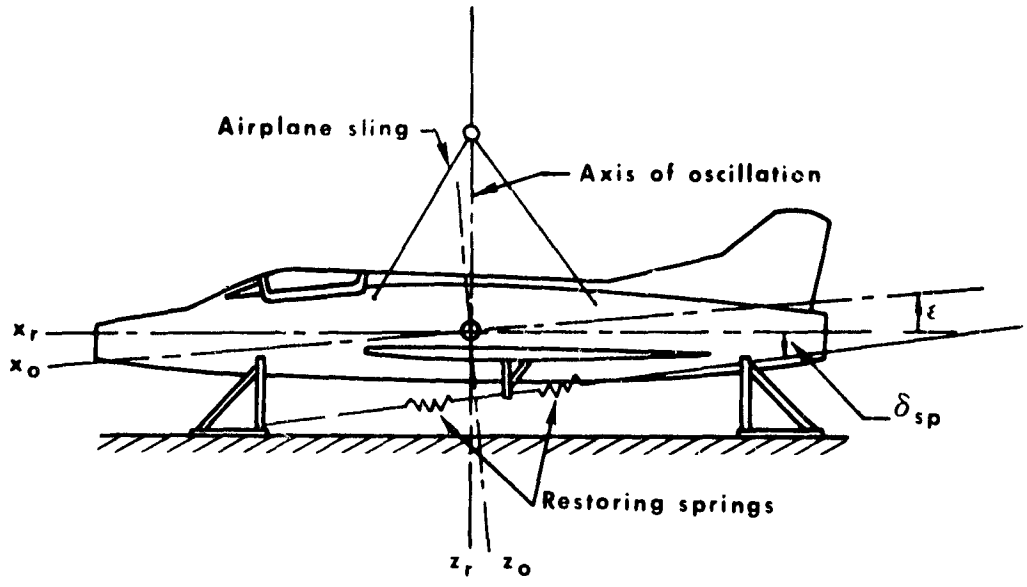

(a) Test setup

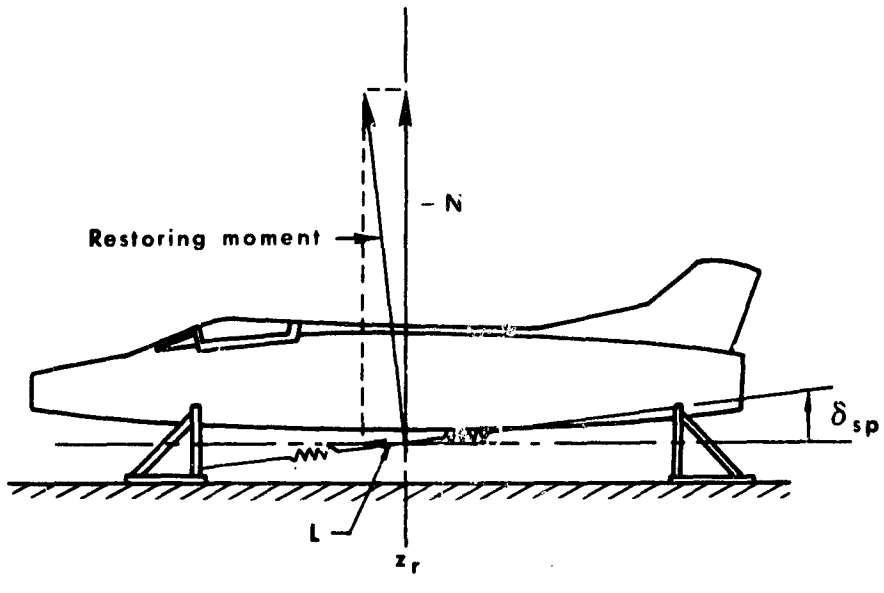

(b) Vector resolution

Fig. 15 Determination of inclination of principal axis and yawing moment of inertia

Fig. 16 Photograph showing a general arrangement for determining inclination of principal axis and yawing moment of inertia. Springs attached to mounting brackets located below wings

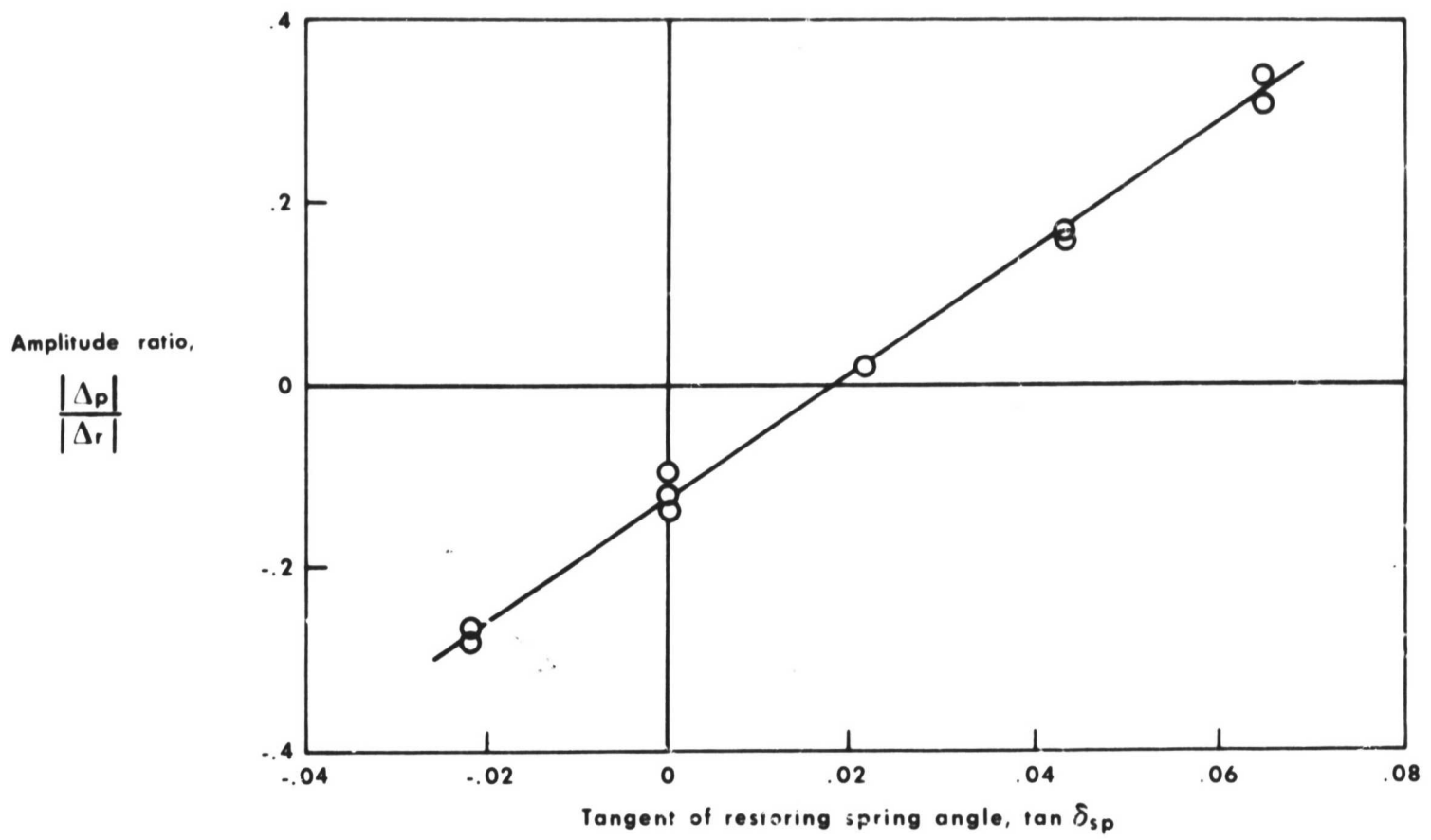

Fig. 17 Amplitude ratio $|\Delta p|/|\Delta r|$ as a function of spring restoring angle

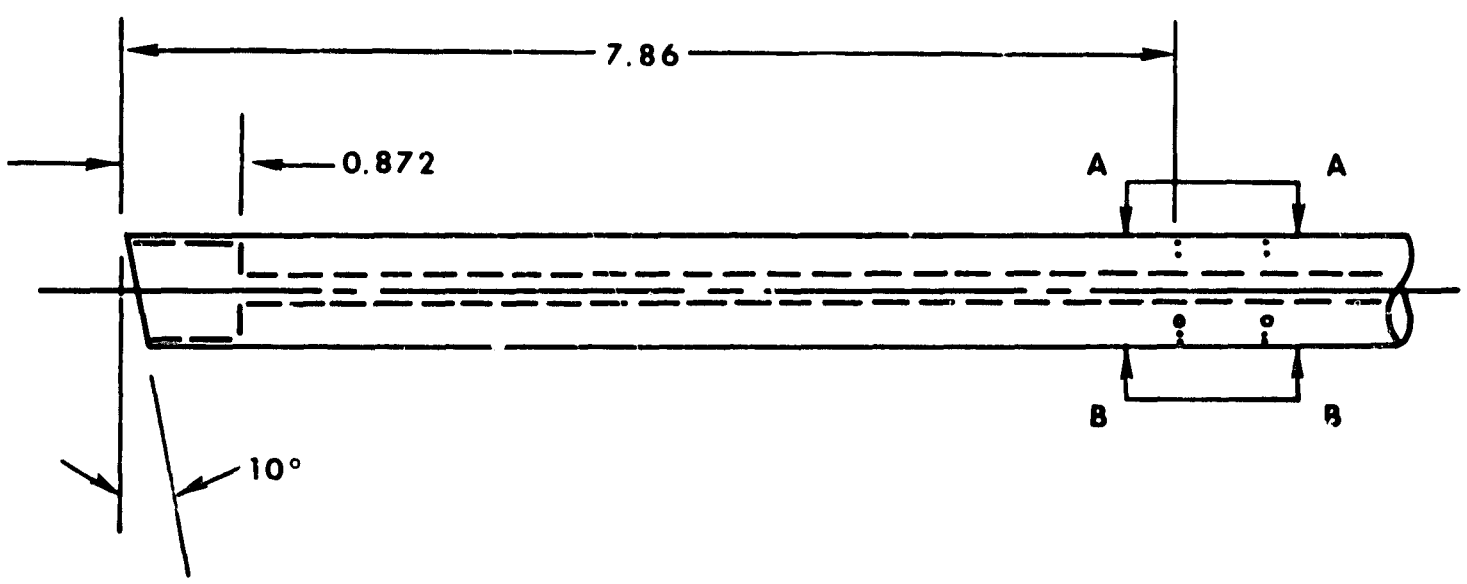

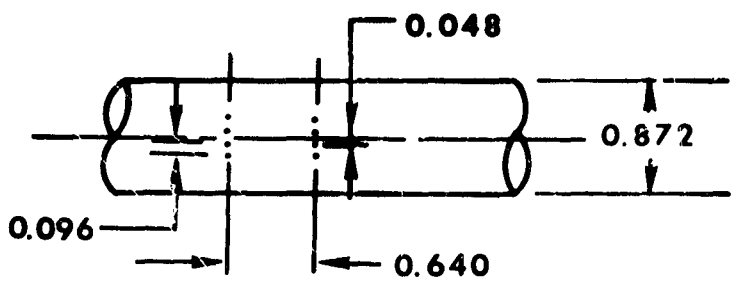

View A-A

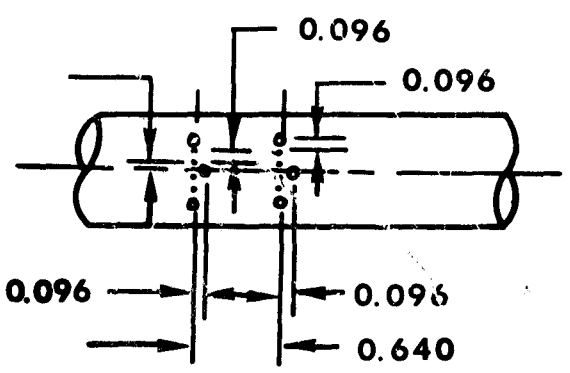

View B-B

• 0.043-inch-diameter orifice

o 0.052-inch-diameter orifice

Fig. 18 Details of total-pressure chamber and static-pressure orifices. Reproduced from Reference 24

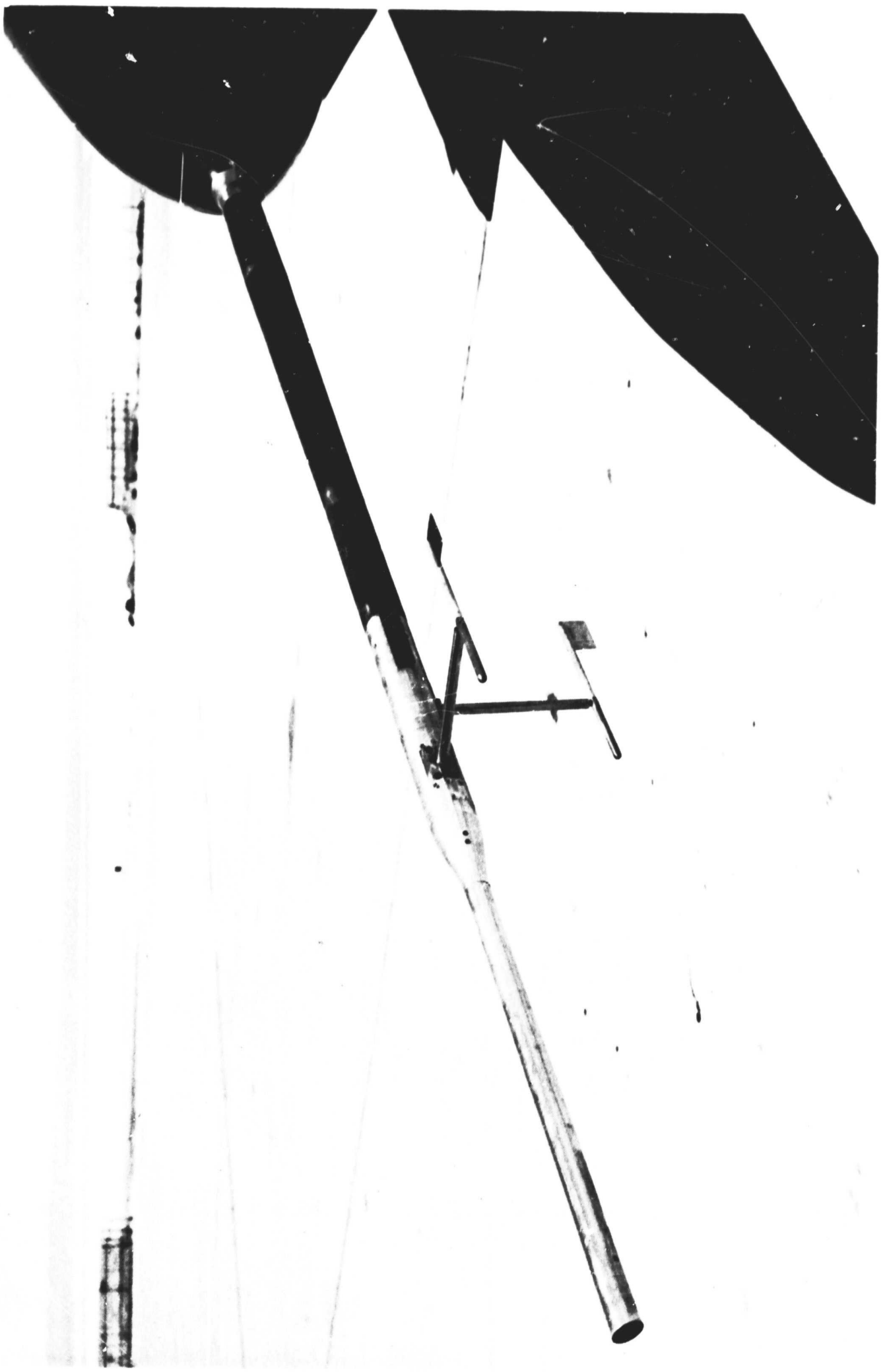

Fig. 19 Photograph of a typical NASA installation of angle-of-attack and sideslip vanes on nose boom

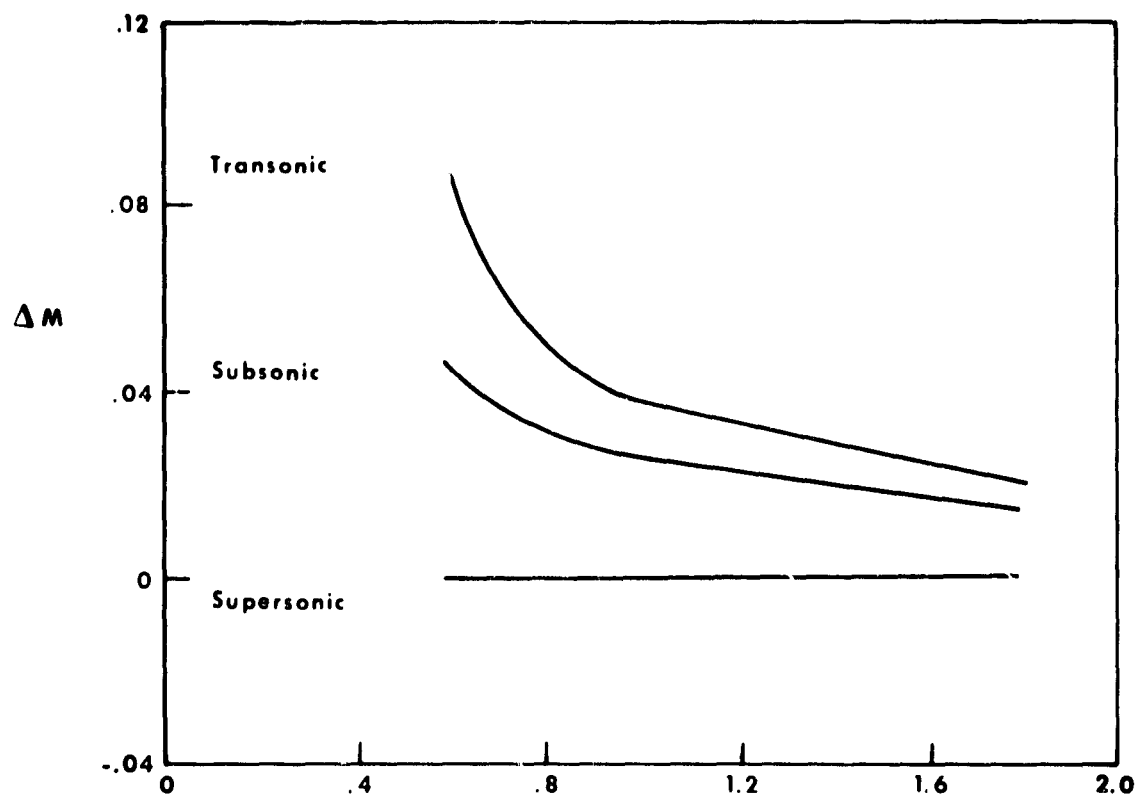

Fig. 20 Effect of ratio of boom length to fuselage diameter on Mach number error. Reproduced from Reference 30

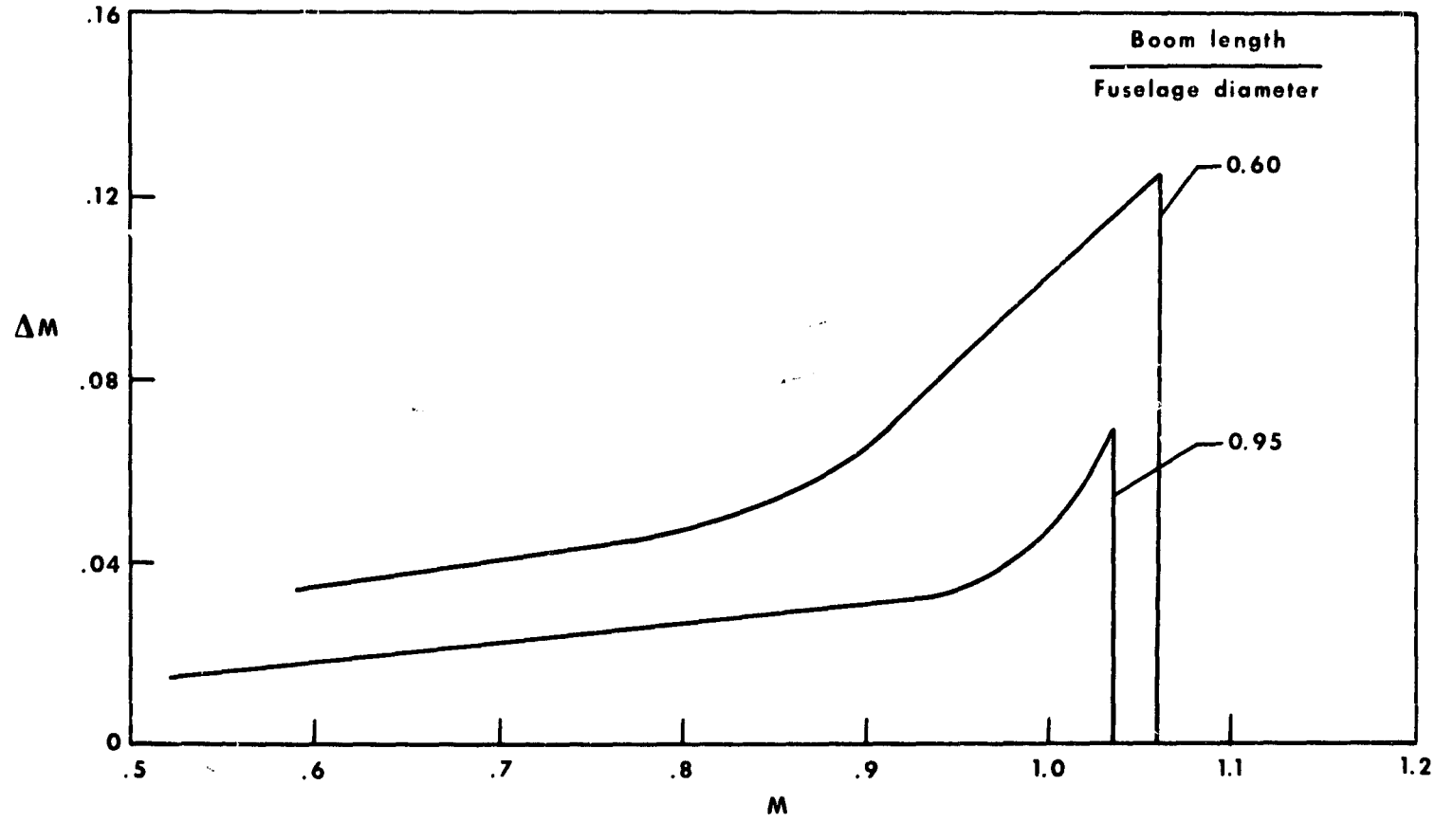

Fig. 21 Variation of Mach number error with Mach number. Reproduced from Reference 30

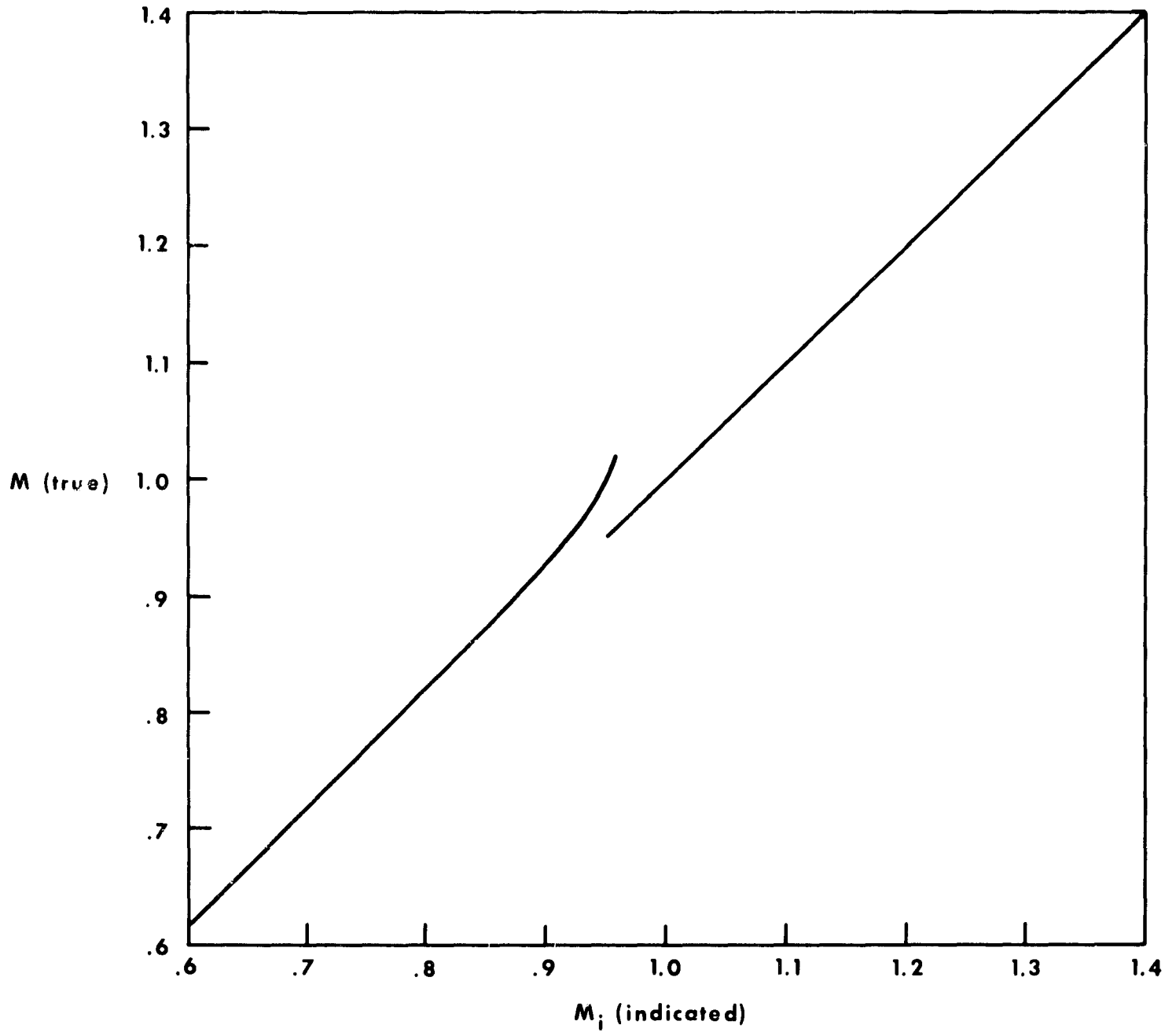

Fig. 22 A typical calibration curve for determination of true Mach number

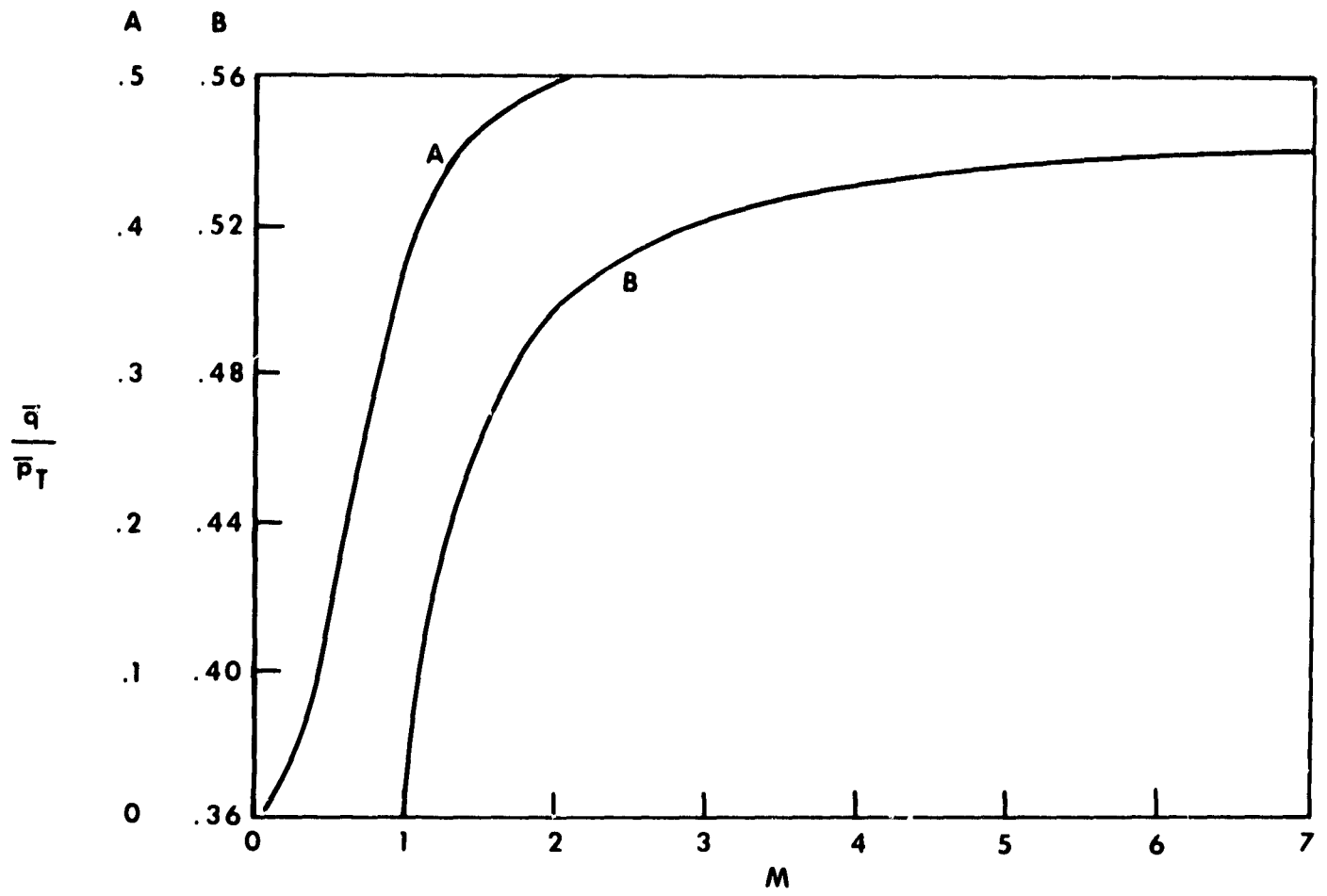

(a) Variation of $\bar{q}/\bar{p}_T$ with Mach number

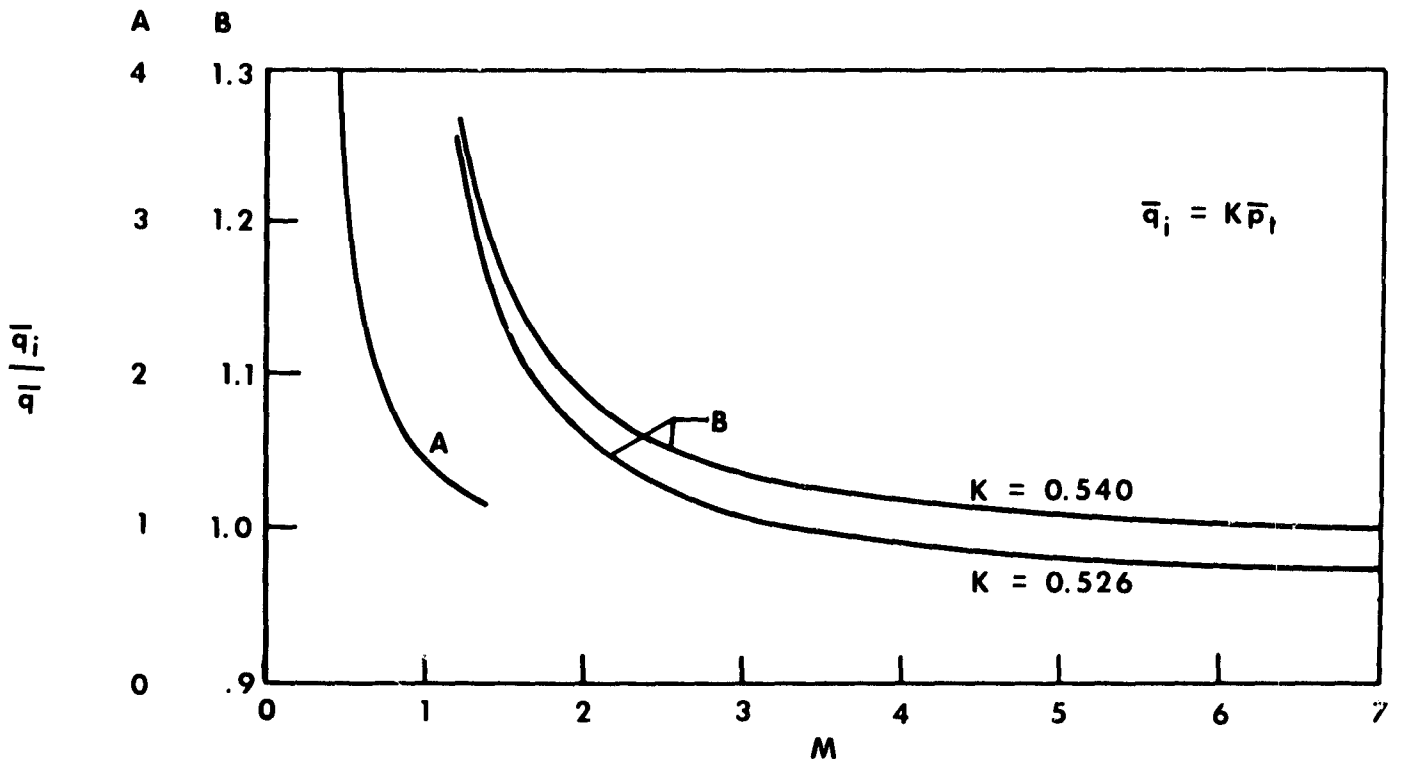

(b) Variation of $\bar{q}_i/\bar{q}$ with Mach number

Fig. 23 Determination of dynamic pressure from total pressure

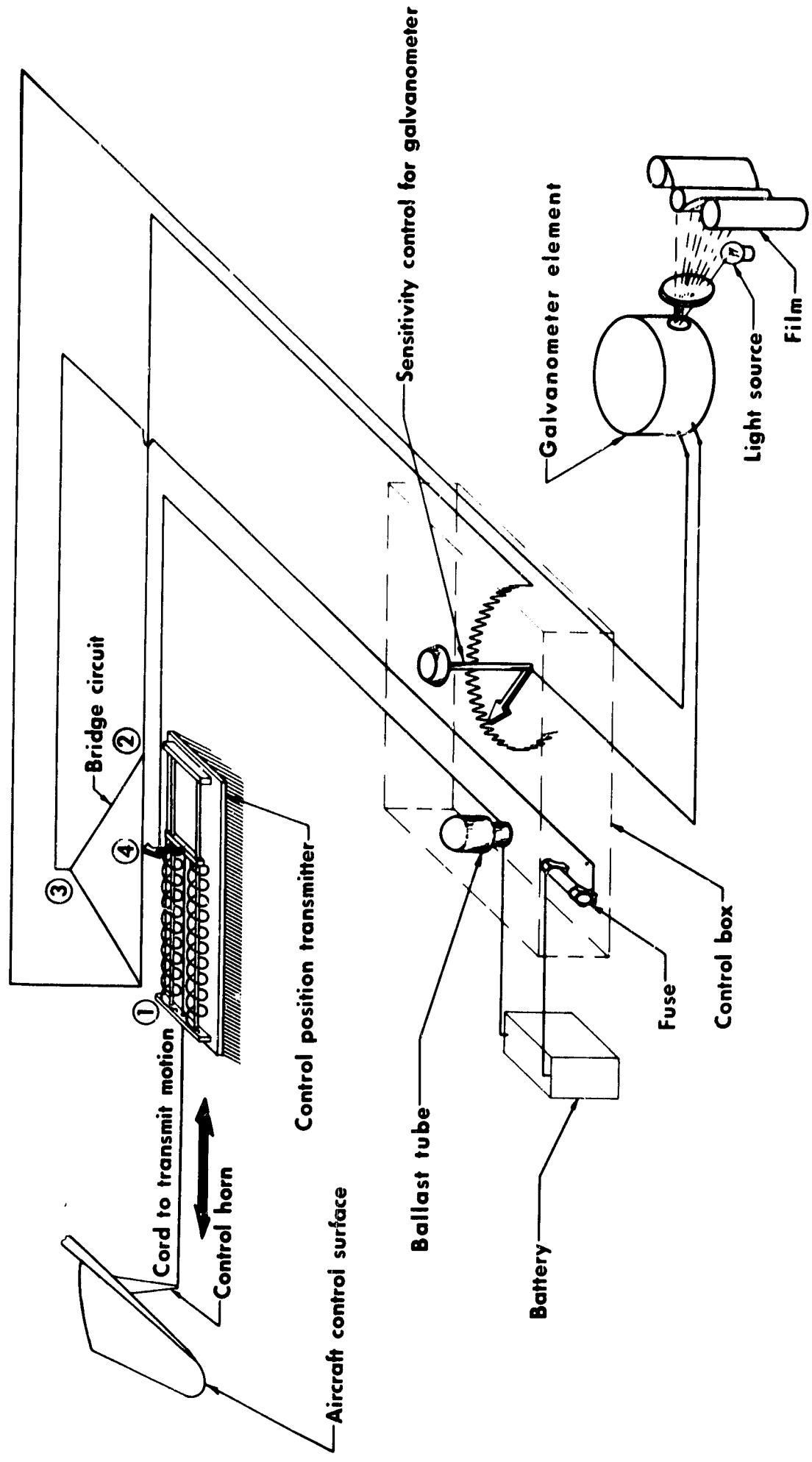

Fig. 24 Control position transmitter and recorder

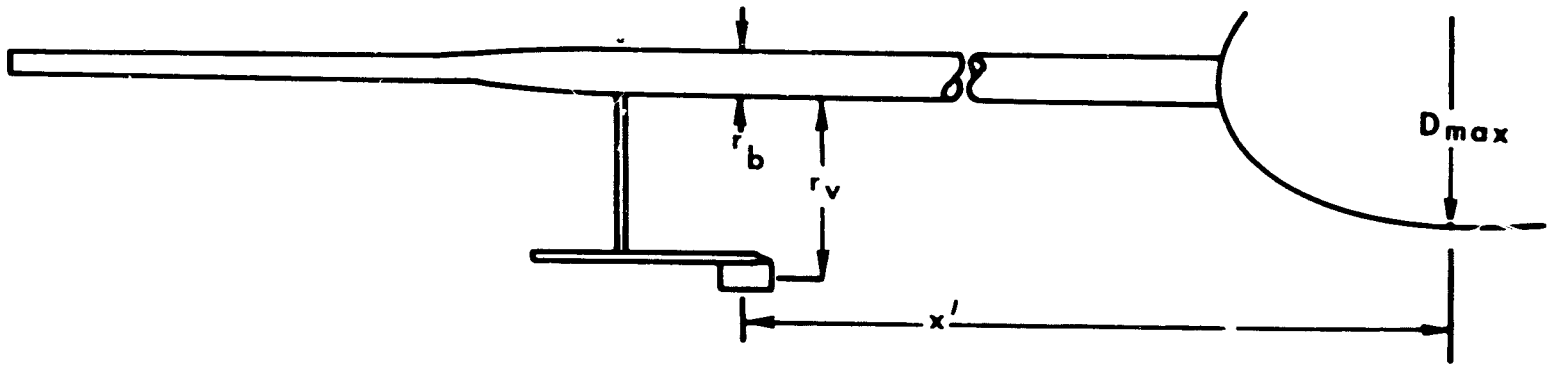

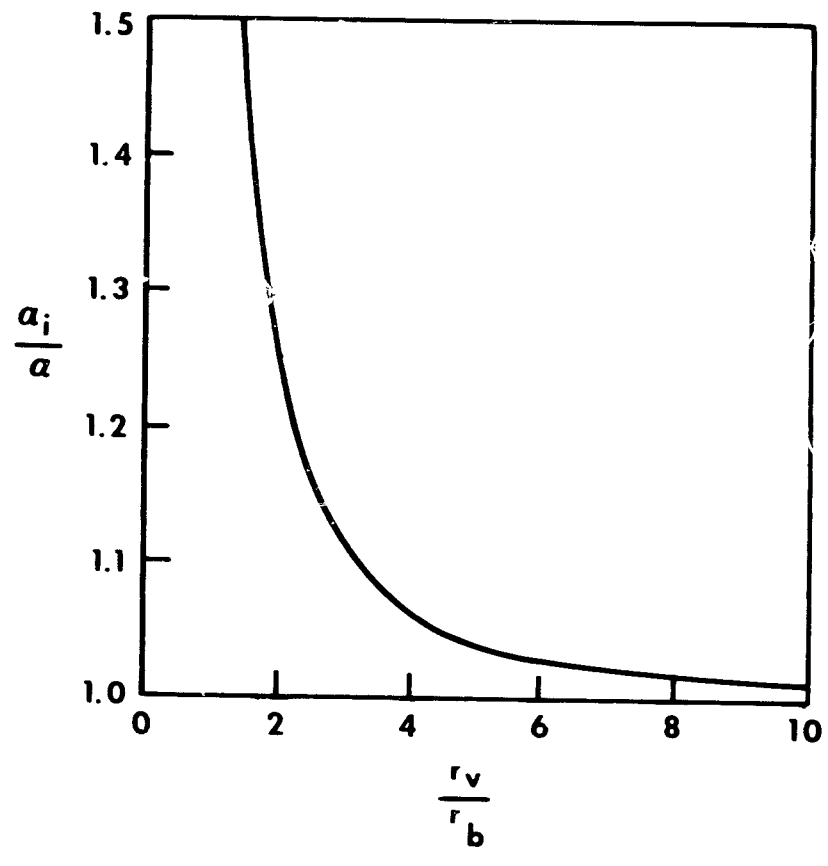

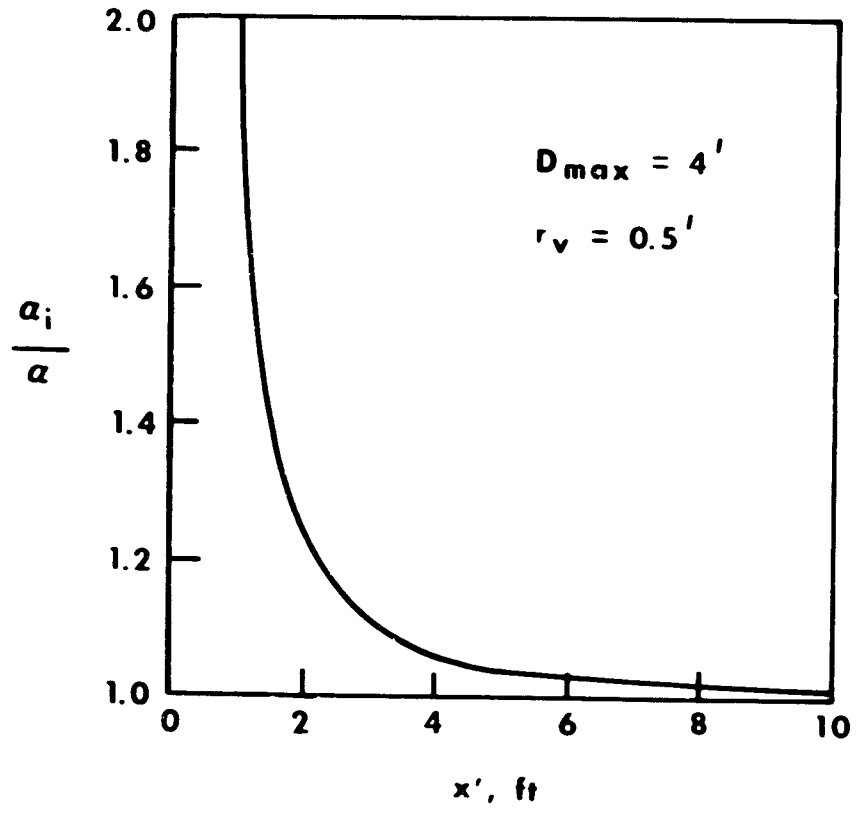

Fig. 25 Theoretical effects on angle-of-attack measurements of upwash from the nose boom and fuselage at low speeds. Reproduced from Reference 30

$$\tan \Delta\alpha_c = \frac{x_v}{R} \quad \text{where} \quad R = \frac{V^2}{g(a_n - \cos\theta \cos\phi)}$$

$$\text{therefore} \quad \Delta\alpha_c = \tan^{-1} \frac{x_v g (a_n - \cos\theta \cos\phi)}{V^2}$$

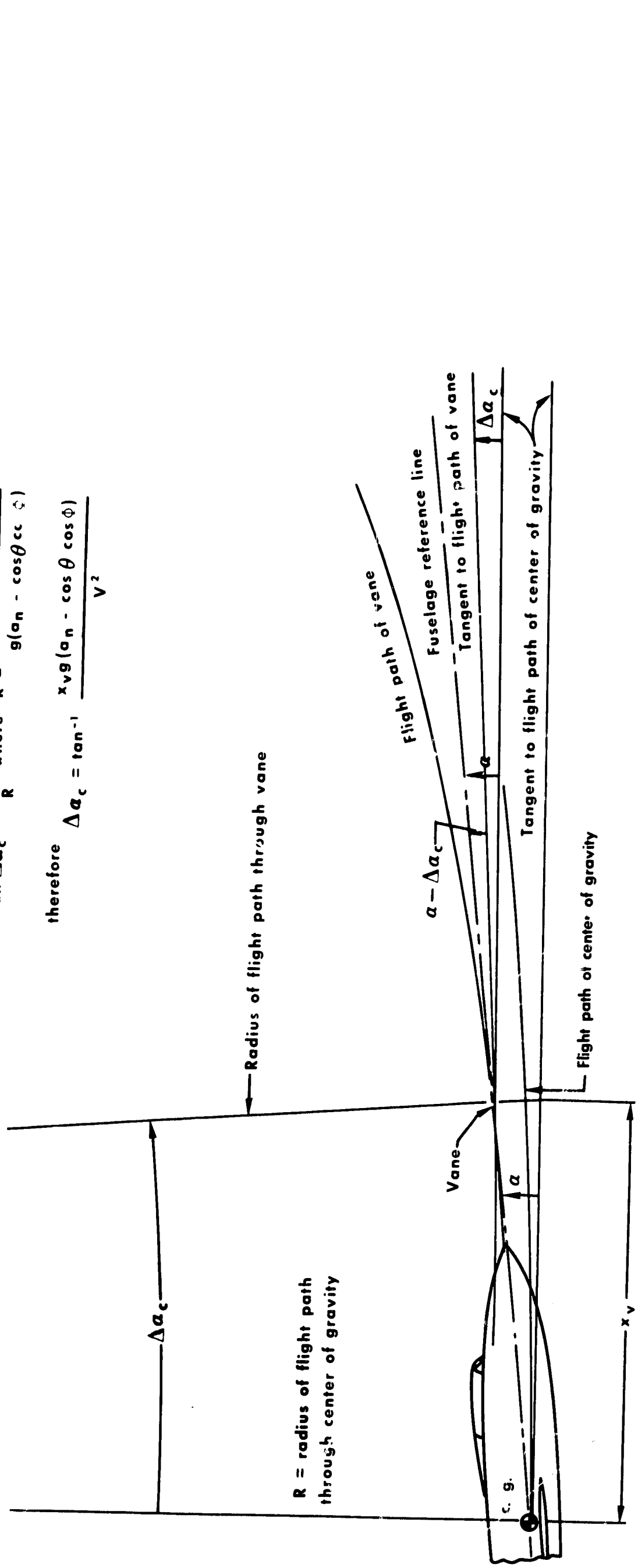

Fig. 26 Influence of flight-path curvature on vane indications of angle-of-attack

$$\frac{|\Delta\alpha|}{|\Delta\alpha_i|}\angle\Phi_{\alpha\alpha_i} = 1 + \frac{x_v g}{V^2}\frac{|\Delta a_n|}{|\Delta\alpha_i|}\angle\Phi_{a_n\alpha_i} + \frac{x_v}{V}\frac{|\Delta q|}{|\Delta\alpha_i|}\angle\Phi_{q\alpha_i}$$

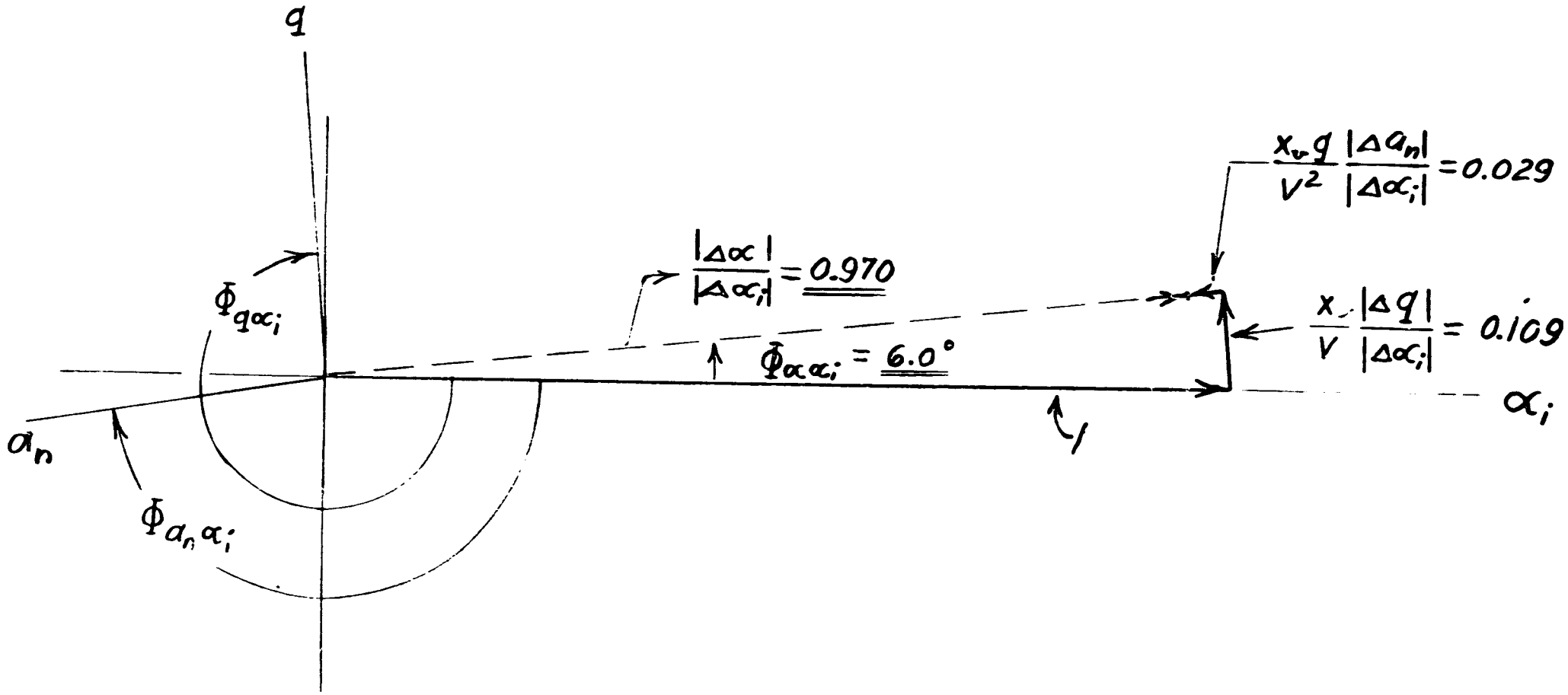

Fig. 27 Time-vector solution for correcting angle-of-attack records to the center-of-gravity of the aircraft

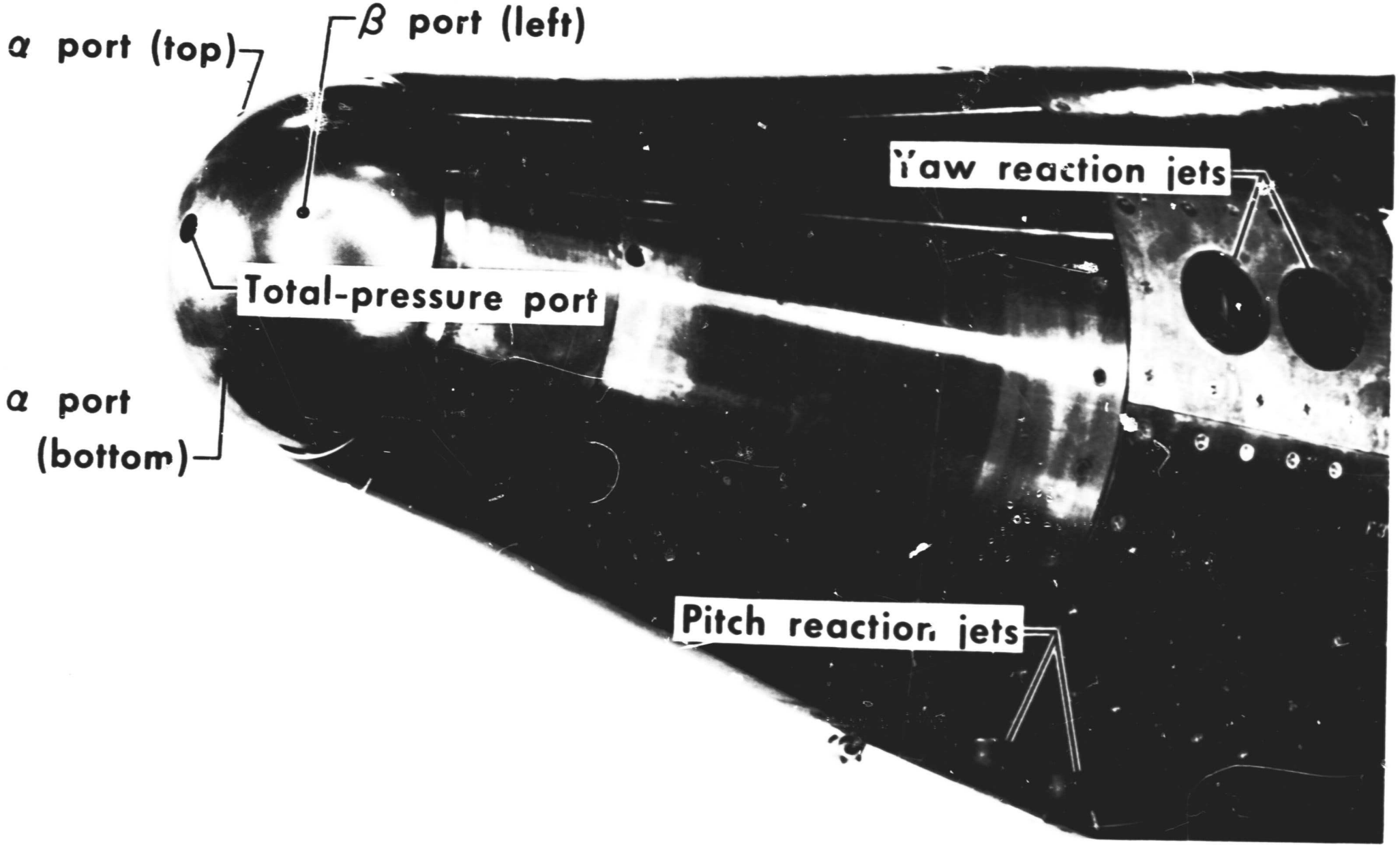

Fig. 28 Spherical flow-direction sensor. (Note location of pitch and yaw reaction-control nozzles of the airplane.)

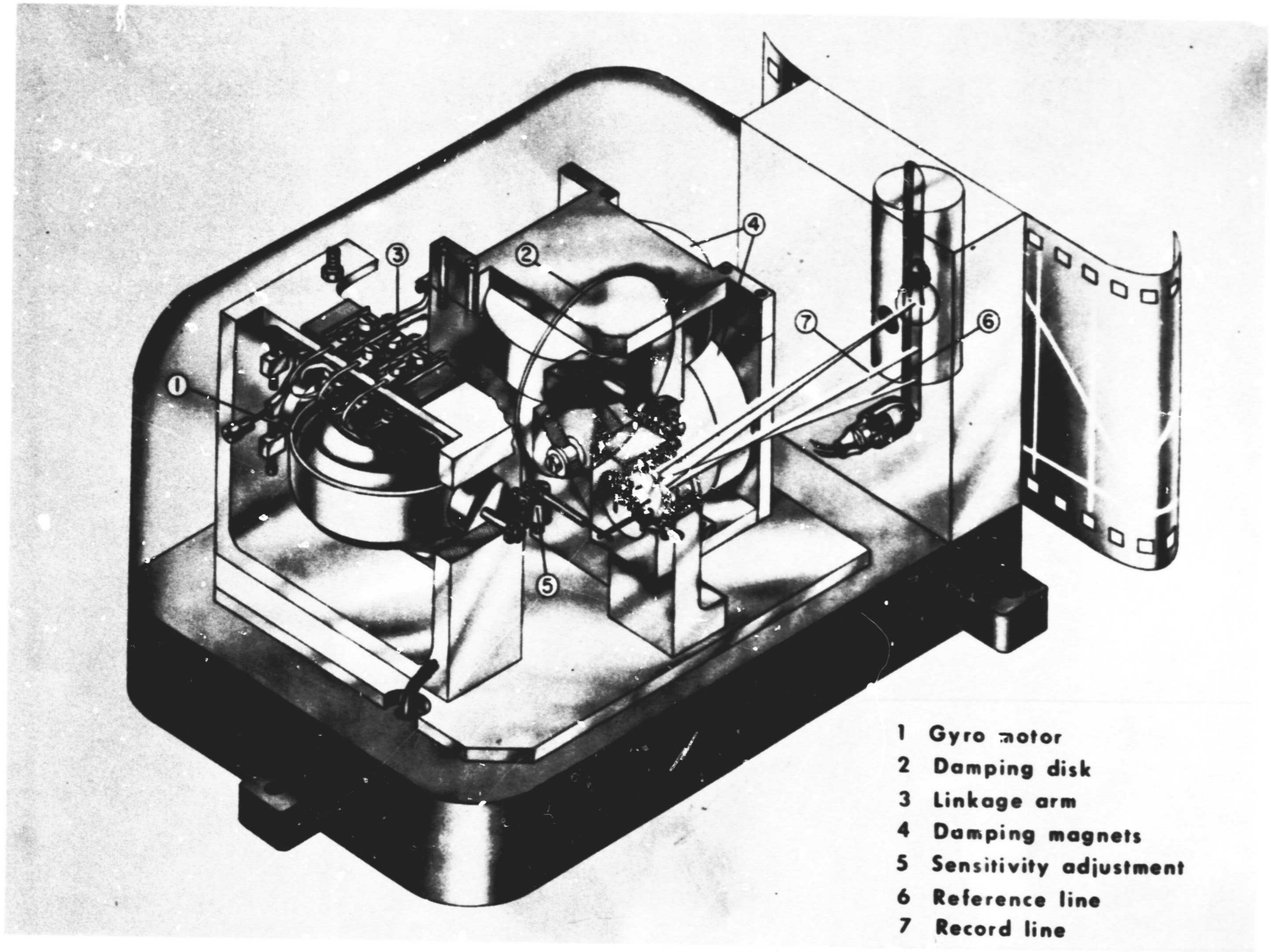

Fig. 29(a) Magnetically damped angular-velocity recorder

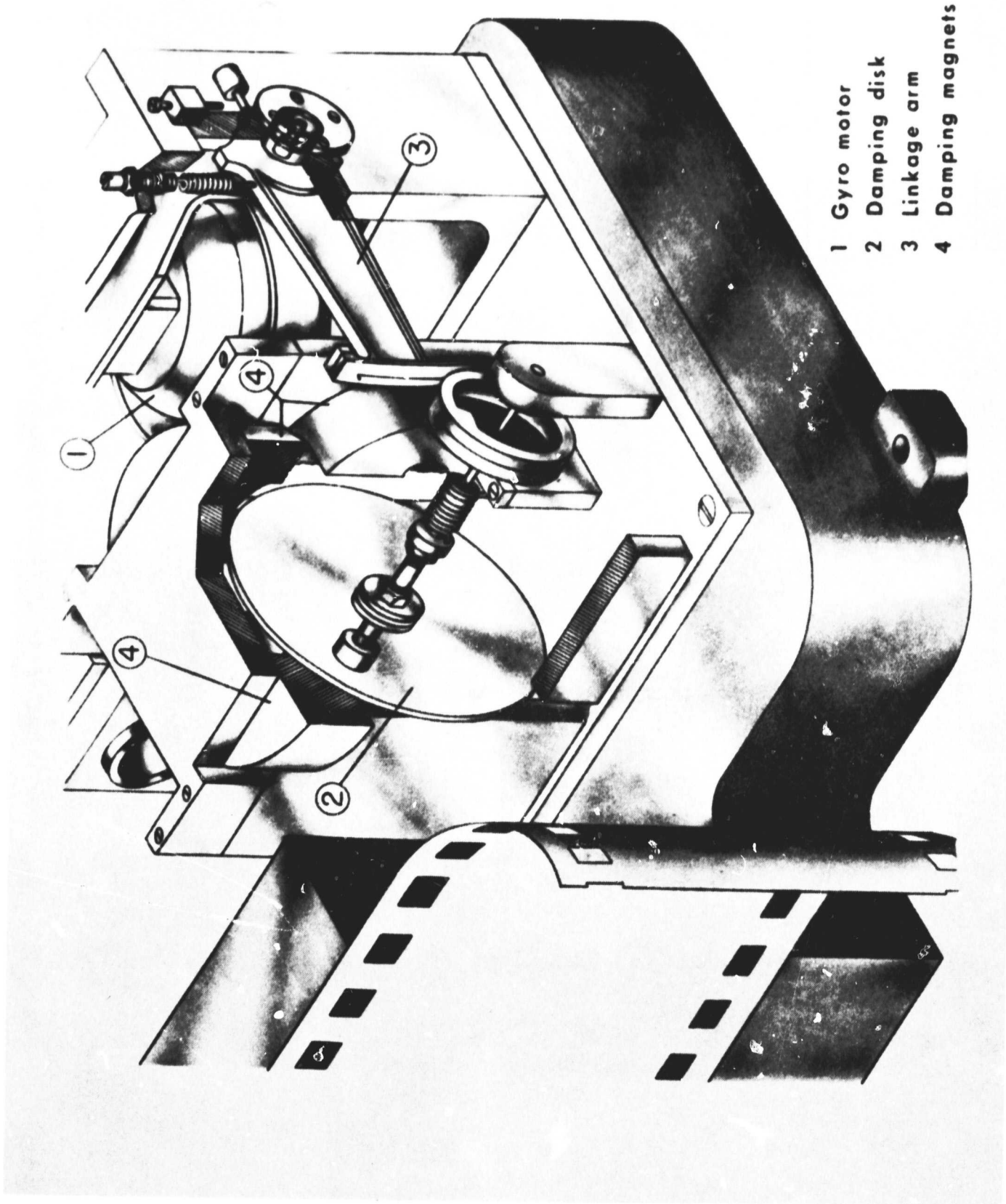

Fig. 29(b) Detail of linkage and damping system

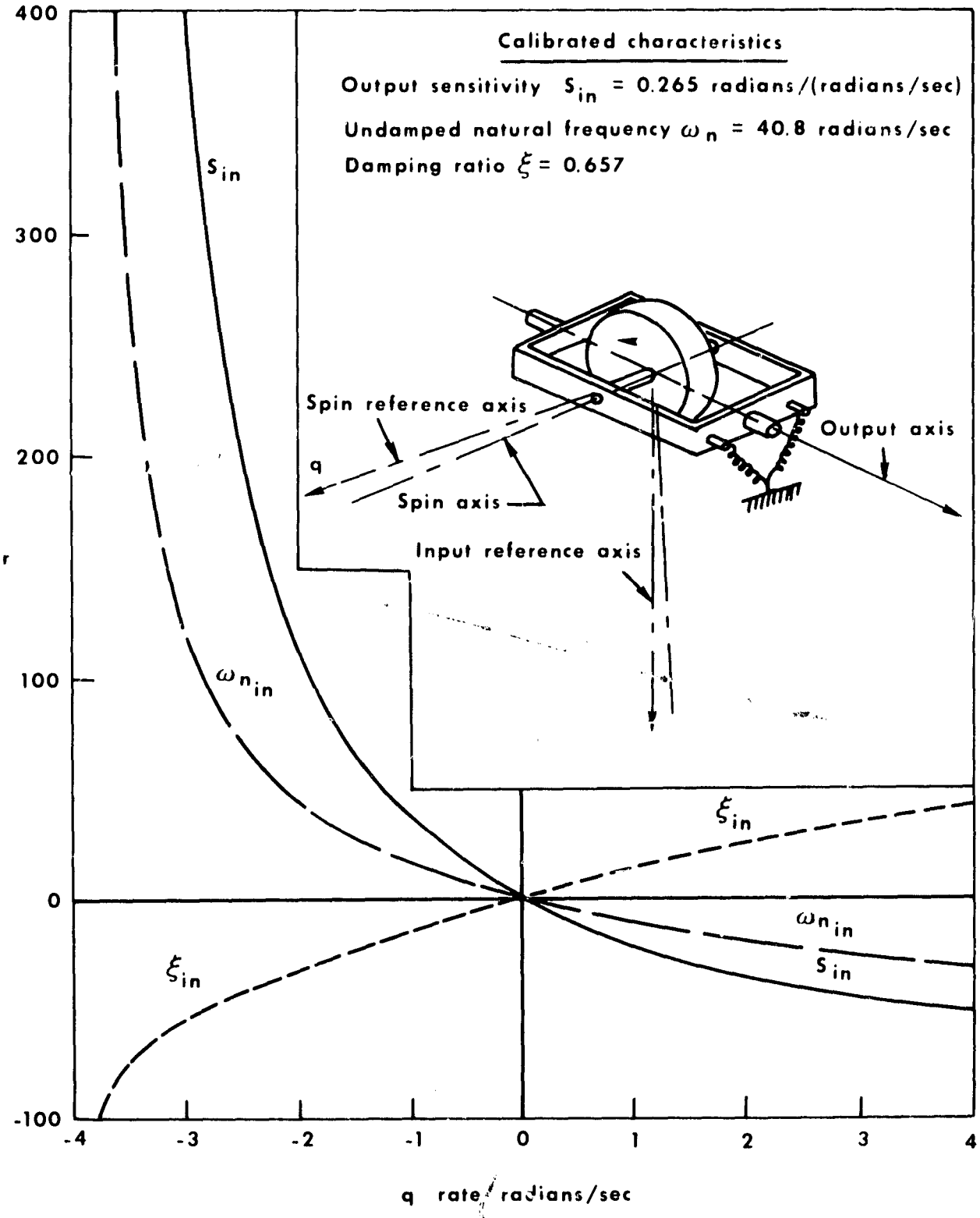

Fig.30 Influence of interference angular velocity ("q" rate) about spin reference axis of a sensitive rate gyro

$$p_i = p \cos\theta_1 \cos\psi_1 + q \cos\theta_1 \sin\psi_1 - r \sin\theta_1$$

$$q_i = p(\cos\psi_2 \sin\theta_2 \sin\varphi_2 - \sin\psi_2 \cos\varphi_2) + q(\sin\psi_2 \sin\theta_2 \sin\varphi_2 + \cos\psi_2 \cos\theta_2) + r(\cos\theta_2 \sin\varphi_2)$$

$$r_i = p(\cos\psi_3 \sin\theta_3 \cos\varphi_3 + \sin\psi_3 \sin\varphi_3) + q(\sin\psi_3 \sin\theta_3 \cos\varphi_3 - \cos\psi_3 \sin\varphi_3) + r(\cos\theta_3 \cos\varphi_3)$$

Instrument	Mounting error
p_i	ψ_1 θ_1 φ_1
q_i	ψ_2 θ_2 φ_2
r_i	ψ_3 θ_3 φ_3

Note: Solve for p, q, and r

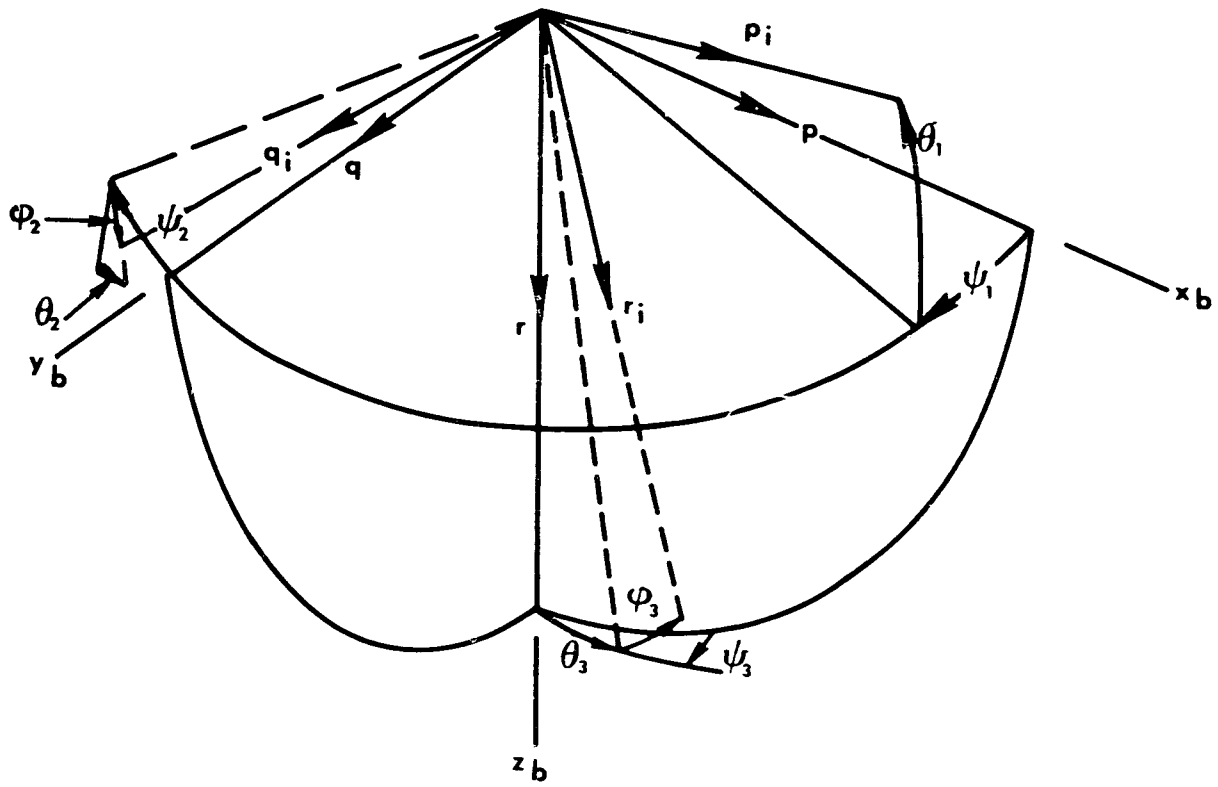

Fig. 31. Equations for correcting rate gyro records for instrument misalinement

$$a_x = a_{x_i} - \frac{z\dot{q}}{g} + \frac{y\dot{r}}{g} + \frac{xq^2}{g} + \frac{xr^2}{g}$$

$$a_t = a_{t_i} - \frac{x\dot{r}}{g} + \frac{z\dot{p}}{g} + \frac{yr^2}{g} + \frac{yp^2}{g}$$

$$a_n = a_{n_i} - \frac{x\dot{q}}{g} + \frac{y\dot{p}}{g} - \frac{zq^2}{g} - \frac{zp^2}{g}$$

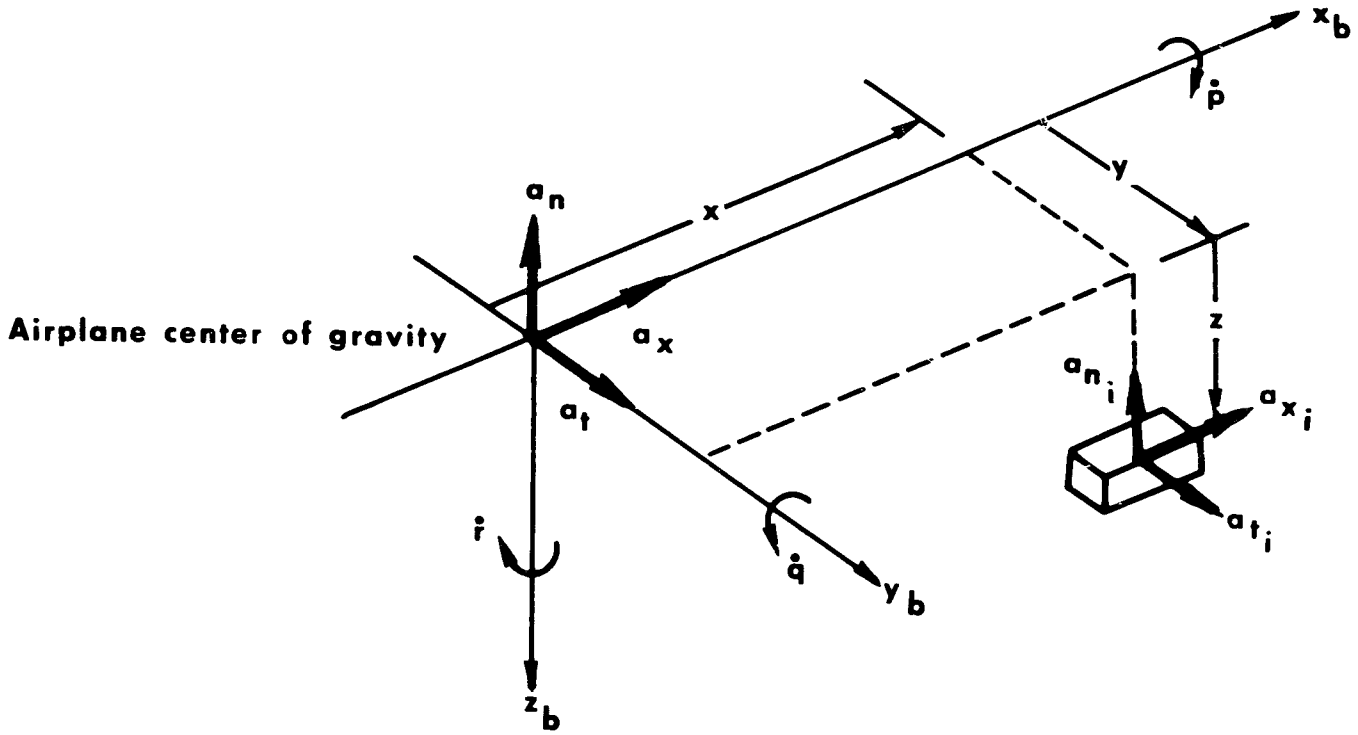

Fig. 32 Equations for correcting records of linear accelerometers to the center-of-gravity of the aircraft

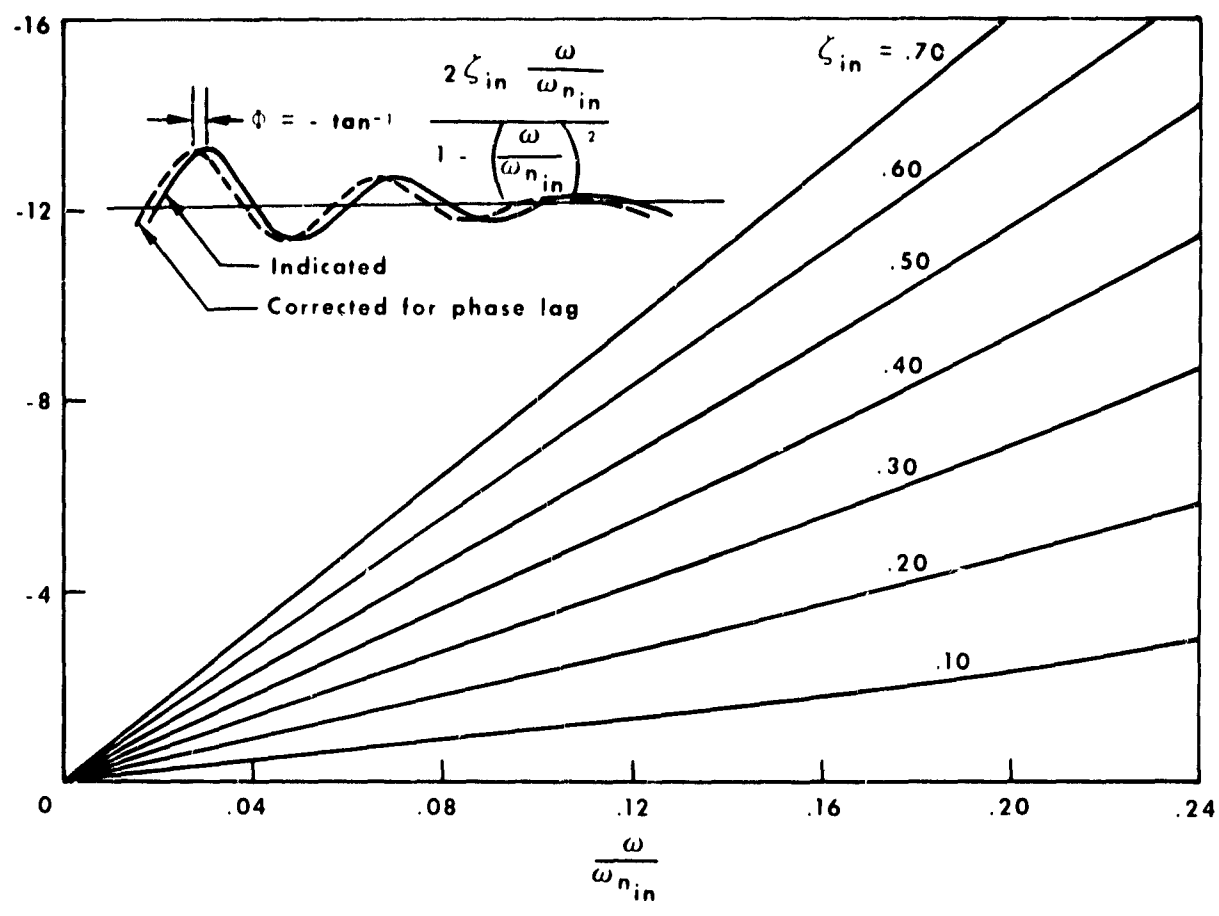

Fig. 33 Chart for correcting sensing-recording circuit of instrument for phase lag

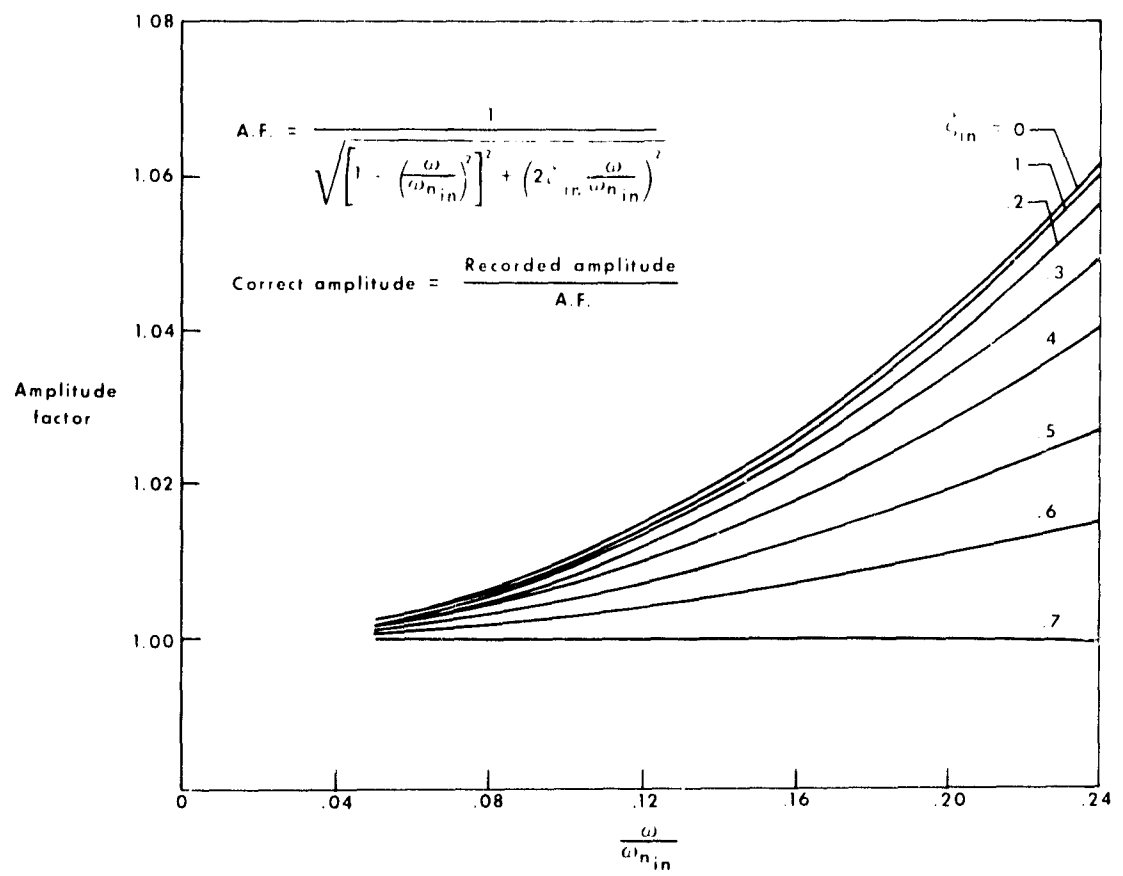

Fig. 34 Chart for correcting sensing-recording circuit of instrument for dynamic amplification

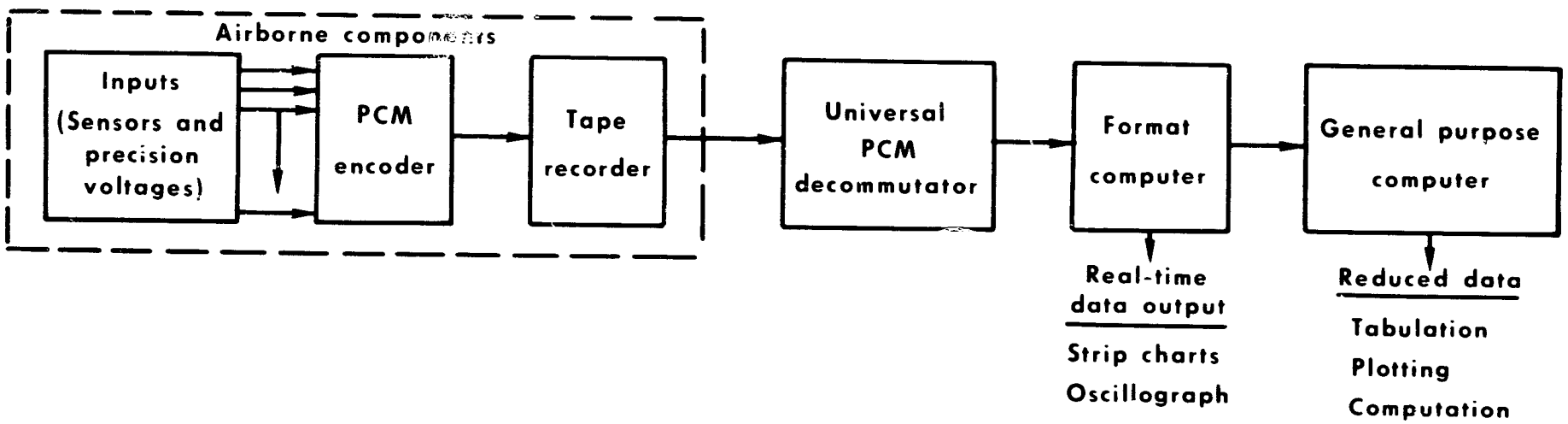

(a) PCM system with airborne recorder

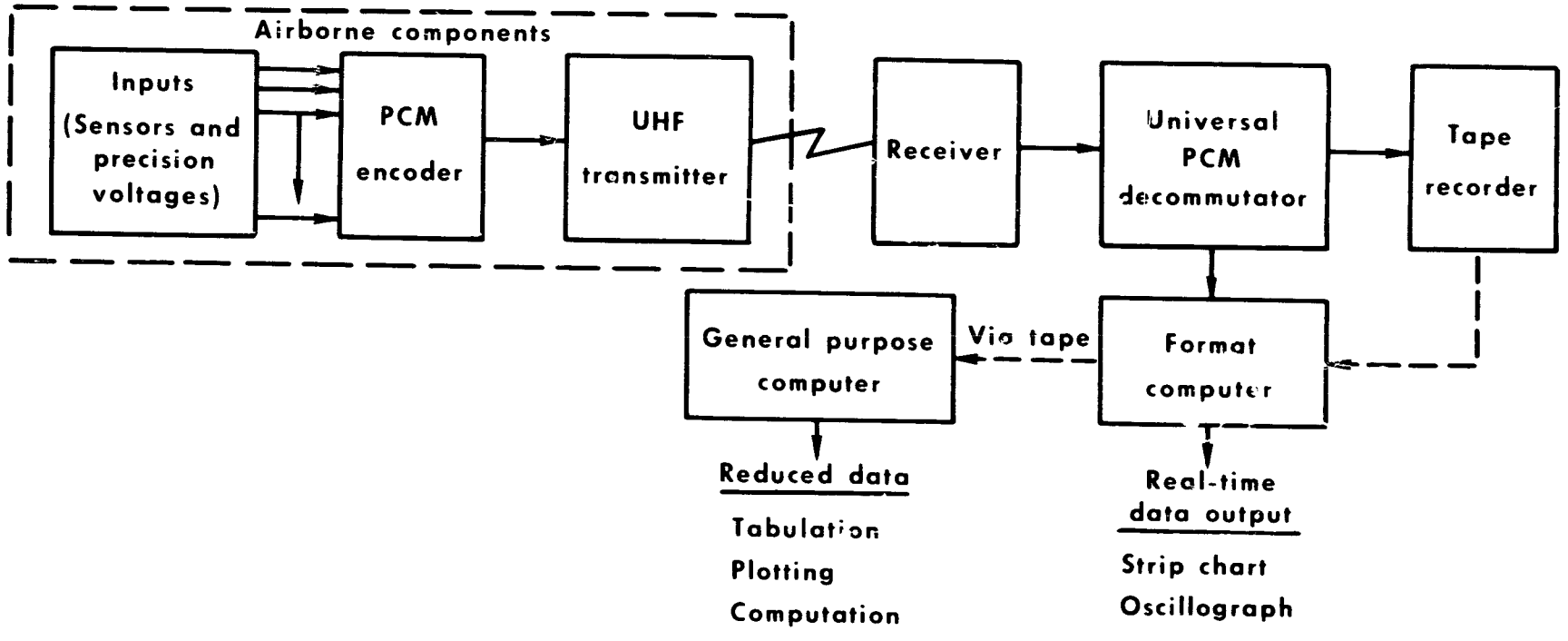

(b) PCM system using telemetry to record data

Fig. 35 Functional schematics of pulse code modulation (PCM) data-acquisition systems

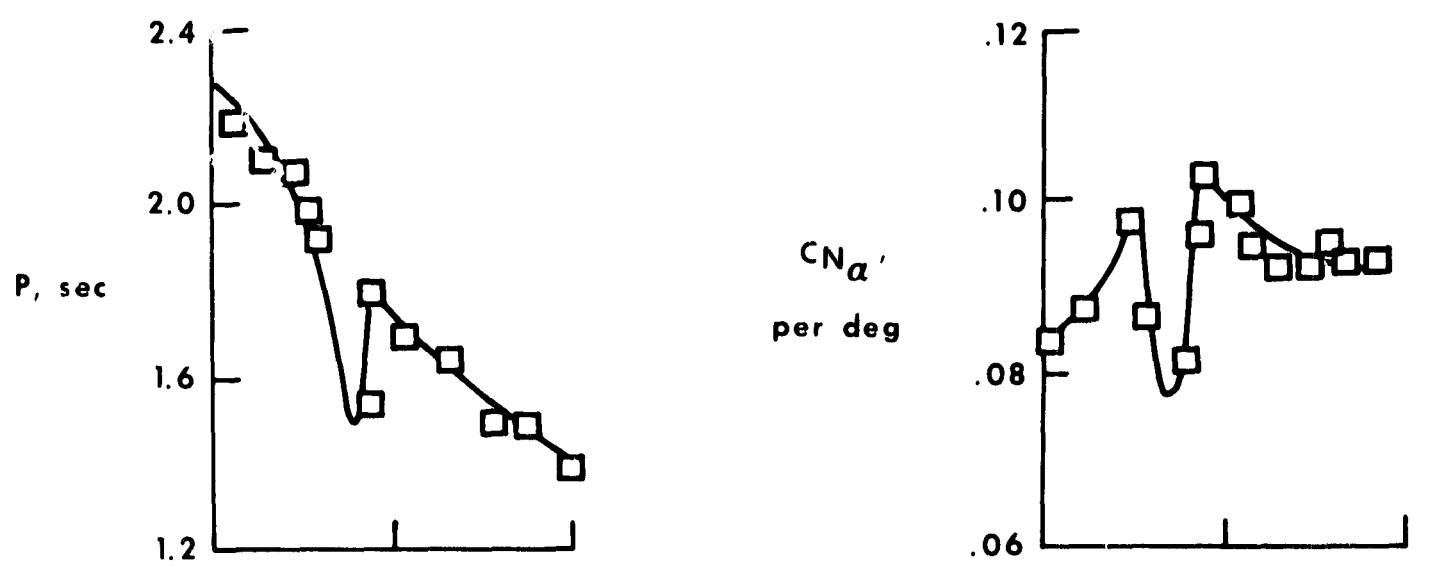

Fig. 36 Results of analysis of flight data in region of rapid changes in aircraft characteristics

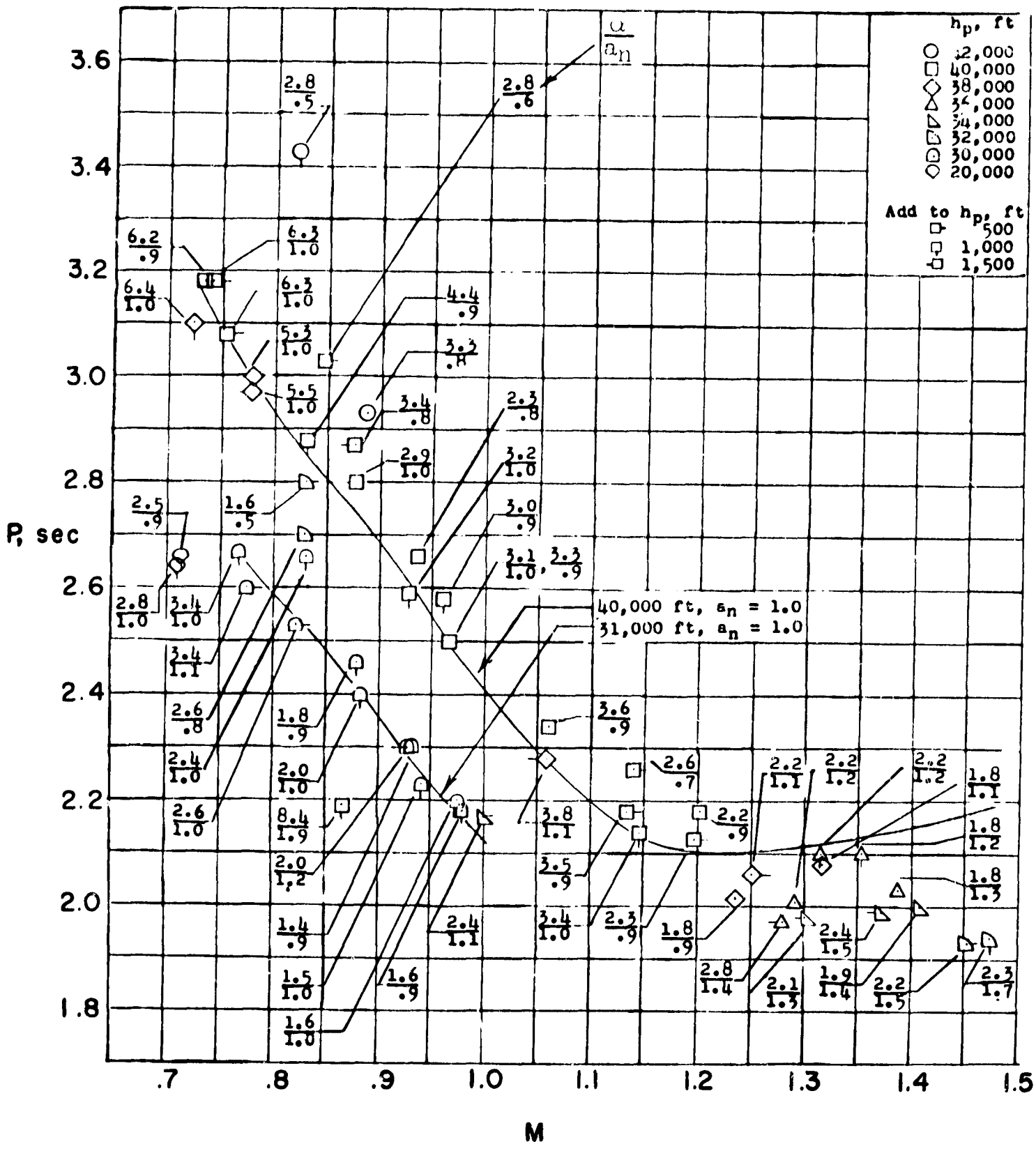

Fig. 37 Variation of the period of an F-100 series airplane as a function of Mach number, altitude, angle-of-attack, and load factor (from Reference 41)

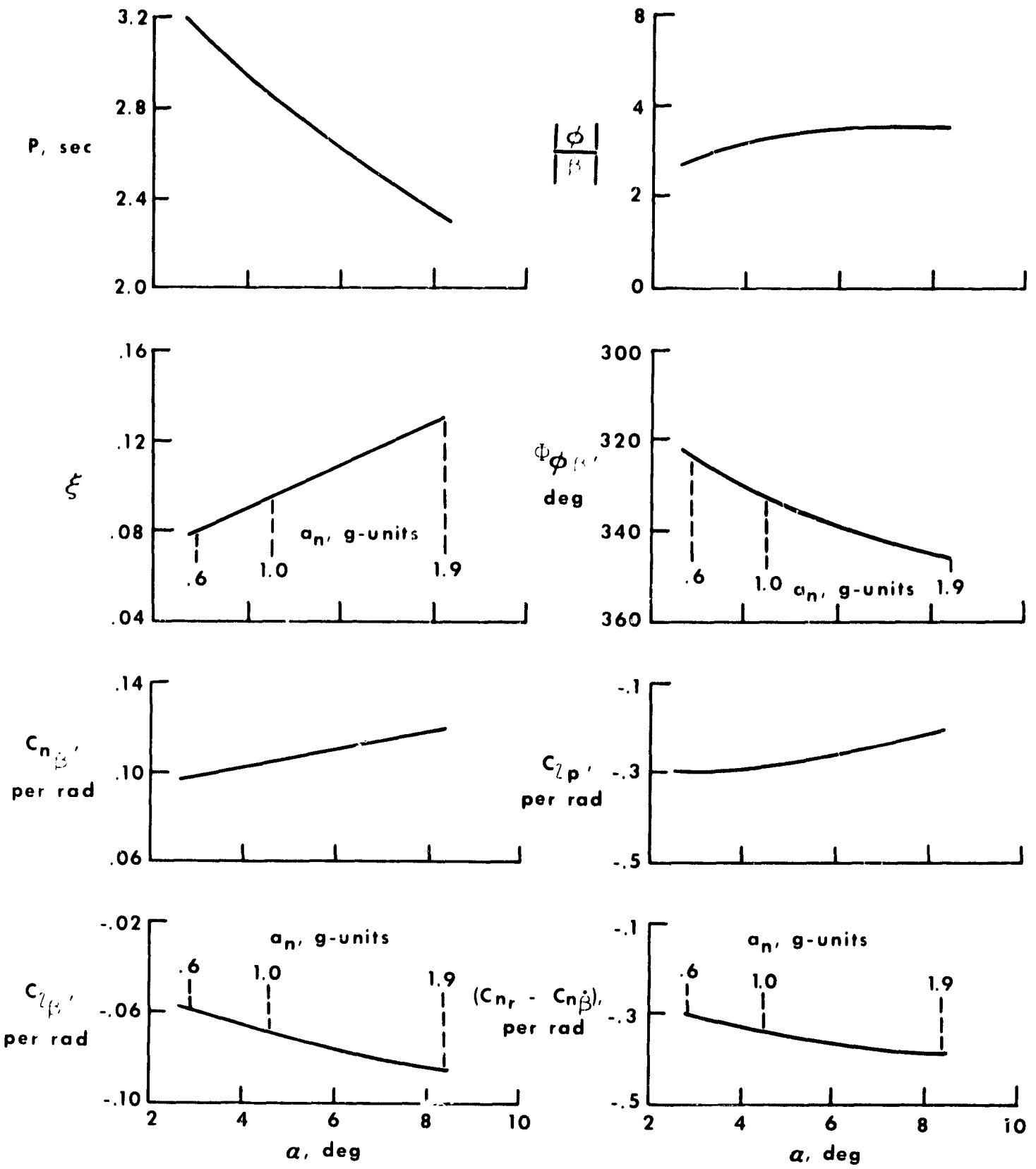

Fig.38 Influence of angle-of-attack and load factor upon lateral characteristics of one aircraft

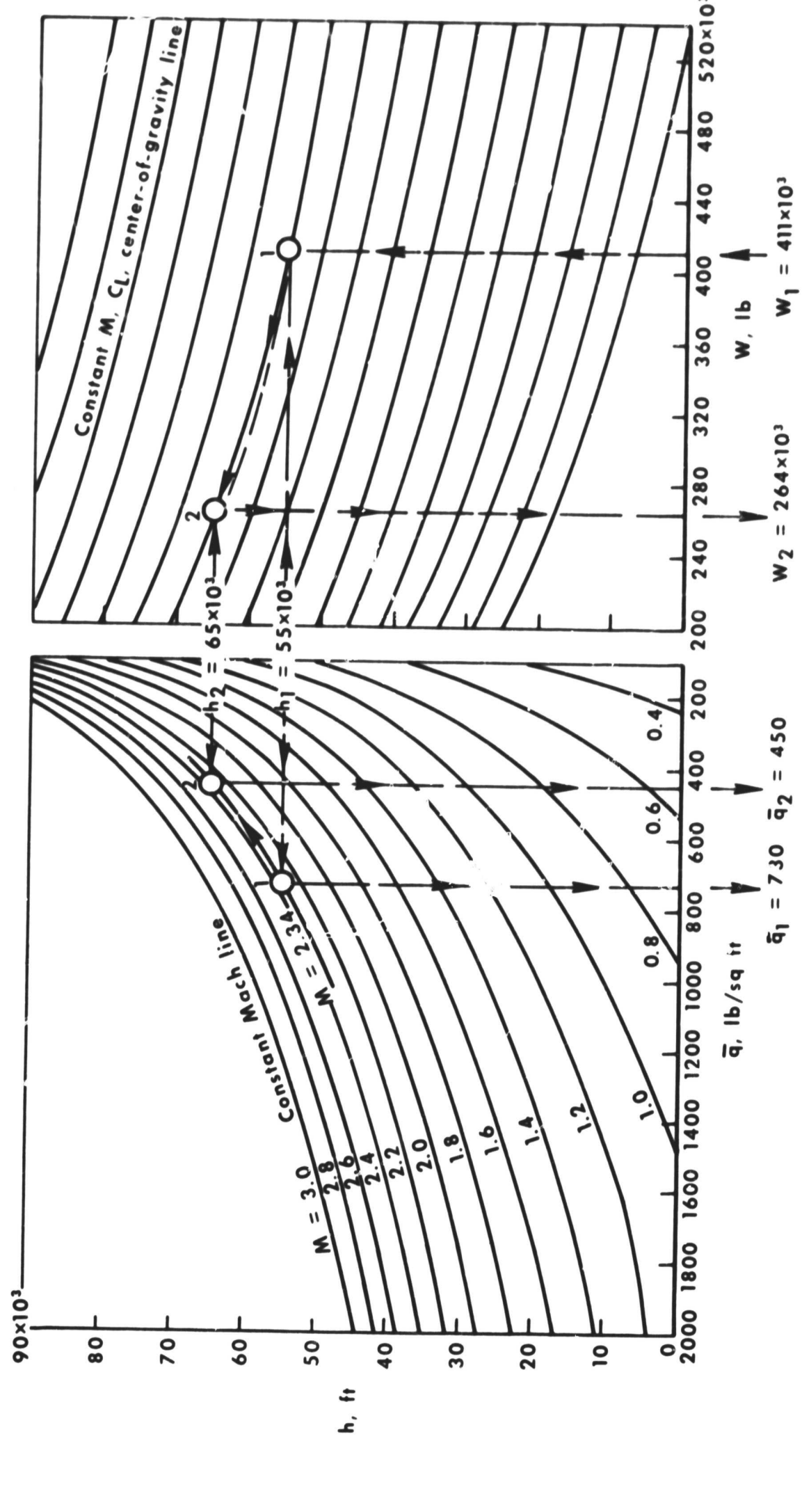

Fig. 39 A nomograph for planning flight test conditions in investigating aeroelastic effects on stability and control

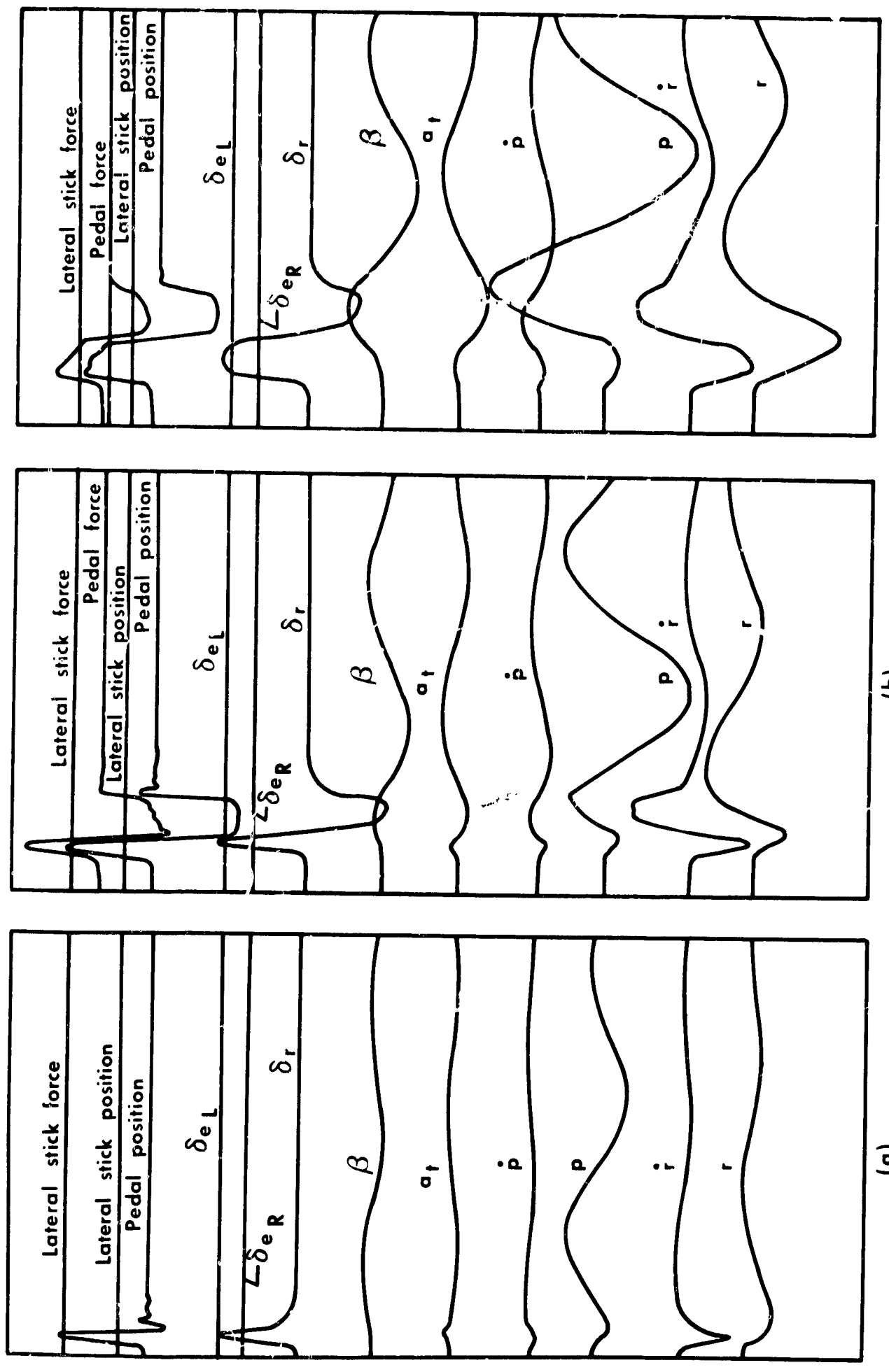

Fig. 40 Comparison of lateral-directional responses to different types of rudder inputs

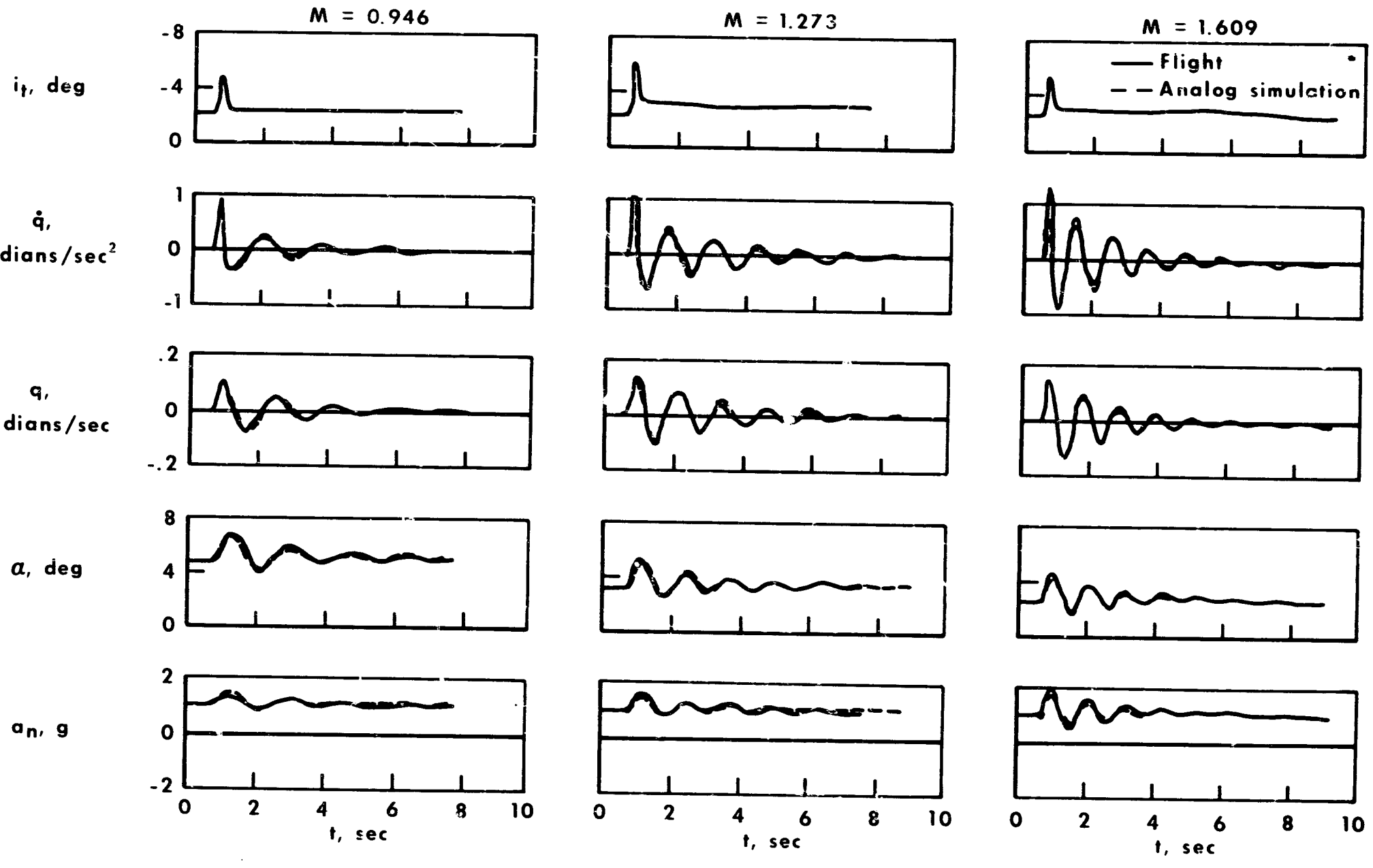

Fig. 41 Typical time histories of the longitudinal response characteristics of the test airplane resulting from abrupt stabilizer deflection

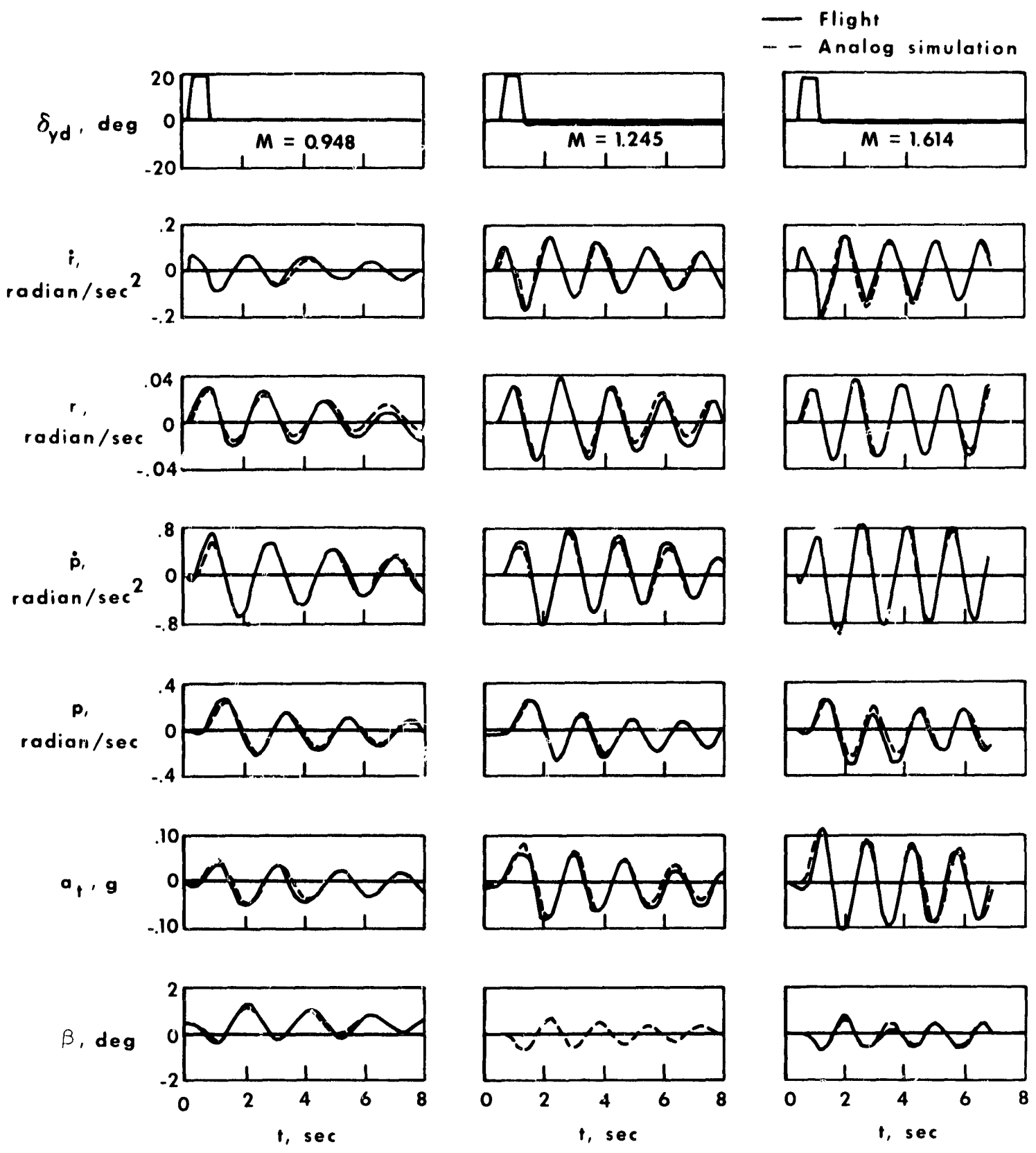

Fig. 42 Typical time histories of the lateral and directional response characteristics of the test airplane resulting from abrupt yaw-damper deflection

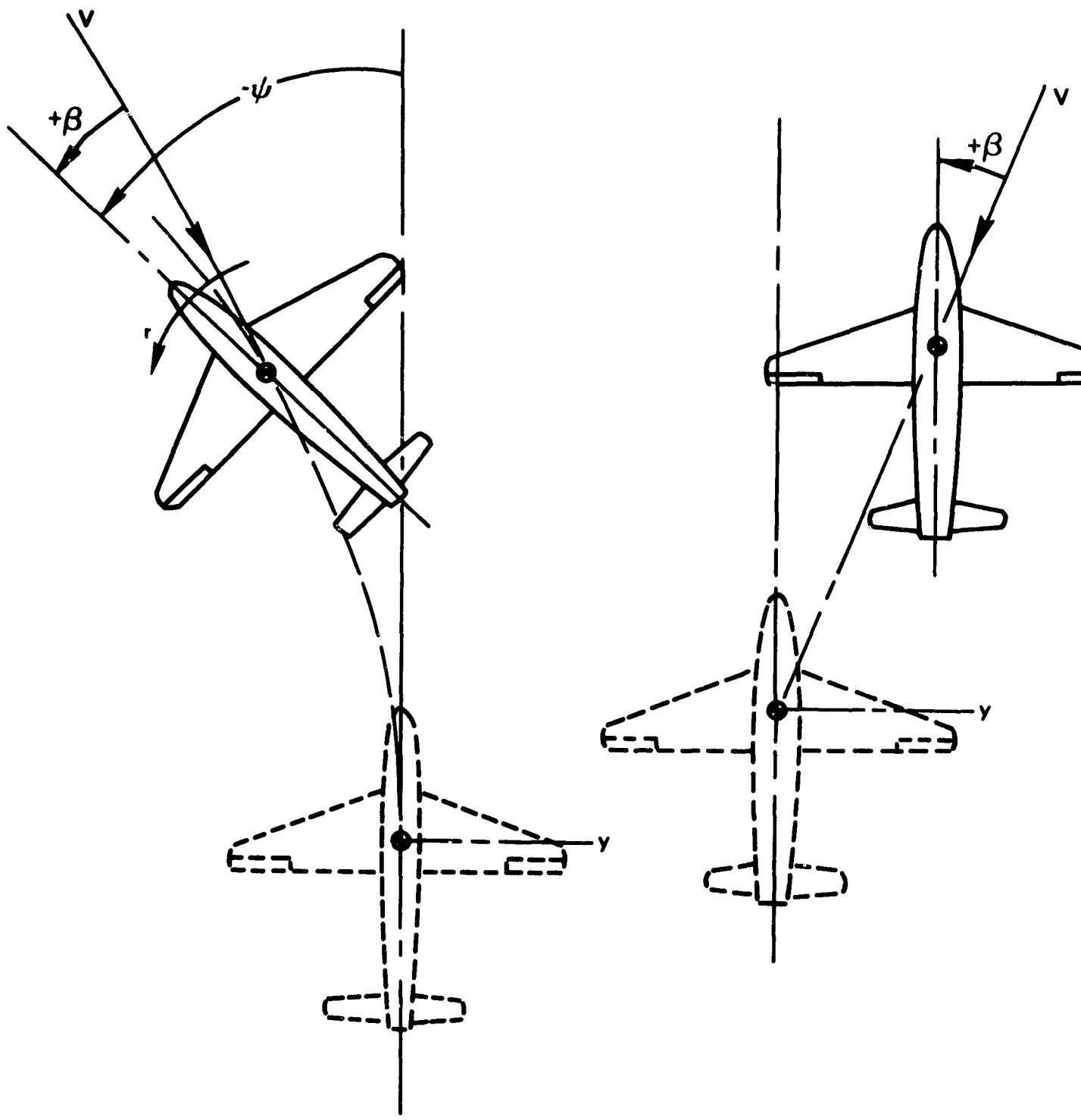

(a) Wings-level sideslip (b) Constant-heading sideslip (r = 0)

Fig.43 Comparison of wings-level and constant-heading sideslips

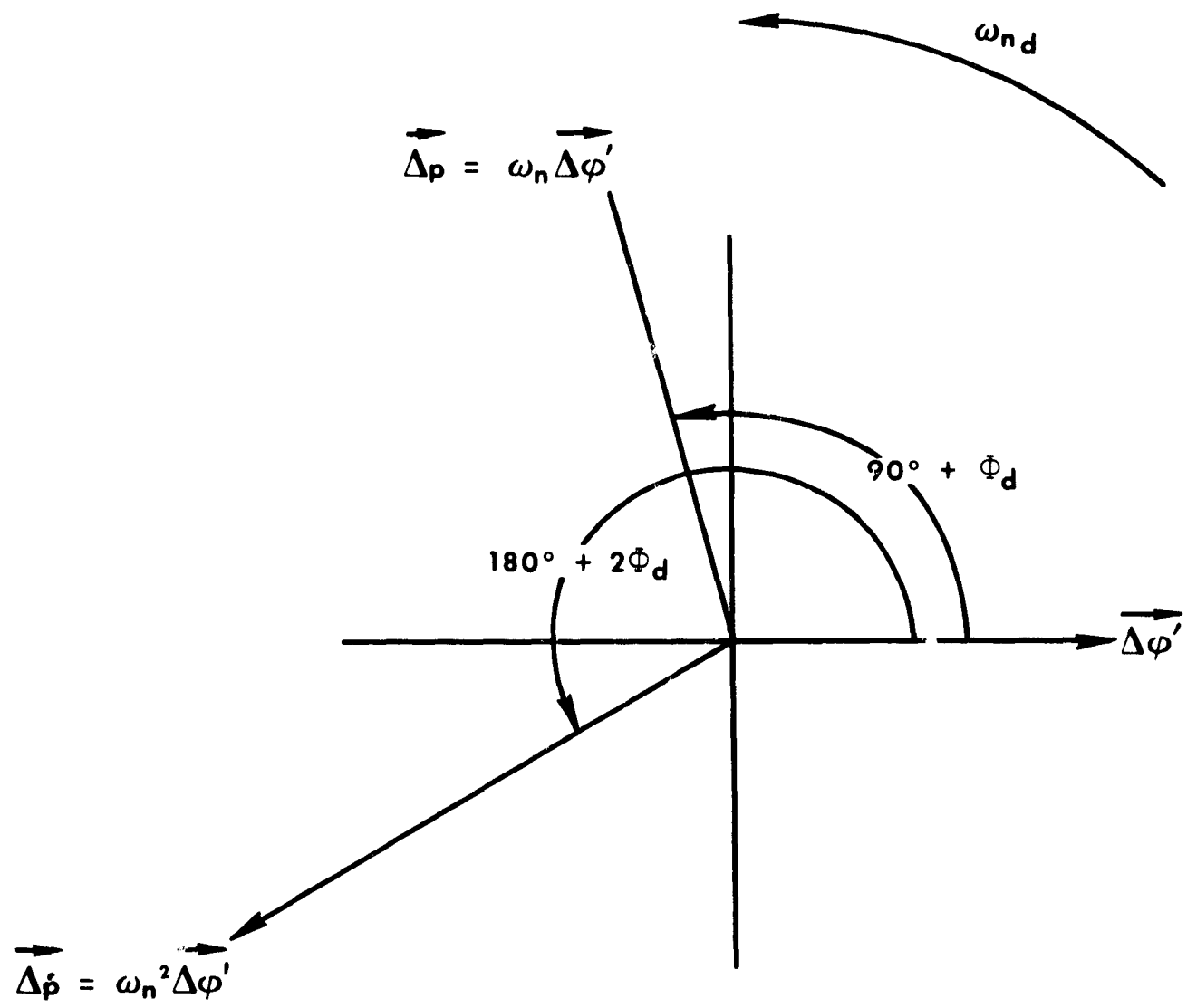

Fig. 44 Relation of small-perturbation rolling velocity and acceleration vectors to small-perturbation roll-displacement vector in a transient oscillation

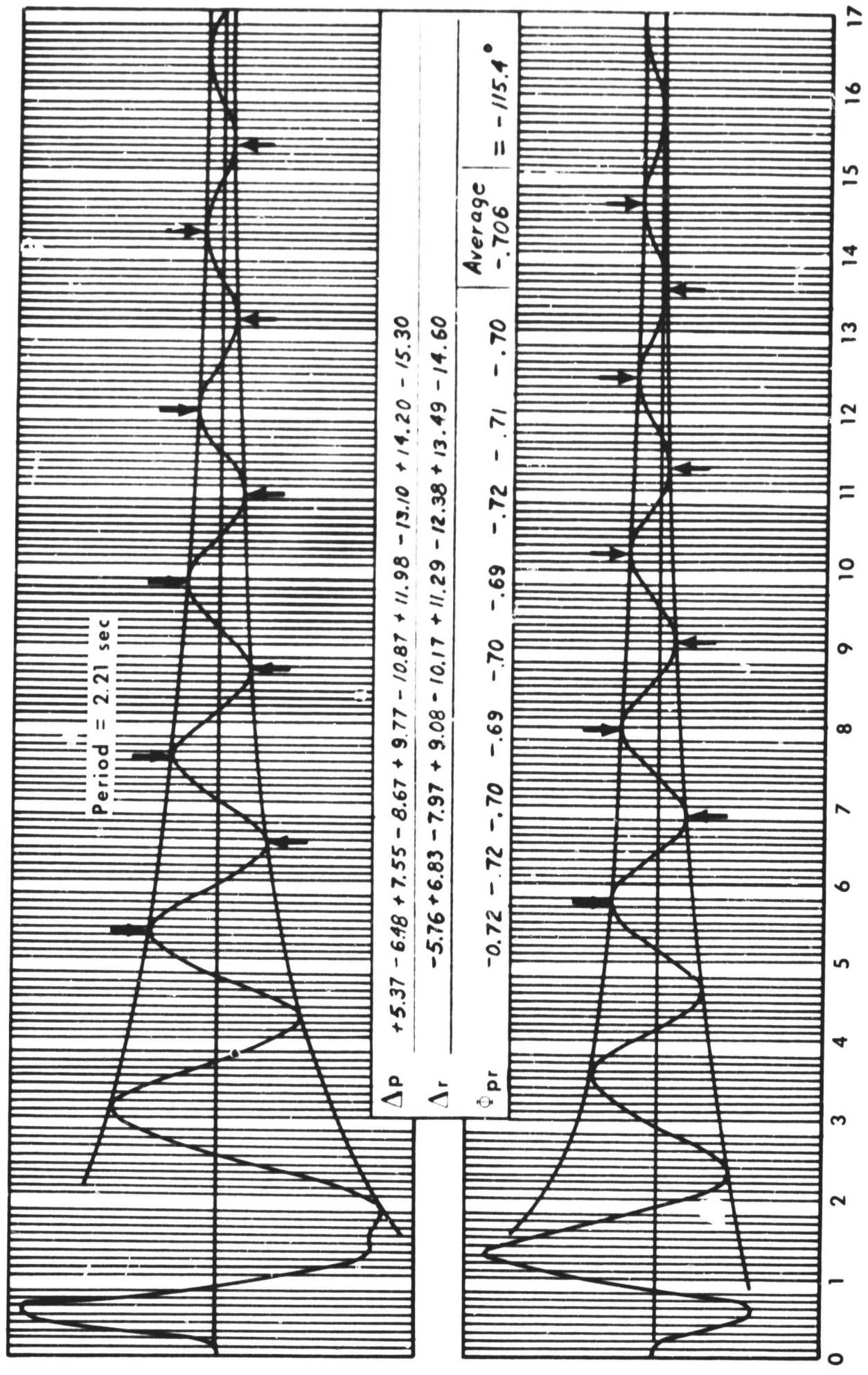

Fig. 45 Determination of period and phase angles from free-oscillation data

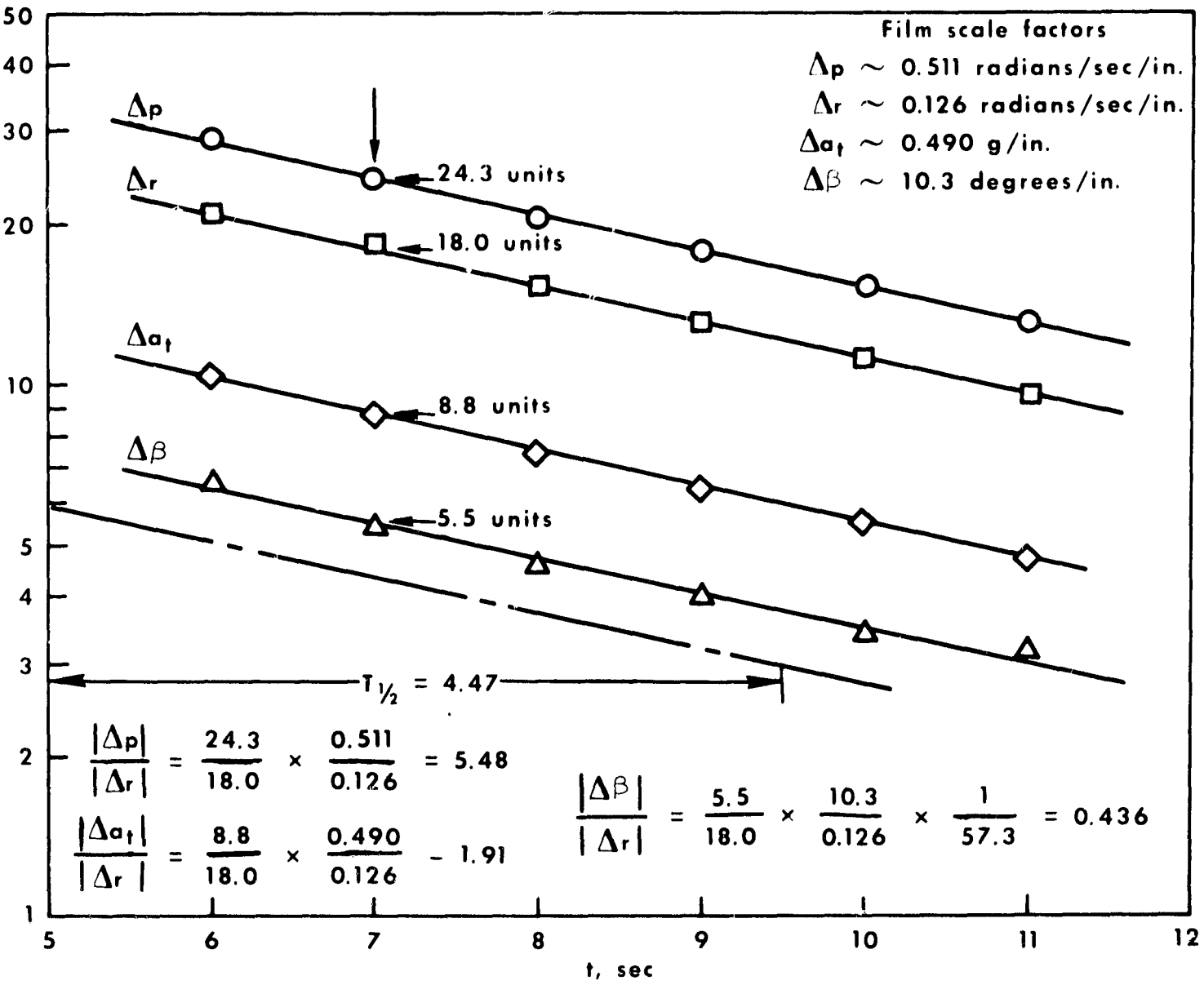

Fig. 46 Determination of time-to-damp to one-half amplitude and amplitude ratios from free-oscillation data

$$\frac{|\Delta a_n|}{|\Delta q|}\angle\Phi_{a_n q} = \frac{|\Delta a_{n_i}|}{|\Delta q|}\angle\Phi_{a_{n_i} q} - \frac{x}{g}\frac{|\Delta \dot{q}|}{|\Delta q|}\angle\Phi_{\dot{q}q}$$

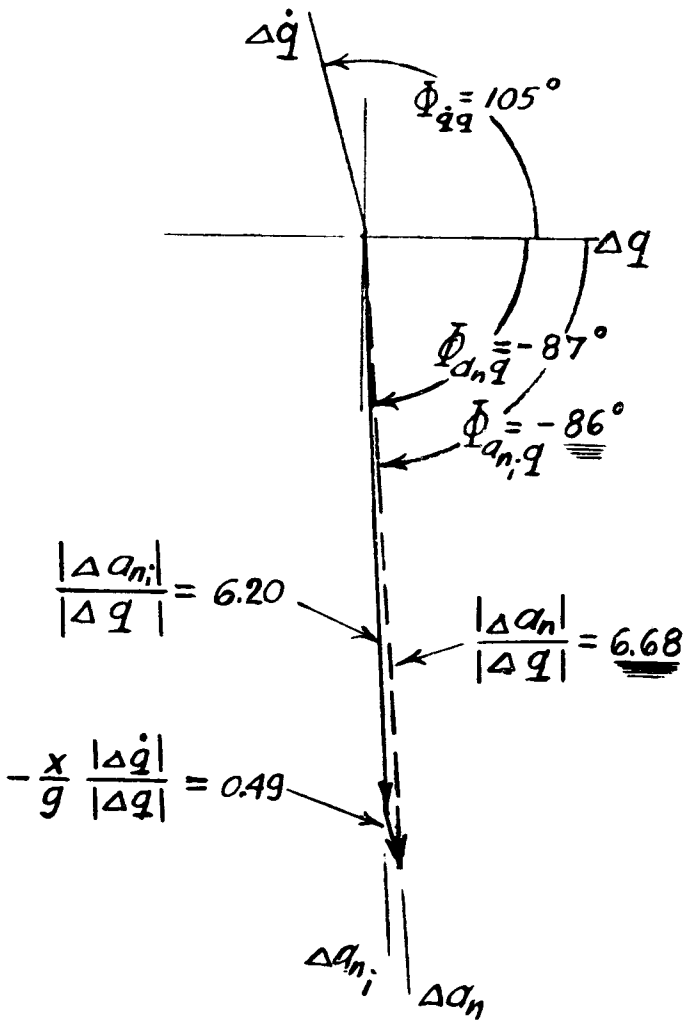

(a)

$$\frac{|\Delta a_n|}{|\Delta q|}\angle\Phi_{a_n q} - \frac{V}{g}\frac{|\Delta q|}{|\Delta q|}\angle\Phi_{qq} + \frac{V}{g}\frac{|\Delta \dot{\alpha}|}{|\Delta q|}\angle\Phi_{\dot{\alpha}q} = 0$$

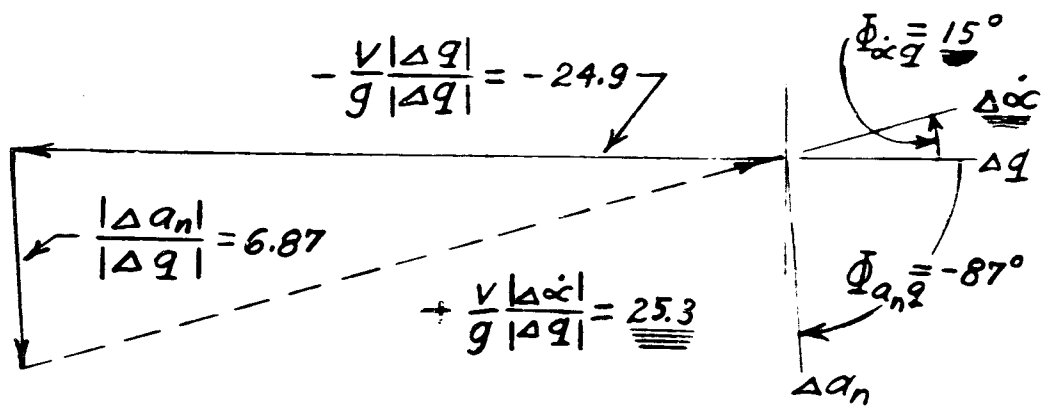

$$\frac{|\Delta\alpha|}{|\Delta q|} = \frac{\frac{V}{g}\frac{|\Delta\dot{\alpha}|}{|\Delta q|}}{\frac{V}{g}\omega_n} = \frac{25.3}{72.5} = .349$$

$$\frac{|\Delta a_n|}{|\Delta\alpha|} = \frac{\frac{|\Delta a_n|}{|\Delta q|}}{\frac{|\Delta\alpha|}{|\Delta q|}} = \frac{6.68}{.349} = 19.15$$

(b)

Fig. 47 Vector solution of $|\Delta a_n|/|\Delta\alpha|$ using pitch rate as base for amplitude ratio when angle-of-attack records are unavailable

$$\frac{|\Delta a_t|}{|\Delta r|}\angle\Phi_{a_t r} = \frac{|\Delta a_{t_i}|}{|\Delta r|}\angle\Phi_{a_{t_i} r} - \frac{x}{g}\frac{|\Delta \dot{r}|}{|\Delta r|}\angle\Phi_{\dot{r}r} + \frac{z}{g}\frac{|\Delta \dot{p}|}{|\Delta r|}\angle\Phi_{\dot{p}r}$$

$$2\tau\frac{|\Delta\dot{\beta}|}{|\Delta r|}\angle\Phi_{\dot{\beta}r} + 2\tau\frac{|\Delta r|}{|\Delta r|}\angle\Phi_{rr} - 2\tau\alpha\frac{|\Delta p|}{|\Delta r|}\angle\Phi_{pr} - C_{L_T}\frac{|\Delta\phi|}{|\Delta r|}\angle\Phi_{\phi r} - C_{L_T}\frac{|\Delta a_t|}{|\Delta r|}\angle\Phi_{a_t r} = 0$$

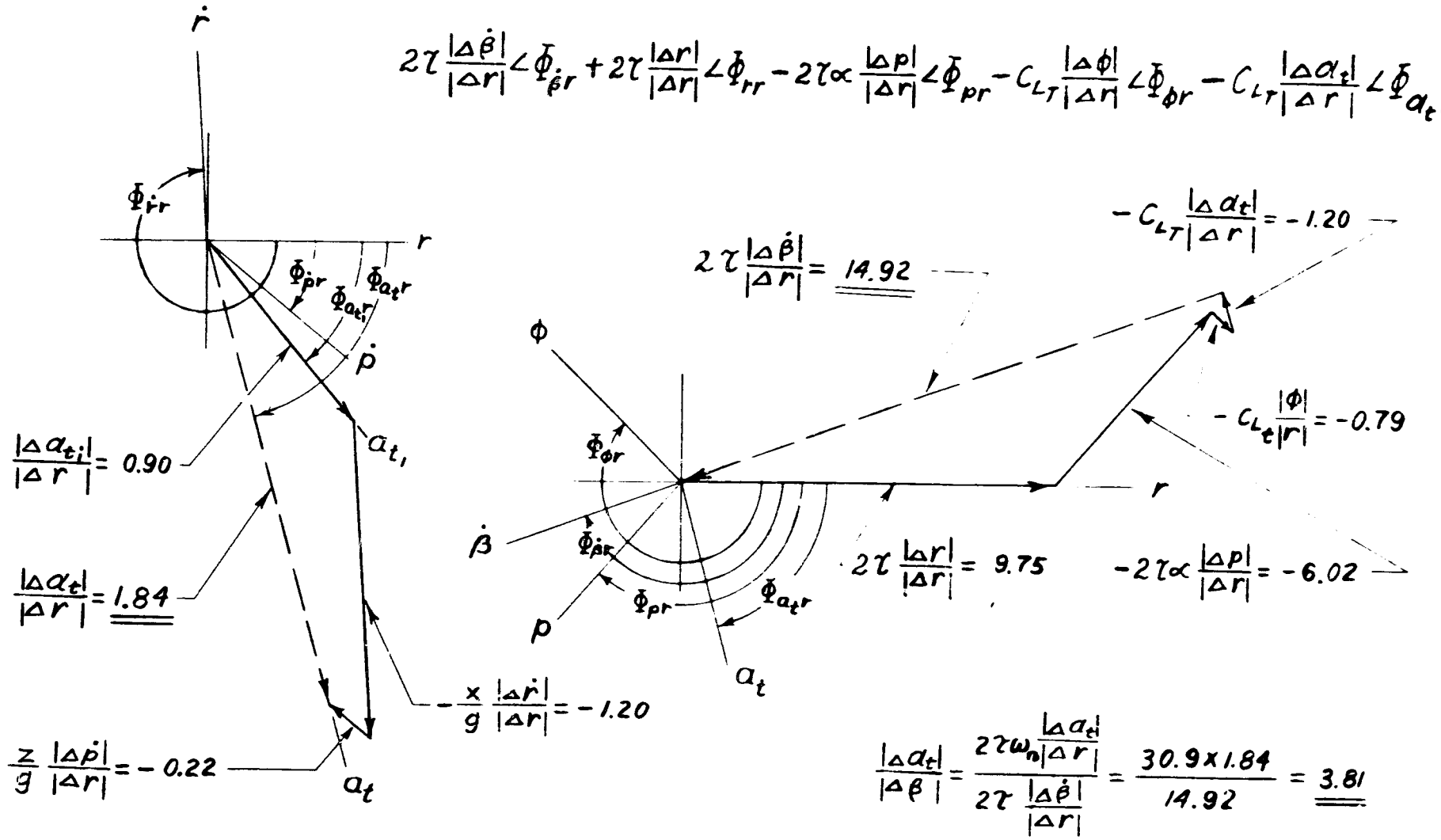

Fig. 48 Vector solution of $|\Delta a_t|/|\Delta\beta|$ using yaw rate as base for amplitude ratios when sideslip records are unavailable

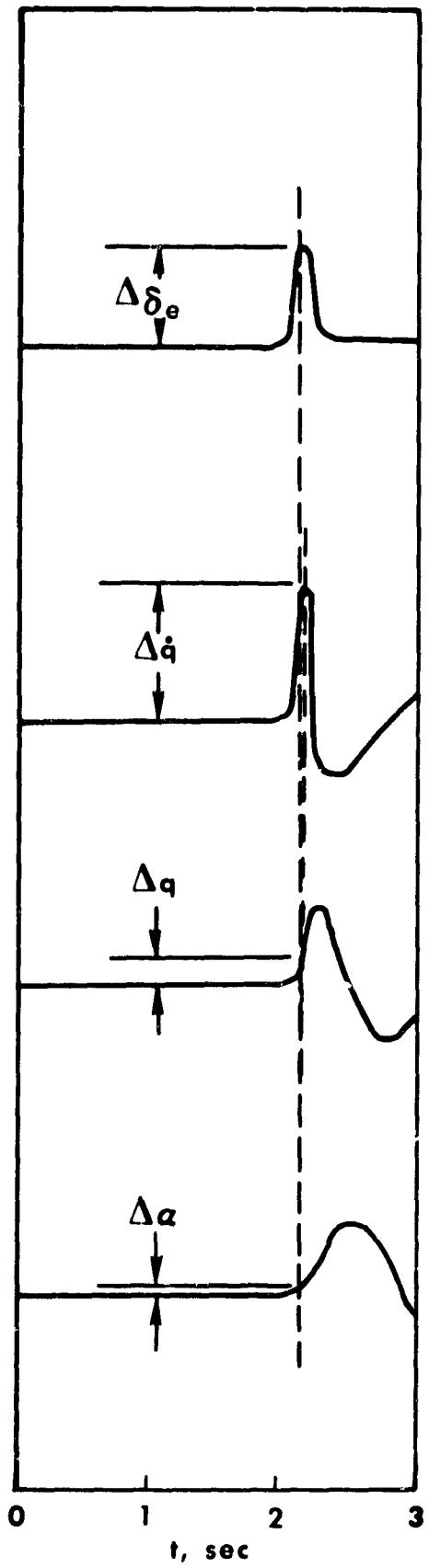

Fig. 49 Typical determination of flight quantities for the evaluation of longitudinal control derivatives

$$C_{L_T}\frac{|\Delta a_n|}{|\Delta q|}\angle\Phi_{a_n q} - C_{N_\alpha}\frac{|\Delta\alpha|}{|\Delta q|}\angle\Phi_{\alpha q} - (C_{N_q}+C_{N_{\dot\alpha}})\frac{\bar c}{2V}\frac{|\Delta q|}{|\Delta q|}\angle\Phi_{qq}=0$$

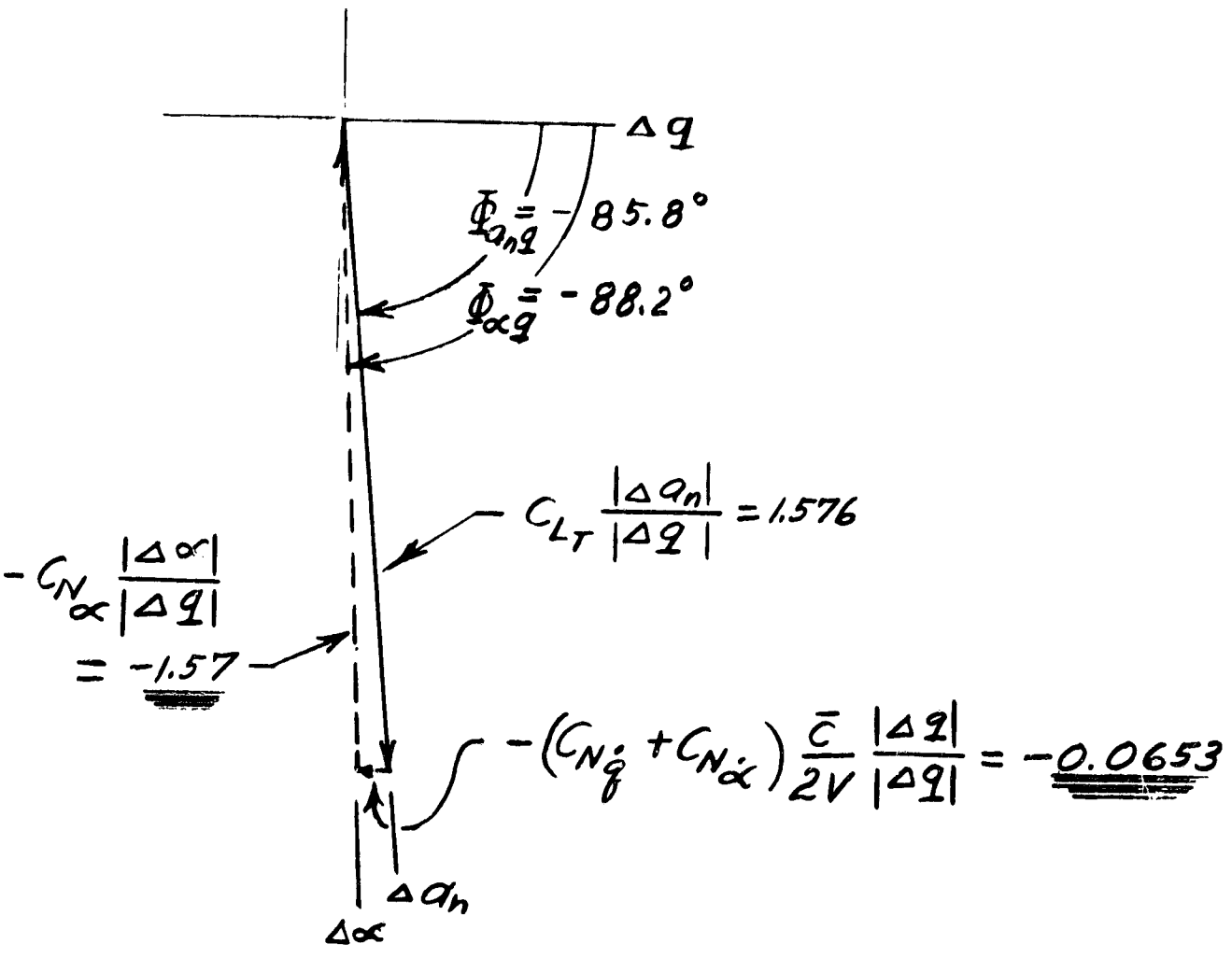

$$C_{N_\alpha} = \frac{1.57}{\frac{|\Delta\alpha|}{|\Delta q|}} = \frac{1.57}{.363} = 4.35$$

$$(C_{N_{\dot q}} + C_{N_{\dot\alpha}}) = \frac{0.0653}{\frac{\bar c}{2V}} = \frac{0.0653}{.00754} = +8.66$$

Fig. 50 A graphical time-vector solution for C_{N_α} and $(C_{N_q} + C_{N_{\dot\alpha}})$

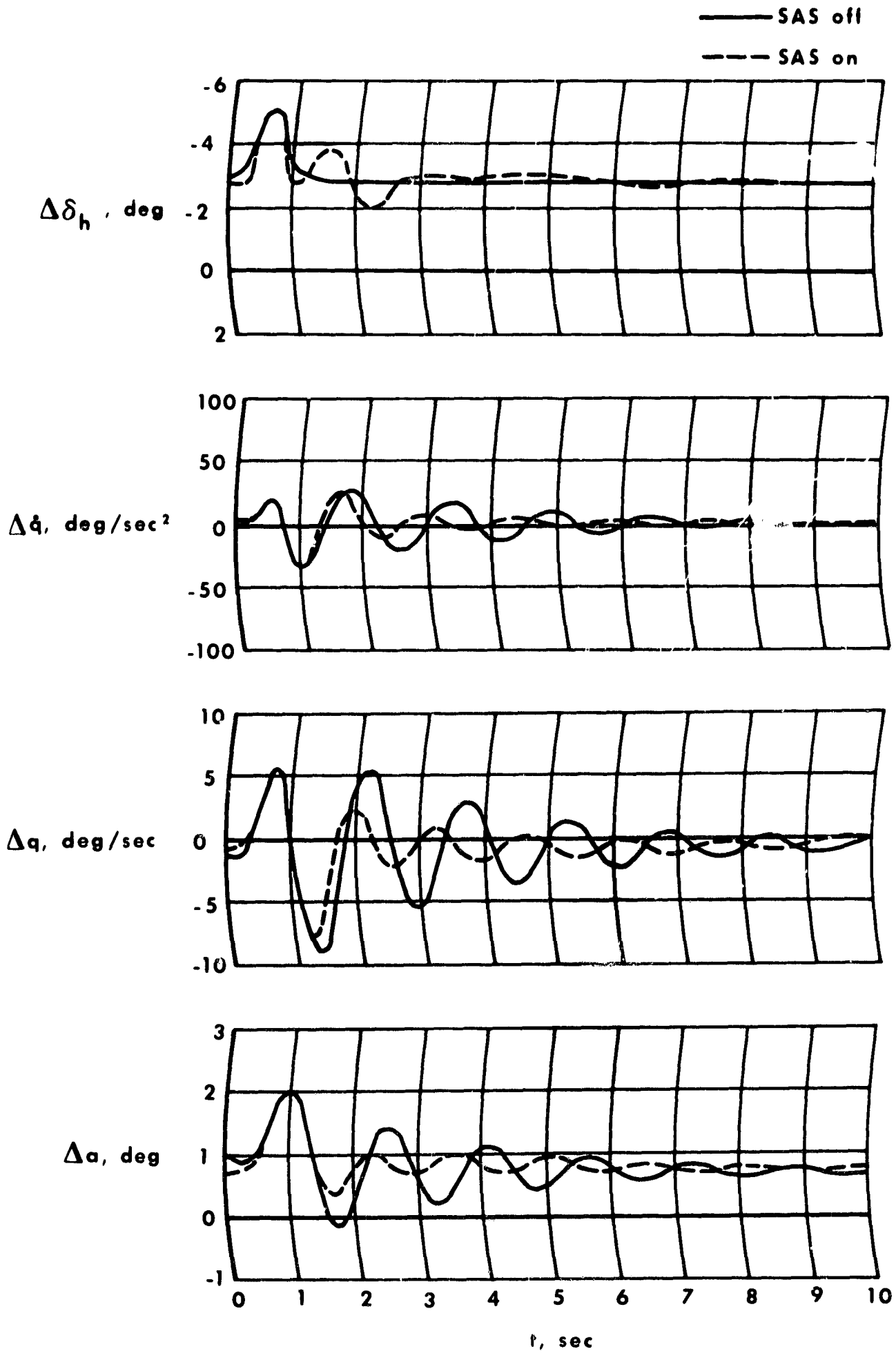

Fig. 51 Time histories of longitudinal pulses performed on the X-15 analog with the stability augmentation system engaged and disengaged (from Reference 42)

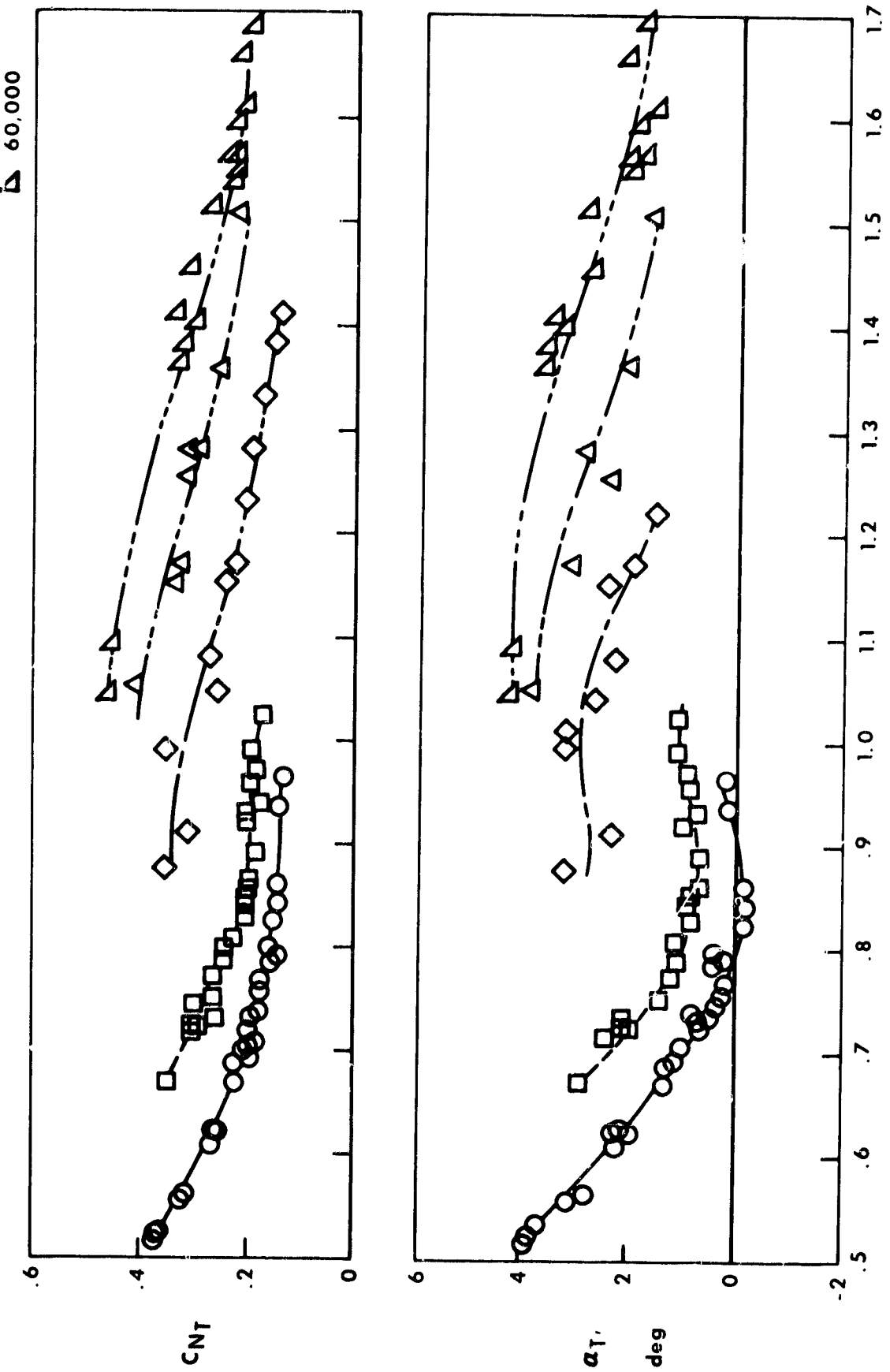

Fig. 52 Variation of lg lift coefficient and corresponding trim angle-of-attack with Mach number (from Reference 43)

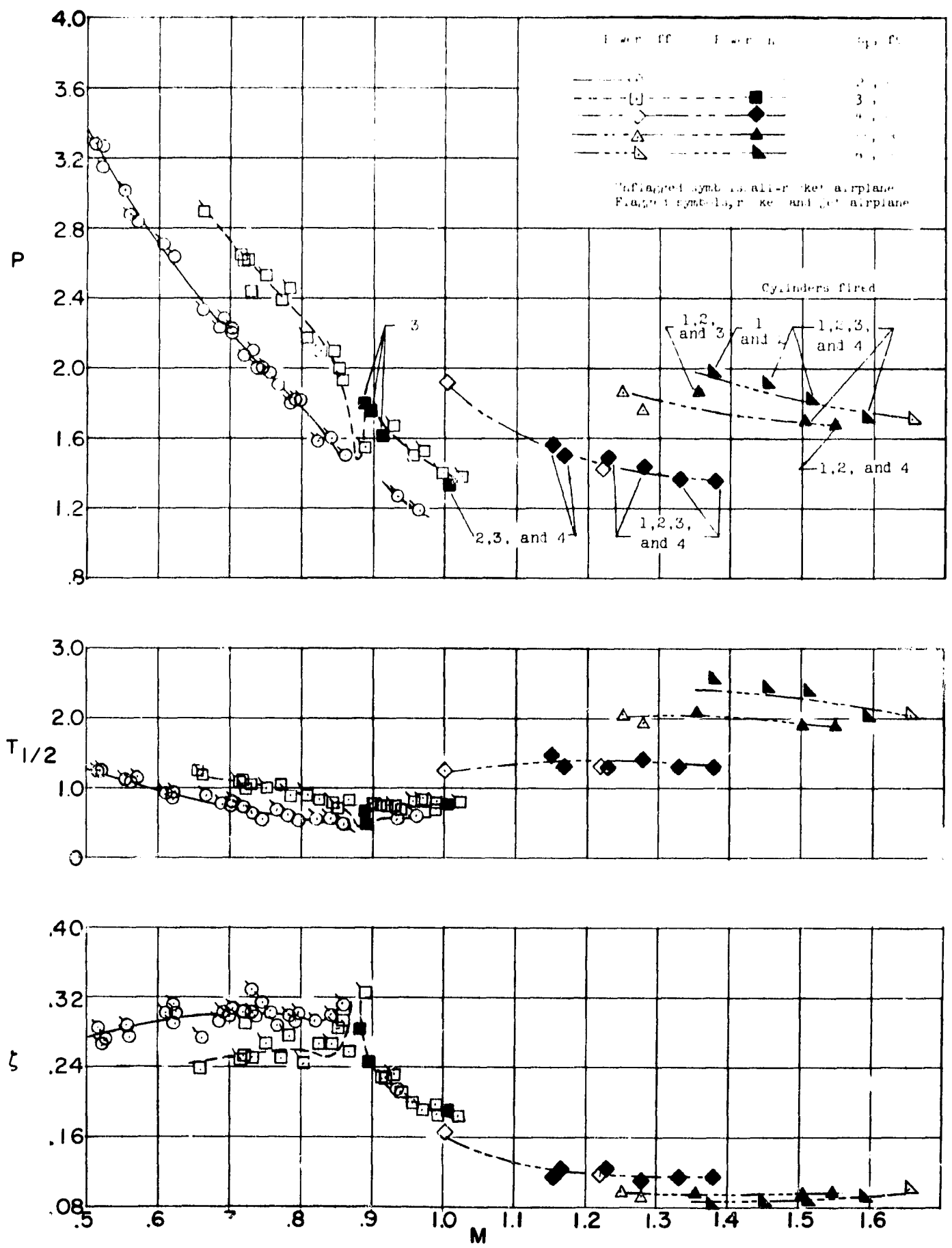

Fig. 53 Longitudinal period and damping characteristics of the D-558-II airplane as functions of Mach number and altitude

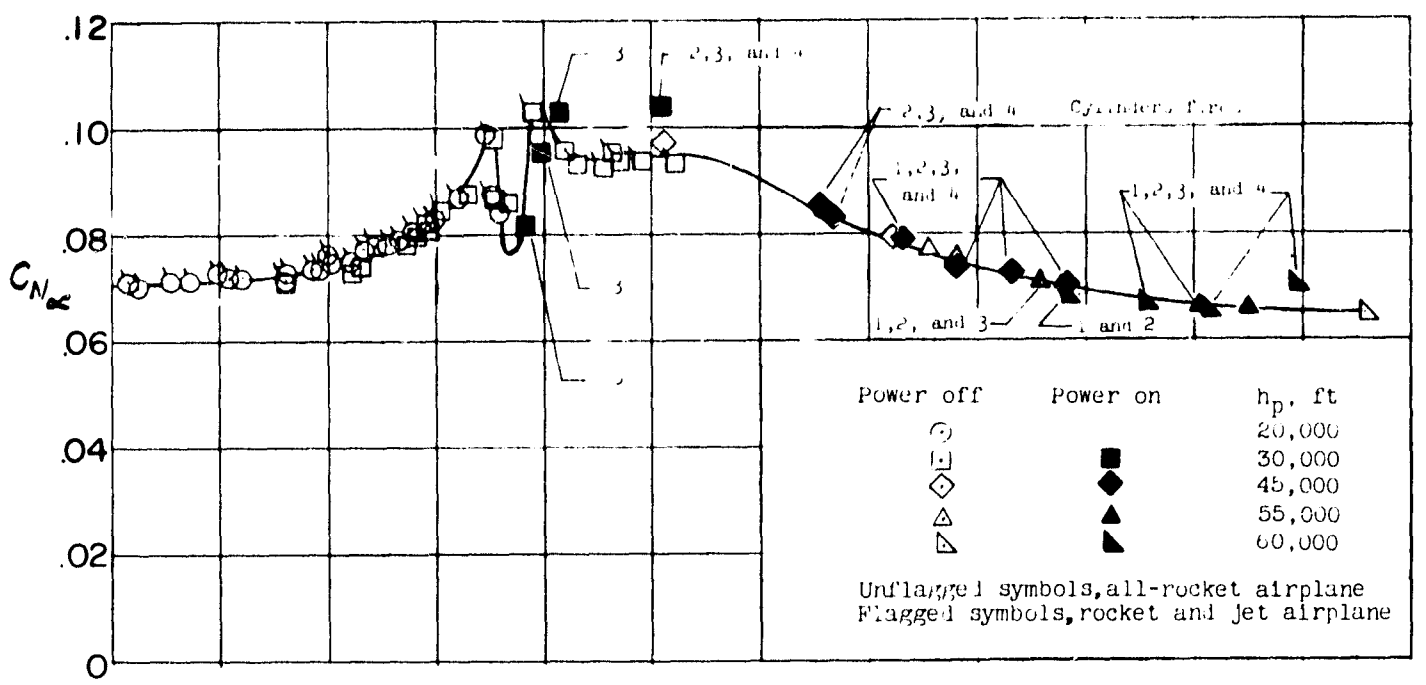

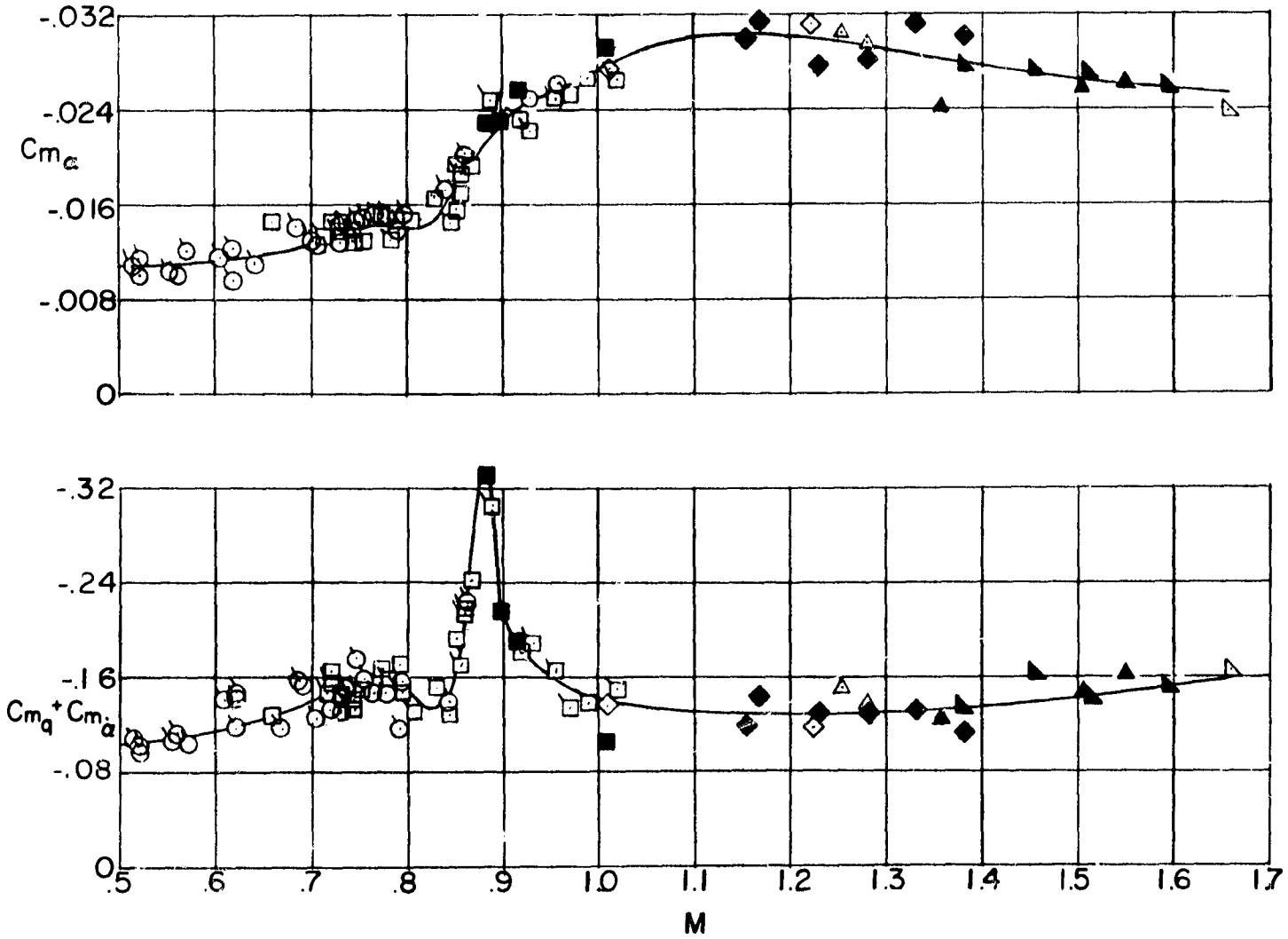

Fig. 54 Variation of static and dynamic longitudinal stability derivatives of the D-558-II airplane with Mach number (from Reference 43)

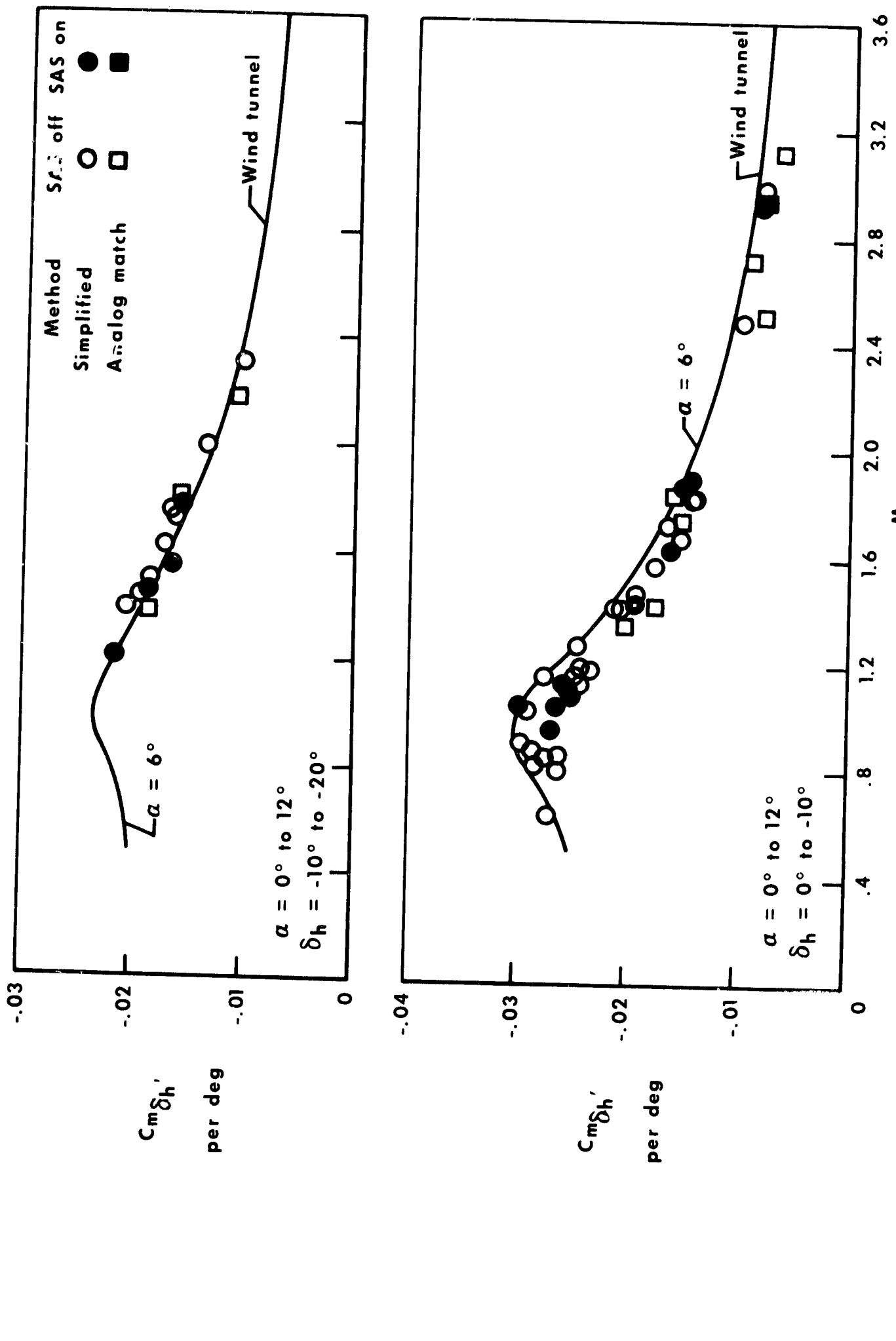

Fig. 55 Comparison of flight-determined horizontal-tail effectiveness with wind-tunnel results

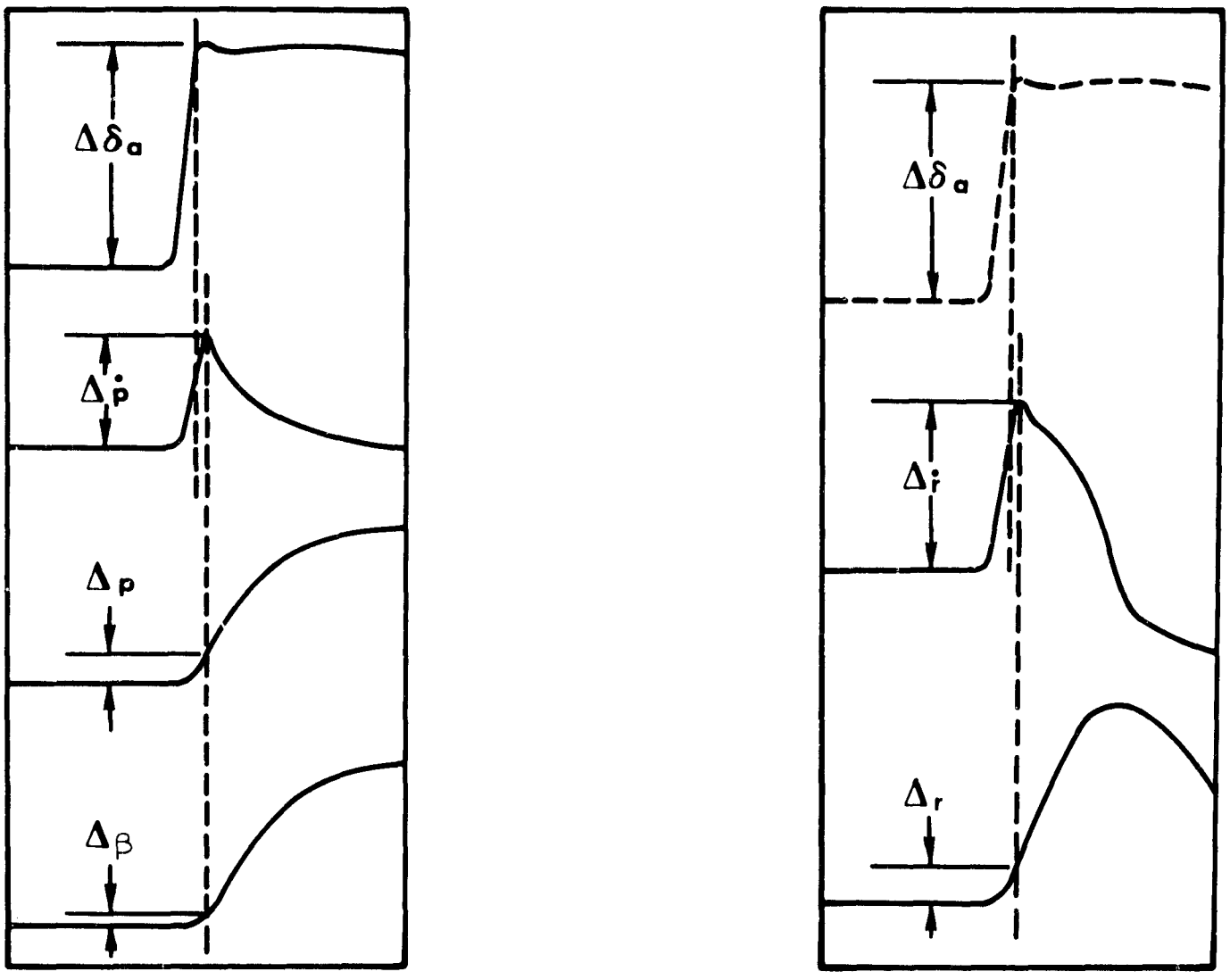

Fig.56 Typical determination of flight quantities for the evaluation of lateral control derivatives

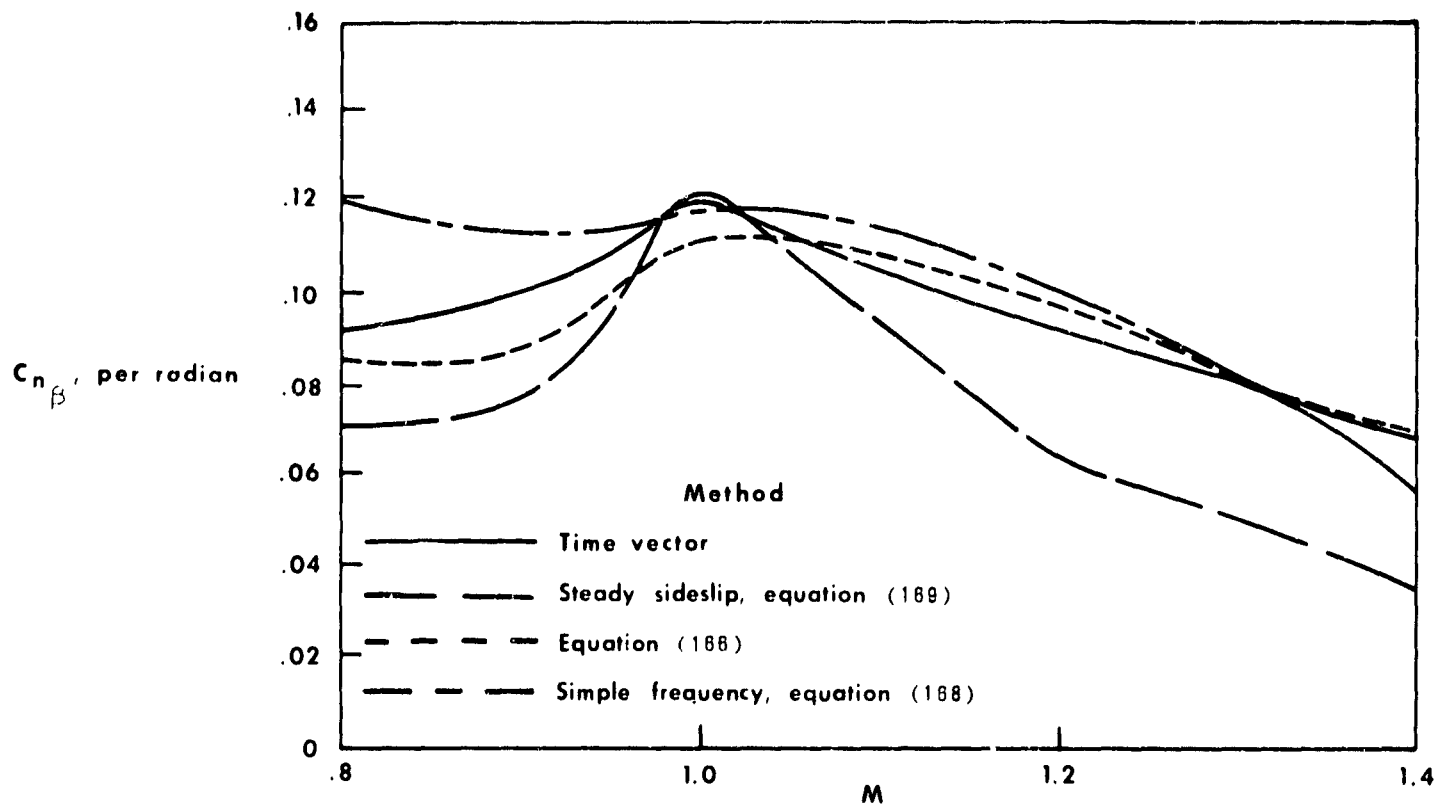

Fig. 57 Comparison of C_{n_β} as determined by several different approximate methods with the time-vector method

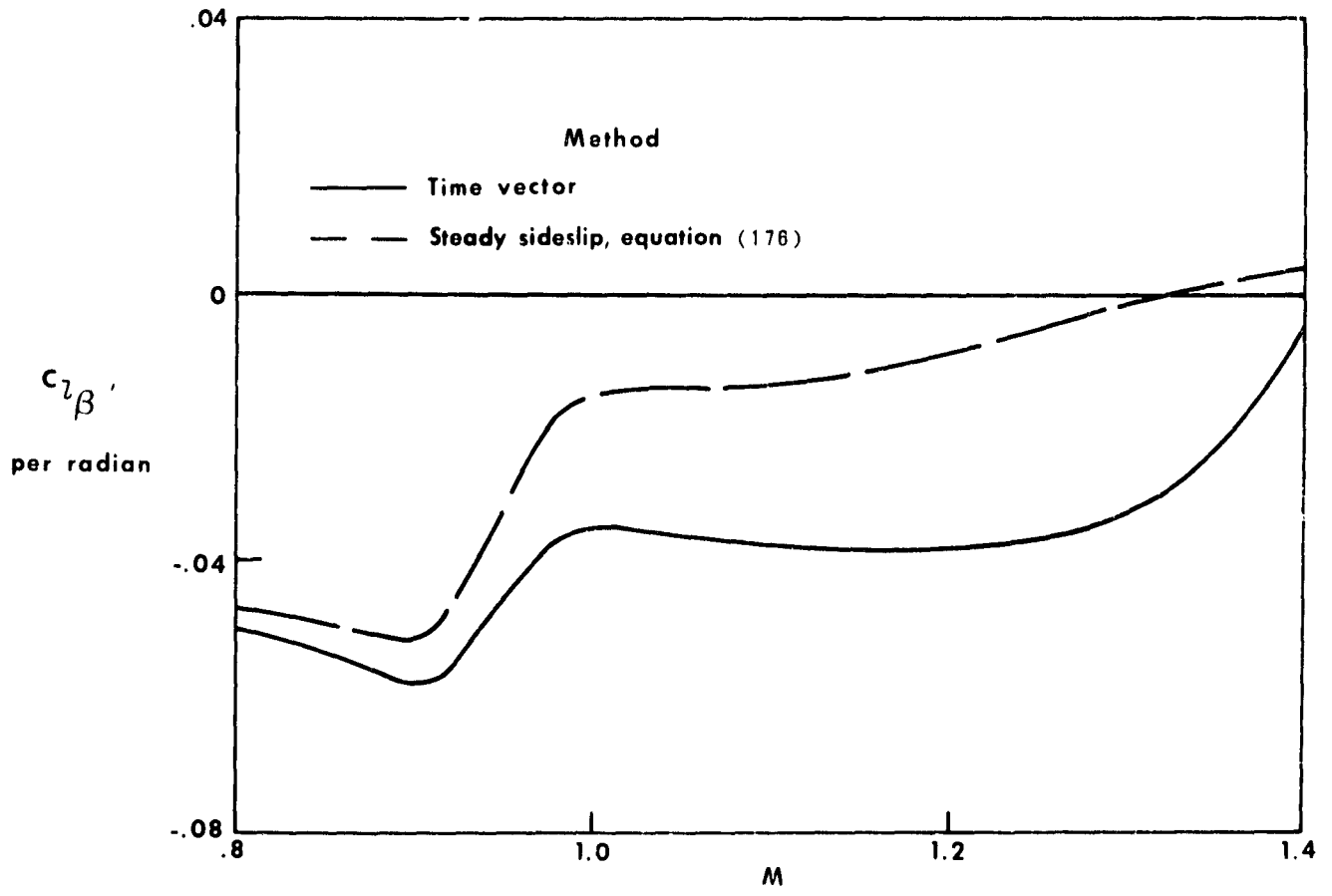

Fig. 58 Comparison of results of determining C_{l_β} by time-vector method and steady-sideslip equations

$$\frac{I_z}{\bar{q}Sb}\frac{|\Delta\dot{r}|}{|\Delta r|}\angle\Phi_{\dot{r}r}-\frac{I_{xz}}{\bar{q}Sb}\frac{|\Delta\dot{p}|}{|\Delta r|}\angle\Phi_{\dot{p}r}-C_{n_\beta}\frac{|\Delta\beta|}{|\Delta r|}\angle\Phi_{\beta r}-C_{n_p}\frac{b}{2V}\frac{|\Delta p|}{|\Delta r|}\angle\Phi_{pr}-(C_{n_r}-C_{n_{\dot{\beta}}})\frac{b}{2V}\frac{|\Delta r|}{|\Delta r|}\angle\Phi_{rr}=0$$

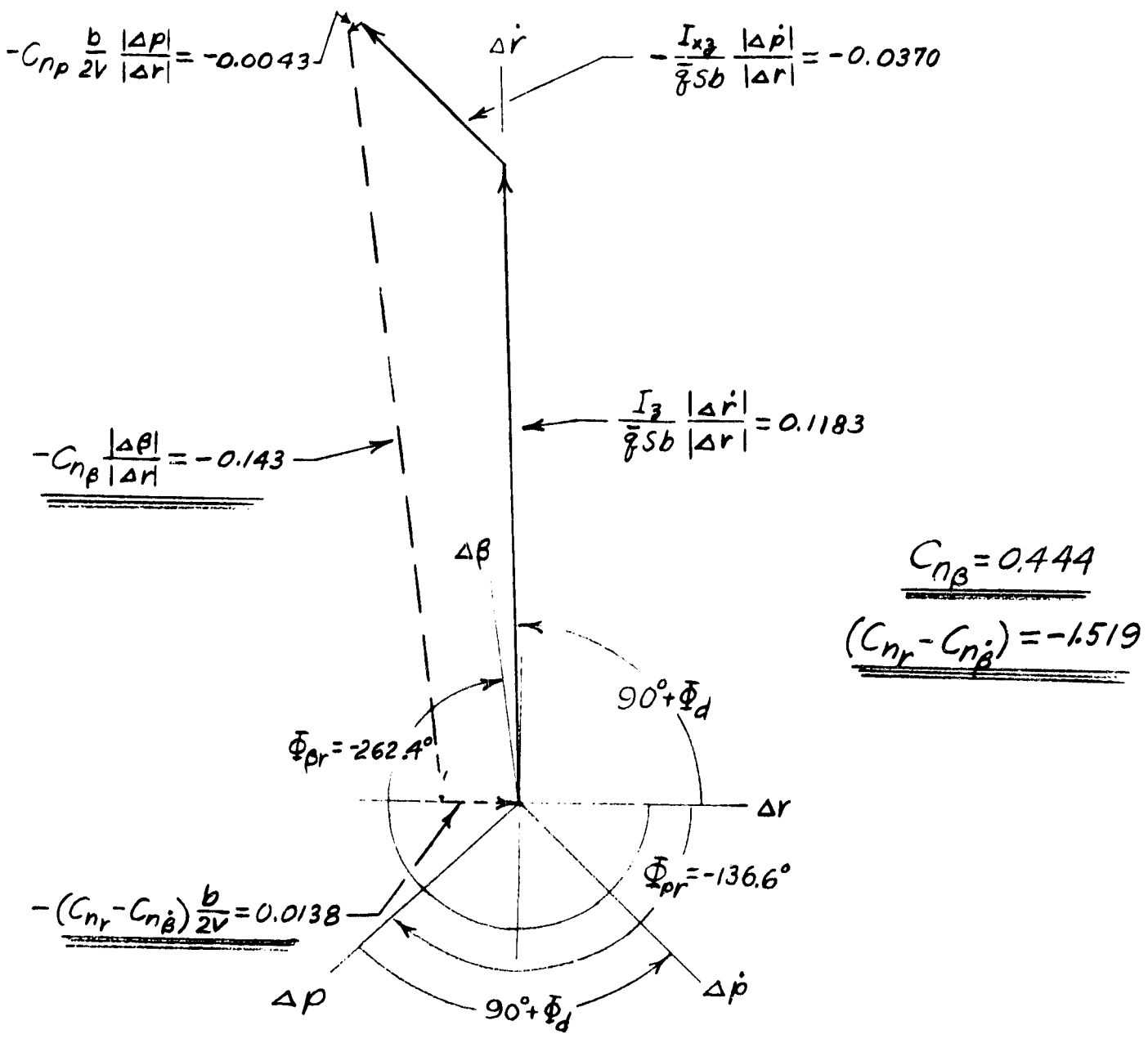

(a) Determination of C_{n_β} and $(C_{n_r} - C_{n_{\dot{\beta}}})$

Fig. 59 A typical graphical time-vector solution of yawing and rolling stability derivatives (continued)

$$\frac{I_x}{\bar{q}Sb}\frac{|\Delta\dot{p}|}{|\Delta r|}\angle\Phi_{\dot{p}r} - \frac{I_{xz}}{\bar{q}Sb}\frac{|\Delta\dot{r}|}{|\Delta r|}\angle\Phi_{\dot{r}r} - C_{l_\beta}\frac{|\Delta\beta|}{|\Delta r|}\angle\Phi_{\beta r} - C_{l_p}\frac{b}{2V}\frac{|\Delta p|}{|\Delta r|}\angle\Phi_{pr} - C_{l_r}\frac{b}{2V}\frac{|\Delta r|}{|\Delta r|}\angle\Phi_{rr} = 0$$

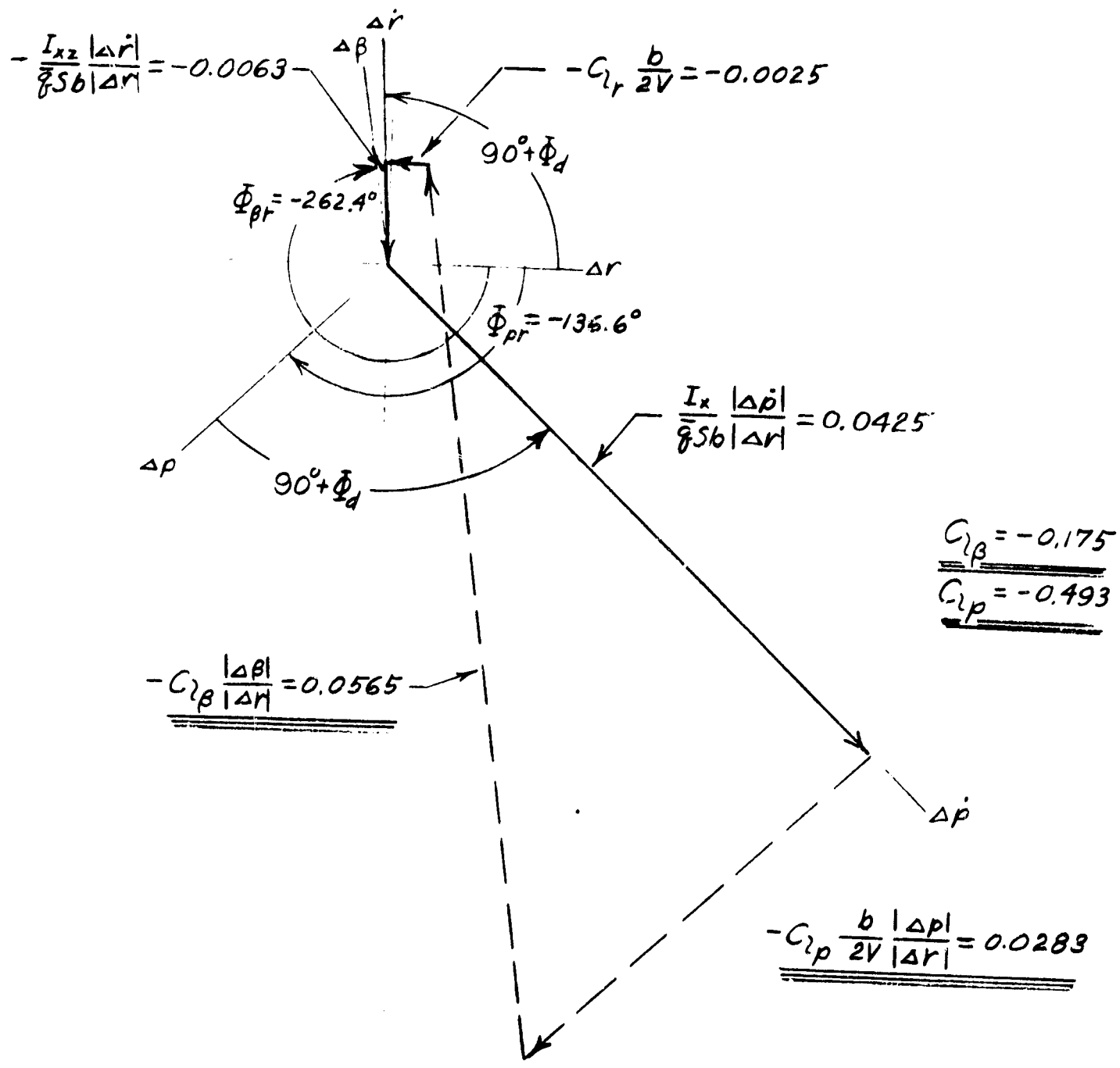

(b) Determination of C_{l_β} and C_{l_p}

Fig. 59 A typical graphical time-vector solution of yawing and rolling stability derivatives (concluded)

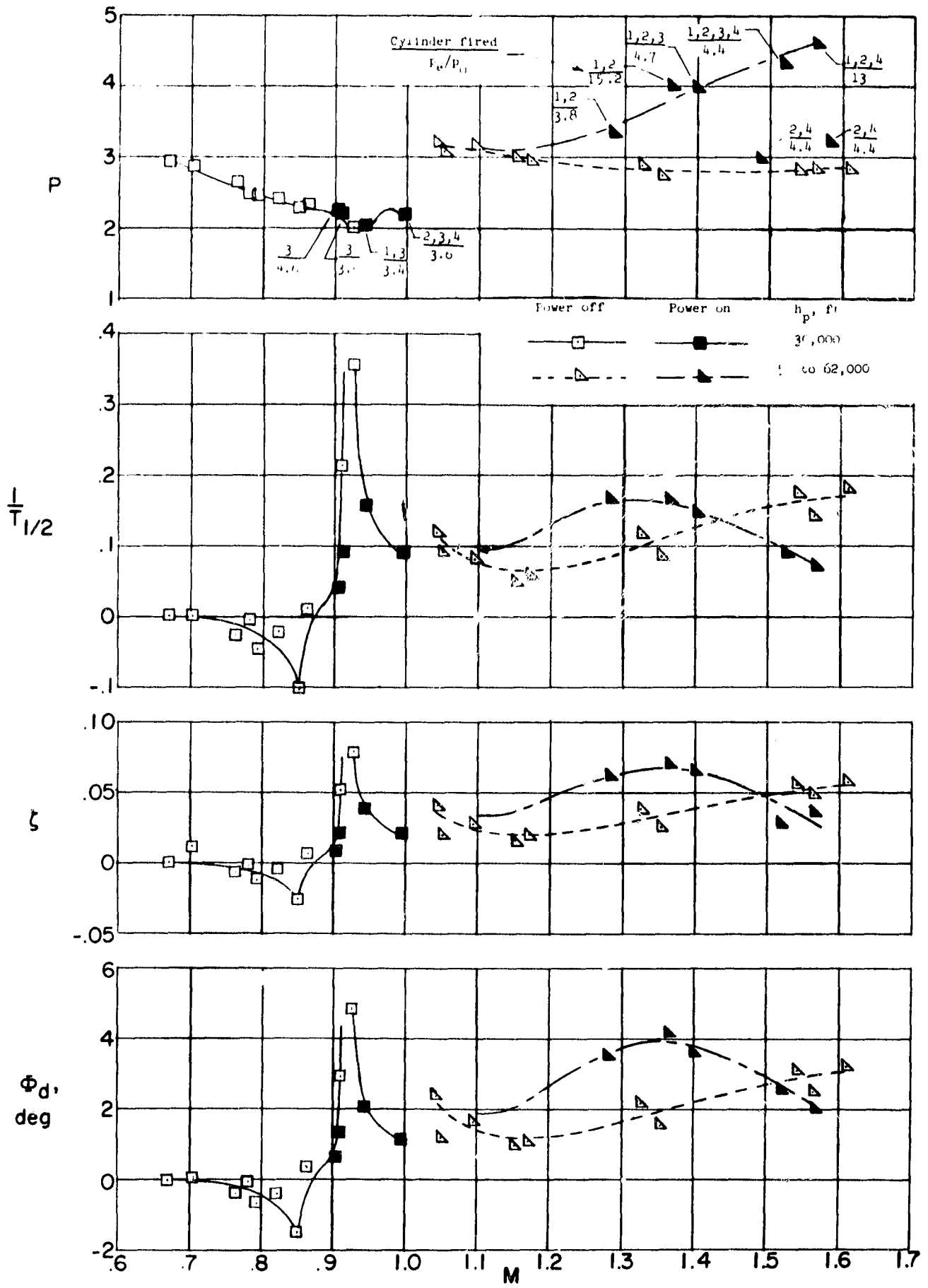

(a) Influence of power on the variation of lateral period and damping

Fig.60 Results of graphical time-vector analysis of the effects of power on the lateral-directional period, damping, and stability derivatives of the D-558-II research airplane (from Reference 43) (continued)

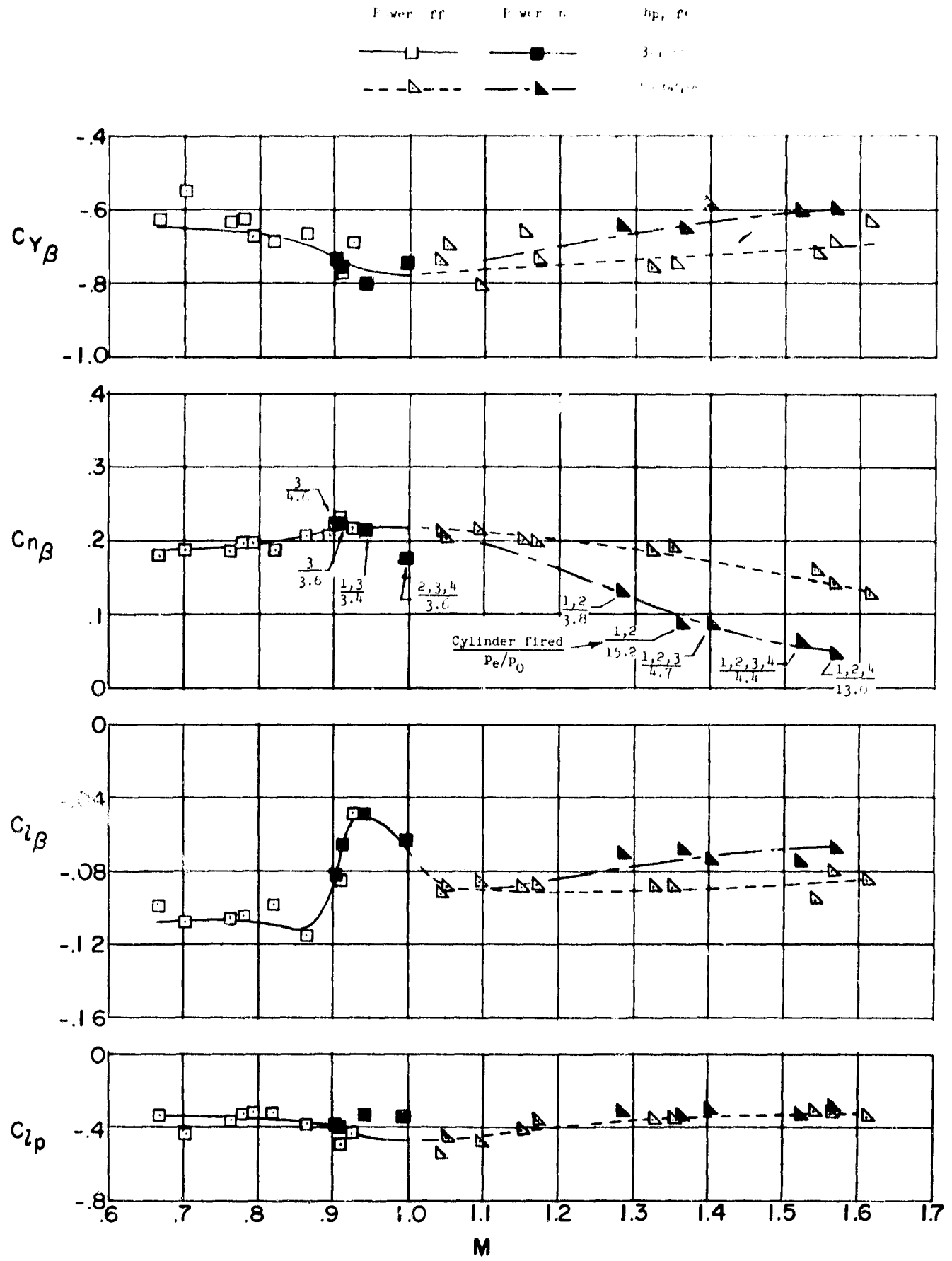

(b) Influence of power on the variation of static and dynamic lateral stability derivatives

Fig.60 Results of graphical time-vector analysis of the effects of power on the lateral-directional period, damping, and stability derivatives of the D-558-II research airplane (from Reference 43) (concluded)

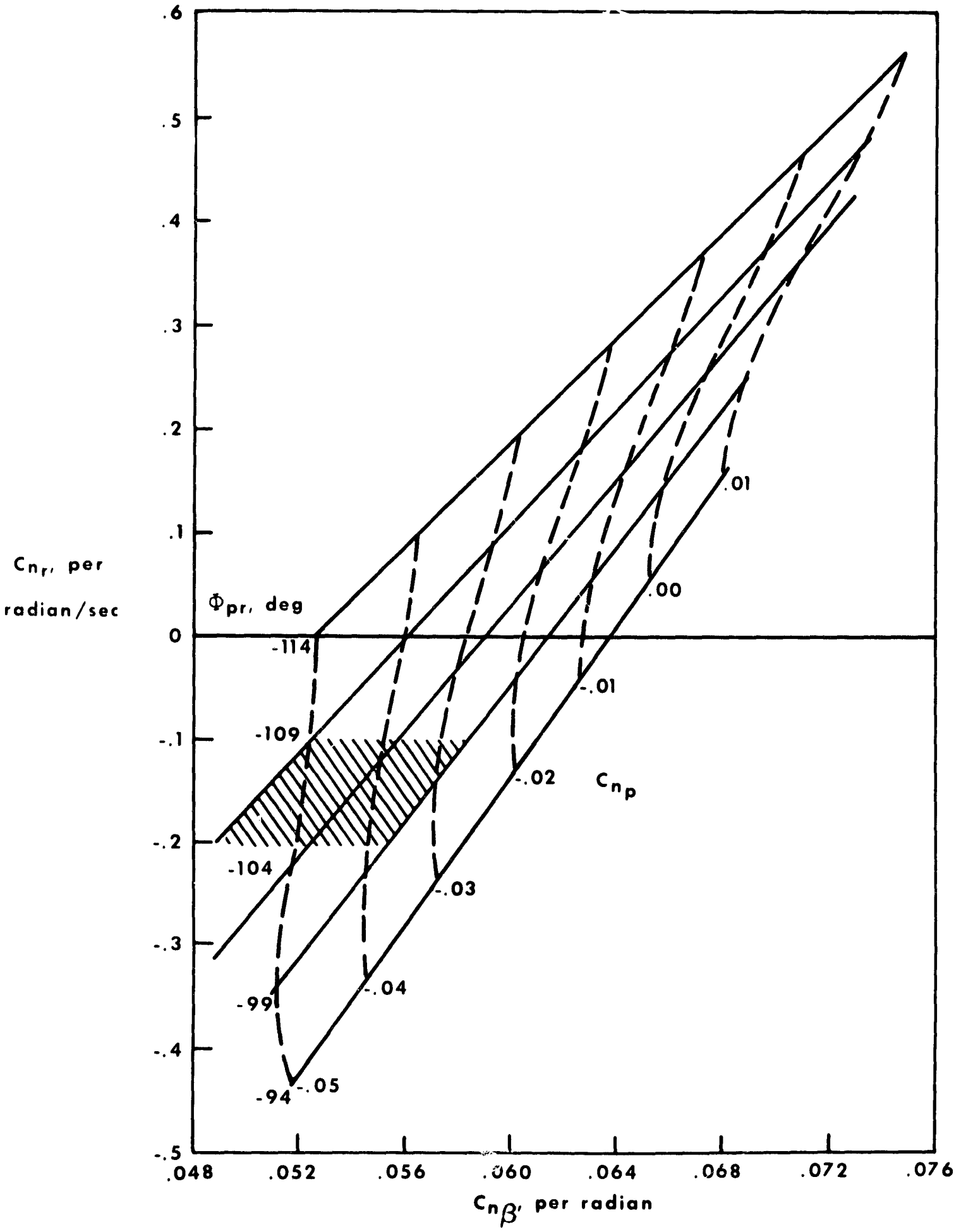

Fig.61 Grid plot used to trace source of incompatibility between flight and wind-tunnel data

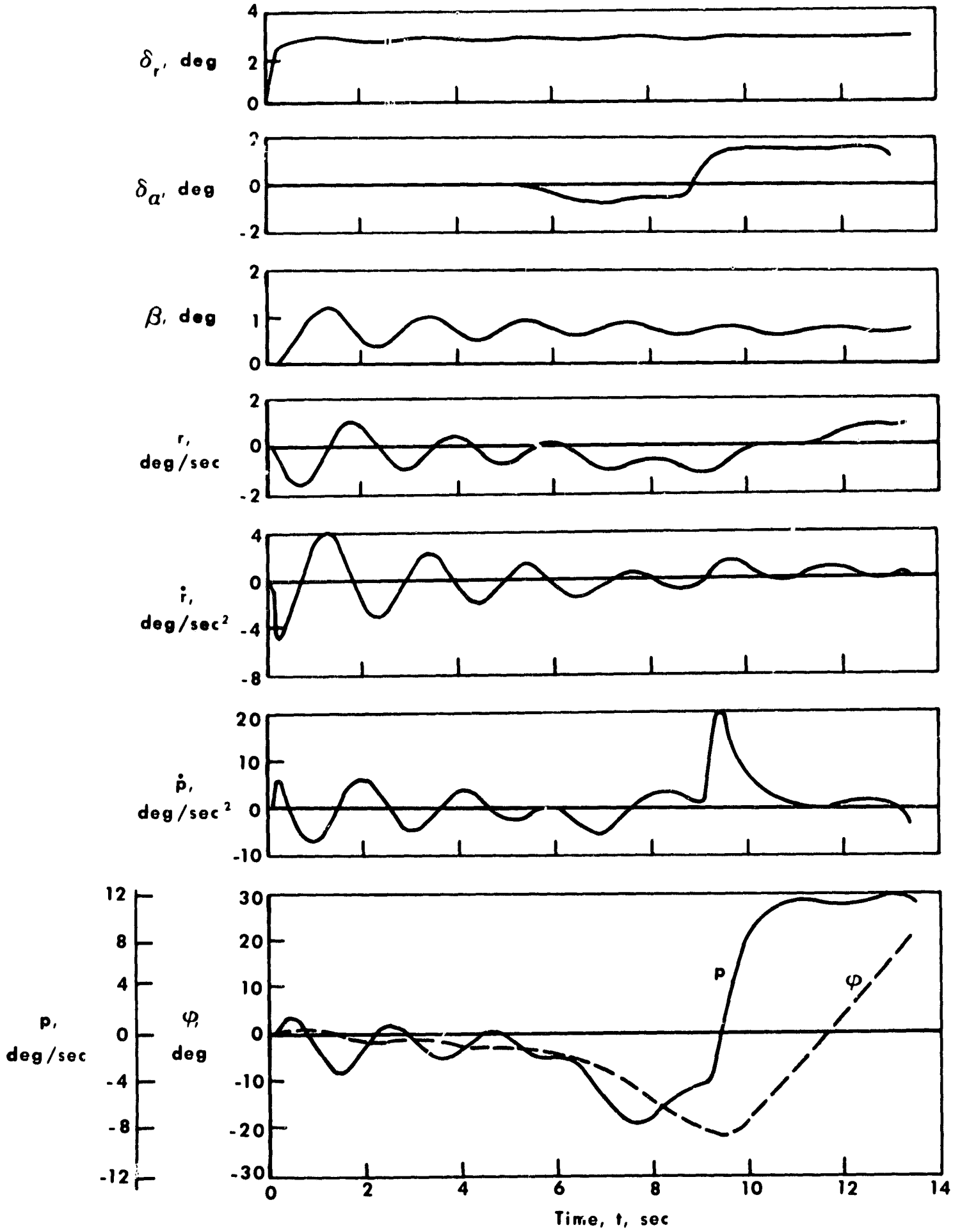

Fig.62 Typical time history of maneuver to determine derivatives by least squaring the equations of motion (Reference 48)

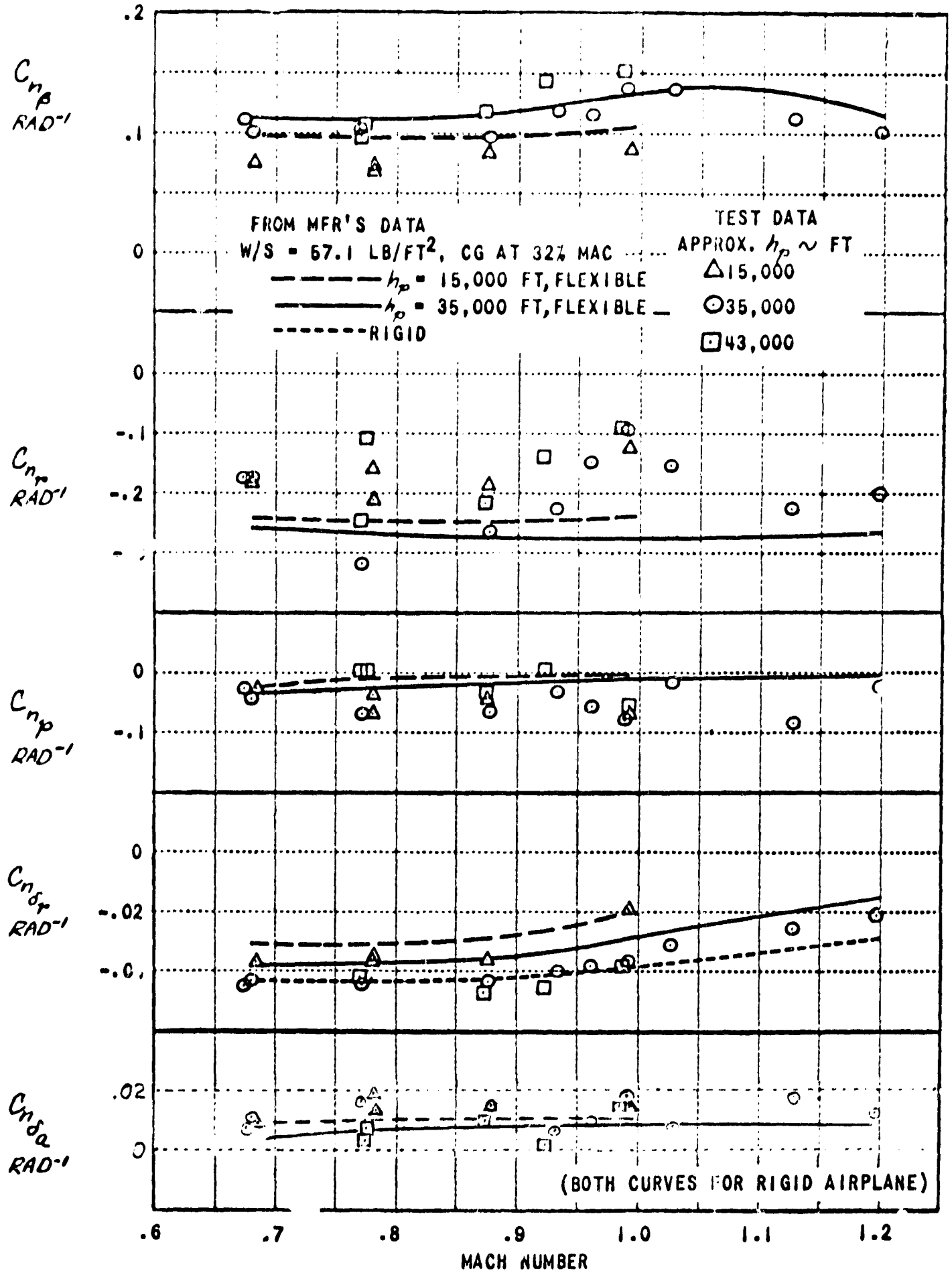

(a) Yawing-moment derivatives versus Mach number, stability-axes system

Fig.63 Lateral-directional derivatives determined by least squaring the equations of motion. as per Reference 43 (continued)

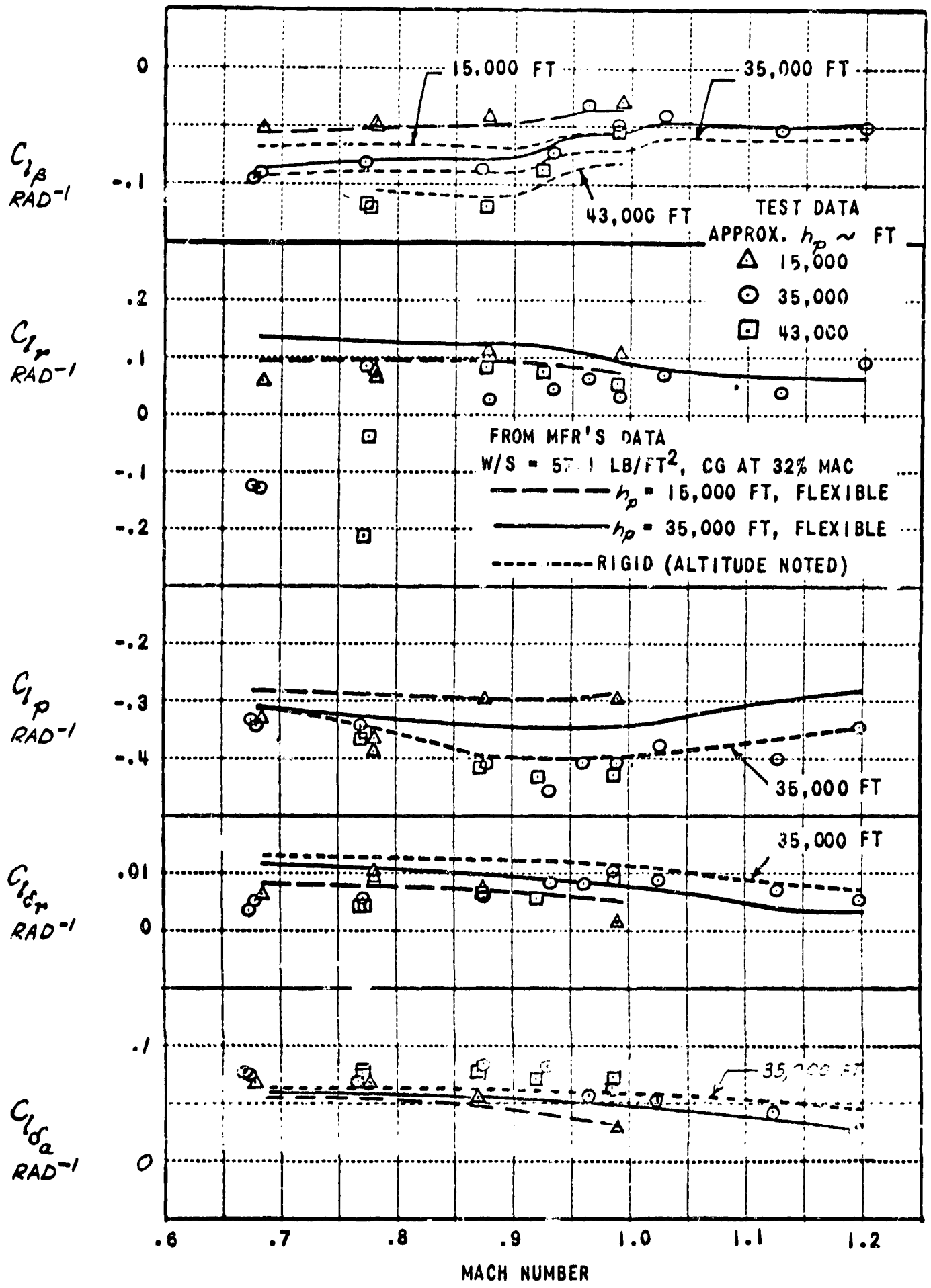

(b) Rolling-moment derivatives versus Mach number, stability-axes system

Fig.63 Lateral-directional derivatives determined by least squaring the equations of motion, as per Reference 48 (concluded)

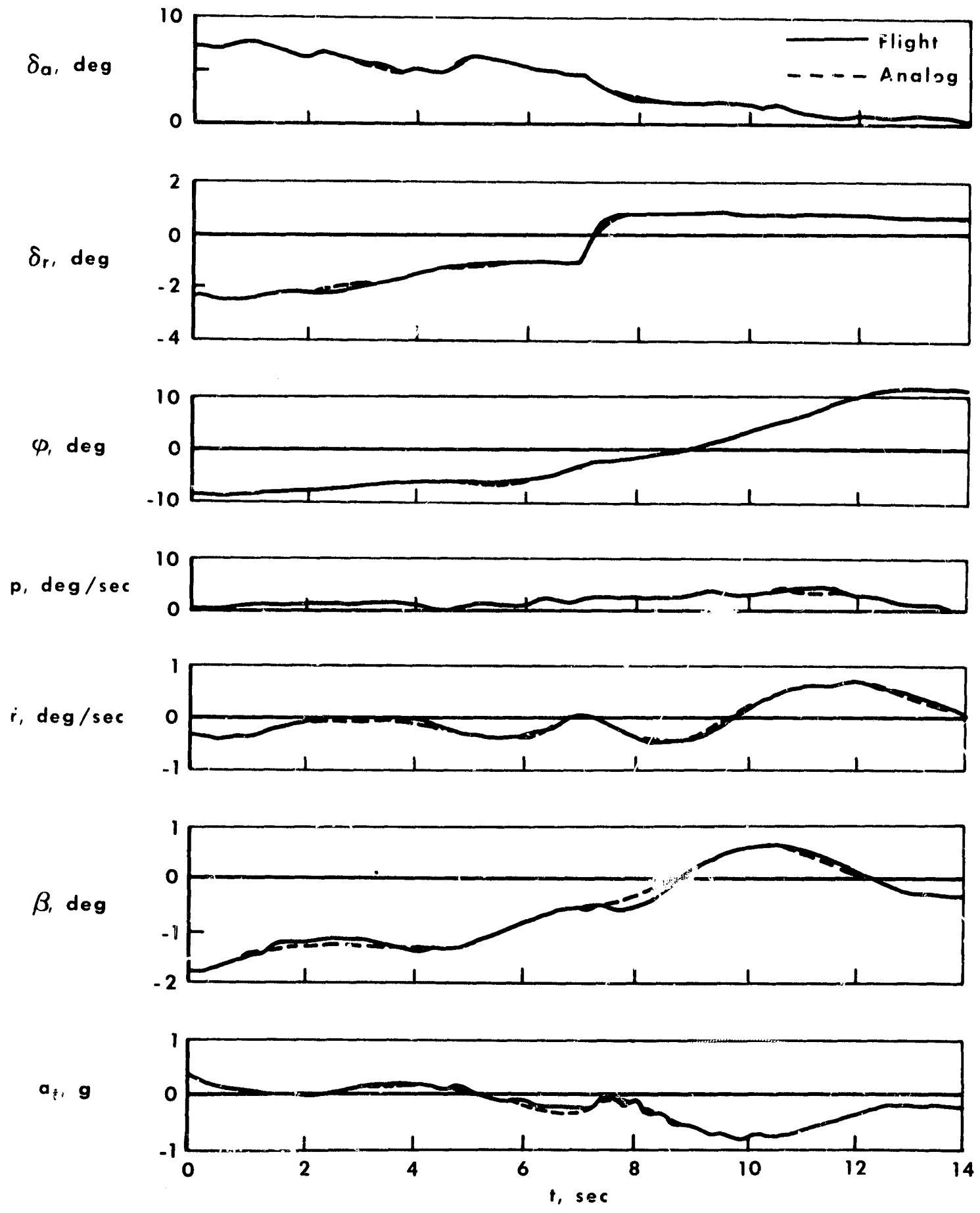

Fig.64 Typical analog-match of a "recovery-from-sideslip" maneuver of an experimental aircraft. M = 1.84 ; altitude = 49,400 ft

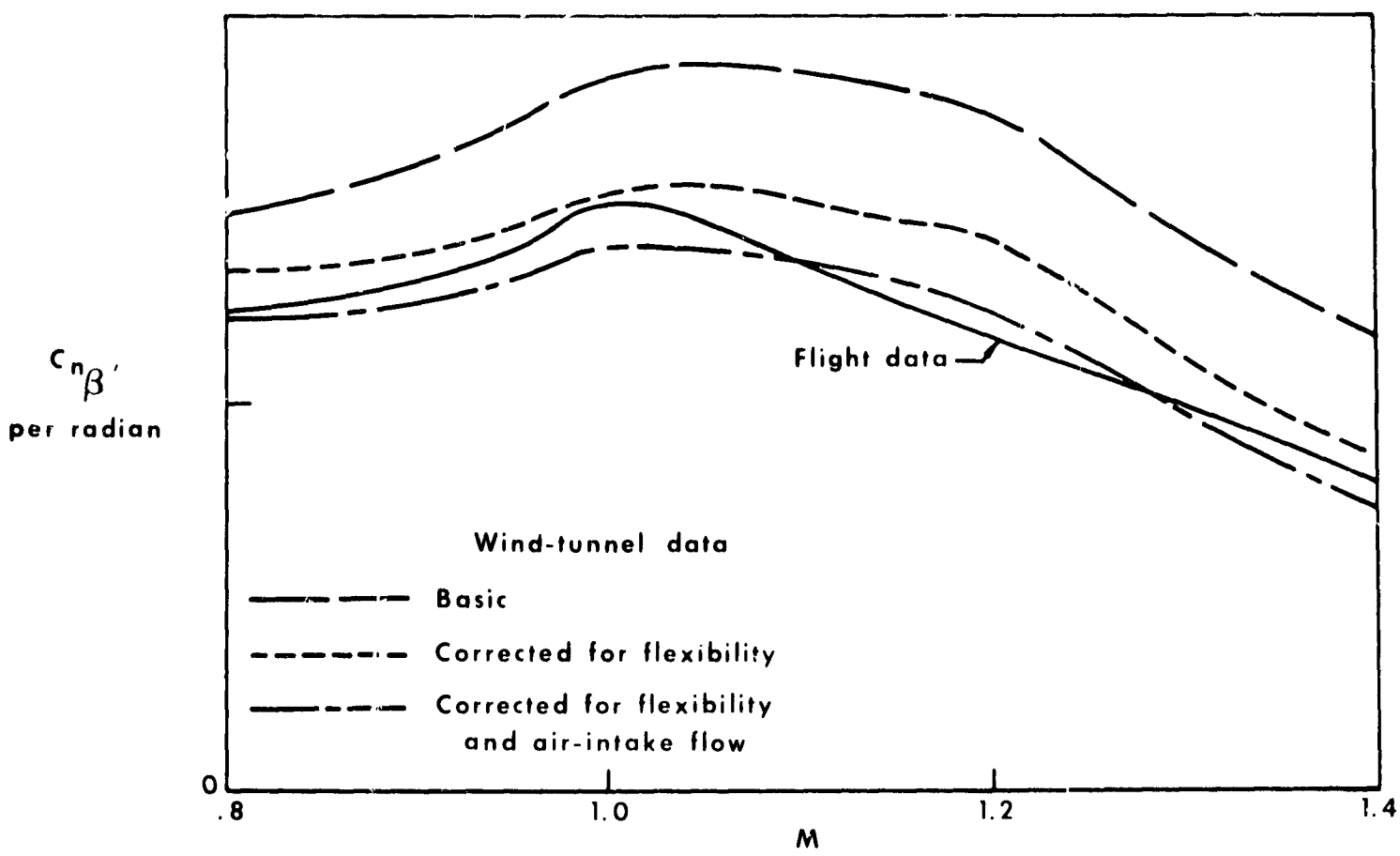

Fig.65 Influence of flexibility and air intake to engine on the directional stability derivative, C_{n_β}

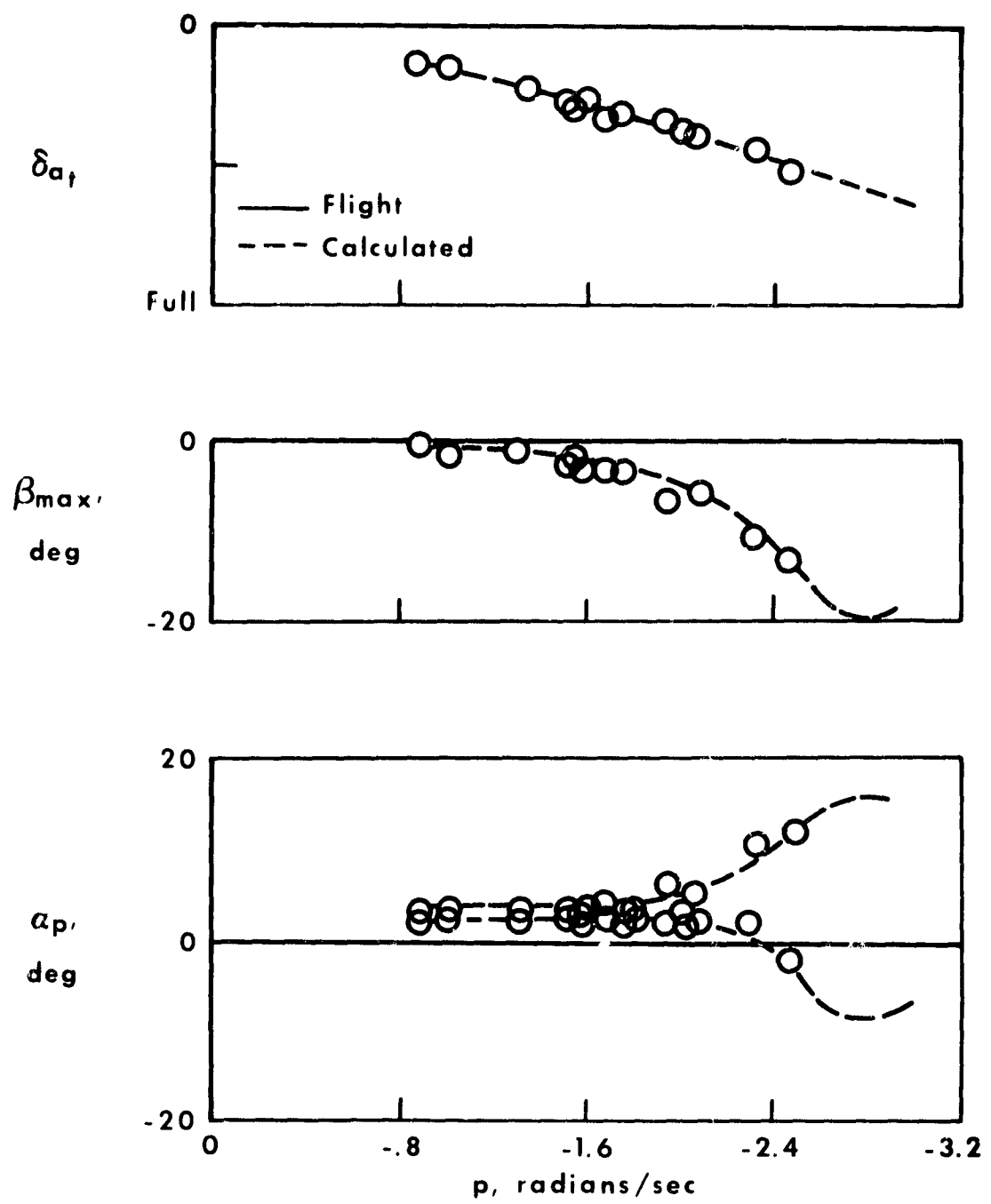

Fig.66 Comparison with flight data of results of analog simulation studies of 360° rolls using flight-determined derivatives